NASA CR-135369

ANALYSIS AND TEST OF DEEP FLAWS IN THIN SHEETS OF ALUMINUM AND TITANIUM

VOLUME 1—PROGRAM SUMMARY AND DATA ANALYSIS

By

R. W. Finger

THE BOEING AEROSPACE COMPANY

Prepared For

NATIONAL AERONAUTICS AND SPACE ADMINISTRATION

NASA Lewis Research Center

Contract NAS3-19697

Gordon T. Smith, Project Manager

1. Report No.	2. Government Accession No.	3. Recipient's Catalog No.
NASA CR 135369		

4. Title and Subtitle	5. Report Date
Analysis and Test of Deep Flaws in Thin Sheets of Aluminum and Titanium (Volume I - Program Summary and Data Analysis)	April 1978
	6. Performing Organization Code

7. Author(s)	8. Performing Organization Report No
R. W. Finger	D180-24613-1
	10. Work Unit No

9. Performing Organization Name and Address	11. Contract or Grant No
Boeing Aerospace Company Research and Engineering Division P.O. Box 3999 Seattle, WA 98124	NAS3-19697
	13. Type of Report and Period Covered Contractor Report July 1976 through December 1977

12. Sponsoring Agency Name and Address	14. Sponsoring Agency Code
National Aeronautics and Space Administration Lewis Research Center 21000 Brookpark Road, Cleveland, Ohio 44135	

15. Supplementary Notes
Project Manager, Gordon T. Smith
Materials and Structures Divsiion
NASA Lewis Research Center
Cleveland, Ohio 44135

16. Abstract

This experiment program was undertaken to further investigate the crack growth behavior of deep flaws in thin sheets. The program was designed to supplement the work performed under contract NAS3-18906 "Proof Test Criteria for Thin Walled 2219 Aluminum Pressure Vessels". Static fracture tests were performed on surface flawed specimens of both the aluminum and titaniumalloys. A simulated proof overload cycle was applied prior to all of the cyclic tests. Variables included in each test series were flaw shapes and thickness. Additionally, test temperature was a variable for the aluminum test series. Results were analyzed and compared with previously developed data to establish a criterion for proof testing thin walled pressure vessels.

17. Key Words (Suggested by Author(s))		18. Distribution Statement
Surface Flaw	Cryogenic	Unclassified, Unlimited
2219-T87 Aluminum	6Al-4V STA Titanium	
Cyclic Flaw Growth	Proof Testing	
Static Fracture		

19. Security Classif. (of this report)	20. Security Classif. (of this page)	21. No. of Pages	22. Price*
Unclassified	Unclassified	173	

* For sale by the National Technical Information Service, Springfield, Virginia 22161

FOREWORD

This report describes an investigation of the flaw growth behavior during proof testing, and its subsequent cyclic crack growth characteristics of deep surface flaws in both 2219-T87 aluminum and 6Al-4O STA titanium performed by The Boeing Aerospace Company from July, 1975, through December, 1977. The work was administered by Mr. Gordon T. Smith of the NASA-Lewis Research Center.

The program was conducted originally by the Research and Engineering and finally by the Boeing Military Airplane Development Division of the Boeing Aerospace Company, Seattle, Washington, under the supervision of Mr. H. W. Klopfenstein (Research and Engineering Division) and Mr. D. E. Strand (Boeing Military Airplane Division). The Program Leader was originally Mr. J. N. Masters and finally Mr. T. E. Dunning. The Technical Leader was R. W. Finger. Mr. H. Lenhart and H. M. Olden provided testing engineering support, and G. Jensen produced the technical illustration and art work. This technical report is also released as Boeing Document D180-24613-1.

TABLE OF CONTENTS

LIST OF FIGURES

LIST OF TABLES

SYMBOLS

K_{IE}	Fracture toughness obtained from test of surface flaw specimen.
K_{CN}	Fracture toughness obtained from center crack panel using initial flaw length and maximum load.
K_{cR}	Critical stress intensity for surface flaw specimen tests (i.e. the stress intensity at failure either fracture or breakthrough) calculated using initial flaw size and gross area failure stress.
K_{Ii}	Stress intensity calculated using initial flaw size and maximum applied stress.
E	Modulus of Elasticity
ϵ	Strain
P	Load
μ	Poisson's ratio
t	Thickness
a	Depth of semi-elliptical surface flaw or semi-minor axis of the ellipse $X^2/a^2 + y^2/c^2 = 1$
2c	Effective width of semi-elliptical surface flaw
Φ	Complete elliptical integral of second kind having modulus K defined. $K = (1-a^2/c^2)^{\frac{1}{2}}$
Q	Flaw shape parameter = $\Phi^2 - 0.212\ (\sigma/\sigma_{y.s.})^2$ (See Figure 7)
σ	Uniform tensile stress applied perpendicular to plane of crack or peak cycle value thereof.
$\sigma_{y.s.}$	Uniaxial tensile yield strength.
2C	Total crack length of center crack panel.
M_K	Magnification factor (see Figure 8).
A	Constant
n	Exponent

1.0 INTRODUCTION

The very high degree of reliability required of aerospace pressure vessels has resulted in the expenditure of considerable effort in developing analytical and experimental procedures for definition and understanding of their associated failure problems. Experience has shown that a realistic representation of failure origins is a semi-elliptical surface flaw. Accordingly, the semi-elliptical surface flaw has been adopted as a model for development of both analytical procedures and experimental data for describing the tank wall failure process.

The initial work, both analytical and experimental, was directed at developing an understanding of the catastrophic (burst) failure problem. The catastrophic (burst) failure process is a consequence of the critical defect depth being less than the wall thickness, thereby precluding the development of a leakage failure by stable crack growth. Initial studies used the stress intensity factor for a semi-elliptical flaw in a finite thickness plate which was proposed by Irwin (1)*. Irwin's original solution was for surface flaws with depth to thickness ratios, a/t, of less than 0.5. Subsequent analytical and experimental efforts (2 through 8) have provided "magnification factor" coefficients which extend the usability by accounting for effects of stress-free rear surface boundary conditions and for limited plasticity about the crack tip. These developments were incorporated into a design methodology (9) which provided a design basis for utilizing nondestructive inspection and proof-testing methods to verify that the design life could be realized in service operations.

Having recognized the intolerance of some materials to crack-like defects, a gradual but marked change in design philosophy has occurred. The most prominent feature of this change has been the development and selection of materials which exhibit a high level of tolerance to crack-like defects inherent in raw material or resulting from manufacturing processes. A good example of this was the selection of 2219 aluminum, rather than a higher

*Numbers in parentheses refer to references at the end of the report.

strength aluminum alloy, for many of the space shuttle components. The use of such flaw-tolerant materials has presented some unique problems. These problems are a consequence of the defect size which will cause failure (burst) during proof testing, being greater than the wall thickness. The procedures developed for assuring the service lives of vessels produced from brittle material (Reference 9) are no longer directly applicable. Although the procedures for minimizing service failures are available for the "brittle" vessels, the possibility of costly proof test failures and resultant schedule problems was sufficient incentive to cause the selection of the more flaw tolerant alloy. Although the selection of flaw tolerant materials such as 2219-T87 aluminum could virtually eliminate the possibility of a catastrophic failure during proof test or operation, deep flaws which survived the proof test cycle could grow through the thickness during service causing leakage and thereby compromising mission objectives or possibly causing a total loss of the mission.

An evaluation of the applicability of the proof testing methodologies to thin walled vessels was undertaken by references 10 and 11. This program, a follow-on to references 10 and 11, was directed towards developing a better understanding of and the procedures for proof testing thin walled tanks. The program has two major sections, the first directed at determining the crack growth behavior of surface flaws during the application of a simulated proof test cycle, and the second designed to evaluate the use of a proof test cycle in assuring subsequent service life. The program consisted of an experimental effort which employed specimens fabricated from both 2219-T87 aluminum and 6Al-4V STA titanium base metal. A variety of flaw shapes were tested at room temperature 295 K (70°F) and at 20 K (-423°F) for the aluminum and exclusively at room temperature for the titanium. Thicknesses tested varied from 0.64 mm (0.25 inch) to 4.77 mm (0.188 inch) for the aluminum and 1.02 mm (0.040 inch) to 3.18 mm (0.125 inch) for the titanium.

The following sections of the report present a brief review of related background data, definitions and terminology, a description of the materials and experimental procedures, and a discussion of the results and a summary of the significant conclusions. Applicable data from other studies are incorporated into the analysis of the results.

2.0 BACKGROUND

Significant progress had been made in developing procedures for handling the shallow flaw problem when experimental work devoted to the deep flaw problem was initiated in 1967. This work, published in Reference 2, involved static and cyclic tests of thick and thin gages of material, using a variety of different flaw shapes in order to bound the influence of flaw depth to thickness ratio and flaw shape on the failure process. Two materials were tested during the conduct of that program, 2219-T87 aluminum and 5Al-2.5 Sn titanium in both base and weld metal form. The results were used to empirically derive deep flaw magnification factors to be applied to Irwin's surface flaw stress intensity solution. Instrumentation for determining wall penetration prior to fracture was not available although it was suspected that such behavior had occurred and influenced the results.

A subsequent experimental program (8) was undertaken to explore the static and cyclic behavior for combinations of flaw depth, flaw shapes and thicknesses through that range where failure mode changed from "catastrophic failure" to leak-before-failure. Instrumentation was added to detect flaw breakthrough (leakage) prior to failure. The data from the program was used to establish the empirical formula

$$t - a = 0.10 \left(K_{IE}/\sigma_{ys}\right)^2 \qquad (1)$$

for determining ligament length at which the failure mode changes from fracture to leakage-before-fracture. Additionally, the results of that study indicated that K_{IE} values obtained from any of three available deep flaw solutions (2, 3, 4) could be used to describe fracture stress/flaw size loci for a wide range of thicknesses, flaw shapes, alloys, and stress loads. These ranges were:

a. maximum failing stresses of about 0.90 σ_{ys}
b. minimum thickness of about 0.25 $(K_{IE}/\sigma_{ys})^2$;
c. ligament length greater than about 0.10 $(K_{IE}/\sigma_{ys})^2$

For ligaments less than this value, prior to failure leakage occurred. The final fracture strength was dependent on flaw length and the appropriate through-crack toughness.

The primary emphasis of these initial studies (2, 8) was on the fracture and cyclic flaw growth behavior of aluminum and titanium base metal specimens. These studies had established that significant surface flaw crack growth can occur during loading and had also determined the range of applicability of the available stress intensity solutions in determining the fracture stress/flaw size loci.

The mechanical properties of as-welded 2219 welds are significantly different from the T87 base metal properties. The program reported in reference 10 was conducted to evaluate the weldment flaw growth characteristics of both 2219-T87 aluminum and 6Al-4V STA titanium weldments. Tests were conducted both at room and cryogenic temperatures and on several thicknesses. K_{IE} values (gross stress levels less than yield) were obtained only on the thicker gage-lower temperature combinations of the titanium specimens. Leakage occurred on several of the titanium tests and substantiated the ligament restrictions developed in reference 8. Validity of the ligament restriction could not be evaluated on the aluminum weldment tests because the surface flaw toughness could not be measured in the thicknesses of interest. As expected, fracture prior to leakage was not observed except with small flaws which caused fracture well in excess of the weld metal yield strength.

Cyclic tests on both proof loaded and non-proof loaded specimens were conducted under the reference 10 study. Three major observations resulted from the analysis of the cyclic test data:

a. Cyclic lives of proof tested specimens always equalled or exceeded the lives of unproofed specimens. Although significant growth often occurred during the proof loading, the subsequent cyclic growth was retarded due to the proof overload, and the resultant cyclic life was not adversely affected by the initial proof cycle.

b. The cyclic lives of the specimens increased with increasing initial flaw shape ratio (a/2c). For specimens loaded to equal percentages of their failure (leakage) load at proof, the stress intensity associated with the subsequent cyclic loading is less for the

rounder flaws; therefore, the growth rate will be less and their subsequent cyclic life greater.

c. In tests of several dozen specimens which were proof tested to incipient leakage, measurable subsequent cyclic life (at stresses of 85 percent of the proof stress) was realized. Results from static failure tests were used to determine the maximum proof stress which would be applied without causing leakage. This result was significant in that it indicated that safe life can be assured by proof testing of thin walled tankage fabricated from high toughness materials.

Reference 11 was a comprehensive study of the stable flaw growth during loading and post proof test cyclic lives of deep surface flaws in 2219-T87 aluminum, both base and weld metal. The objective of this study was to determine proof testing procedures which would guarantee a minimum service life capability subsequent to proof test. Three gage thicknesses of both base and weld metal specimens were tested at temperatures ranging from room temperature to 20 K (-423°F). The post-proof test cyclic life capability of nearly 100 specimens, all of which had been subjected to a proof test which would maximize the stable proof test flaw growth, leaving the specimen in an incipient penetration mode, were evaluated. The incipient penetration condition was established by crack opening displacement gage instrumentation and prior static tests.. The major conclusion of this study was that a proof test could be used to assure, not absolutely but with a very high degree of confidence,a subsequent cyclic life capability.

The key observations of the preceding discussion are:

- The failure stress-flaw size locus for surface flaw specimens can be divided into three regions,
  - Region I - inelastic range ($\sigma \geq 0.90\sigma_{ys}$)
  - Region II - elastic fracture
  - Region III - leakage prior to fracture.

- A complete description of the failure locus in Region I is not yet available; however, it appears that the failure locus lies along a relatively straight line extending from ultimate strength at zero flaw size to the point at about 0.90 σ_{ys}, where Region II begins.

- Region II can be described using available surface flaw stress intensity solutions (which account for a/t effects) up to the point where the initial ligament (t-a) is less than about 0.10 $(K_{IE}/\sigma_{ys})^2$, whereupon Region III begins.

- Final fracture in Region III is preceded by leakage and can be described by consideration of original surface flaw length and the through-crack toughness, K_{CN}, of the material.

- Limited data available suggests that resistance curve techniques may be a powerful tool for describing both the leakage and fracture type failures of surface flaw specimens.

- Flaw growth "damage" occurring during proof testing appears to be compensated for by subsequent retarded flaw growth rates.

- For equally critical (i.e. loaded to an equal percent of their failure load) long and short flaws surviving a given proof cycle, the long flaw has the shortest subsequent cyclic life.

- A proof test to assure with a very high degree of reliability a subsequent cyclic life of a thin-walled pressure vessel.

The above points had a very significant influence on the design of the experimental program reported herein. The Region III leakage failure prediction remains uncertain and is a major objective of the program reported herein. The subject program was a follow-on to the reference 11 study and draws heavily on the results of that program in the analysis of the data and the expansion or modification of the above points. These discussions are presented in Section 5 of the report, "Discussion of Results."

3.0 DEFINITIONS AND TERMINOLOGY

It has been established by numerous investigators that significant stable crack growth can occur prior to catastrophic failure. Crack growth resistance curves have been used in attempts to better understand this phenomenon and establish the true instability points and associated fracture toughness values for materials.

For structural application, the initial flaw size will be established either by proof testing or non-destructive testing (NDT) procedures and the flaw growth associated with the design service life requirements will be incorporated. The service life will be the time required to grow the initial defect to the size which will produce failure at limit load. The limit load stress in conjunction with the flaw size at the start of limit load application will establish the failure condition. Service failure is not limited to the catastrophic fracture mode but can be leakage for some applications, such as pressure vessels.

The objective of this study was the development of proof testing procedures for thin walled pressure vessels and the investigation of the stable crack growth behavior of both surface flaws and through cracks. The failure mode for the pressure vessels (surface flaws) could be by leakage or fracture whereas, the center crack panel would fracture. The stress intensity concept is used in developing the proof testing procedures and also in evaluation of the stable flaw growth behavior. A list of symbols denoting the stress intensity synonymous with numerous events are listed below together with a brief explanation.

K_{CN} - The toughness calculated from equation 3 using the initial crack length in conjunction with the maximum load. General stable crack growth precedes failure, therefore, this is a measure of the minimum stress intensity present at failure.

K_C - The fracture toughness as determined by tests of center crack panels using equation 3 in conjunction with the maximum load

and crack length (i.e. the crack length at the tangency of the resistance and driving curve).

K_{ICG} - The stress intensity at the initiation of crack growth in center crack panels. Calculated using equation 3 in conjunction with initial crack length and stress which initiated stable crack growth determined by crack propagation gages.

K_{Ii} - The stress intensity calculated from equation 2 using the initial flaw dimensions and the maximum stress.

K_{CR} - The stress intensity calculated from equation 2 using the initial flaw dimensions and the stress at failure either by breakthrough or catastrophic failure.

K_{IE} - Apparent fracture toughness as determined by test of surface flaw specimens whose failure mode was fracture using maximum stress and initial flaw dimensions in conjunction with equation 2.

The stress intensity concept is a powerful tool for analyzing the behavior of flaws; an actual stress intensity can only be calculated if the state of stress and the flaw dimensions are known. The inability of NDT techniques to reliably establish the size of pre-existing flaws necessitated the development of quantitative interpretations of proof testing procedures. The use of the stress intensity concept in the determination of required proof to operating stress ratio requires an assumption of initial flaw size. Since proof testing is meant only to assure a minimum service life potential, the initial flaw size assumed is the maximum which could exist without causing failure during proof testing. The successful completion of a proof test establishes the maximum initial flaw size. For the pressure vessels whose failure mode at proof is leakage, the post proof test flaw size is not known. Rather than trying to establish the maximum flaw size after proof and use that as the starting point for the crack growth during operational loading, all of the cyclic tests in this program were conducted after a simulated proof test was applied and the original (prior to proof test) flaw dimensions were used in all of the subsequent stress intensity calculations for the surface flaw specimens.

4.0 MATERIALS AND PROCEDURES

The materials and experimental procedures are described in this section. ASTM standard mechanical property tests were conducted on the materials; results of these tests are discussed in Section 5.0. A detailed description of material composition and heat treat procedures follow in Section 4.1. Details of specimen preparation and experimental approaches are included in Section 4.2.

4.1 Materials

All of the specimens were fabricated from either 2219-T87 aluminum or 6Al-4V STA titanium. The aluminum material was originally purchased for NASA CR-134679 (Effect of Thermal Profile on Cyclic Flaw Growth in Aluminum), and subsequently used on NASA CR-135036 (Proof Test Criteria for Thin-Walled 2219 Aluminum Pressure Vessel) and the subject program NAS3-19697 (Analysis and Test of Deep Flaws in Thin Walled Vessels.) The sheet material 6.35 x 1219 x 2438 mm (0.25 x 48 x 96 inch) was purchased per Boeing Specification BMS7-105C (equivalent to Military Specification MIL-A-8920A). The chemical composition of the material as required by the specification and as measured for NASA CR-134679 is presented in Table 1.

The 6Al-4V titanium material was purchased in Sheet form 6.35 x 914 x 2134 mm (0.25 x 36 x 84 inch) per Military Specification MIL-T-9046F, Type III, Condition C (annealed condition). The chemical composition of the material as required by the specification and as certified by the supplier (Reactive Metals, Inc.) is presented in Table 1.

The 2219 aluminum was purchased in the T87 condition, the 6Al-4V titanium was purchased in the annealed condition and heat treated to the STA condition. The heat cycle selected for the titanium was identical to that employed in NASA CR-134587, "Fracture Characteristics of Structural Aerospace Alloy Containing Deep Surface Flaws":

a. Solution Treat at 1227K (1750°F) for 30 minutes
b. Water quench with 6 second maximum delay
c. Age at 769K (925°F) for 8 hours.

The quench cycle produced some distortion, most of which was eliminated by aging the parts while they were clamped flat. The remaining distortion was eliminated by machining away excess material.

4.2 Procedures

Procedures used for specimen preparation and testing are described in this section. The specimen preparation section (4.2.1) covers the details of flaw preparation and specimen fabrication. Details applicable to the testing of specimens are covered in Section 4.2.2, Test Procedures.

4.2.1 Specimen Preparation

All of the specimens were prepared using conventional machining procedures. The detailed specimen configurations are presented in Figures 1 through 4. All specimen blanks were removed from the parent sheet material so that loading would be applied parallel to the long transverse direction of the material.

Fatigue crack starter slots were introduced into both the surface flawed and center crack panel specimens by electric discharge machining. The electrodes used in the electric discharge machining were fabricated from 1.5 mm (0.06 inch) thick Packanite sheet. The starter slots had a maximum of 30 degrees included angle terminated by an 0.08 mm (0.003 inch) root radius. Fatigue cracks were produced at the root of the starter notches by means of tension-tension cyclic fatigue applied at 30 Hz, peak stresses of 69 MN/m^2 (10 ksi) to 110 MN/m^2 (16 ksi) were used to precrack the titanium center crack panels, and a maximum stress range of 41 MN/m^2 (6 ksi) to 69 MN/m^2 (10 ksi) was used for the aluminum center crack panels. The precracking of the center crack panels was monitored visually with the aid of a 10 power magnifier. The precracking operation was terminated when the desired final crack length had been obtained. Generally 20,000 to 50,000 cycles were sufficient to produce the desired results. The surface flaw specimens were divided into groups which had nominally the same flaw size. All of the specimens within a given group were precracked at the same stress level. For the titanium specimens the stress levels ranged from 207 MN/m^2 (30 ksi) to 276 MN/m^2 (40 ksi) and for the

aluminum specimens the range of stress levels varied from 69 MN/m^2 (10 ksi) to 83 MN/m^2 (12 ksi). The precracking operation was monitored visually with the aid of a 30 power microscope. Generally 10,000 cycles were sufficient to produce the desired precrack for the surface flawed specimens.

4.2.2 Testing

Three different types of tests were conducted during the program (static fracture, load/unload, cyclic). Static fracture tests were performed on all center crack panels and some surface flawed specimens. These tests consisted of monotonically increasing the load until specimen fracture. A loading rate sufficient to produce failure in 1 to 2 minutes was used for all of these tests. The load/unload and cyclic tests were applied exclusively to the surface flawed specimens. The load-unload tests consisted of monotonically increasing the specimen load at a rate which would produce the desired load in approximately one minute and then rapidly unloading the specimen. Cyclic tests were conducted using either a sinusoidal or trapezoidal profile. Cyclic tests conducted at 10 or 3 cpm employed the sinusoidal loading profile, where the 1 cpm tests used a trapezoidal loading profile. The trapezoidal loading profile was equally divided into four 15 second portions (i.e., 15 seconds to load, 15 seconds at load, 15 seconds to unload and 15 seconds at zero load). The minimum load in all the cyclic tests was less than 5 percent of the maximum value.

4.2.3 Environments

All of the testswere conducted at either room temperature or at liquid hydrogen temperature 20K (-423°F). For the liquid hydrogen temperature the specimens were enclosed within a cryostat. The liquid hydrogen level within the cryostat was monitored by means of liquid level sensors. Liquid sensors were located periodically inside the cryostat and coupled to an automatic triggering system to assure maintenance of the desired liquid level. This system had been used to control the liquid hydrogen depth in the cryostat to within 25 mm (1 inch) of the desired level for reference 12. The entire test section

the specimen was submerged in the liquid hydrogen during testing. A minimum soak time of 30 minutes was allowed after filling the cryostat to ensure that the specimen had stabilized at the desired test temperature.

4.2.4 Instrumentation

The center crack panels were instrumented to provide a continuous record of crack opening displacement and crack length. An EDI (Electrical Displacement Instrumentation) clip gage was used in monitoring the crack opening displacement. The gage was either inserted directly into the flaw or attached to brackets which were micro spot welded to the specimen as shown in Figure 5. The EDI gage was connected to an X-Y plotter which produced plots of load versus crack opening displacement. In addition to the load crack opening displacement records, instrumentation for load-crack length determination was also applied to the center crack panels. Crack propagation gages (CPG) (Type TK040CPC03-003) consisting of 20 parallel filaments spaced 2.03 mm (0.08 inch) apart in a 39.6 x 19.1 mm (1.56 x 0.75 inch) frame were used to monitor the crack length. Crack propagation through a filament results in the failure of that filament and an increase in the resistance of the gage. The load-crack length relationship was thereby obtained by recording load versus gage resistance on an X-Y plotter.

The surface flaw specimens were equipped with an EDI gage for monitoring crack opening displacement and pressure cups for detecting breakthrough. The EDI gages were attached to the flaws in the manner described previously (see Figure 5) and load-crack opening displacement records were obtained. Additionally, the surface flawed specimens were instrumented with pressure cups for determination of crack breakthrough. The pressure cup system (see Figure 6) consisted of two cups applied symmetrically on the specimen, one directly over and one directly behind the flaw. The cup over the flaw was pressurized with either nitrogen or helium gas and the pressure in the rear cup was monitored. Breakthrough was denoted by an abrupt increase in pressure in the rear cup. The rear cup pressure was plotted versus the applied load on an X-Y plotter, thereby providing a permanent record for determination of breakthrough load. For cryogenic tests the rear cup was vented immediately prior to testing to relieve any partial vacuum which might

have been produced by the cool-down cycle. During fracture or load-unload testing, both the crack opening displacement and rear cup pressure were recorded versus load, however, for cyclic tests the crack opening displacement was recorded on a strip chart recorder as was the rear cup pressure.

4.2.5 Flaw Size Determination

All of the flaw sizes presented in the tables were measured directly from the fracture faces of the specimens. The measurements were made visually with the aid of a 30 power microscope and polarized light. A load sequencing procedure designed to produce visible bands of growth for each load-unload or cyclic loading was used throughout the experimental portion of the program. The load sequencing procedure was successful in producing visible bands for each loading segment, therefore, the crack size measurements were made directly from the fracture faces. The crack opening displacement records were used as guidelines and provided further substantiation of the visual measurements.

4.3 Stress Intensity Solutions

Surface Flawed Specimens

The surface flaw stress intensity values reported in the tables were calculated using the Irwin Surface Flaw Equation presented in reference 1, modified by the deep flaw magnification term presented in Figure 58 of reference 2. The resulting equation is:

$$K_I = 1.1\ (\pi\ a/Q)^{1/2}\ M_K\sigma \qquad (2)$$

See the list of Symbols for definition of the terms and Figures 7 and 8 for values of Q and M_K.

Center Crack Panel Stress Intensity

The stress intensity values presented for the center crack panels were calculated using the following formula:

$$K = Y \frac{P(c)^{1/2}}{B W} \qquad (3)$$

See the list of Symbols for definition of the terms and Figure 9 (from reference 13) for values of Y.

5.0 RESULTS AND DISCUSSION

5.1 Mechanical Property Tests

The tensile properties, of the 2219-T87 aluminum and 6A-4V STA titanium are presented in Tables 2 through 4. The aluminum alloy was tested at 295K (72^{o}F) and 20K (-423^{o}F), the titanium alloy at 295K (72^{o}F), only. The effects of temperature on yield strength, ultimate strength, elongation and Poisson's Ratio are presented in Figures 10 and 11. The uniaxial yield strength values presented were calculated using the 0.2% offset method for a 50.8 mm (2.0 inch) gage length.

Poisson's Ratio was determined from continuous strain gage recording of both longitudinal (ε_L) and transverse strain (ε_T). The elastic Poisson's ratios were then calculated using the following formula:

$$\mu = \frac{d\varepsilon_T}{dP} \div \frac{d\varepsilon_L}{dP} \qquad (4)$$

where μ is Poisson's Ratio and P is the load.

5.2 Center Crack Panel Tests

Results of all of the center crack panel tests are presented and discussed in this section. The discussion is separated by alloy, the aluminum being first followed by the titanium results.

5.2.1 2219-T87 Aluminum Center Crack Panel Tests

Static fracture tests were conducted on the aluminum alloy panels at both room temperature and 20K (-423^{o}F). All specimens were monotonically loaded at a rate which produced failure in approximately 1 minute. The results have been summarized and are presented in Tables 5 through 8. All of the specimens were instrumentated with both crack opening displacement (COD) and crack propagation gages (CPG).

The relationship between initial crack length and gross area failure stress are presented in Figures 12 and 13. Curves of constant toughness (K_{CN}) calculated from the initial crack length and maximum gross area stress have been passed through the data. K_{CN} values of 68 MN/m$^{3/2}$ (62 ksi $\sqrt{in}$) and 86 MN/m$^{3/2}$ (78 ksi $\sqrt{in}$) correlate the data for the room temperature and 20K (-423^{o}F) results, respectively. The data fall within 10 percent of the K_{CN} lines presented in Figures 12 and 13, except when the net section failure stress exceeds 80% of yield. The net section stresses are calculated on the basis of initial crack length. The apparent reduction in K_{CN} value at the high stress levels ($\sigma_{net} > 0.80\ \sigma_{ys}$) is normal for this type of testing. Specimen thickness did not significantly influence the test results. At room temperature the thinnest gage consistently failed at a slightly lower stress than the thicker gages. This trend, however, was reversed for the liquid hydrogen temperature tests. Buckling restraints were applied to all of the thinner gage specimens to prevent local buckling at the crack tip from significantly influencing the failure stresses. Although general buckling can be easily prevented, it is difficult to eliminate totally all buckling at the crack tip. For specimens which are instrumented with CPG gages the problem is compounded because the application of any force directly on the gage could cause erroneous gage output. The panels were therefore restrained in such a manner that generalized buckling would not occur, but very localized buckling at the crack tip was possible. Buckling would tend to reduce the apparent toughness of the material. Toughness is generally considered to increase with decreasing thickness because of the failure mode change from plane strain to plane stress; the former producing flat fracture faces while the latter is characterized by a shear type fracture face. For the 2219-T87 aluminum, however, applying the criteria

$$t \geq 2.5\ (K_{Ic}/\sigma_{ys})^2 \qquad (5)$$

for determining the required thickness to produce flat fracture conditions a gage thickness in excess of 40 mm (1.6 inch) would be required to produce flat fracture. Since the gages tested ranged from 0.64 to 4.77 mm (0.025 to 0.188 inches) the expected failure mode would be a shear type for all specimens. A review of the fracture faces of the specimen reveals a

predominance of shear, especially for the room temperature tests. Reference 11 tested 2219-T87 aluminum base metal center crack panels in thicknesses of 3.18, 6.35 and 9.53 mm (0.125, 0.250 and 0.375 inches). A K_{CN} value of 68 $MN/m^{3/2}$ (62 ksi $\sqrt{in}$) correlated the data within a plus or minus 10% scatter band. For room temperature tests of 2219-T87 aluminum base metal center crack panels a K_{CN} of 68 $MN/m^{3/2}$ (62 ksi $\sqrt{in}$) can be used to correlate the data for thicknesses up to 9.53 mm (0.375 inch) within a plus or minus 10% scatter band.

Decreasing temperature from 295K (72°F) to 20K (-423°F) generally increases the K_{CN} of the 2219-T87 aluminum alloy. This was found to be the case for the center cracked panels tested for this program. A limited number of tests were conducted and half of those conducted failed at high net section stresses. The remaining specimens exhibit a K_{CN} of 86 $MN/m^{3/2}$ (78 ksi $\sqrt{in}$). This increase of 25 percent over the room temperature K_{CN} value is an abnormally high increase in toughness. An increase in toughness of 10 percent is more typical; however, due to the very limited number of tests conducted, the high value is probably a consequence of data scatter. If the K_{CN} values of the three specimens having the largest flaws are averaged with the K_{CN} values of reference 11 for specimens machined from the same lot of material and tested at 20K (-423°F),a value of 83.0 $MN/m^{3/2}$ (75.6 ksi $\sqrt{in}$) is obtained. The five specimens, three from this program and two from reference 11, were all machined from the same lot of material to the same planform configuration, thickness being the only variable. Also, the initial flaw lengths of the five specimens were all within 1 percent of each other. The effect of thickness on K_{CN} for these specimens is presented in Figure 14. Although the spread between the maximum and minimum values is only 27 percent, it does appear that the thickness did have an influence on K_{CN} since it is the only variable. At room temperature the thickness did not significantly influence the measured K_{CN} value. The average room temperature K_{CN} values, calculated from the specimens that failed at net section stress below 80% of yield, are presented in Figure 14. Examination of the fracture faces of the specimens revealed a shift in failure mode from shear to mixed mode (both flat and shear) for the liquid hydrogen tests, but no change for the

room temperature tests. Although the fracture faces of the thinnest liquid hydrogen specimens were all shear, the thickest specimens exhibit a significant amount of flat fracture, indicative of a mixed mode failure. The fracture faces of the room temperature specimens were almost totally shear for the range of thickness being considered (0.64 mm (0.025 inch) to 6.35 mm (0.25 inch).

All of the center crack panels were instrumented with crack propagation gages, the outputs of which have been used in constructing the plots of applied load versus crack length presented in Figures 15 through 18. These results have been used further to calculate the crack growth resistance curves presented in Figures 19 through 23. The maximum crack length shown and the corresponding load or stress intensity represents the minimum crack length at maximum load. That is, there was not any discernible increase in applied load after the reported crack length was obtained; the crack growth resistance curve was therefore tangent to the stress intensity or driving curve at that point. From Figures 19 through 23 the K_c values can be determined which will be the end point of the resistance curves. The effect of thickness on K_c is presented in Figure 24. K_c is calculated using the maximum gross area stress and the minimum crack length at maximum stress. Data taken from reference 11 has also been included in Figure 23. At 20K (-423^{o}F) thickness did influence the measured K_c values, however there wasn't any influence of thickness on the measured K_c values at room temperature. The effect of temperature and thickness on measured K_c values is consistent with that found on K_{CN} values (Figure 14).

Plots of the stress at initiation of crack growth versus initial crack length are presented in Figures 25 and 26. Initiation of crack growth was determined from the CPG gages and was considered to be the point at which the first gage wire broke. The gages were mounted on the panels such that the centerline of the first wire was 2.03 mm (0.80 inch) from the end of the crack tip. The initiation of crack growth therefore corresponds to a discernible increase in crack length. A reasonable approximation of the stress at the initiation of crack growth can be made if a K_{ICG} of 53 MN/m$^{3/2}$ (48 ksi $\sqrt{in}$) and 58 MN/m$^{3/2}$ (53 ksi $\sqrt{in}$) are used for the room temperature and 20K (-423^{o}F) test results,

respectively. Although the room temperature K value for initiation of crack growth is equal to the values measured in reference 11, the 20K ($-423^{o}F$) value is somewhat higher. The thickness tested in this program was generally less than in reference 11, therefore the increase in K_{ICG} at the initiation of crack growth for the liquid hydrogen tests was probably a result of the increased toughness of the thinner material gages. The stress intensity values at which crack growth initiated was relatively constant for the range of initial flaw lengths tested. Most of the specimens experienced crack growth at net section stress levels below 80 percent of yield.

A plot of initial crack length versus critical crack length is presented in Figure 27. Neither thickness nor test temperature significantly influenced the relationship between the initial and final crack lengths. Knowing the initial crack length,a reasonable approximation of the critical crack length can be calculated from

$$(2C)_{cr} = 1.24\ (2C_i) + B \qquad (6)$$

where

$$B = 14.7 \text{ mm } (0.58 \text{ inch})$$

Equation 6 can also be used in conjunction with Equation 3 to calculate K_c directly. The resulting equation would be:

$$K_c = Y\sigma\sqrt{1.24\ C_i + B/2} \qquad (7)$$

Y = determined from Figure 9 and

$$2c/_W = \frac{2(1.24)\ C_i + B}{W} \qquad (8)$$

All of the test data presented and the instrumentation records obtained indicated that for 2219-T87 aluminum center crack panels crack growth initiates at a stress intensity level significently below critical and the crack propagation continues at an increasingly higher velocity until fracture. During the failure process the load must be continually increased until the

point at which the crack growth resistance curve becomes tangent to the driving curve; thereafter a further increase in load is not required to perpetuate failure.

The results of the 2219-T87 aluminum center crack panel tests can be summarized as follows:

- Over the range of thicknesses tested at room temperature the measured K_{CN} and K_c values were insensitive to thickness. (Figures 14 and 24.)

- At liquid hydrogen temperature the range of thickness did influence both the measured K_{CN} and K_c values. Both K_{CN} and K_c were found to increase with decreasing thickness. (Figures 14 and 24.)

- Failure stresses can be predicted within 10% for specimens which fail at net section stresses below 80 percent of yield if the appropriate K_{CN} value is considered. (Figures 12 and 13.)

- All of the specimens experience significant crack growth prior to failure. The failure process can be divided into two distinct regions; the first requires an increase in load to create an increase in crack length, the second region does not require any increase in load to produce crack growth. The dividing point between the regions is defined by the point at which the crack growth resistance and driving curves become tangent.

- The stable crack growth experienced in the first region is insensitive to both temperature and thickness, but is dependent on initial crack length.

5.2.2. 6Al-4V STA Titanium Center Crack Panel Tests

Static fracture tests were conducted on nine 6Al-4V STA titanium center crack panels at room temperature. The results of these tests have been summarized

and are presented in Table 9. A plot of gross area failure stress versus initial crack length is presented in Figure 28. All of the specimens failed at net section stress significantly below 80 percent yield, therefore the results were not influenced by yielding to the same extent as the aluminum results. K_{CN} values of 72 $MN/m^{3/2}$, 80 $MN/m^{3/2}$ and 92 $MH/m^{3/2}$ (66 ksi $\sqrt{in}$, 73 ksi $\sqrt{in}$ and 84 ksi $\sqrt{in}$) provide reasonable prediction of the failure stesses for the 3.18 mm, 2.03 mm and 1.02 mm (0.125 in, 0.080 in., and 0.040 in.) thick specimens, respectively. Inspection of the fracture faces of the specimen shows the thinnest gage to have failed in shear, all other gages had areas of flat fracture. Using the 72 $MN/m^{3/2}$ (66 ksi $\sqrt{in}$) toughness obtained from the 3.18 mm (0.125 inch) thick specimen and the yield strength reported in Table 4 a thickness of 12 mm (0.47 inch) was required for flat fracture (minimum toughness) conditions (using Equation 5). Since the thickness rangedfrom 10 to 30 percent of that required to produce flat fracture conditions, and the fracture faces indicate a transition from full shear to mixed mode, the variation in measured K_{CN} is as would be anticipated.

The results obtained from the crack propagation gages were summarized and presented in Figure 29 as a plot of gross area stress versus crack length. Further, the data was reduced to stress intensity versus crack length, presented in Figure 30. The final crack length for each specimen presented in Figures 29 and 30 corresponded to the minimum crack length at maximum load. That is, after obtaining the crack length presented, no further increase in load was required to produce additional crack propagation. The final crack lengths presented were therefore synonymous with the crack growth resistance and driving curves being tangent. K_c values can be obtained directly from Figure 30. There was significant variability in the measure K_c values present in Figure 30. There was also considerable variation in the amounts of stable crack growth that occurred prior to failure. Figure 31 presents a summary of the titanium center crack panel K_{CN} data. Although the average K_{CN} values obtained from the specimens were inversely proportional to thickness there was overlap in K_{CN} values between gage thickness. Rather than consider the overall amount of flat fracture as compared to shear fracture, the amount of flat fracture at the crack length corresponding to the resistance and driving curves becoming tangent could lend some insight into the variations in measured K_c. The ratio of shear to total area at

the critical crack length was measured for the individual specimens and presented in Figure 32 in terms of measure K_c versus percent shear fracture. There is a very definite trend to the data; the greater the amount of shear the greater the apparent K_c. All of the 1.01 mm (0.040 in.) chick specimens failed under pure shear and correspondingly they had the highest K_c values. The other gages failed with varying amounts of shear. The greatest spread in both K_c and percent of shear fracture was for the 2.03 mm (0.080 in.) thick specimens.

Since the specimens were all cut from the same piece of material,the variation in the results should not be relatable to chemistry. Prior to machining,all of the specimen blanks were heat treated in their nominal plate thickness. The solution treat and quench portion of the heat treatment cycle was performed individually on each blank. All of the parts were heat treated per the BMS specifications, however, there was a variation in individual quench times. A maximum quench delay of 6 seconds is allowed by the BMS specification. Controlling mechanical properties is the major function of the heat treatment specifications. A maximum quench delay of 6 seconds is indicative of a material which is quench critical (e.g. a material whose properties depend critically on the quench step). Fracture properties may be even more sensitive to quench delays than are the mechanical properties. Reference 14 has shown that the microstructure can be made to vary significantly through the thickness of 25 mm (1.0 in.) 6Al-4V titanium plate by heat treatment. The most probable cause of the disparity in the K_c values is the specimen to specimen variation in quench time. This non-uniformity in fracture properties can be anticipated in large structures fabricated from the subject alloy since there will be significant variations in quench times for structural elements of varying thickness. The impact of variability on developing proof testing procedures for 6Al-4V titanium tank pressure vessels is discussed in a later section of this report.

A plot of stress at the initiation of crack growth versus initial crack length is presented in Figure 33. The crack propagation gages which were used in the determination of crack length were mounted with the first strand approximately 2.03 mm (0.080 inch) from the crack tip; the initiation of crack growth corresponds to the failure of the first wire of the gage. The stress intensity required to initiate crack growth was inversely proportional to the specimen thickness (Figure 34). The consistency of the results presented in Figure 33

is somewhat surprising considering the variation in K_{CN} and K_c values previously discussed. Indeed the best ordered set of data, the 2.03 mm (0.080 inch) thick specimen results, offered the greatest variation in the K_{CN} and K_c calculations. K_{CN} and K_c are both related to failure stress and failure stress for these specimens was not directly dependent on the stress at which crack growth initiated. The measured K_c values are dependent upon the amount of stable crack growth the specimen can tolerate prior to becoming critical. A comparison of initial and critical crack length for the titanium specimen is presented in Figure 35 although there was a consistent relationship between initial and critical crack lengths for the aluminum center crack panels, there was considerable variability in the titanium results. The specimens which were capable of withstanding a greater percentage of crack growth exhibited higher K_c values (see Figure 36).

The results of the room temperature 6Al-4V STA titanium center crack panel tests can be summarized as follows:

- K_{CN} values based on maximum gross area stress and initial crack length can be used to predict failure stresses. Decreasing thickness will increase the K_{CN} values required to cause failure.

- For the range of thicknesses and flaw sizes tested, the stress intensity required to initiate crack growth was consistent within a gage thickness but decreased as thickness increased.

- The amount of stable growth a specimen could tolerate was not relatable to its thickness. It was, however, influenced by the toughness (K_c) of the specimen.

- There was a definite relationship between measured K_c and the percentage of flat fracture at the critical crack length.

5.3 Surface Flaw Specimen Tests

The results of the surface flaw specimen tests are presented in this section. Individual discussions are presented for each alloy and test type conducted. The two alloys tested were 2219-T87 aluminum and 6Al-4V STA titanium, base

metal only. Tests were conducted to determine the stable flaw growth characteristics during loading, the parameters controlling thickness penetration prior to fracture and the post proof test cyclic life. The aluminum alloy results are presented first.

5.3.1 2219-T87 Aluminum Growth-on-Loading Tests

The results of the aluminum growth on loading tests have been summarized and are presented in Tables 10 through 21 and Figures 37 through 40. The growth on loading tests were conducted on three different flaw shapes and thicknesses at room temperature and on three thicknesses, but only one flaw shape at 20K (-423°F).

The flaw sizes were selected so that the typical failure loads would correspond to 90 percent of the material's minimum yield strength at the test temperature. Ninety percent of yield is a commonly used proof pressure for spacecraft pressure vessels, and therefore was selected as the test stress. The flaw sizes were selected after a review of available literature (8, 11) had been made. The targeted failure stress was 310 MN/m^2 (45 ksi) for the room temperature tests and 407 MN/m^2 (59 ksi) for the liquid hydrogen temperature tests. Generally, the actual failure stresses were within 10 percent of the targeted values; and, deviations from the selected flaw sizes were not made. For all of the combinations of thickness-temperature-flaw size the failure mode was leakage, except for the 4.77 mm (0.188 inch) a/2c = 0.15 specimens at 20K (-423°F). The flaw shapes selected for the room temperature testing were a/2c = 0.15, 0.30 and 0.45 for the 4.77 and 1.91 mm (0.188 and 0.075 inch) thickness specimens and a/2c = 0.05, 0.15 and 0.30 for the 0.64 mm (0.025 imch) thick specimens. An a/2c of 0.05 was substituted for the 0.45 for the thinnest gage because it was difficult to get a half-circle defect in this gage. Only one flaw shape was scheduled at 20K (-423°F), therefore, an a/2c = 0.15 was used because it proved to be the most severe case for the thicker gages.

The test data is presented in terms of applied gross area stress versus flaw depth in Figures 37 thorugh 40. Individual plots for each thickness-flaw shape-temperature combination are presented. Initial flaw depths are denoted by open symbols and final flaw depths are represented by the closed symbols.

A single open symbol is used when no discernible crack growth was evident on the fracture face. The data is being presented in terms of flaw depth not only because stress intensity is more dependent on crack depth than other crack dimensions but also because the objective of this portion of the program is to characterize the flaw growth behavior which can cause a pressure vessel containing a surface flaw to reach an incipient wall penetration condition after proof testing. Variations in flaw length were generally restricted to the higher aspect ratio flaws and were less frequent than variation in crack depth. A discussion of the variation in crack length will be presented later. Although there is considerable scatter in the data, there are several observations that can be made which are worth noting.

The results of the room temperature 4.77 and 1.91 (0.188 and 0.075 inch) thick specimens are discussed followed by the results of the 0.64 mm (0.025 inch) thick room temperature tests. The discussion has been divided because of testing problems encountered with the thinnest gage specimens. In all of the thicker gage tests (Figures 36 and 37) flaw growth initiated at stress levels significantly below the failure stress levels. After initiation, flaw growth continued until breakthrough. The loading was applied at constant rate, and the crack growth initiated and continued at increasing velocity to failure. As the load approached the failure load, there was a rapid increase in the crack tip velocity. There was no reason to believe, either from the data presented in these figures or the crack opening displacement records presented in Volume II of this report, that there was an instability associated with the breakthrough phenomenon.

From Figure 41 (which is Figure 37 of reference 11) it can be seen that for a given increment of load the associated increment of crack growth increases as failure is approached. Since all of the tests were conducted at a constant loading rate, the crack tip velocity versus stress intensity relationship would be as schematically presented in Figure 42. Prior to the crack tip velocity becoming asymptotic to the stress intensity line, a failure by ligament penetration will occur. When the material thickness is sufficient to allow the crack tip velocity to become asymptotic to the stress intensity line, a catastrophic failure occurs. Regardless of failure mode, a significant amount of stable flaw growth will be encountered prior to failure. Figure 43 presents the relationship between K_{cR} and thickness for 2219-T87 aluminum base

metal. K_{cR} was calculated from equation 2 using the initial flaw size and the gross area stress at either fracture or breakthrough. The figure demonstrates that it is possible to have failure by leakage in the range of stress intensity where failure by fracture is expected. The failure process appears to be one of stable crack growth at an increasing velocity (for constant loading) until the flaw has either penetrated the rear surface or attained sufficient velocity to cause fracture.

To develop the resistance curves, a stress-flaw size relationship must be established. The data presented in Figures 37 and 38 was used to develop the stress-flaw size relationship presented in Figure 44. Resistance curves have been derived from the data presented in Figure 44 and are presented in Figures 45 and 46. Equation 2 was used in calculating the stress intensity values; the deep flaw magnification term presented in Figure 8 was truncated at an a/t of 0.90. Although there are several deep flaw magnification factors available (References 2, 3, and 4) which adequately correlate the data from specimens which failed at elastic stress levels and had flaws which were less than 80 percent deep, the data being considered here does not fall in this range of flaw depths. The shallowest initial flaws are 80 percent deep and all of the final flaw depths are equal to the specimen thickness.

It has been established (6, 10, 11) that plastic deformation extending completely through the ligament occurs prior to failure of deep surface flaws. For the cases being considered, the ligament was plastically deformed during the failure process; therefore, perhaps an elastic deep flaw magnification term should not be included in the calculation of the stress intensity factor. In Figures 47 and 48, the resistance curves are again presented; however, the stress intensity calculations did not include the deep flaw magnification corection (M_K) presented in Figure 8. Although the initial flaw depth to thickness ratios (a/t's) did vary slightly with flaw shape, for a given thickness, all of the failures are by leakage; therefore, the final a/t in all cases was equal to one. At failure (i.e., leakage) the variations in the M_K correction term was a consequence of the flaw shape variations only. It is apparent from Figures 45 and 46 that the modified Irwin surface flaw stress intensity equation (i.e., Equation 2) was inadequate for correlating the data.

The elimination of the deep flaw magnification term in the stress intensity formulation does help in the correlation of the data as can be seen in Figures 47 and 48. Although the data correlation was greatly improved, there is still a systematic effect of flaw shape on the calculated critical stress intensity. Additionally, the gage thickness significantly influences the critical stress intensity values obtained, the critical values obtained for the 1.91 mm (0.075 inch) thick specimens are typically 65 percent of the values obtained for the 4.77 mm (0.188 inch) thick specimen of the same flaw shape (a/2c). It has been established (2, 8) that Equation 2 can be used to correlate failure data when the specimen thickness is sufficient to produce a failure by fracture. From Figure 43 it is apparent that the minimum required thickness is somewhat dependent upon flaw shape. Equation 2, with any of a number of M_K correction terms (2, 3, 4), can be used to correlate fracture data when specimens are sufficiently thick. The problem being considered here, i.e., failure by leakage case, is significantly more complex and Equation 2 is not satisfactory for correlating the failure data. Equation 2 does not account for the influence of thickness and it overcompensates for the effect of flaw shape. The major portion of the overcompensation for flaw shape is in the M_K term; however, even the exclusion of this term still leaves a systematic influence of flaw shape on the results. Plotting the data in terms of remaining ligament (t-a) versus thickness (Figure 49), or flaw depth to thickness ratio (a/t) versus flaw shape (a/2c (Figure 50) only verifies the significance of flaw shape on the breakthrough failure mode. The remaining ligament (t-2) (Figure 49) which caused failure was dependent upon both thickness and flaw shape, as well as stress; therefore, it does not simplify the problem to consider this parameter alone. For a given flaw shape and failure stress, the a/t which caused failure by leakage (Figure 50) was somewhat insensitive to variations in thickness. This is in agreement with reference 11 where it was observed that for a given flaw shape, the percentage increase in flaw depth prior to failure was independent of thickness, but dependent upon flaw shape.

The extent of flaw growth that can be encountered prior to failure is presented in Figures 41, 52 and 53 in terms of K_{Ii}/K_{cR} versus percent increase in flaw depth. K_{Ii} and K_{cR} were calculated using Equation 2 in conjunction with the maximum applied stress and the initial flaw size. The K_{cR} used for the calculations were the average values of all the failure points for each thickness--

flaw shape--temperature combination. Either breakthrough or fracture was considered to be a failure. The percent increase in flaw sizes were calculated from the initial flaw depth and the extent of flaw growth that occurred during loading. The percent increase in flaw depth was dependent on initial flaw shape only and was independent of temperature or gage thickness. This is as would be expected from reference 11 and Figure 47. From the figures, it is apparent that an increase in flaw depth of 10 percent or more will only occur very near failure. Presenting the data in terms of K_{Ii}/K_{cR} is a representation of the proximity of failure which minimizes the effects of M_K, a parameter which is of questionable value for these calculations. Since the initial flaw sizes were nearly identical for any given thickness and flaw shape tested the M_K terms in both the numerator and denominator of the K_{Ik}/K_{cR} calculation are self-cancelling. The K_{Ii}/K_{cR} terms are very nearly equal to the σ_i/σ_{cR} but were selected for correlating the data because K accounts for the minor differences in initial flaw size.

A plot of K_{Ii}/K_{cR} versus percent increase in flaw depth is presented in Figure 54 for the thinnest gage aluminum specimens tested (0.64 mm (0.025 inch)). The results from these tests were similar in all cases to the thicker specimen results. The data scatter was slightly more severe due to the problems associated with introducing flaws which were within 0.13 mm (0.005 inch) of the rear surface. For all of the gages tested, there was considerable scatter in the results. The lack of specimen to specimen repeatability, however, was not surprising for this type of testing. The emphasis of this portion of the program was to determine the parameters controlling stable flaw growth for specimens subjected to incipient failure. Micro delaminations, grain boundary positions, local microstructural variations could all have had a significant impact on the results. None of the previously mentioned parameters would be revealed when the fracture faces were viewed with a microscope, nor could anything be done to circumvent them during testing. Considerable specimen to specimen scatter was therefore inherent in this type of testing and the degree of scatter could be expected to increase as test gages decrease. For the 0.64 mm (0.025 inch) thick specimen, the only flaw shapes which experienced flaw growth prior to failure were the $a/2c = 0.05$ and 0.15. The behavior of the thinnest gage specimens were similar in all respects to the heavier gages.

The specimen thickness had a significant influence on the stress intensity at which stable flaw growth initiated. From the data developed in reference 11, it appears that stable flaw growth initiated at stress intensity factors approximately 70 percent of the critical value. The stress intensity factor at 70 percent of critical for the thickest specimen (of reference 11) was greater than the maximum stress intensity factor which can be obtained in the thinnest specimen. Therefore, if the specimen thickness did not influence the flaw growth during loading behavior, it would be impossible to have a failure by leakage in the thinnest gage specimen.

The most significant observations made so far in the discussion of the stable crack growth during loading phenomenon can be summarized as:

- Crack growth during loading is a stable process which will only occur under increasing load.

- The critical stress intensity at breakthrough is dependent upon specimen thickness and flaw shape.

- Inclusion of the deep flaw magnification term of reference 2 in the stress intensity formula results in a greater variation in calculated critical stress intensity at breakthrough, than if it is excluded in the calculation.

- For a given flaw shape, the initial flaw depth to thickness ratio which will cause failure by leakage is independent of specimen thickness.

- The stress intensity at which stable crack growth initiates during loading is dependent upon specimen thickness and initial flaw shape.

- The flaw shape parameter Q in the stress intensity formula overcompensates for the effect of flaw shape on the critical stress intensity for breakthrough.

- o The crack growth resistance curves do not become tangent to the stress intensity curves prior to the flaw penetrating the thickness.

For thick specimens whose failure mode is fracture, it has been demonstrated that Equation 2, with any of several (2, 3, 4) deep flaw magnification factors, can be used to correlate the data. For these cases, the plastic zones are small with relation to remaining ligaments and the Q and M_K terms adequately account for the effects of flaw shape and a/t. For the case of failure by breakthrough, there is significant plastic deformation and the parameters of Equation 2 are inadequate. Additionally, specimen thickness has a significant influence on the stress intensity at breakthrough and initiation of crack growth.

An empirical modification of Equation 2 could be accomplished which would correlate the breakthrough data. Deletion of the M_K term from the equation helps to reduce the data scatter (see Figures 45 through 48); therefore, it would be dropped. Exclusion of the M_K term does not totally alleviate the data scatter within a given thickness. Therefore, a modification of the Q term would be required to further reduce the scatter within a thickness. The influence of thickness must now be accounted for by introduction of a multiplication term which would be empirically derived. The final formula would have the form:

$$K_{BT} = C\ \sigma\ \sqrt{a}\ F\ (a/2c)\ G\ (t) \qquad (9)$$

where F(a/2c) and G(t) are empirically derived correction factors

where $K_{B.T.}$ = Stress Intensity at Breakthrough

C = Constant

a = Flaw depth

F(a/2c) = Flaw shape parameter (empirically derived)

G(t) = Empirical factor to account for thickness

The F(a/2c) term would be somewhat less sensitive to variations in flaw shape than the Q term presented in Figure 7. G(t) would account for thickness and would increase as thickness decreases. It might also be necessary to make G(t) a function of flaw shape if all the data were to be correlated within generally acceptable bounds. The final equation would merely be a reiteration

of the data and its usefulness would be restricted to the parameters tested. The interface of the solution for failure by breakthrough and the solution for failure by fracture (Equation 2) would be cumbersome.

5.3.2 6Al-4V STA Titanium Growth-on-Loading Tests

The results of the titanium growth on loading tests have been summarized and are presented in Tables 22 through 30 and Figures 55, 56 and 57. All of the titanium tests were conducted at room temperature on three thicknesses of material with three different flaw shapes per thickness.

The initial flaw sizes for the titanium specimens were selected to cause failure at 90 percent of the design allowable yield strength of the material. The Boeing Design Manual lists a 1020 MN/m^2 (148 ksi) "B" allowable yield for 6Al-4V STA titanium, therefore, the target failure stress was selected to be 90 percent of this value (918 MN/m^2 (133 ksi)). The flaw sizes selected were based on a data search of 6Al-4V STA titanium fracture properties. Generally, the failure stresses obtained were below the targeted failure stress. Although the titanium test program consisted of 33 surface flaw tests, there were 9 different combinations of specimen thickness and flaw shape. A maximum of 5 specimens were allocated per flaw shape-gage combination, thus, it was not possible to deviate from the pre-selected flaw sizes without severely limiting the number of specimens available for investigating each condition. Additionally, there was considerable variations in failure stress for seemingly identical specimens. The same specimen configuration was used for both the titanium center crack and surface flawed specimens. The variation in failure stress for the surface flawed specimen was synonymous with the variations in toughness of the center cracked panels discussed in Section 4.2.2. The specimen-to-specimen variation in toughness experienced in both the surface flaw and center crack results is probably typical of location variations in pressure vessels made of 6Al-4V STA titanium. The only variable to which the toughness variation can be attributed was quench delay during heat treatment; a variable which will most certainly be encountered in the heat treatment of even moderate sized titanium structure.

A better understanding of the data presented in Figures 55 through 57 and Tables 22 through 30 can be obtained if the crack opening displacement records for the individual specimens are considered. The crack opening displacement records have been reproduced on Figures 58 through 66. The records have been divided in such a manner that all the records for a given thickness and flaw shape are presented on the same figure. It is apparent from the crack opening displacement records that some of the specimens were at an incipient failure condition when unloading occurred. When the crack opening displacement records are considered, it is apparent that those specimens which experienced a significant amount of flaw growth at a stress level significantly below that at which similar specimens failed did so because the toughness of that particular specimen was lower and it was in an incipient failure mode when unloading occurred. Perhaps, a better characterization of the stable crack growth during loading behavior of the alloy can be obtained if a comparison is made between the flaw growth and proximity of failure at unloading.

The crack opening displacement records presented in Figures 58 through 66 were used to estimate the proximity of failure when unloading occurred. The estimated load which would have caused failure was divided into the maximum load and considered to be K_{Ii}/K_{cR}. Unlike the aluminum results where there was not a significant variation in specimen-to-specimen toughness and an average K_{cR} was used for each gage-flaw shape-temperature combination for the titanium, each specimen was treated individually. The percentage flaw growth was determined for each specimen (i.e., the stable crack growth during loading compared to the initial flaw size) and is compared with its K_{Ii}/K_{cR} value in Figures 67, 68, and 69. As with the aluminum data, the growth on loading was a uniform process initiating at a stress intensity significantly below critical and continuing until failure had occurred. The crack tip velocity increased as failure approached, the loading rate was constant; however, there was no point of instability. The lack of an instability point was well demonstrated by the crack opening displacement records of specimens 2TR14-1 and 2TR81-2 (Figures 58 and 59). Specimen 2TR14-1 experienced a 22.7 percent increase in flaw depth during the loading and unloading procedure. From the crack opening displacement records it appears a portion of the crack growth occurred when the applied loading was being decreased. Had the load remained constant, no further increase would have been required to cause failure (of

specimen 2TR14-1) certainly; if the failure process was an instability process, unloading without failure would have been impossible. Specimen 2TR81-2 experienced a 32 percent increase of flaw depth during the loading and unloading process, a portion of which also apparently occurred during decreasing load. The amount of crack growth, if any, that occurred during decreasing load for these two specimens only occurred during the very initial reduction in loading. Since crack growth apparently occurred during decreasing and peak load, it could be inferred that the loading rate could influence failure load. Crack growth during either constant or decreasing load will only occur, however, at loads very nearly the failure point. Therefore, variations in loading rates will not produce any discernible change in failure stress.

The plots of K_{Ii}/K_{cR} versus percent increase in flaw depth presented in figures 67, 68 and 69 are very similar to the aluminum curve presented in previous figures. As with the aluminum results, the crack growth during loading process appears to have been a stable process from initiation to failure. The crack grew at an increasing velocity until failure occurred either by breakthrough or fracture. For specimens of sufficient thickness, the crack tip velocity was of sufficient magnitude that breakthrough and fracture occur simultaneously. A minor variation in toughness can be sufficient to produce a leakage failure rather than a fracture-type failure. An example of this is given in Figure 57. Two of the 1.02 mm (0.040 inch) thick titanium specimens having an $a/2c = 0.15$ failed by fracture, while one failed by breakthrough. The resistance curve for these specimens can be determined from an assumed flaw growth during loading behavior. For the two fracture-type failures, the assumed flaw growth behavior is given in Figure 70. For the breakthrough failure, the K_{Ii}/K_{cR} versus percent increase in flaw depth behavior presented in Figure 67 was used to calculate flaw depths at various stresses approaching critical. The assumed relationship is given in Figure 70. As with the aluminum data, the resistance and stress intensity curves were calculated, both with and without the deep flaw magnification term presented in Figure 8. The results of these calculations are presented in Figures 71 and 72. Independent of whether the deep flaw magnification term was used or not, it is interesting to note that the breakthrough failure occurred at a lower stress intensity than the fracture-type failure. Flaw growth also initiated at a lower stress intensity for the breakthrough failure than for the fracture-type failures.

The breakthrough specimen was apparently less resistant to crack growth due to loading, thereby allowing the flaw to grow through the thickness before the crack tip velocity was sufficient to cause a simultaneous breakthrough and fracture. Although the "fracture" specimens could withstand a higher stress intensity without failing, their increased toughness did not produce a leakage failure. The author has observed fracture tests of surface flaw specimens of other alloys which produced similar results. One specimen will fracture at a higher stress intensity than another, but the crack opening displacement record of the tougher specimen will be linear to fracture, whereas the record of the other one will indicate significant crack growth prior to fracture. Therefore, the fracture toughness of a material is not necessarily indicative of the amount of stable crack growth the specimen can experience during loading.

Although flaw growth behavior could be assumed for the other titanium specimens and resistance curves generated, any trends in the data would be indistinguishable because of the specimen-to-specimen variation in toughness. The more significant points pertinent to the stable crack growth due to loading behavior of the titanium specimen are summarized below:

- Crack growth during loading is a stable process occurring primarily under increasing load.

- Crack growth can occur at constant load and even during the initial relaxation of loading, but only at load levels extremely close to critical.

- Minor variations in Quench-Delay Times can produce significant variations in the critical stress intensity.

5.3.3 Effect of Growth-on-Loading on Crack Length

Thus far, the discussion has been limited to the extent of crack growth experienced in the crack depth direction during loading. The primary emphasis has been placed on the crack depth growth because it controls breakthrough and is a primary variable in the stress intensity equation. The crack length

as measured at the specimen surface did not vary in any of the specimens during the growth-on-loading tests. Where an increase in crack length occurred, it was at some depth, not at the surface. In all cases the crack lengths presented in the tables are the maximum lateral crack dimension; they are not necessarily the crack length at the surface. The manner in which the various flaw shapes grew is illustrated in Figure 73. Some typical examples of the behavior are presented in Figure 74 for the aluminum specimen and Figure 75 for the titanium specimens.

The only aluminum specimens which experienced an increase in flaw length prior to failure were the 4.77 mm (0.188 inch) thick specimens having initial a/2c's of 0.30 and 0.45. None of the other aluminum specimens experienced any lateral flaw growth prior to failure. All of the specimens which experienced increases in crack length in excess of 5 percent did so only when failure was imminent. A plot of K_{Ii}/K_{cr} versus percent increase in crack length is presented in Figure 76. The results presented in Figure 76 are very comparable to the results reported in reference 11. Reference 11 tested the same alloy and flaw shapes in thicknesses from 3.18 mm (0.125 inch) to 9.53 mm (0.375 inch) and reported lengthwise crack growth in all thicknesses tested. The magnitudes of the crack growth observed are the same between the reference and this program. Considering the results of the two programs, the following conclusion can be made pertinent to lateral crack growth during loading in 2219-T87 aluminum base metal.

- Lateral crack growth can be experienced during loading but only at load levels in excess of 70 percent of critical.

- Lateral crack growth will be most predominant with round flaws, i.e, a/2c $\geq$0.30.

- Lateral crack growth will be most prominent in gages in excess of 1.91 mm (0.075 inch). The data available suggests that lateral crack growth will not occur in gages less than 1.91 mm (0.075 inch).

- Lateral crack growth will not occur at the surface, but rather at some depth. The intersection of the crack front and the surface will not vary during loading.

None of the titanium specimens having initial a/2c's of 0.15 or 0.05 experienced any lateral crack growth prior to failure. Lateral flaw growth was experienced in the 2.03 and 1.02 mm (0.080 and 0.040 inch) thick specimens having an initial a/2c of 0.30. For the specimens having an initial a/2c of 0.45, lateral flaw growth occurred in both the gages tested (3.18 and 2.03 mm (0.125 and 0.080 inch)). As with the aluminum specimen, lateral crack growth did not occur at the surface but rather at some depth. Even for the cases where very significant growth occurred, the surface dimension remained constant. The percent increase in flaw length of the titanium specimens was significantly greater than aluminum results (see Figures 76 and 77). The magnitude of the increases in flaw length suggests that the failure of the titanium specimen may be predominately controlled by the lateral crack growth rather than depthwise crack growth. If lateral crack growth does indeed exhibit a significant influence on the failure process, it would be a result of the material being significantly more resistant to crack growth in the depth than in the lateral direction. The results of the center crack panel tests, which were a measure of the lateral toughness of the material, however, yielded K_{CN} values which were higher than the K_{IE} measured for the surface flaw specimens. There is insufficient data to determine whether or not the lateral crack growth is the controlling parameter in the failure process; however, the data does suggest that lateral crack growth has a significant impact on the failure process for specimens which have relatively round flaws ($a/2c \geq 0.30$). The more significant facts pertinent to lengthwise crack growth during loading for both alloys can be summarized as:

- Lateral crack growth will only occur for initial $a/2c > 0.15$.
- Lateral crack growth will only occur at load levels approaching failure.
- Very pronounced crack growth can occur but only when failure is imminent.
- Lateral crack growth will not occur at the surface, but rather at some interior point.

5.3.4 Summary of Growth-on-Loading Tests

Individual summaries of the aluminum and titanium results have been presented in Sections 5.3.1 and 5.3.2, respectively. The following is a summary of the observations which were common to both sets of data. The test results presented in reference 11 have also been incorporated in this summary.

- Significant stable crack growth can occur under increasing load. Significant specimen-to-specimen variation in the extent of crack growth obtained can be expected for seemingly identical specimens tested under carefully controlled laboratory conditions.

- Low aspect ratio (a/2c) flaws will experience more depthwise flaw growth, on a percentage basis, than high aspect ratio flaws.

- High aspect ratio flaws will experience more lengthwise flaw growth, on a percentage basis, than low aspect ratio flaws.

- It appears possible to experience crack growth at constant load and initially decreasing load in 6Al-4V STA titanium specimens but only when the maximum applied load was nearly equal to the failure load.

- The extent of flaw growth which will occur, either depthwise or lengthwise, is dependent upon initial flaw shape.

- For a 2219-T87 aluminum specimen, lengthwise flaw growth, prior to failure, will only occur in gage thicknesses in excess of 1.91 mm (0.075 inch).

5.4 Static Fracture Toughness Tests

It was not possible to obtain fracture toughness values from any of the room temperature aluminum surface flaw specimen results because the failure mode was leakage. Several of the titanium specimens, however, failed by fracture; therefore, fracture toughness values were obtained for these specimens. The fracture toughness values obtained have been summarized and are presented in

Table 31 and Figure 78. The average toughness value obtained from the seven specimens was 58 $MN/m^{3/2}$ (53 $ksi\sqrt{inch}$). There was considerable variability in the K_{IE} values obtained. The variability in results is not relatable to either flaw shape or thickness. Like the center crack results, the variability in the results are most probably a result of variation in quench time of the individual specimen blanks. Unlike the center crack results, there was no systematic increase in toughness associated with a decrease in thickness.

5.5 Single Cycle Penetration Criteria Tests

The results of the single cycle penetration tests are presented in this section. These tests were conducted to determine the parameters controlling failure by leakage. The geometric variables examined for each alloy were flaw shape and specimen thickness. All of the tests of a given alloy were conducted at approximately the same stress; therefore, failure stress was not a variable investigated. The discussion of the results is initially divided by alloy and a final discussion of commonalities is offered.

5.5.1 2219-T87 Aluminum Single Cycle Penetration Criteria Tests

Presently, two methods for predicting failure mode are considered. The first was presented in reference 8 and the second in reference 11. Both of these methods were empirically derived at least partially from 2219-T87 aluminum test results. The reference 8 procedure assumes that the remaining ligament which separates failure by leakage from failure by fracture can be calculated using the following formula:

$$t - a = 0.10(K_{IE}/\sigma_{ys})^2 \qquad (1)$$

The second, or reference 11, procedure is more lengthy and can be used to determine the failure mode for a selected failure stress. A comparison of the predicted failure mode and the actual failure modes obtained during the course of this program is presented in Figure 79.

The failure mode for all of the aluminum tests, with the exception of the 4.77 mm (0.188 inch) thick specimen tested in liquid hydrogen, was leakage. The first method (reference 8) predicted all of the failure modes correctly. The actual remaining ligaments were generally significantly less than the predicted transition remaining ligament. The reference 11 or Method II procedure also accurately predicted all of the failure modes. From the results presented here, it appears that either procedure can be used to satisfactorily predict failure mode.

5.5.2 6Al-4V STA Titanium Single Cycle Penetration Criteria Tests

The actual failure mode of the titanium surface flaw specimen can also be compared to the predicted mode. Both methods of predicting failure mode, however, require the K_{IE} of the material to be known. Unlike the aluminum results where K_{IE} was known, there appeared to be a specimen-to-specimen variation in the titanium tests as a result of the heat treatment of the specimen blanks. The maximum and minimum K_{IE} values presented in Table 31 and Figure 78 have been used to determine the range of remaining ligaments which separate failure by leakage from fracture. Using the reference 8 or Method I procedure, the comparison of predicted and actual failure modes is presented in Figure 80. If the maximum K_{IE} value is considered for the prediction, the actual and predicted failure modes are in agreement with one exception. Considering the specimen-to-specimen variation in toughness and flaw growth during loading behavior, the one erroneous prediction was not surprising. Generally, this procedure provided accurate predictions of the failure modes.

The basic premise of the second failure mode prediction method (reference 11) is that for a given material-flaw shape combination, there is a maximum amount the flaw can grow stably prior to failure. Further, the maximum amount of growth is a percentage of the initial flaw depth. Therefore, for a given elastic failure stress, it is possible to determine the failure mode if the critical stress intensity (K_{IE}) is known. The maximum size flaw which would cause fracture rather than breakthrough can be calculated as follows:

$$a_{max} = t - \Delta a \qquad (10)$$

where Δa = stable growth during load which will be a certain percentage of the material thickness depending on initial flaw shape (see Figures 67 through 69).

$$\text{If, } 1.95\sigma M_K \sqrt{a_{max}/Q} > K_{IE}\text{, fracture will occur.}$$

$$\text{If, } 1.95\, M_K \sqrt{a_{max}/Q} < K_{IE}\text{, fracture cannot occur,}$$

therefore, a deeper flaw will be required to produce a failure at the selected stress. Since the remaining ligament for a larger flaw will be less than the stable growth which can be encountered, the failure mode will be by leakage. For the titanium surface flaw specimens tested here, it appears the maximum percentage increases in flaw depth which can be encountered prior to failure are 35, 35, 25 and 25 for a/2c's of 0.05, 0.15, 0.30 and 0.45, respectively. Therefore, all of the specimens having flaws with a/2c of 0.05 and 0.15 should have failed by breakthrough if their initial a/t was 0.74 or greater, and all of the specimens having a/2c's of 0.30 and 0.45 should have failed by breakthrough if their initial a/t was 0.80 or greater. All of the specimens failed at elastic stress levels, therefore, a comparison of the actual and predicted failure modes can be made using the reference 11 procedure (see figure 81). In general, the predicted and actual failure modes are in agreement, the three erroneous predictions are close to the predicted transition line.

5.5.3 Summary of Single Cycle Penetration Test Results

There was insufficient data to conclusively prove or disprove the validity of either of the two failure mode prediction criteria. Both methods accurately predicted all the aluminum results and produced satisfactory predictions for the titanium results. Considering the variations in toughness encountered in the titanium specimens, some errors in predicted failure mode could be expected.

The first criteria is useful in predicting failure mode if the flaw depth and thickness is known. The procedure can then be used to predict failure mode when failure occurs and is not influenced by flaw shape or stress. The second procedure can be used to predict the failure mode for a selected failure stress. This procedure considers the effects of flaw shape and is useful in determining the potential failure mode at a selected proof stress level.

5.6 Surface Flawed Specimen Cyclic Test Results

The results of the surface flawed specimen cyclic tests are presented and discussed in this section. The initial discussion is divided by alloy followed by a review of commonalities in the results.

5.6.1 2219-T87 Aluminum Surface Flawed Specimen Cyclic Tests

Cyclic tests were conducted at both room temperature and 20K (-423^{o}F) at cyclic frequencies between 1 and 10 cpm. The cyclic tests were generally terminated at failure, either breakthrough or fracture; however, some tests were terminated prior to failure. The results of the tests have been tabulated and are presented in Tables 10 through 21. The results are also presented in Figures 82 and 83 in terms of K_{Ii}/K_{cr} versus cycles to failure; Equation 2 was used in the calculation of K. For the K_{Ii} calculation, the initial (prior to simulated proof test) flaw size was used in conjunction with the cyclic stress level. The K_{cr}'s used in the calculation were the average critical stress intensities for each individual combination of temperature, a/2c and thickness. The K_{Ii}/K_{cr} ratios are directly comparable to the ratio of operating to proof stress ($\sigma_{op}/\sigma_{proof}$). Figures 82 and 83 can therefore by used directly to determine the ratio of operating to proof stress which is required to assure a minimum service life requirement.

The curves of K_{Ii}/K_{cr} versus cycles to failure from reference 15 have been plotted on the curves. These curves were "best-fit", rather than "lower bound" curves generated from tests of specimens varying in thickness from 10.2 to 31.8 mm (0.40 to 1.25 inch). All of the test data presented in reference 15 were for cyclic tests with no prior overload whose failure mode was fracture. The room temperature data is evenly distributed about the reference curve except for the longest flaw (a/2c-0.05) thinnest gage [0.635 mm (0.025 inch)] data, which all fall to the left of the curve. The limited data from the liquid hydrogen temperature tests all fall very close to the reference curve. Superficially it may appear the remaining flaw growth life should be a minimum for the thinnest gages, however, there are several self-compensating factors which tend to equalize the cyclic lives. If the crack growth behavior is expressed as

$$\Delta a/\Delta N = C\, K_{max}^{\ n} \tag{11}$$

or

$$\Delta a/\Delta N = C(1.95\, M_K \sigma \sqrt{a/Q})^n \tag{12}$$

For two specimens of different thickness but the same initial flaw shape (a/2c), flaw depth to thickness, (a/t), and cyclic stress the relative growth rates are

$$\frac{(\Delta a/\Delta N)_1}{(\Delta a/\Delta N)_2} = \frac{C\,[1.95\sigma M_K \sqrt{\frac{(a/t)}{Q}}\ \sqrt{t}]_1^n}{C\,[1.95\sigma M_K \sqrt{\frac{(a/t)}{Q}}\ \sqrt{t}]_2^n} \tag{13}$$

However, since the flaw shapes, flaw depth to thickness ratios and stresses are equal, equation 13 reduces to:

$$\frac{(\Delta a/\Delta N)_1}{(\Delta a/\Delta N)_2} = \left(\frac{t_1}{t_2}\right)^{\frac{n}{2}} \tag{14}$$

The residual cyclic life will be proportional to the size of the remaining ligament.

$$\Delta a = [1-(a/t)i]t \tag{15}$$

where (a/t)i = initial flaw depth to thickness ratio

Therefore,

$$\frac{\Delta a_1}{\Delta a_2} = \frac{[1-(a/t)i]t_1}{[1-(a/t)i]t_2} \tag{16}$$

However, the initial a/t's were assumed equal; therefore,

$$\frac{\Delta a_1}{\Delta a_2} = \frac{t_1}{t_2} \tag{17}$$

combining equations 12 and 15

$$\frac{(\Delta a/\Delta N)_1}{(\Delta a/\Delta N)_2}\frac{(\Delta a_2)}{(\Delta a_1)} = \left(\frac{t_1}{t_2}\right)^{n/2}\left(\frac{t_2}{t_1}\right) \qquad (18)$$

$$\frac{\Delta N_2}{\Delta N_1} = \left(\frac{t_1}{t_2}\right)^{\frac{n}{2}-1} \qquad (19)$$

A review of available cyclic crack growth rate data for 2219-T87 aluminum reveals that n = 3.5 does a satisfactory job of correlating the data. This value can, therefore, be used in equation 19.

For the subject program all of the cyclic tests were conducted subsequent to an overload. Since overloads retard crack growth rates, any comparison of relative lives must consider overload effects. The crack growth rate retardation occurs throughout the plastic zone caused by the overload and is dependent upon the magnitude of the overload. Since all the overload plastic zones were greater than the remaining ligaments, for specimens having the same overloads and cyclic stress, equation 19 is valid if the initial flaw shapes and flaw depth-to-thickness ratios are equal. Within these constraints the relative lives of the 0.635 mm (0.025 inch) specimens should be 2 and 4 times the lives of the 1.91 mm and 4.77 mm (0.75 and 0.188 inch) thick specimens, respectively. A comparison of initial flaw depth-to-thickness ratios (a/t's) and cyclic life is presented in Figure 84 for the room temperature specimens having a/2c's of 0.15 and 0.30. Only the specimen which had a cyclic stress of 248 MN/m^2 (36 ksi) and an overload of approximately 310 MN/m^2 (45 ksi) were considered in the comparison. Although not conclusive, there definitely is a trend towards the thinnest gages having the longest lives for equal initial a/t's. The trend is most apparent for the longer flaws (a/2c = 0.15) than for the shorter flaws.

For the 0.635 mm (0.025 inch) room temperature tests an a/2c of 0.05 was substituted for the a/2c of 0.45. These specimens consistently had the shortest cyclic lives of all the room temperature aluminum tests. For very thin material the most probable flaw shape is a very long (low a/2c)

defect such as a scratch. The flaws in the specimens under consideration were twenty times the depth dimensions in length, therefore, they are representative of a long scratch. Going to lower aspect ratio flaws could not be expected to have a significant influence on service life.

A plot of K_{Ii}/K_{CR} versus cycles to failure for the 20 K (-423^{o}F) aluminum data is presented in Figure 83. The cycles to failure curve from reference 15 is also included on the figure so that a comparison can be made. All of the data falls very close to the reference curve. Although the thinner gage specimen tests were terminated prior to failure, it is apparent their cyclic lives would have been at least equivalent to the lives of the thicker specimens and possible longer.

Generally, the room and liquid hydrogen temperature data agrees well with the reference cycles to failure curves. Since the reference curves were generated from thick gage data (up to 31.8 mm (1.25 inch)) it can be concluded that the cycles to failure curves are realistic for all 2219-T87 aluminum. Although the curves are valid for determining proof test factors for short life structure, the (Figure 82 and 83) should not be considered in the analysis of long life structure. Typical spacecraft structure is subjected to a minimum of cyclic loadings. Assuming cycles to failure is uniquely related to K_{Ii}/K_{CR} means cyclic crack growth rate (da/dN) is inversely proportional to cyclic stress level. This analysis procedure was originally developed for short life spacecraft tankage. Appropriate test data was developed at stress levels commensurate with the operating stresses and the test durations similar to required service lives. Within these constraints the procedure is valid and extremely useful for determining proof test factors.

Among the test results in reference 11 were three specimens which failed on the first cycle subsequent to a simulated proof test. The intent and procedure applied on the subject program were identical to reference 11; being the determination of the minimum guaranteed service life subsequent to a proof test. During the course of this program there were not any first cycle failure even though the tests were designed to inflict the

maximum damage possible during the simulated proof test. Reference 11 speculated that first cycle failures would be rare even under carefully controlled laboratory conditions; the results of this investigation substantiate that speculation.

5.6.2 6Al-4V STA Titanium Surface Flawed Specimen Cyclic Tests

The titanium cyclic tests were conducted exclusively at room temperature. The test results have been summarized and are presented in Tables 22 through 30. All of the tests were conducted at either 1 or 10 cpm and were continued until failure (generally by breakthrough) had occurred. The test results are also presented in Figure 85 in terms of K_{Ii}/K_{CR} versus cycles to failure. Because of the specimen to specimen variation in K_{CR} (see Section 5.2.2) the K_{Ii}/K_{CR} ratio was estimated for each specimen individually. The EDI records were used to estimate the K/K_{CR} ratio at the simulated proof load and this was reduced by the ratio of operating to proof stress to obtain the final K_{Ii}/K_{CR} ratio.

For the heavier gages the failure mode was generally fracture whereas breakthrough was the failure mode for the two thinner gages. For comparison purpose the cycles to failure curve from Figure 82 has been plotted on the figure. All of the titanium data falls very close to the line and is evenly dispersed about it. Therefore, a given operating to proof stress ratio will yield similar cyclic lives for either titanium or aluminum. As with the aluminum data the failure mode, either breakthrough or fracture did not influence significantly the cycles to failure. Variations in flaw shape from a/2c's of 0.05 to 0.45 also did not influence the required cycles to failure.

As with the aluminum results it was not possible to produce a first cycle failure subsequent to the proof test cycle. The proof test cycle for all of the specimens was designed to produce the maximum damage possible. It is apparent from Figures 58 through 66 that failure was imminent at the proof test level for most of the cyclic specimens, therefore, it is reasonable to postulate that first cycle failures after proof testing will be rate even under laboratory conditions.

The variations in toughness of the specimens resulted in a variety of proof and cyclic stress being used for the actual tests. It was not possible therefore to assess the influence of gage thickness on cyclic life for specimens of similar proof and cyclic stresses and initial a/t's and a/2c's as was done for the aluminum tests.

5.6.3 Summary of Cyclic Test Results

All of the cyclic tests were conducted after a simulated proof test cycle. Generally the simulated proof test was designed to inflict the maximum possible damage short of causing the flaw to penetrate the specimen. The residual cyclic lives were presented in terms of K_{Ii}/K_{CR} versus cycles to failure. For each alloy-temperature combination, regardless of gage thickness, flaw shape, or failure mode, the cycles to failure were dependent upon the K_{Ii}/K_{CR} ratio. Therefore, it is possible to select an operating-to-proof stress ratio to ensure minimum service life requirements if the relationship between K_{Ii}/K_{CR} versus cycles to failure is known. This is done by assuming the operating to proof stress ratio is equal to K_{Ii}/K_{CR}. This procedure is valid for pressure vessels subjected to a limited number of cycles and attempts to employ it outside of this range should be avoided.

5.7 Proof Testing Thin-Walled Pressure Vessels

Methodologies for proof testing thick walled pressure vessels for assurance of minimum service life capabilities have been developed and documented. An evaluation of the applicability of these procedures to thin walled pressure vessels was the function of this and prior studies (10, 11). If the crack growth associated with leakage was an unstable process (i.e., a pre-existing flaw would "pop" through the thickness, and arrest, at the breakthrough stress) then the maximum flaw size which could exist in a vessel could be established by proof testing. The crack growth mechanism under increasing load, for the alloys considered in the program, was a stable process. Measurable crack growth occurred, however, only when the specimens were loaded close to failure and significant crack growth only occurred when failure was imminent. Therefore, for a given proof stress

material thickness combination,only a very limited band of flaw sizes can produce significant crack growth without causing leakage. The possibility of a proof test producing sufficient crack growth to diminish the vessel's service life capabilities without causing failure of the vessel is extremely remote. A proof test can be used to assure that the service failure mode is leakage as well as providing a high degree of confidence in the residual service life capability of the vessel. Proof testing thin walled pressure vessels, therefore, is an important tool in assuring minimum service life requirements and preventing catastrophic failures during service.

6.0 CONCLUSIONS

The following conclusions were derived from the results of the experimental programs presented in this report and reference 11. Six thicknesses of 2219-T87 aluminum base metal surface flaw and center crack specimens ranging from 9.53 to 0.635 mm (0.375 to 0.025 inch) were tested at temperatures ranging from 295K to 20K (72°F to -423°F). Additionally, 6Al-4V STA titanium base metal specimens were tested in three thicknesses 3.18, 2.03 and 1.02 mm (0.125, 0.080 and 0.040 inch) at room temperature. All of the tests were conducted on uniaxial specimens. Extrapolation of the following conclusions to other conditions without additional experimental verification should be avoided.

1. Significant stable crack growth under increasing load can occur prior to failure.

2. Initial flaw shape and material have a significant influence on the extent of the flaw growth.

3. Test temperature and thickness do not have a significant effect on the flaw growth when the data is viewed in terms of K_{Ii}/K_{CR}.

4. Low aspect ratio flaws (a/2c = 0.15) experience greater depthwise flaw growth than high aspect ratio flaws (a/2c = 0.45).

5. High aspect ratio flaws experience greater lengthwise flaw growth than low aspect ratio flaws.

6. Significant flaw growth (a 10 percent or greater increase in flaw dimension) will occur only when a specimen is loaded near its failure load.

7. Proof testing can be used to assure early service life failures will be leakage rather than catastrophic fractures.

8. Miinimum service lives can be assured, with a high degree of confidence, if a properly designed proof test is employed.

REFERENCES

1. G. R. Irwin, "Analysis of Stresses and Strains Near the End of a Crack Transversing a Plate," Journal of Applied Mechanics, Transactions of ASME, December, 1962.

2. J. N. Masters, W. P. Haese and R. W. Finger, "Investigation of Deep Flaws in Thin Walled Tanks", NASA CR-72606, December, 1969.

3. F. W. Smith, "The Elastic Analysis of the Part-Circular Surface Flaw Problem by the Alternating Method," The Surface Crack: Physical Problems and Computational Solutions, edited by J. L. Swedlow, ASME, November, 1972.

4. R. C. Shah and A. S. Kobayashi, "On the Surface Flaw Problem," The Surface Crack: Physical Problems and Computational Solutions, edited by J. L. Swedlow, ASME, November, 1972.

5. J. R. Rise and N. Levy, "The Part-Through Surface Crack in an Elastic Plate," Journal of Applied Mechanics, Vol. 39, Trans. of ASME, Vol. 94, March 1972.

6. P. H. Francis, D. L. Davidson and R. G. Forman, "An Experimental Investigation into the Mechanics of Deep Semielleptical Surface Cracks in Mode I Loading," Engineering Fracture Mechanics, Vol. 4 No. 4, December, 1972.

7. A. S. Kobayashi and W. L. Moss, "Stress Intensity Magnification Factors to Surface-Flawed Tension Plate and Notched Round Tension Bar," Fracture Proc., 2nd Internation Conference on Fracture (Brighton), Chapman and Krell, London, 1969.

8. J. N. Masters, W. D. Bixler and R. W. Finger, "Fracture Characteristics of Structural Aerospace Alloys Containing Deep Surface Flaws," NASA CR-134587, December, 1973.

9. C. F. Tiffany, "Fracture Control of Metallic Pressure Vessels," NASA SP-8040, 1970.

10. J. N. Masters, W. L. Engstrom and W. D. Bixler, "Study of Deep Flaws in Weldments of Aluminum and Titanium," NASA CR-134649, April, 1974.

11. R. W. Finger, "Proof Test Criteria for Thin Walled 2219 Aluminum Pressure Vessels," NASA CR-135036, August, 1976.

12. L. R. Hall and R. W. Finger, "Stress Corrosion Cracking and Fatigue Crack Growth Studies Pertinent to Spacecraft and Booster Pressure Vessels," NASA CR-120823, December, 1972.

13. W. F. Brown and J. E. Scrawley, "Fracture Toughness Testing Methods," Page 10, ASTM STP 410, 1966.

14. L. R. Hall, R. W. Finger and W. F. Spurr, "Corrosion Fatigue Crack Growth Data for Aircraft Structural Materials," Air Force Materials Laboratory Report AFML-TR-73-204, September, 1973.

15. W. L. Engstrom, "Determination of Design Allowable Properties - Fracture of 2219-T87 Aluminum Alloy," NASA CR-115388, March, 1972.

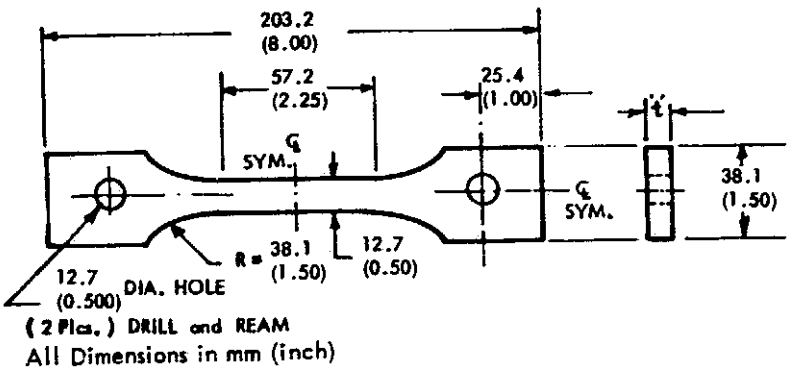

Figure 1 : ALUMINUM AND TITANIUM MECHANICAL PROPERTY SPECIMEN

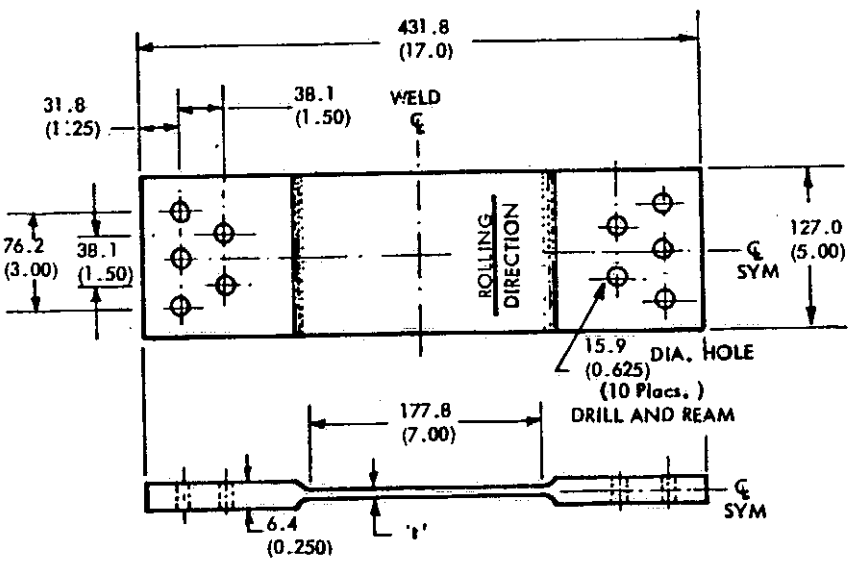

MATERIAL	't' mm (inch)
6 Al-4V STA TITANIUM	31.8(0.125)
	2.03(0.080)
	1.02(0.040)
2219-T87 ALUMINUM	.635(0.025)
	1.91(0.075)

Figure 2 : ALUMINUM AND TITANIUM TEST SPECIMEN

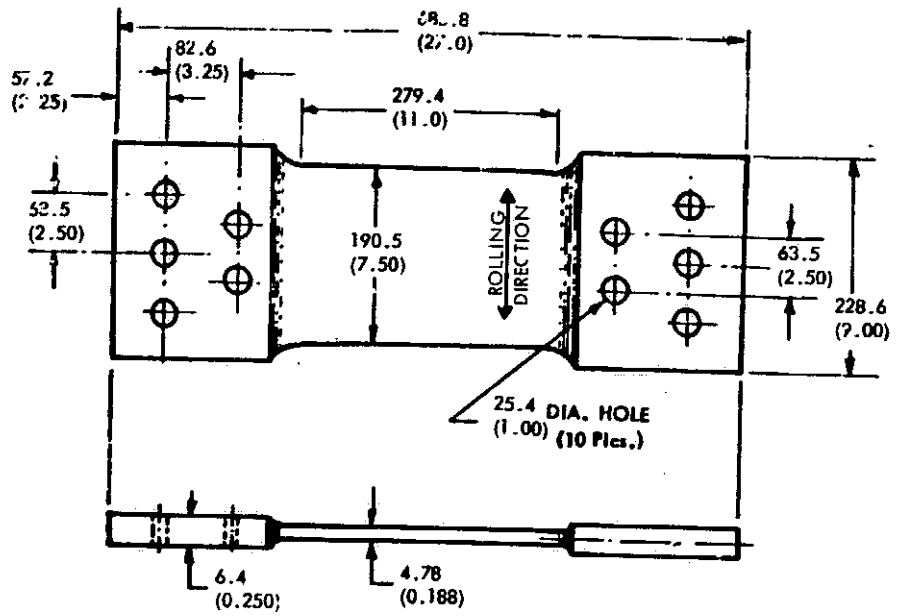

All Dimensions in mm (inch)

Figure 3 : ALUMINUM SURFACE FLAWED SPECIMEN

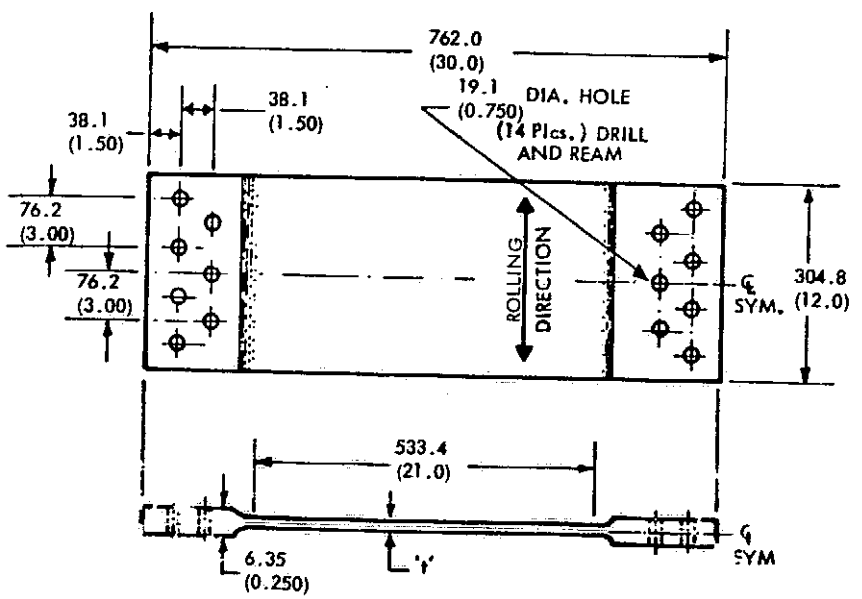

'f' mm (inch)
4.78(0.188)
1.91(0.075)
.635(0.025)

Figure 4 : 2219-T87 ALUMINUM CENTER CRACK SPECIMEN

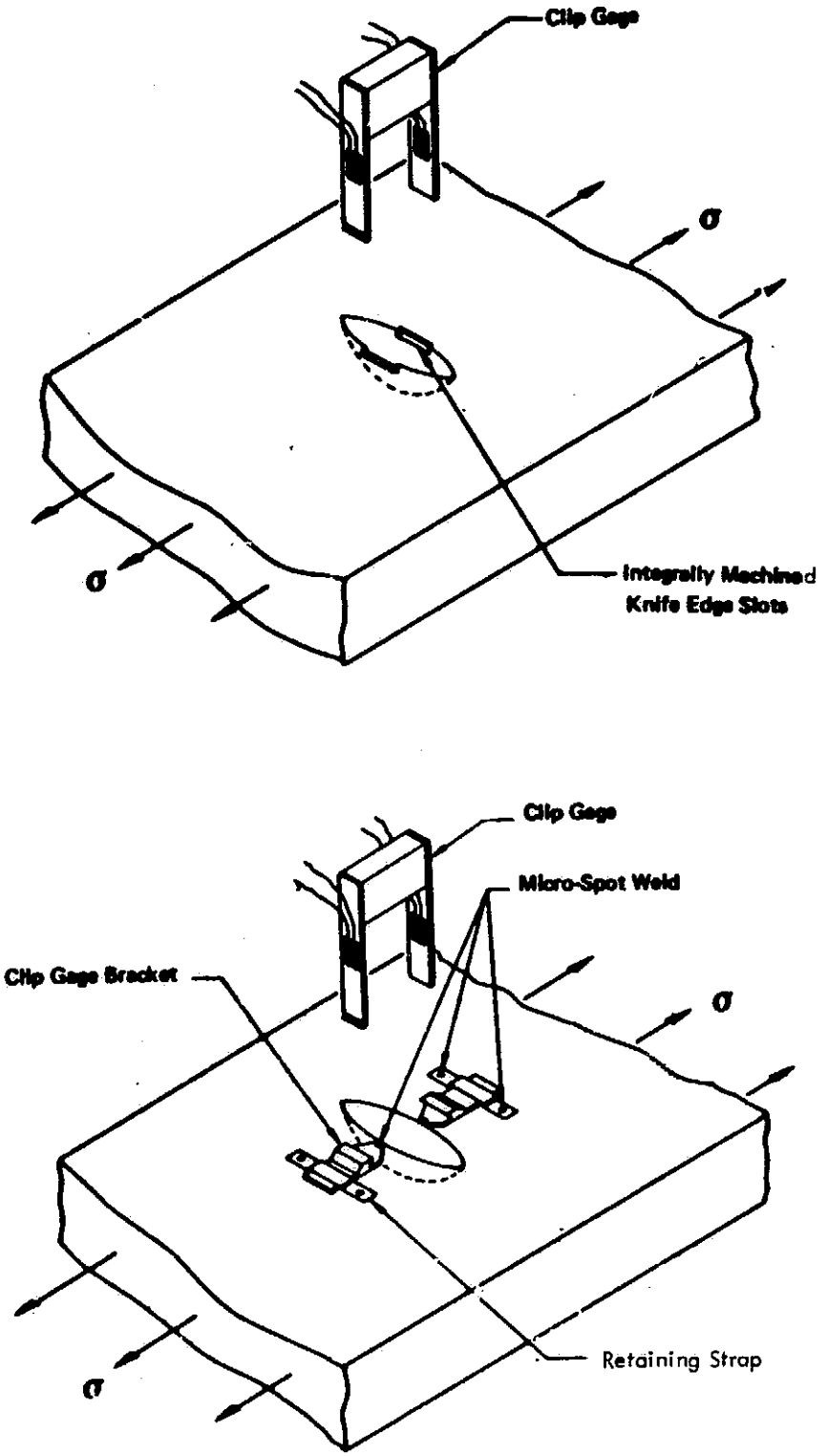

Figure 5: CRACK OPENING DISPLACEMENT MEASUREMENT OF SURFACE FLAW

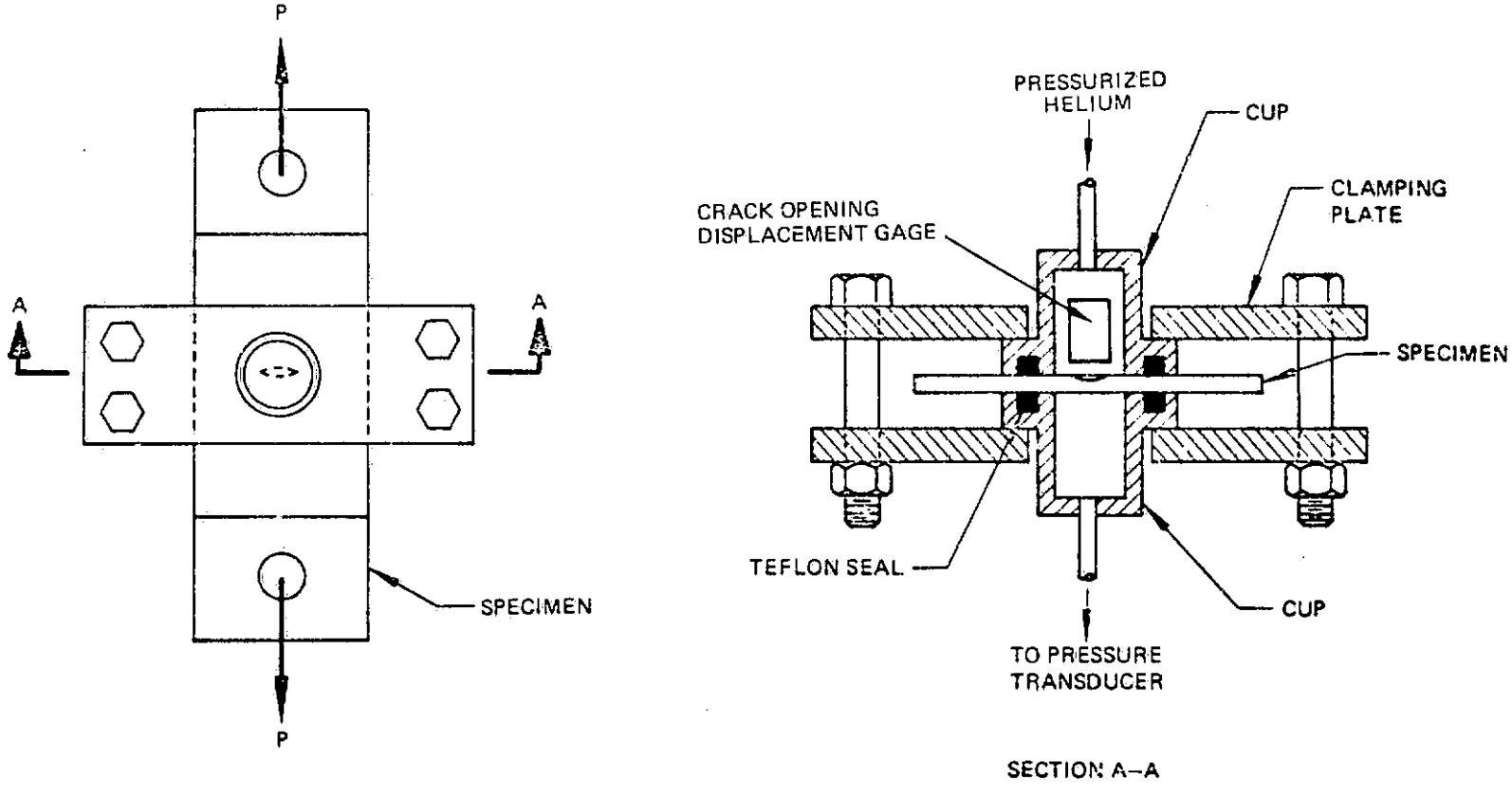

Figure 6: PRESSURE CUPS ASSEMBLY FOR BREAKTHROUGH DETERMINATION

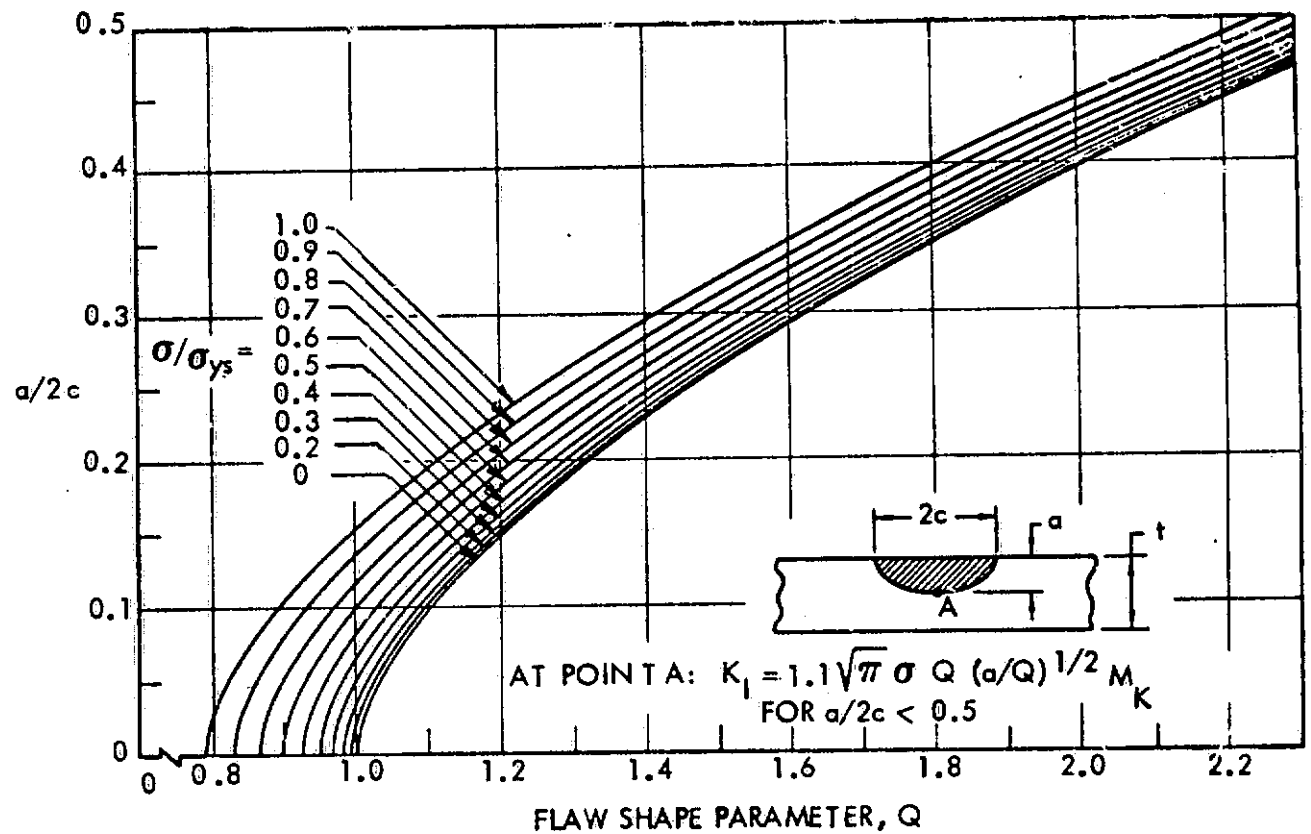

FIGURE 7 : SHAPE PARAMETER CURVES FOR SURFACE AND INTERNAL FLAWS

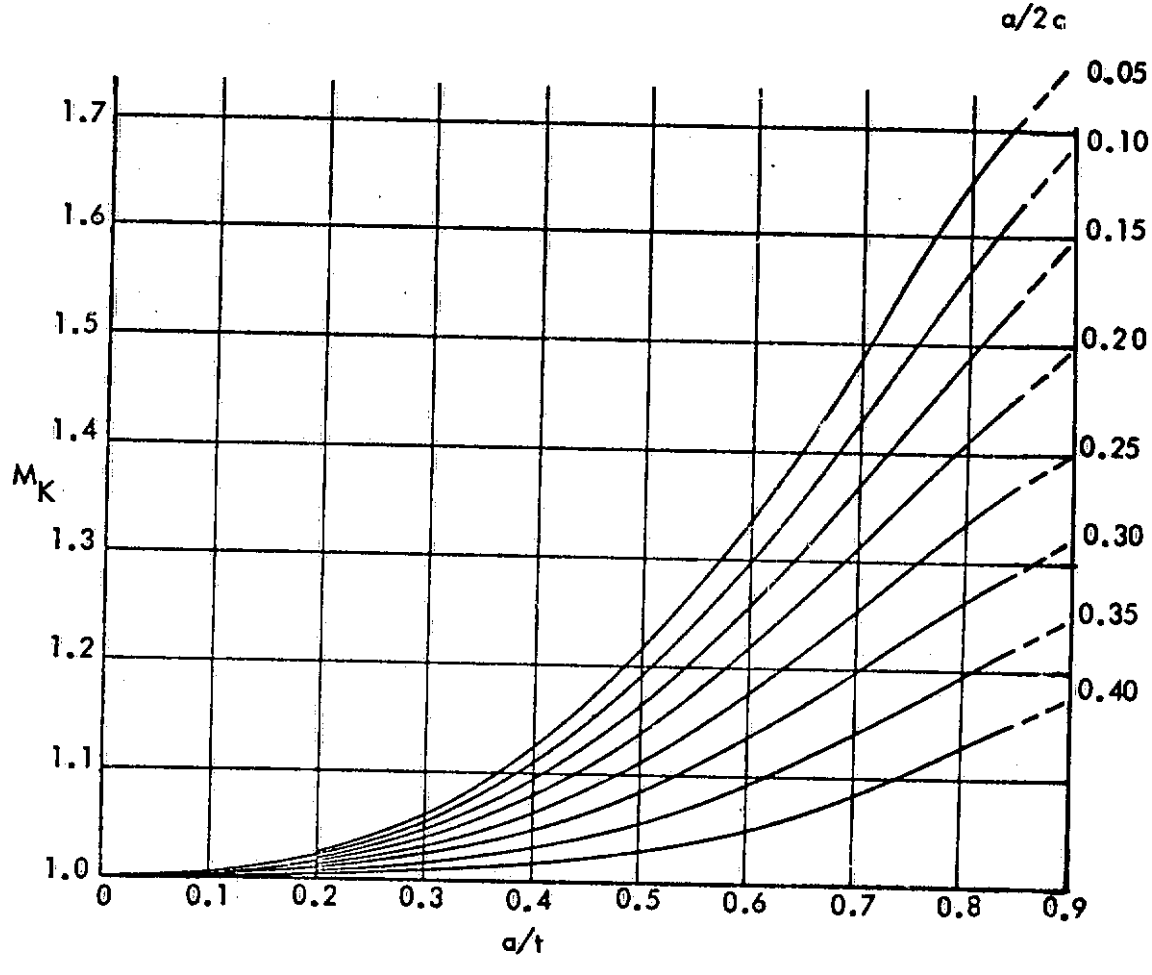

FIGURE 8: DEEP FLAW MAGNIFICATION CURVES (FIGURE 58, REF. 2)

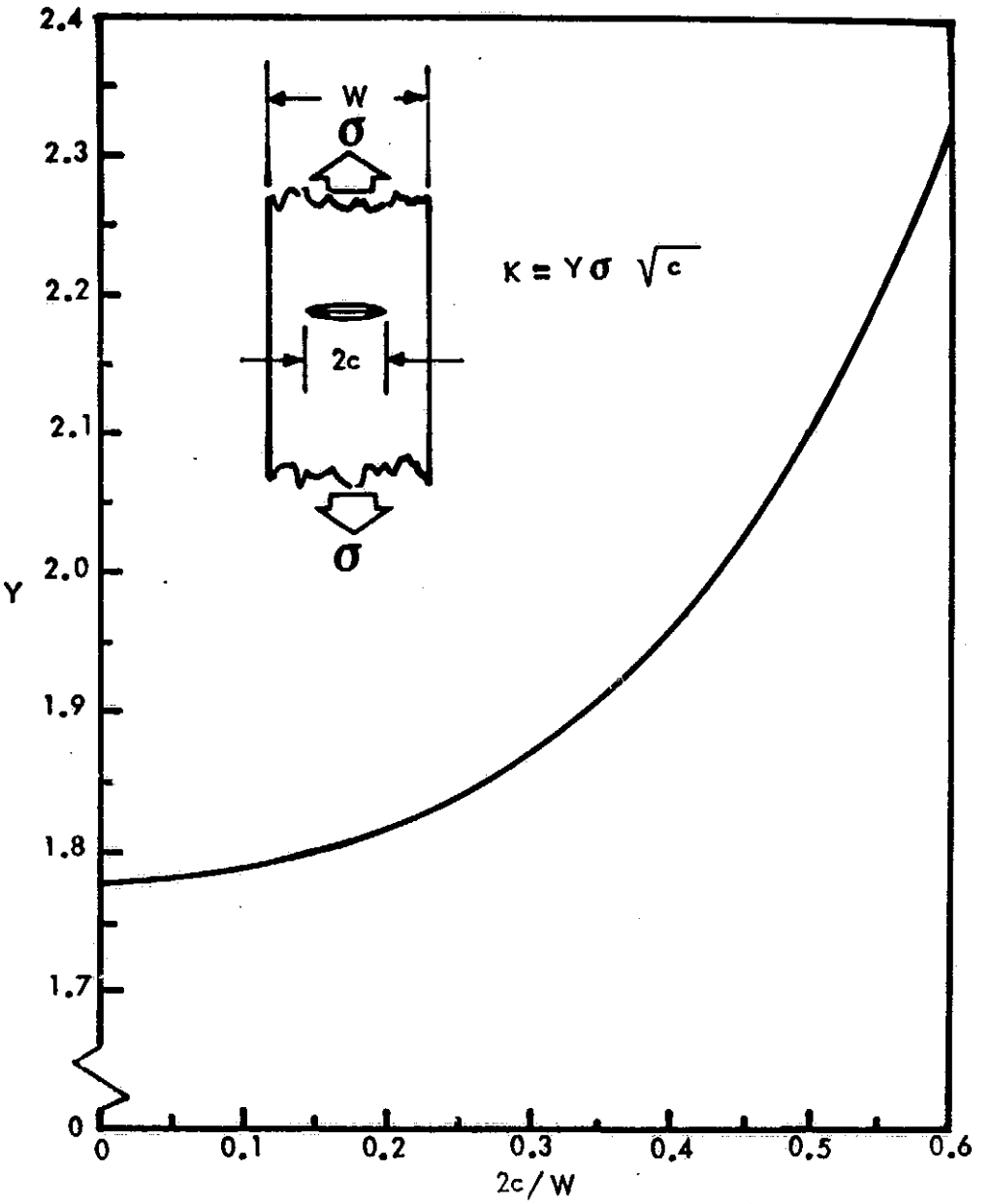

Figure 9: FINITE WIDTH STRESS INTENSITY CORRECTION FACTOR FOR CENTER CRACKED PANELS

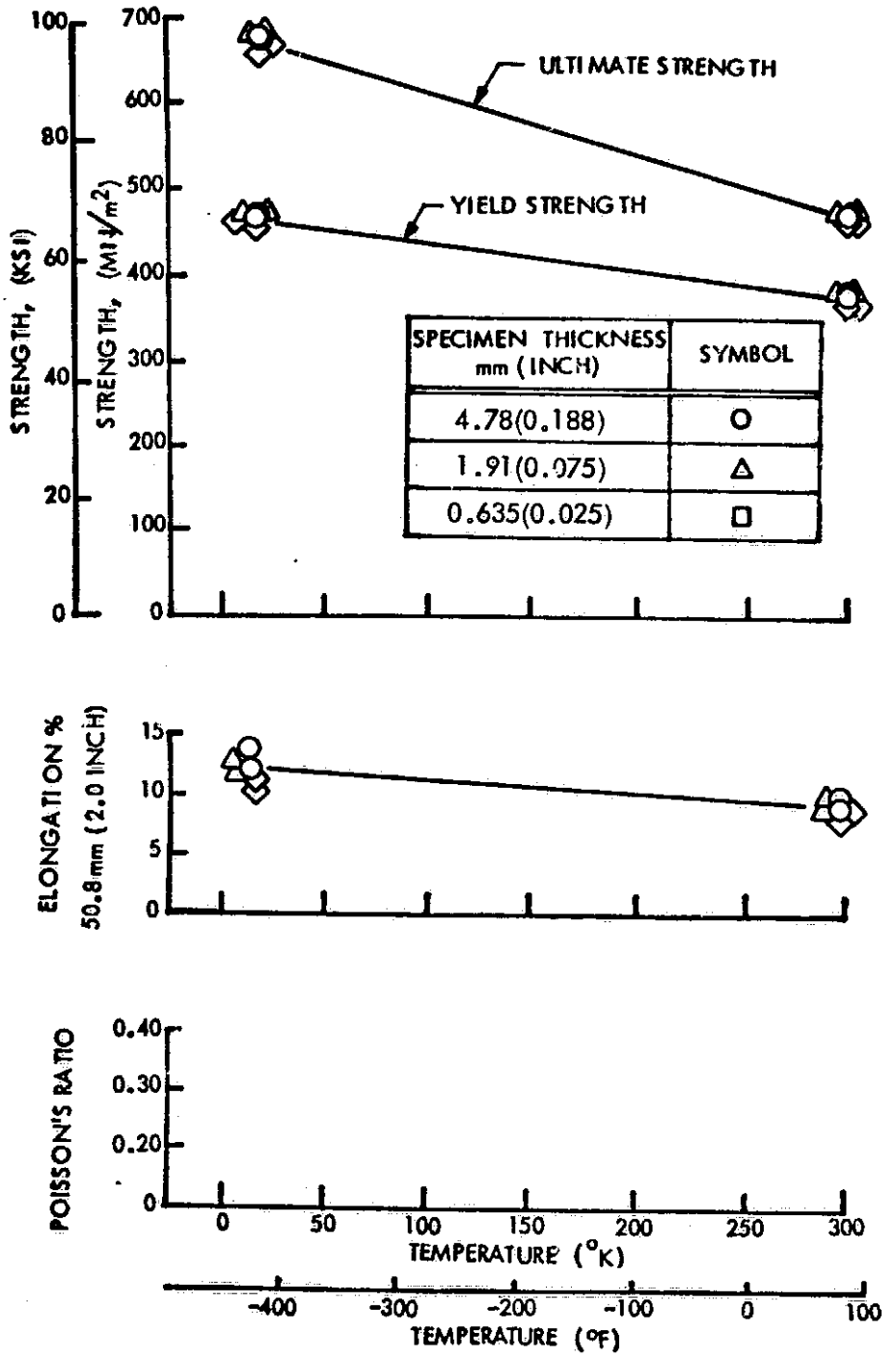

Figure 10 : TENSILE PROPERTIES OF 2219-T87 ALUMINUM BASE METAL TRANSVERSE GRAIN

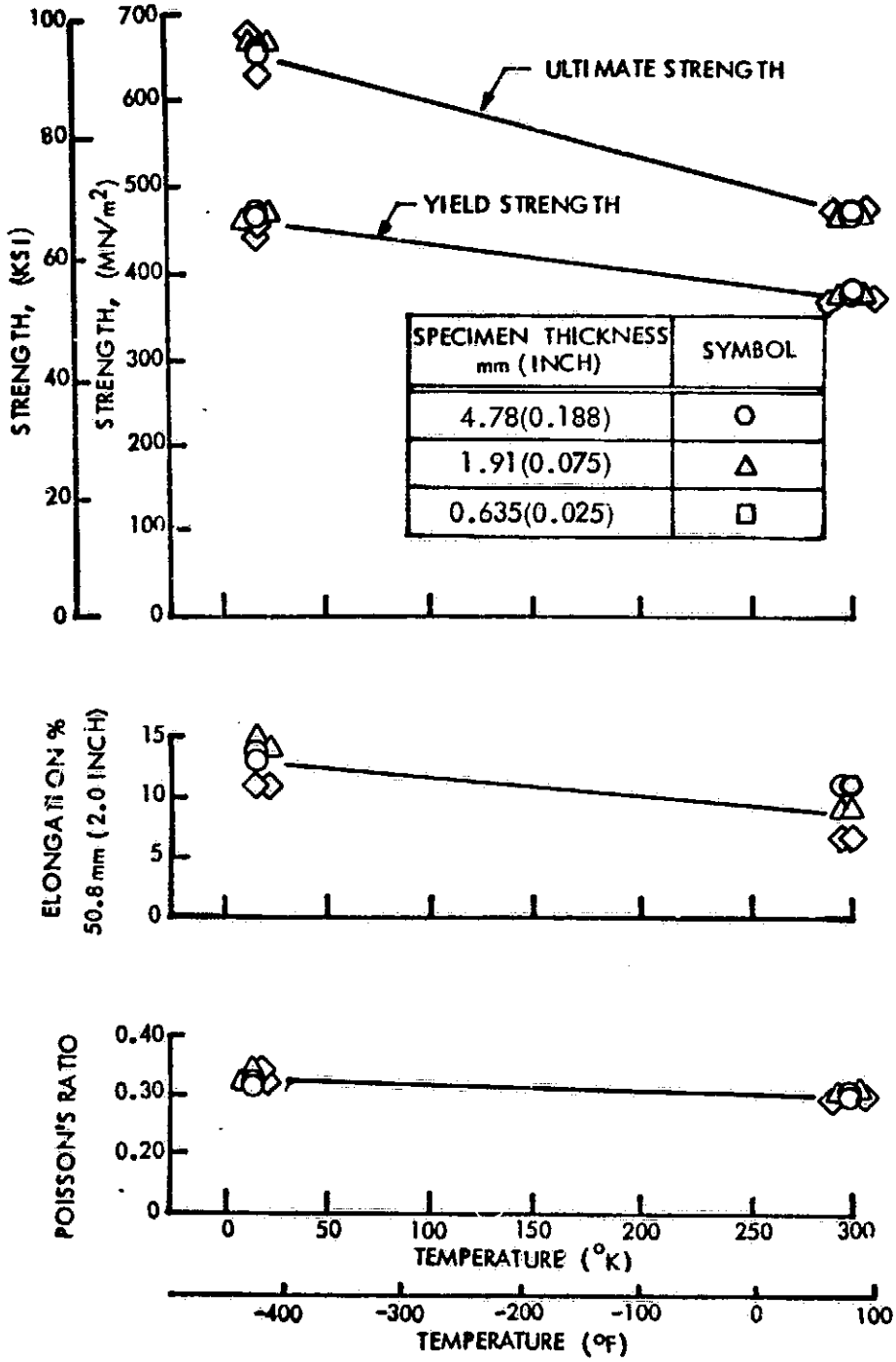

Figure 11 : TENSILE PROPERTIES OF 2219-T87 ALUMINUM BASE METAL LONGITUDINAL GRAIN

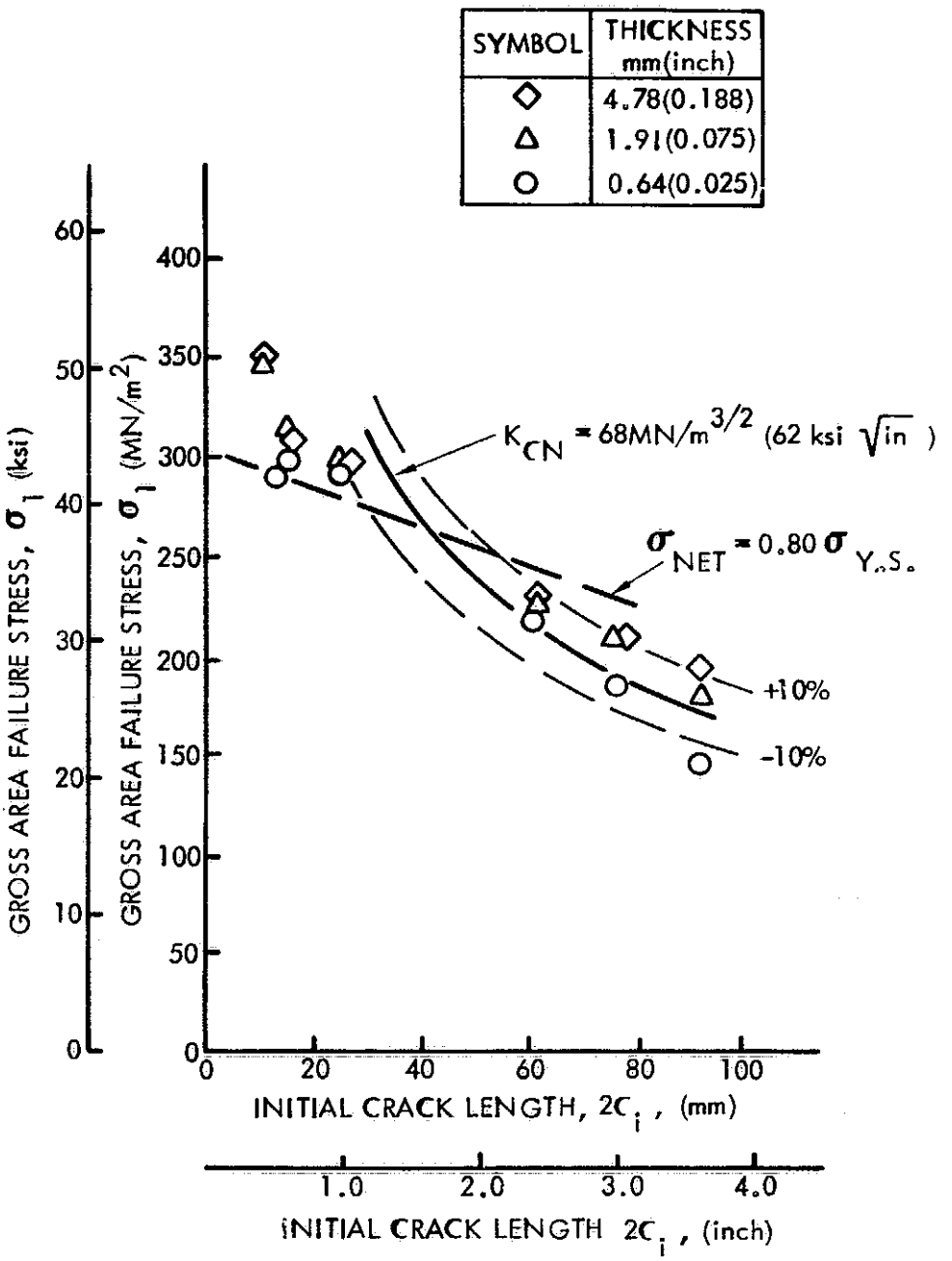

Figure 12 : GROSS AREA FAILURE STRESS VERSUS INITIAL CRACK LENGTH FOR ROOM TEMPERATURE 2219-T87 ALUMINUM CENTER CRACK PANELS

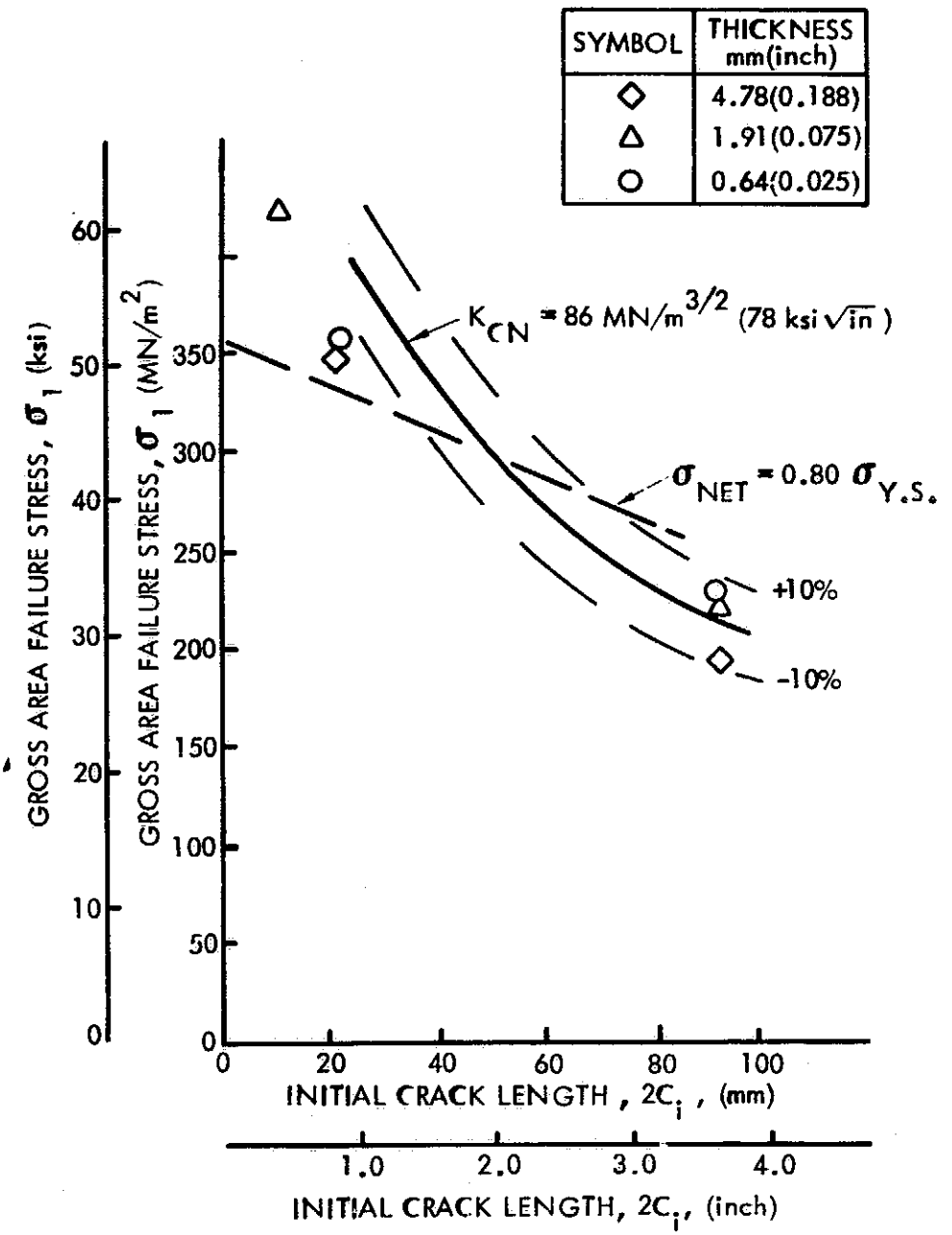

Figure 13 : GROSS AREA FAILURE STRESS VERSUS INITIAL CRACK LENGTH FOR LIQUID HYDROGEN TEMPERATURE 2219-T87 ALUMINUM CENTER CRACK PANELS

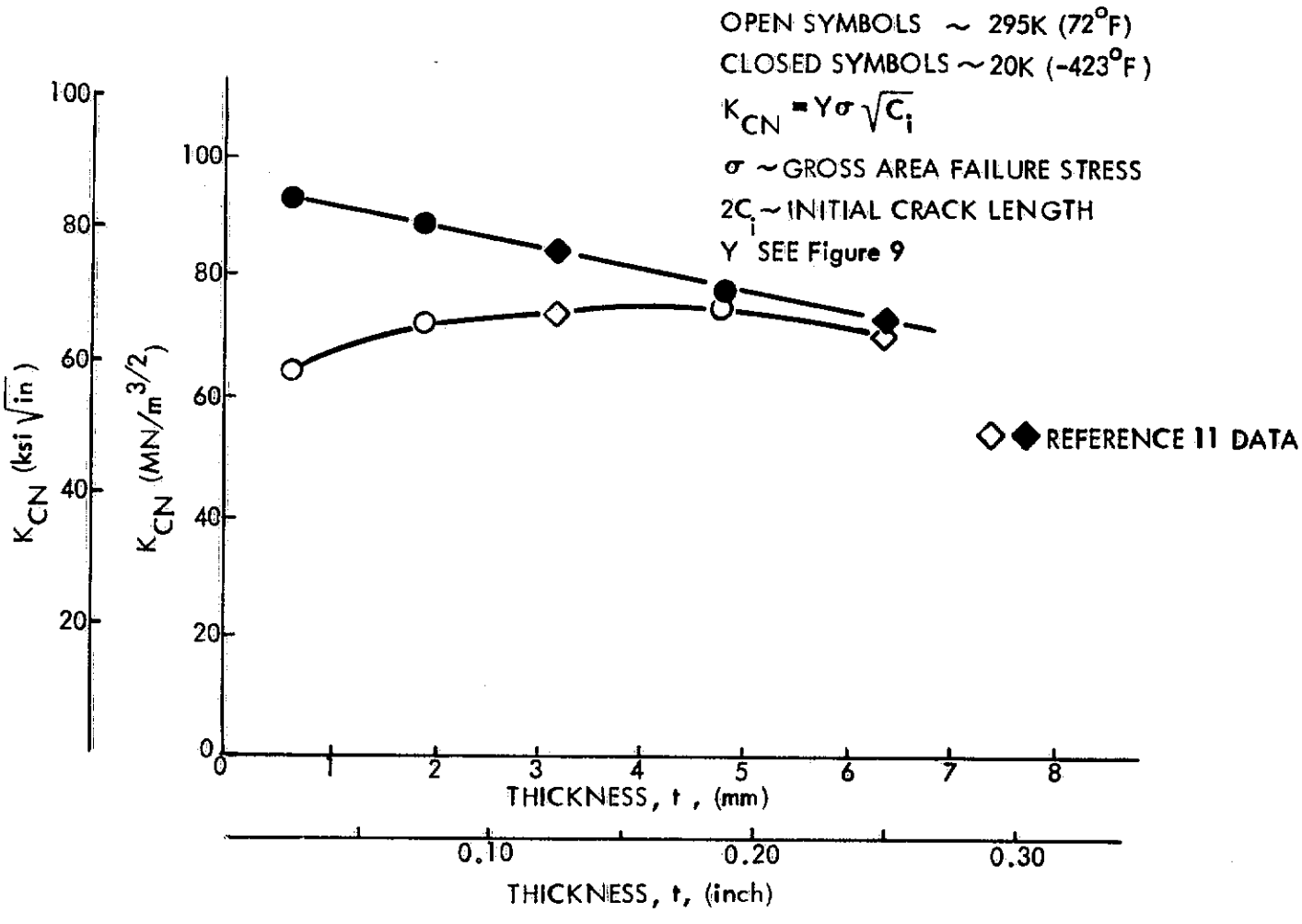

Figure 14 : EFFECT OF THICKNESS ON 2219-T87 ALUMINUM BASE METAL K_{CN} VALUES

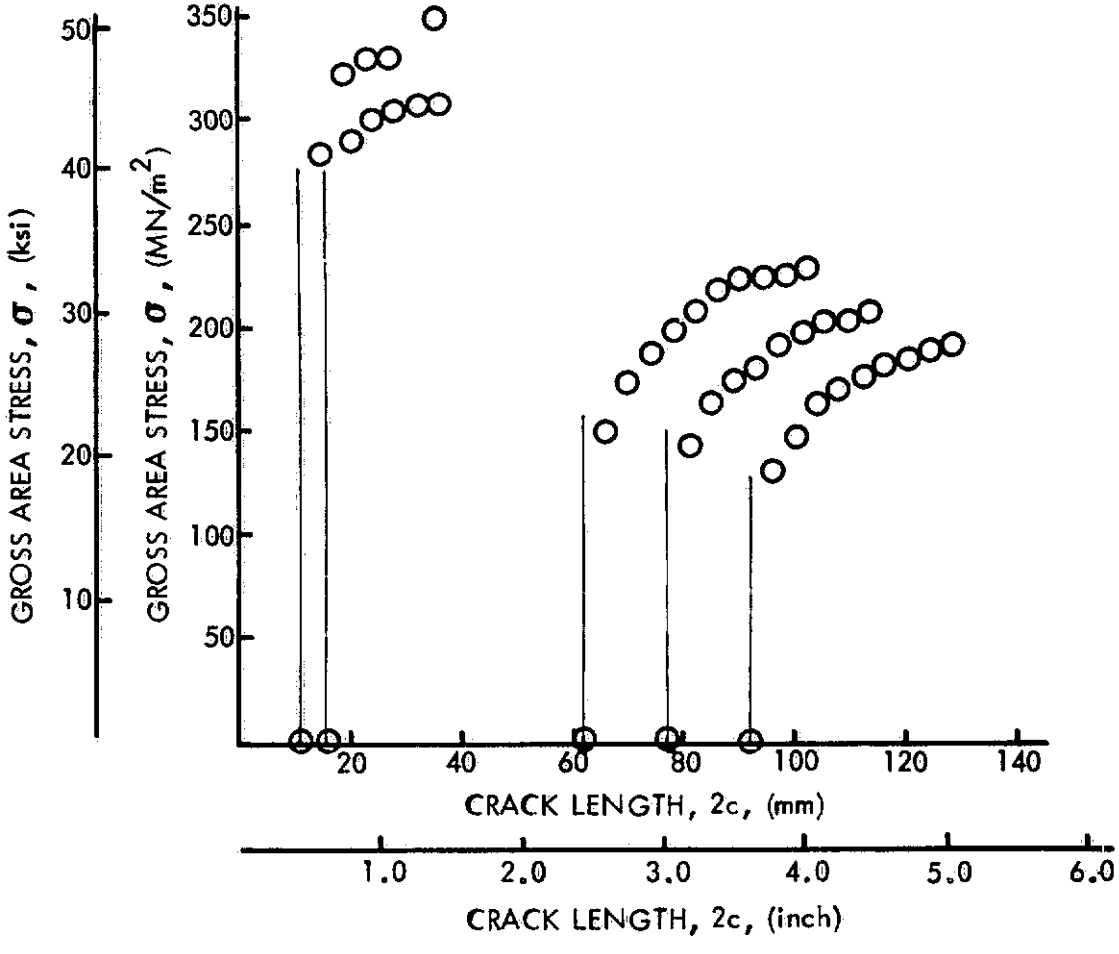

Figure 15 : GROSS AREA STRESS VERSUS CRACK LENGTH FOR 2219-T87 ALUMINUM CENTER CRACK PANEL AT ROOM TEMPERATURE (t = 4.77 mm(0.188 inch))

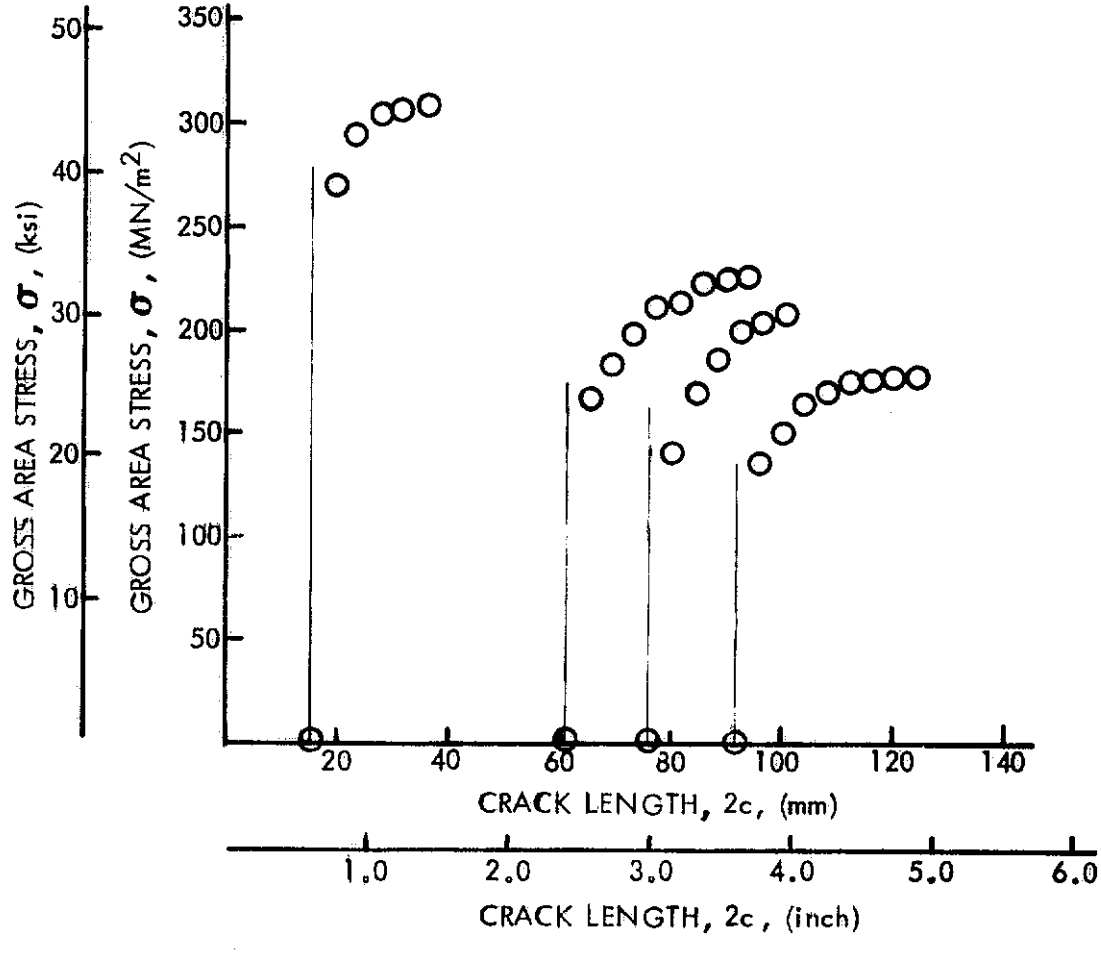

Figure 16 : GROSS AREA STRESS VERSUS CRACK LENGTH FOR 2219-T87 ALUMINUM CENTER CRACK PANELS AT ROOM TEMPERATURE (t = 1.91 mm (0.075 inch))

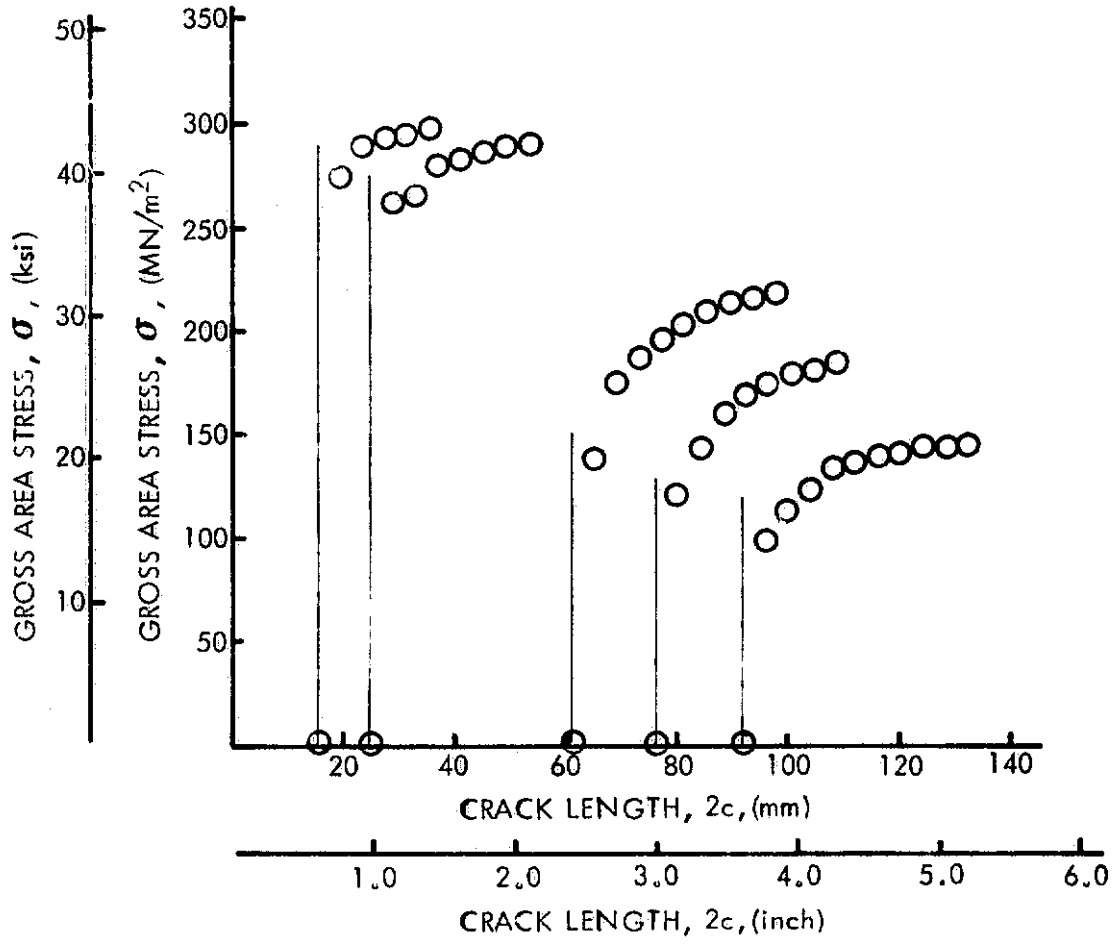

Figure 17 : GROSS AREA STRESS VERSUS CRACK LENGTH FOR 2219-T87 ALUMINUM CENTER CRACK PANEL AT ROOM TEMPERATURE (t = 0.635mm (0.025 inch))

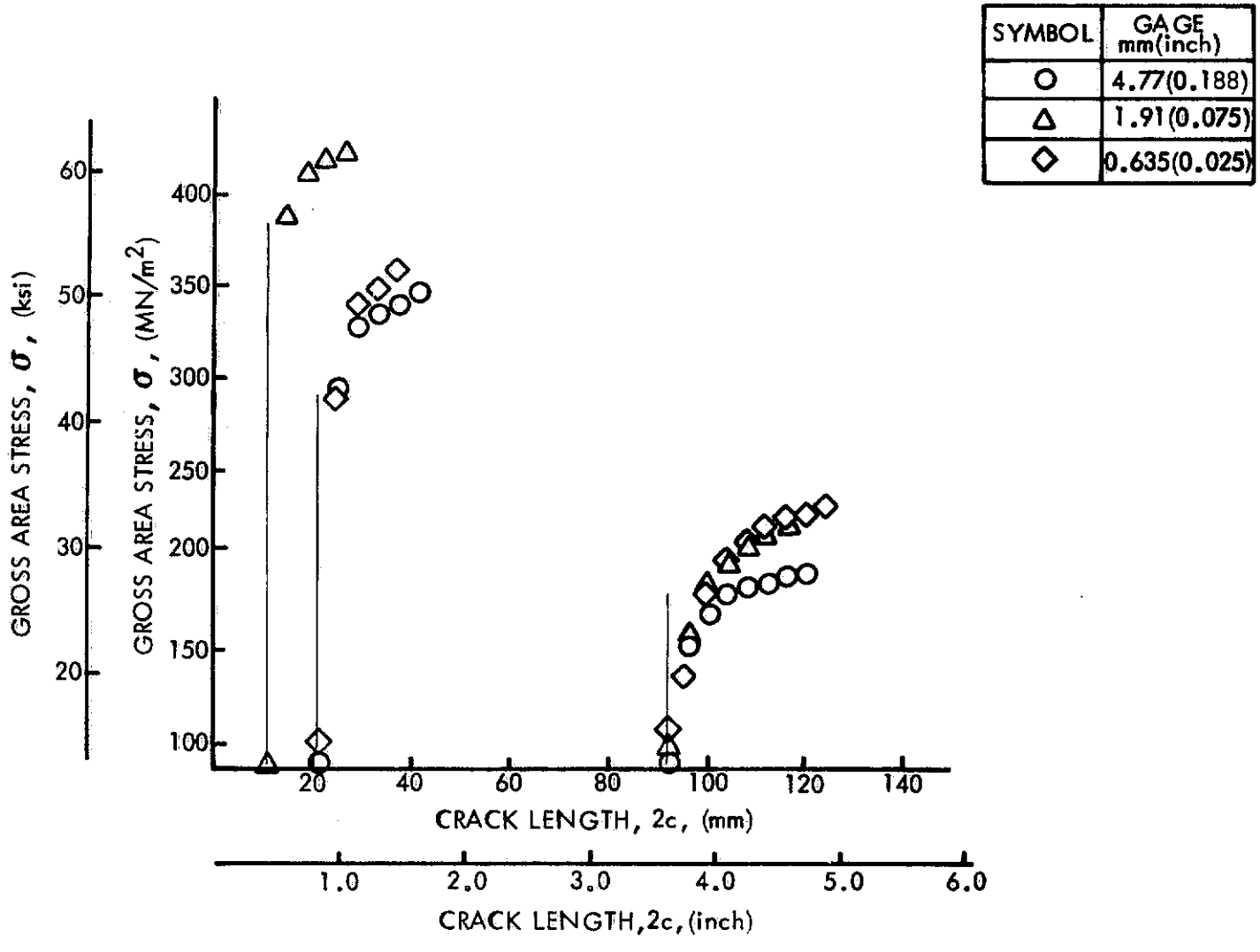

Figure 18 : GROSS AREA STRESS VERSUS CRACK LENGTH FOR 2219-T87 ALUMINUM CENTER CRACK PANEL AT 20°K (-423°F)

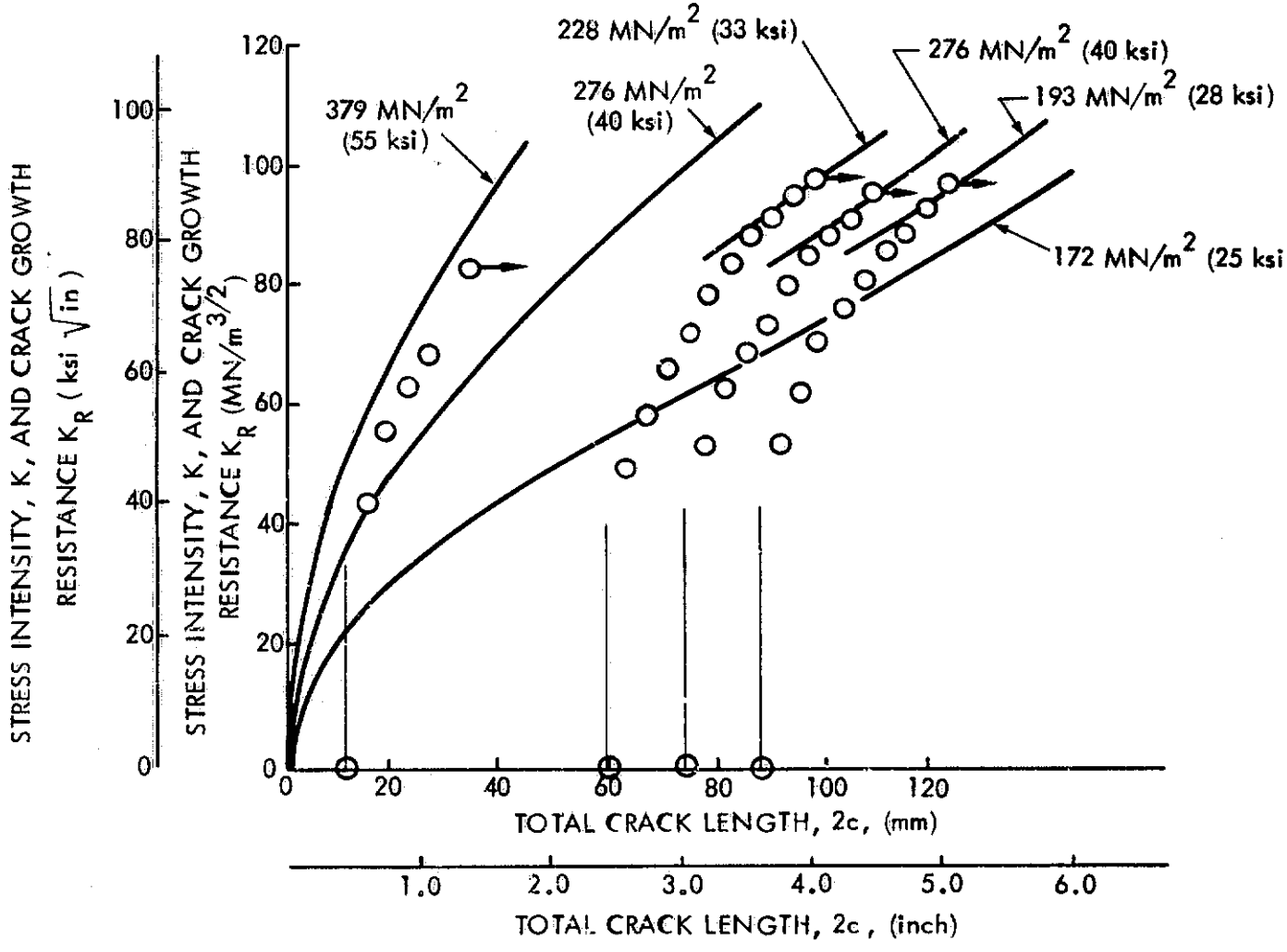

Figure 19 : CRACK GROWTH RESISTANCE AND STRESS INTENSITY CURVES FOR ROOM TEMPERATURE 2219-T87 ALUMINUM BASE METAL (t = 4.77 mm (0.188 inch))

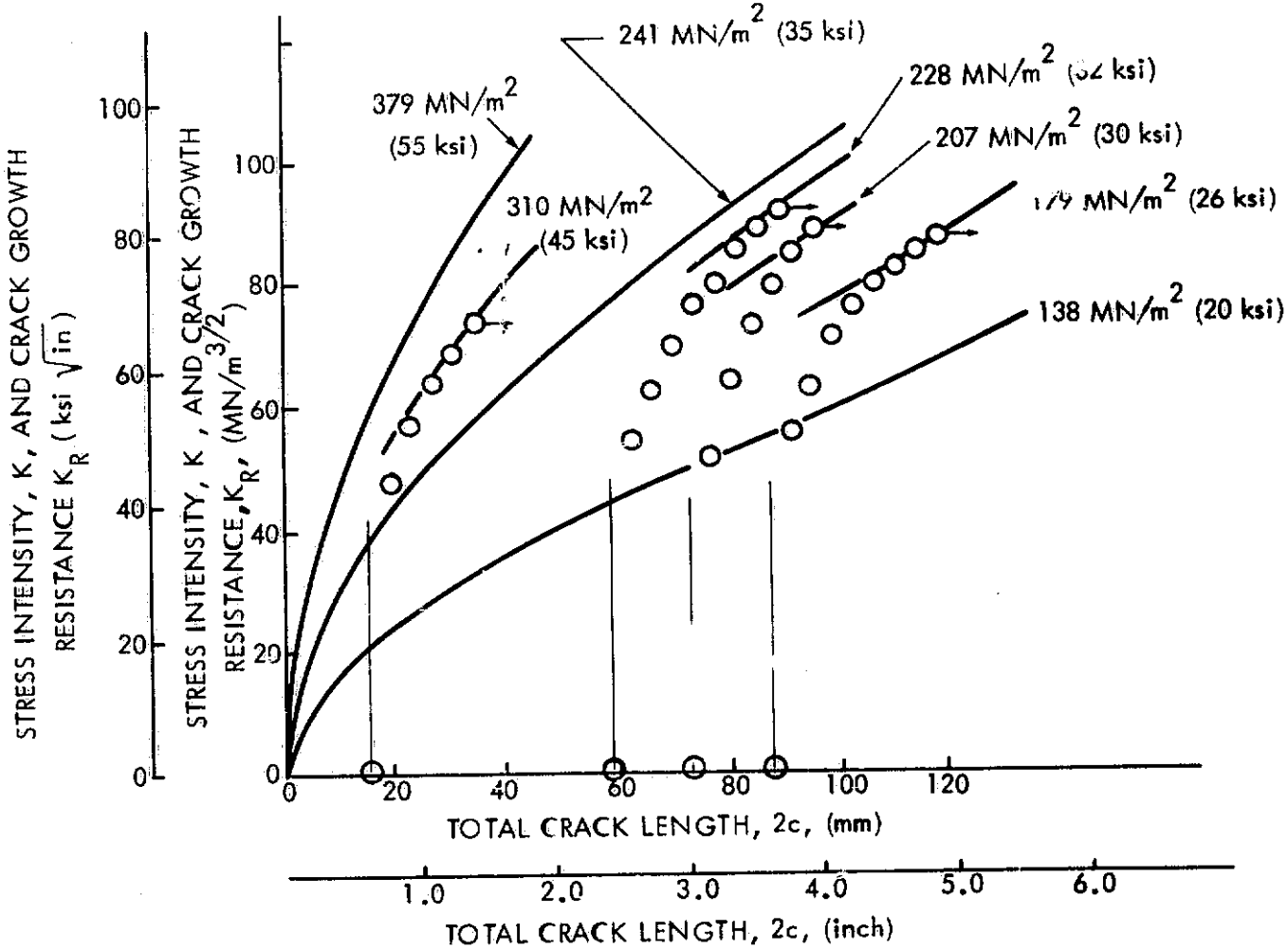

Figure 20 : CRACK GROWTH RESISTANCE AND STRESS INTENSITY CURVES FOR ROOM TEMPERATURE 2219-T87 ALUMINUM BASE METAL (t = 1.91mm (1.00))

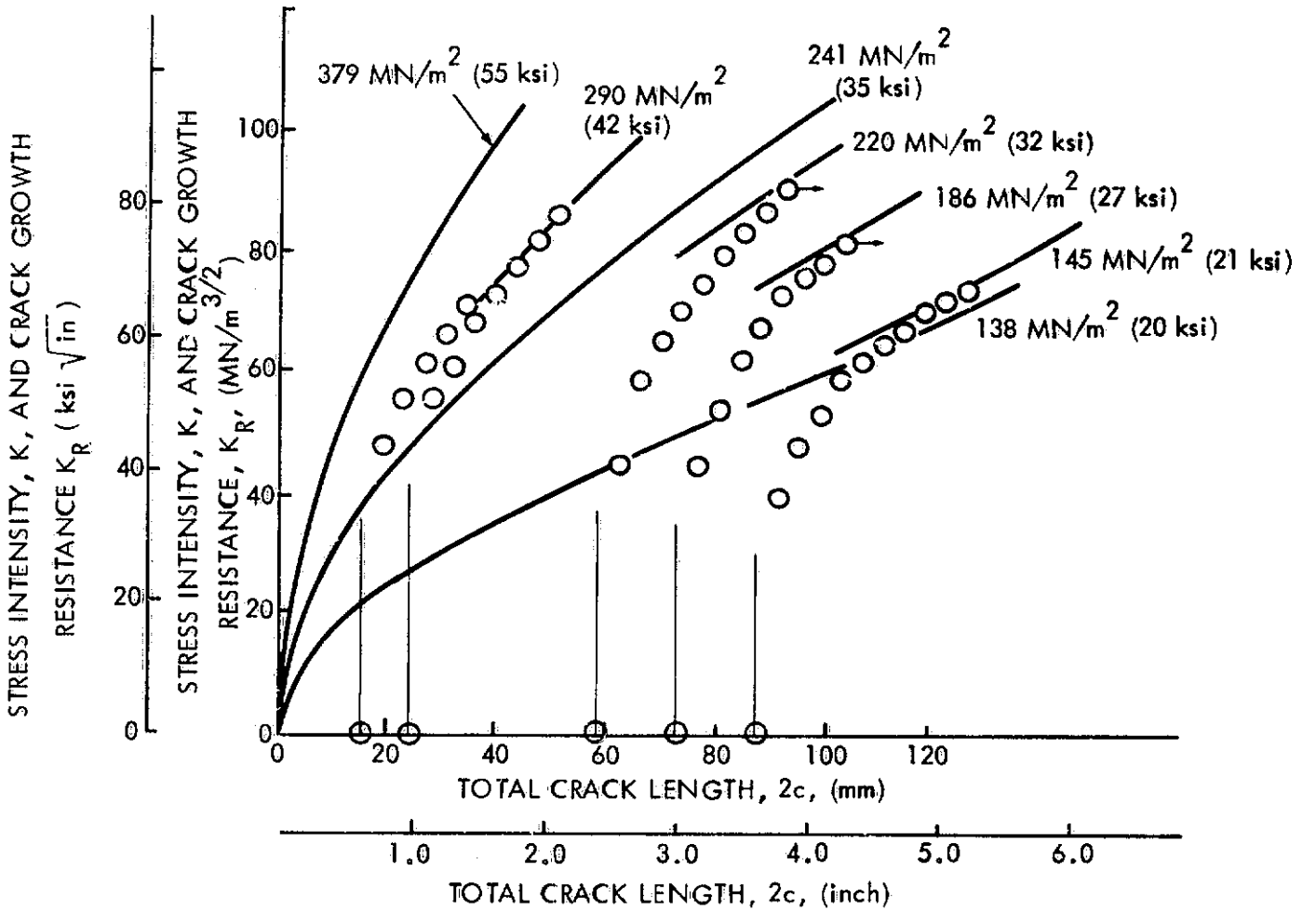

Figure 21 : CRACK GROWTH RESISTANCE AND STRESS INTENSITY CURVES FOR ROOM TEMPERATURE 2219-T87 ALUMINUM BASE METAL (t =0.635mm (0.025 inch))

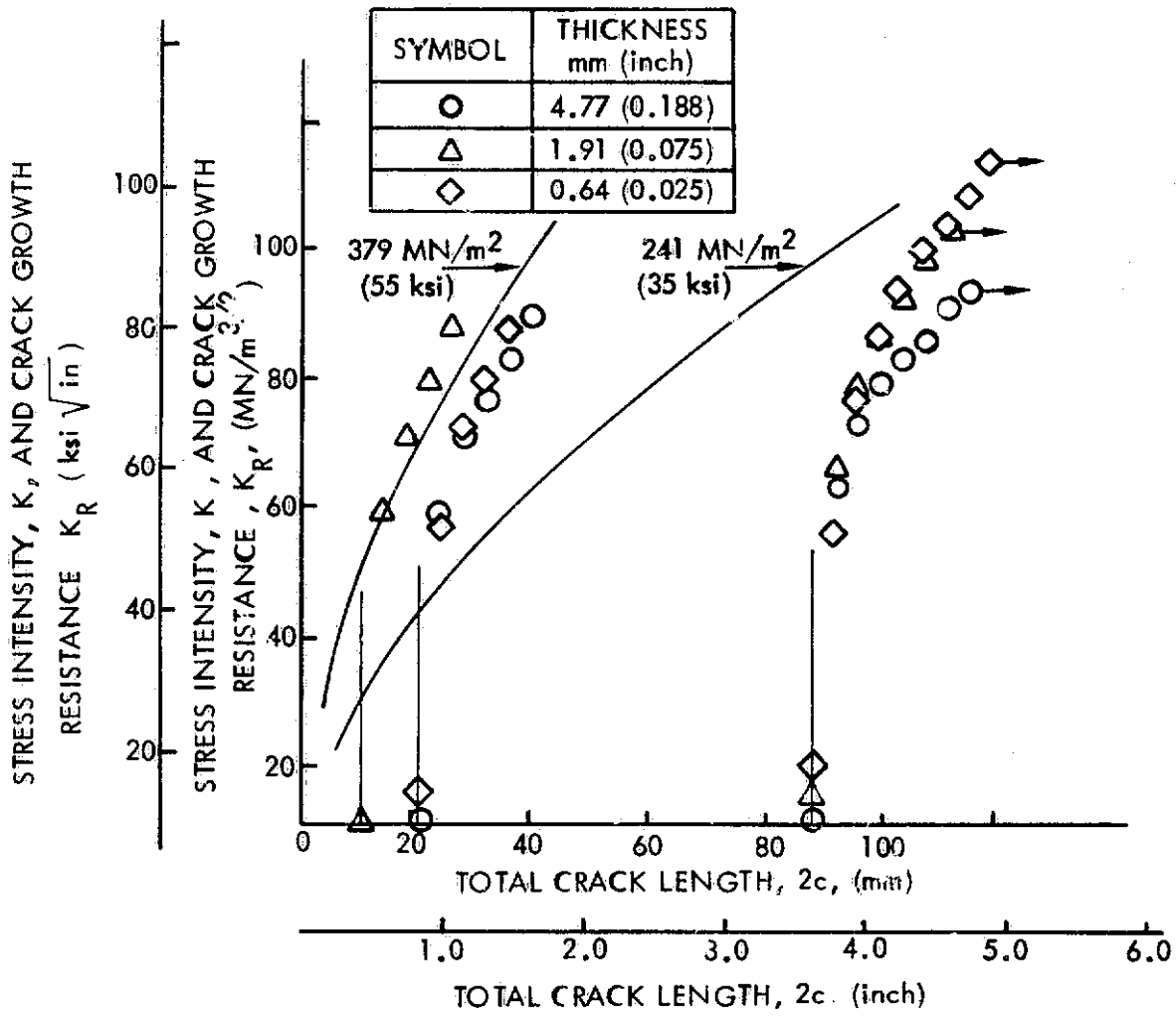

Figure 22 : CRACK GROWTH RESISTANCE AND STRESS INTENSITY CURVES VERSUS TOTAL CRACK LENGTH FOR LIQUID HYDROGEN TEMPERATURE 2219-T87 ALUMINUM BASE METAL

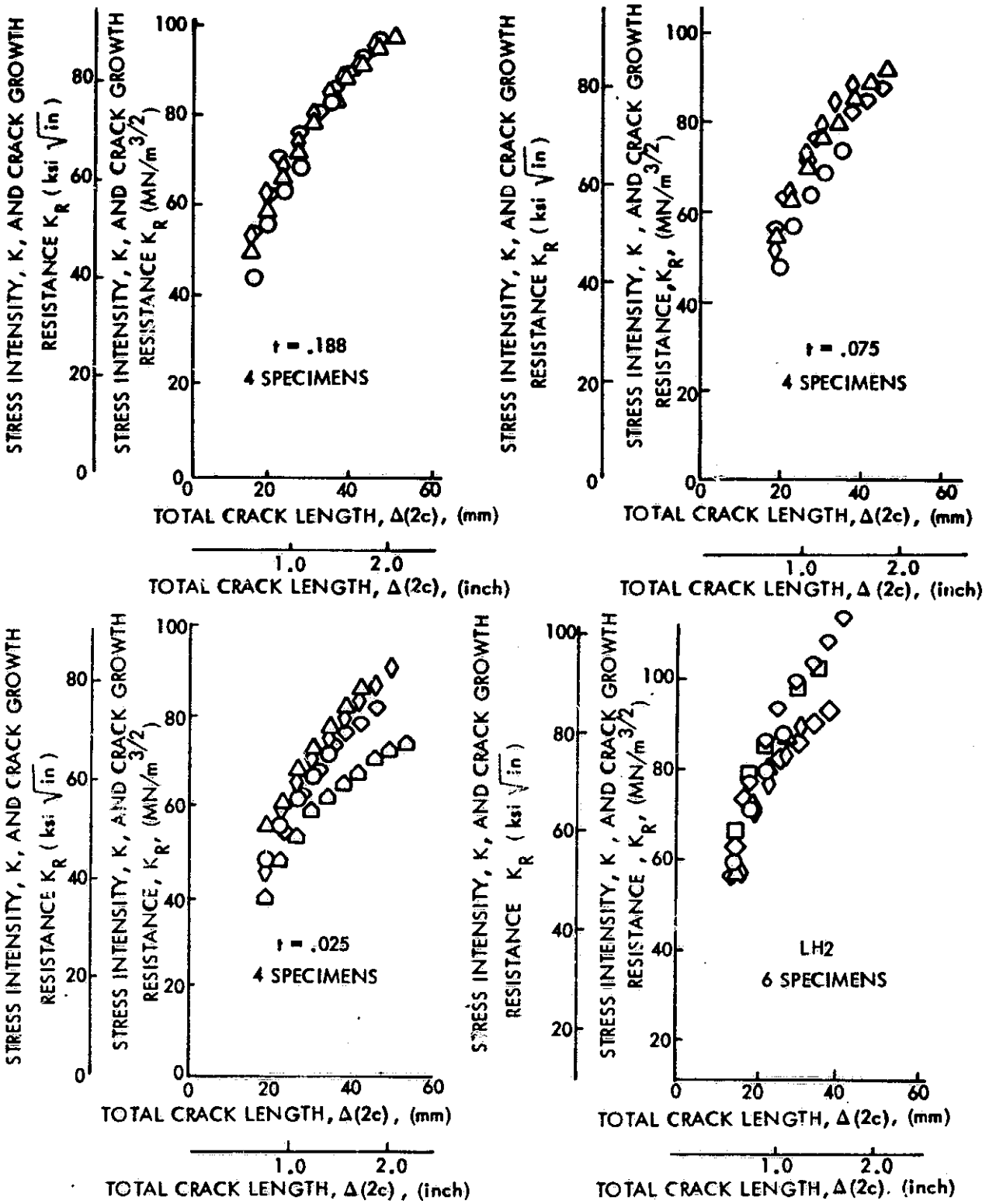

Figure 23: STRESS INTENSITY VERSUS CRACK GROWTH FOR 2219-T87 ALUMINUM CENTER CRACK SPECIMENS

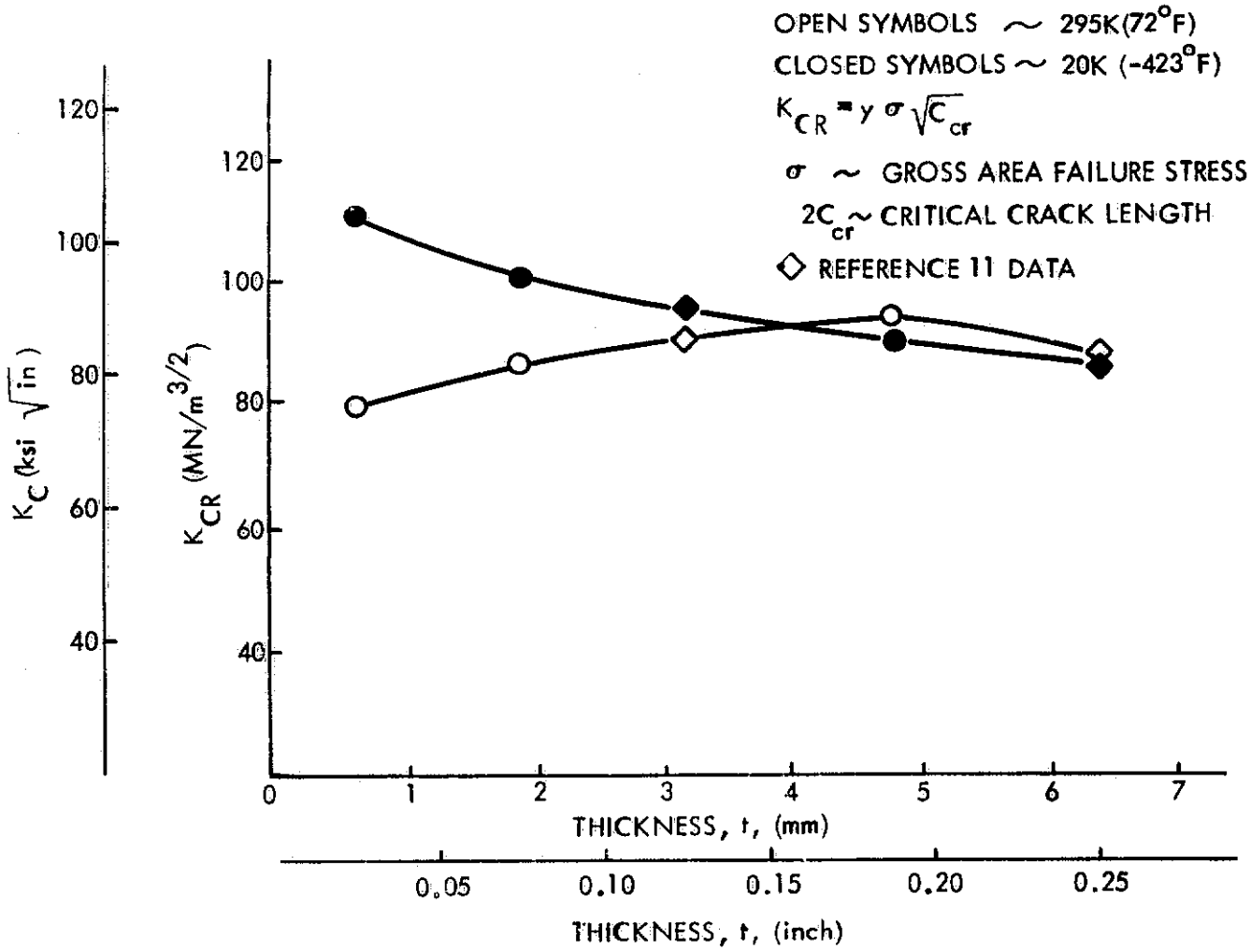

Figure 24: EFFECT OF THICKNESS ON 2219-T87 ALUMINUM BASE METAL K_C VALUES

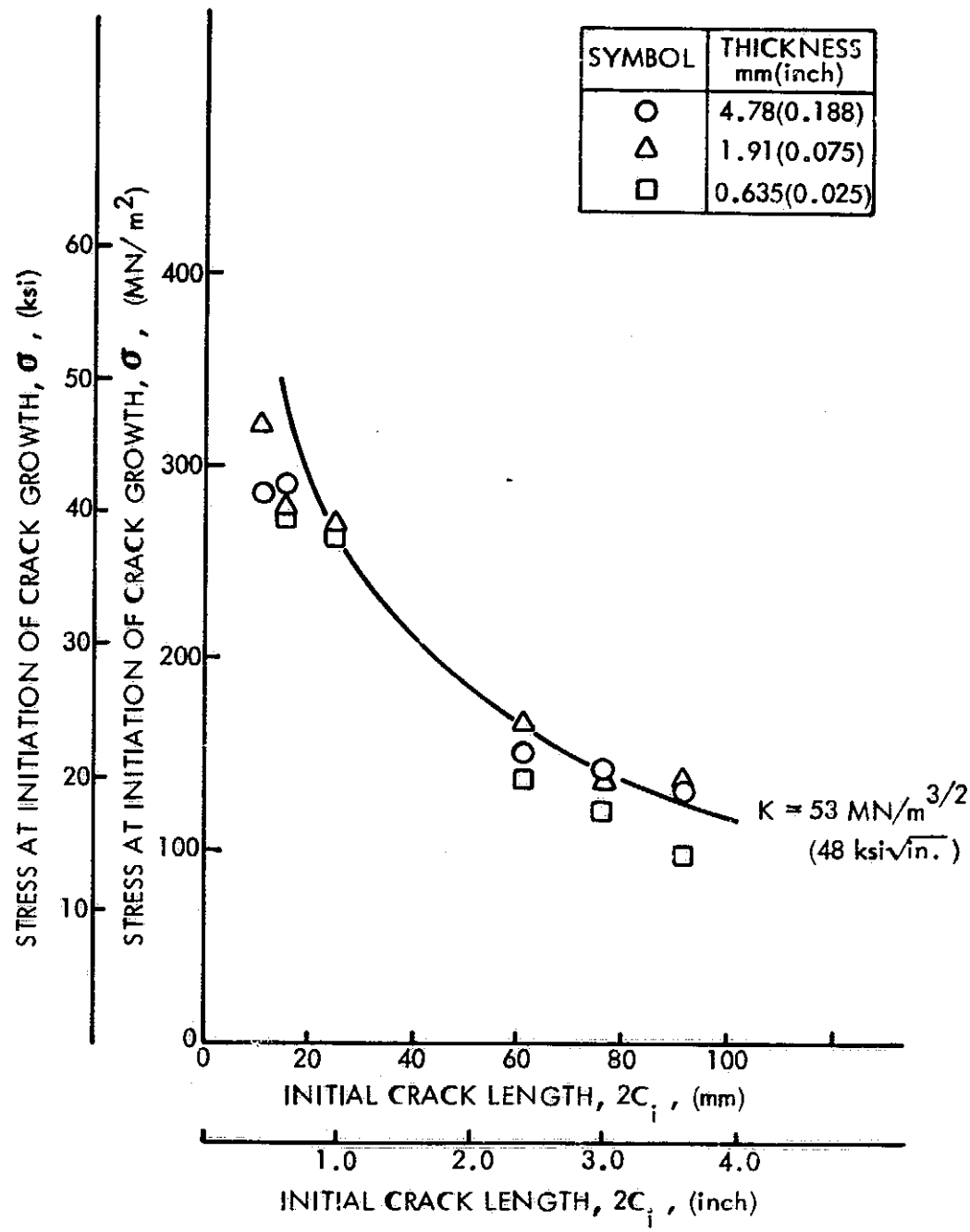

Figure 25 : GROSS AREA STRESS AT INITIATION OF CRACK GROWTH VERSUS INITIAL CRACK LENGTH FOR 2219-T87 ALUMINUM BASE METAL CENTER CRACK PANELS AT ROOM TEMPERATURE

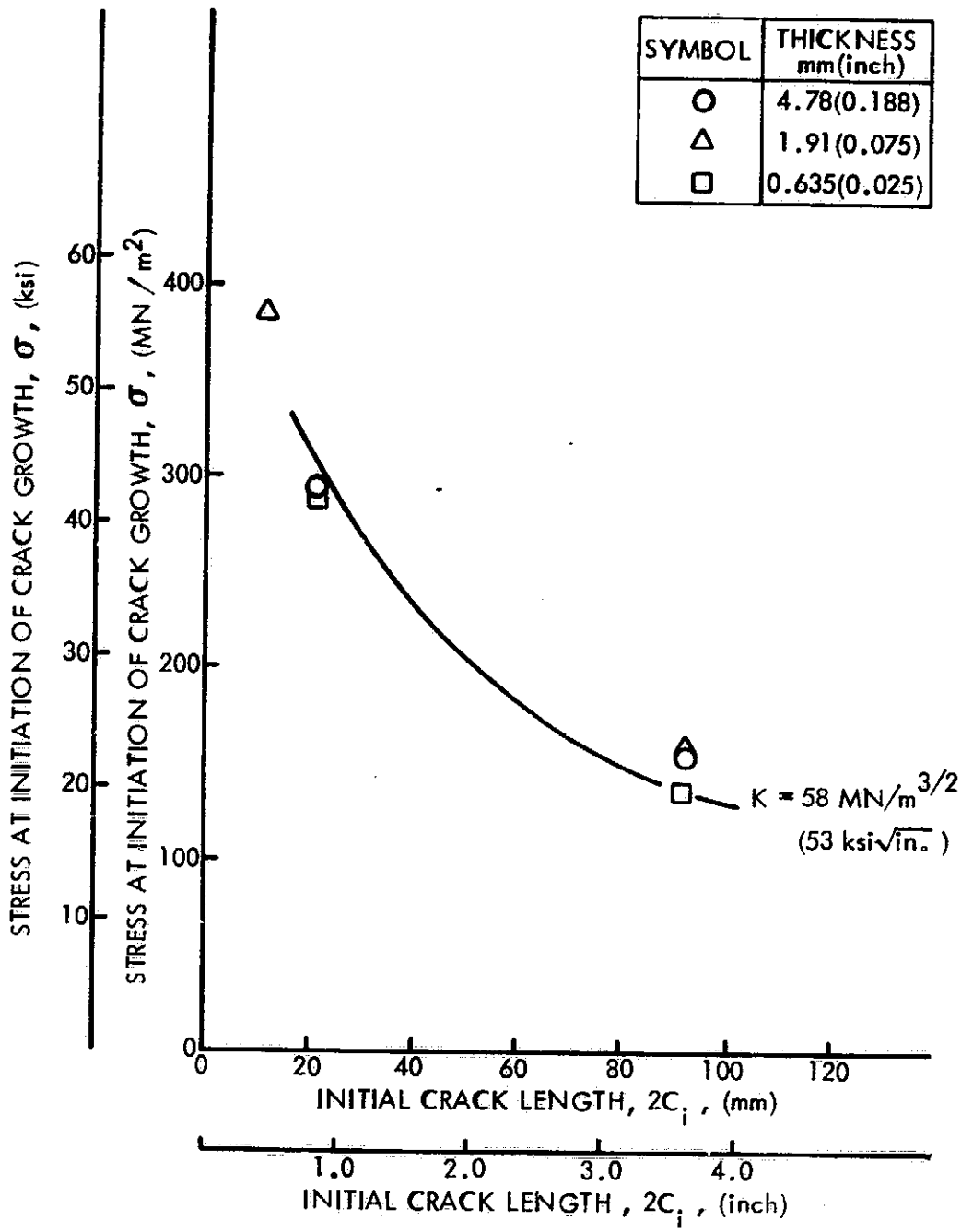

Figure 26 : GROSS AREA STRESS AT INITIATION OF CRACK GROWTH VERSUS INITIAL CRACK LENGTH FOR 2219-T87 ALUMINUM BASE METAL CENTER CRACK PANELS AT LIQUID HYDROGEN TEMPERATURE

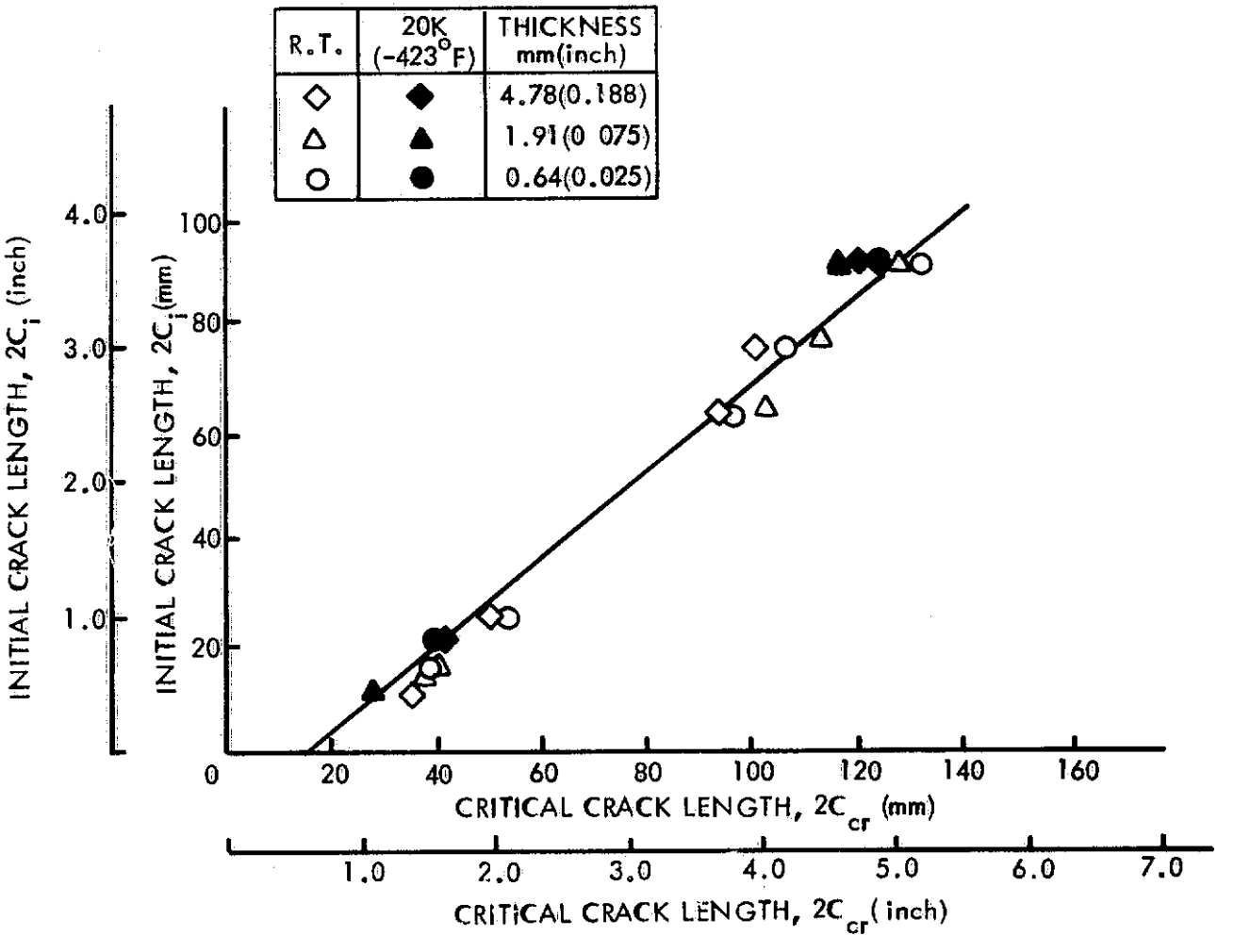

Figure 27 : INITIAL CRACK LENGTH VERSUS CRITICAL CRACK LENGTH FOR 2219-T87 ALUMINUM BASE METAL CENTER CRACK PANELS

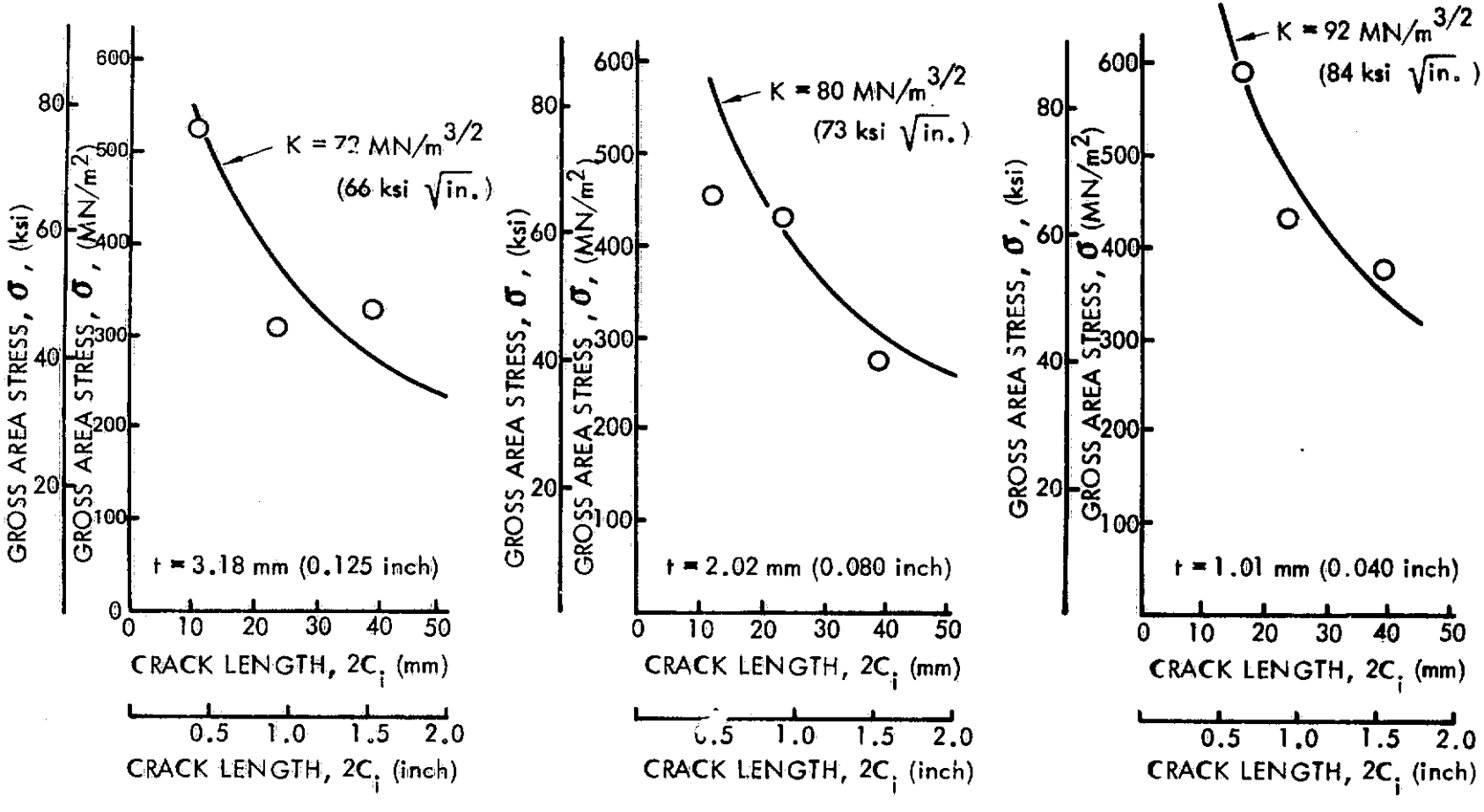

Figure 28 : GROSS AREA FAILURE STRESS VERSUS INITIAL CRACK LENGTH FOR 6Al-4V STA TITANIUM CENTER CRACK PANELS

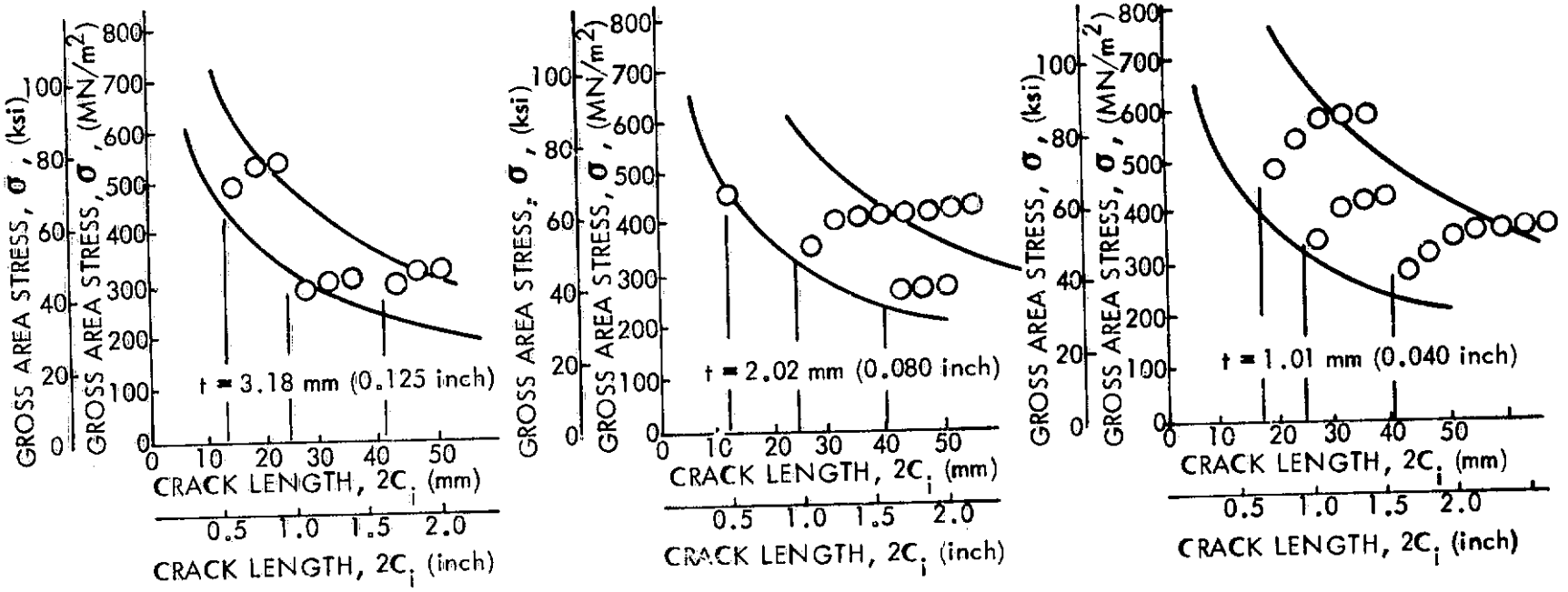

Figure 29: GROSS AREA STRESS VERSUS CRACK LENGTH FOR 6Al-4V STA TITANIUM CENTER CRACK PANELS

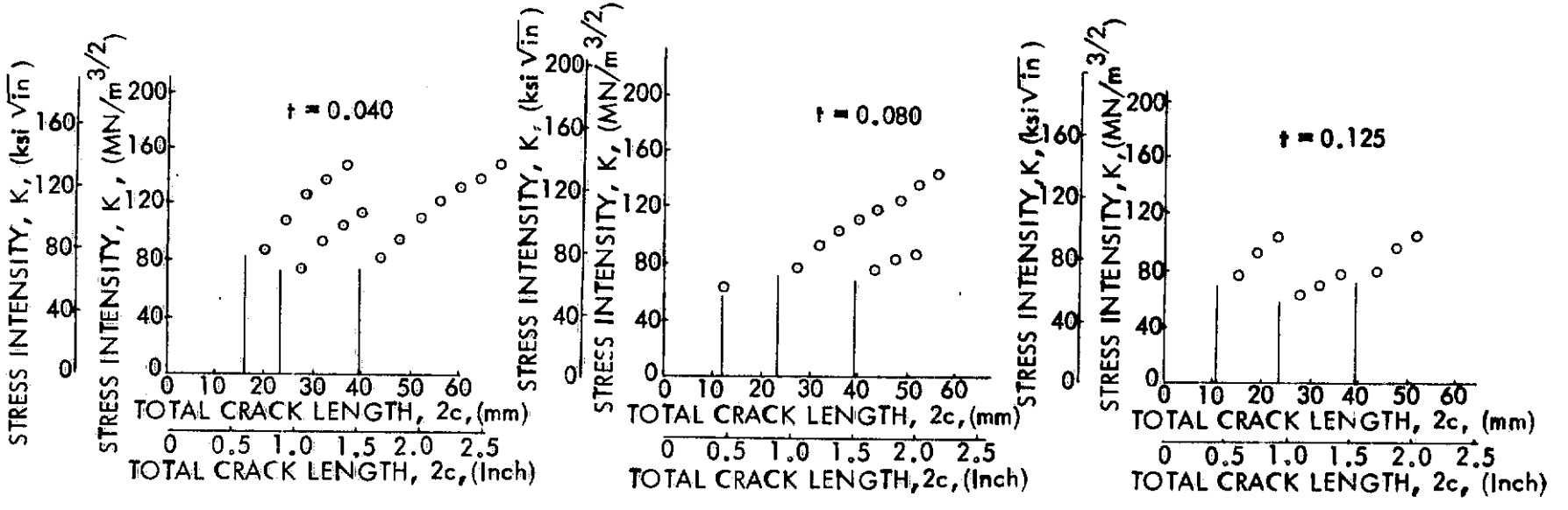

Figure 30: CRACK GROWTH RESISTANCE AND STRESS INTENSITY CURVES VERSUS TOTAL CRACK LENGTH FOR ROOM TEMPERATURE 6AI-4V STA TITANIUM CENTER CRACK PANELS

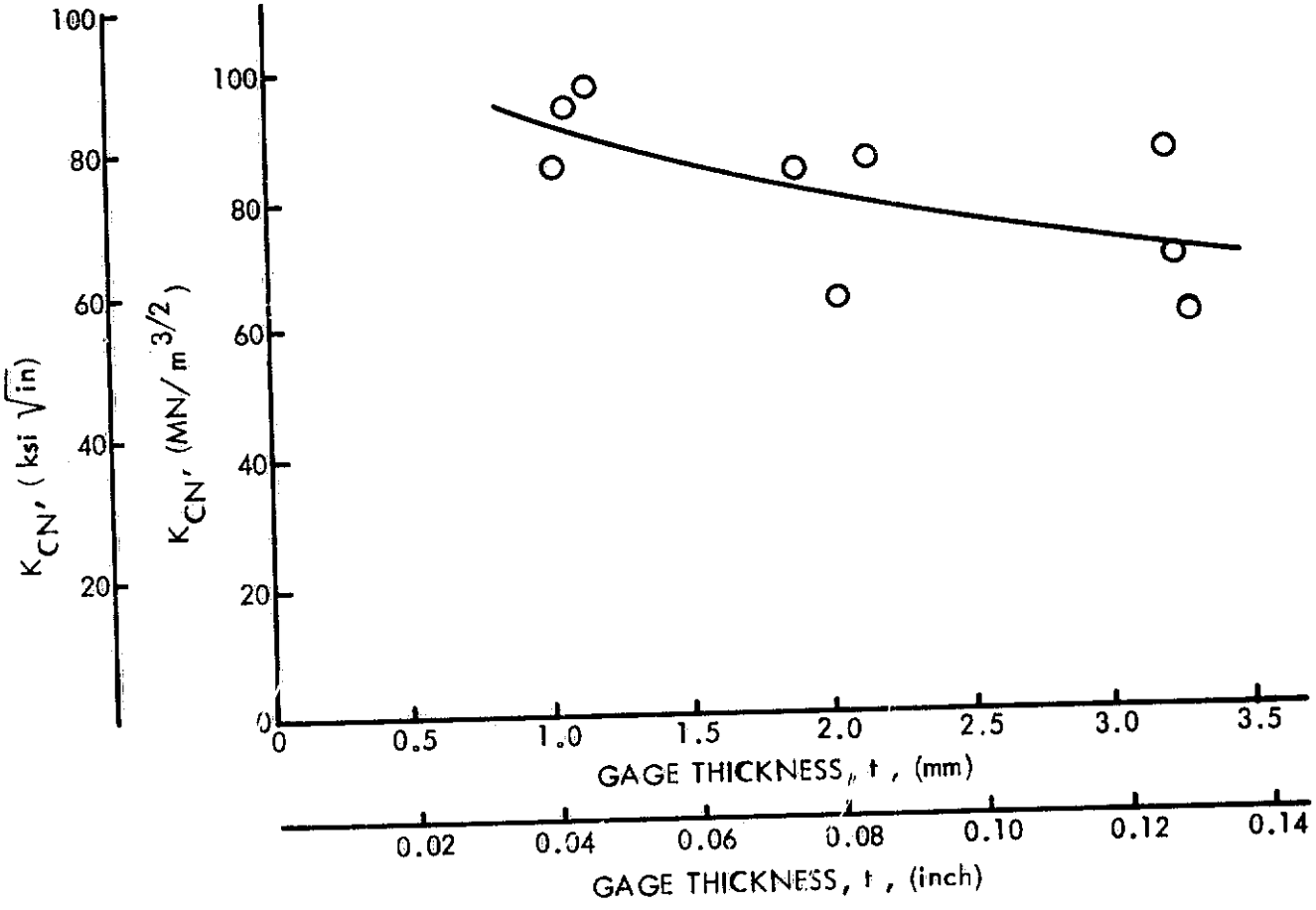

Figure 31 : K_{CN} VERSUS GAGE THICKNESS FOR 6Al-4V STA TITANIUM CENTER CRACK PANELS

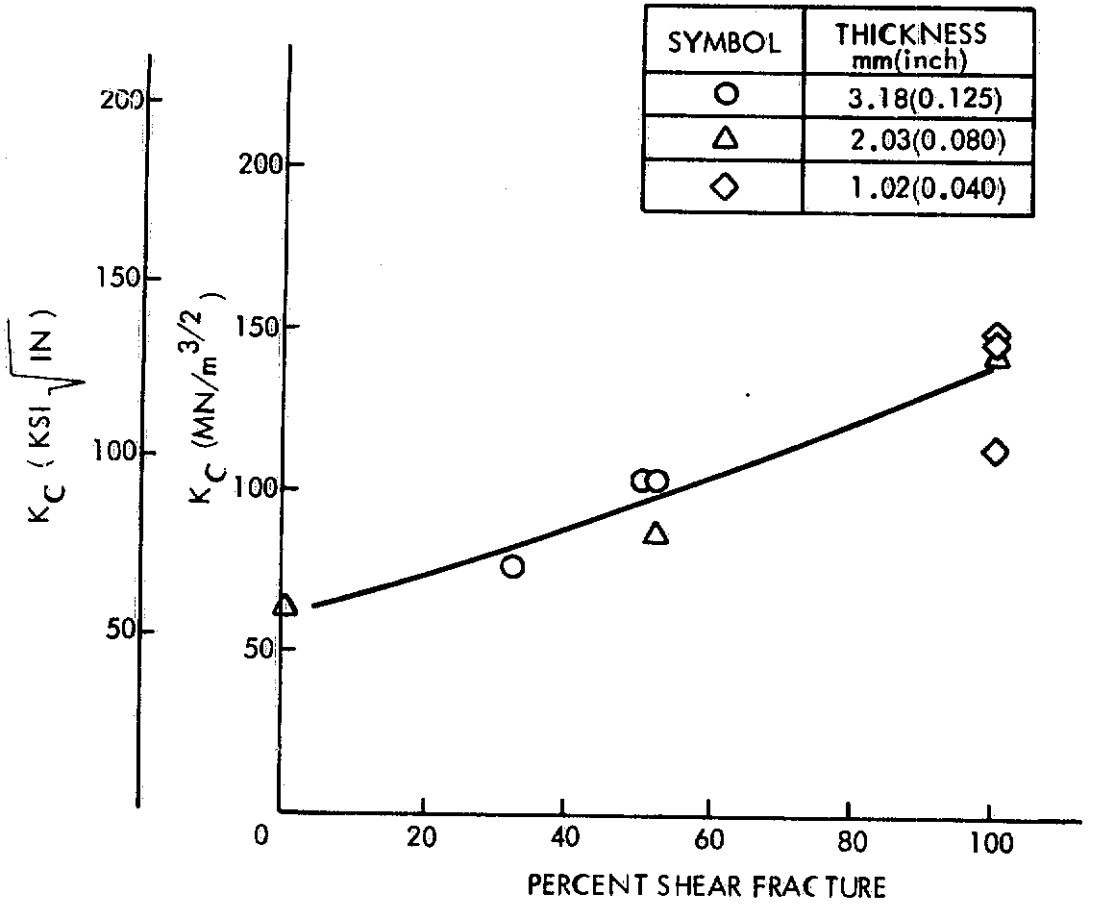

Figure 32: K_C VERSUS PERCENT SHEAR FRACTURE AT CRITICAL CRACK LENGTH FOR 6Al-4V STA TITANIUM CENTER CRACK PANELS

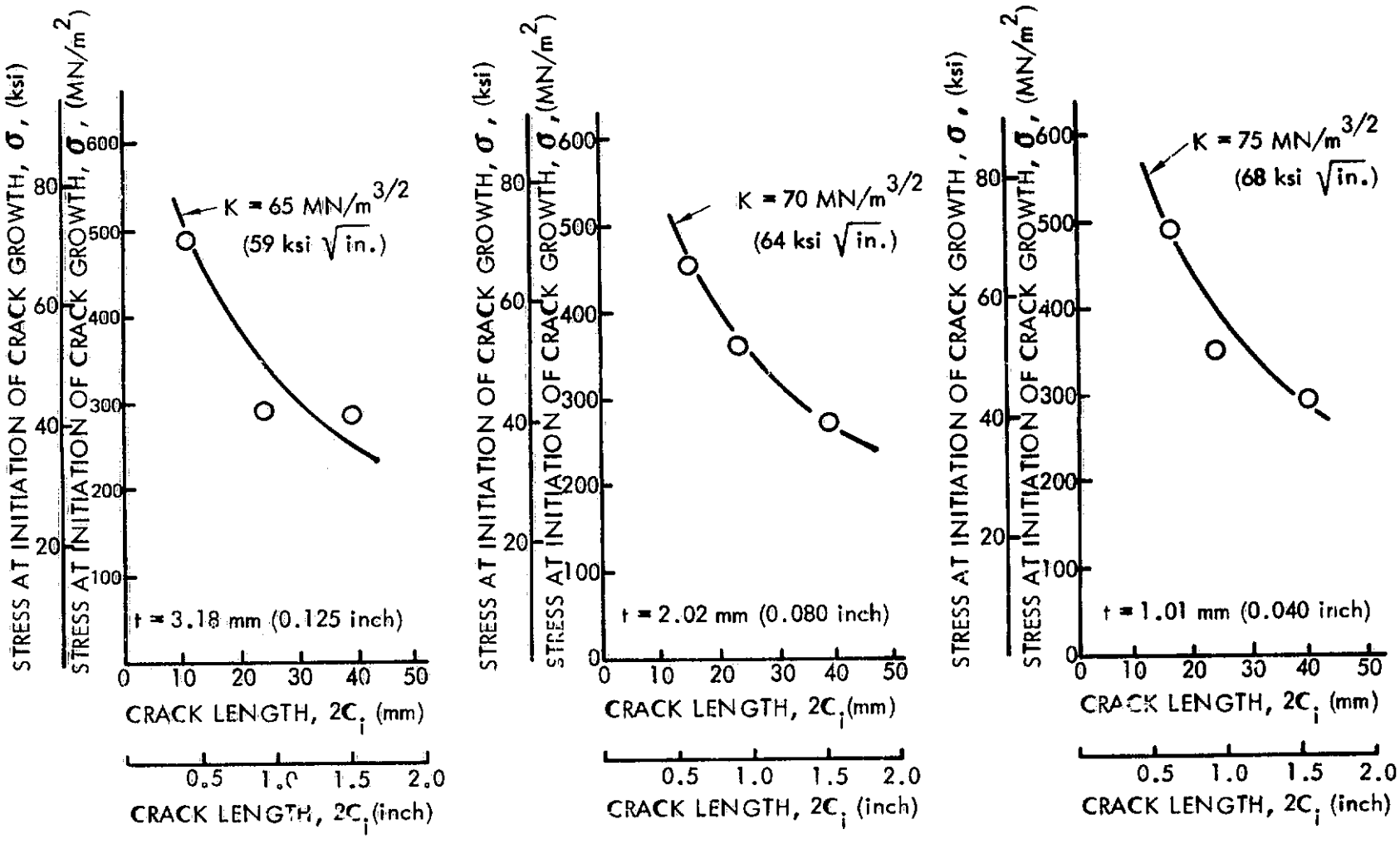

Figure 33 : GROSS AREA STRESS AT INITIATION OF CRACK GROWTH VERSUS INITIAL CRACK LENGTH FOR 6Al-4V STA TITANIUM CENTER CRACK PANEL AT ROOM TEMPERATURE

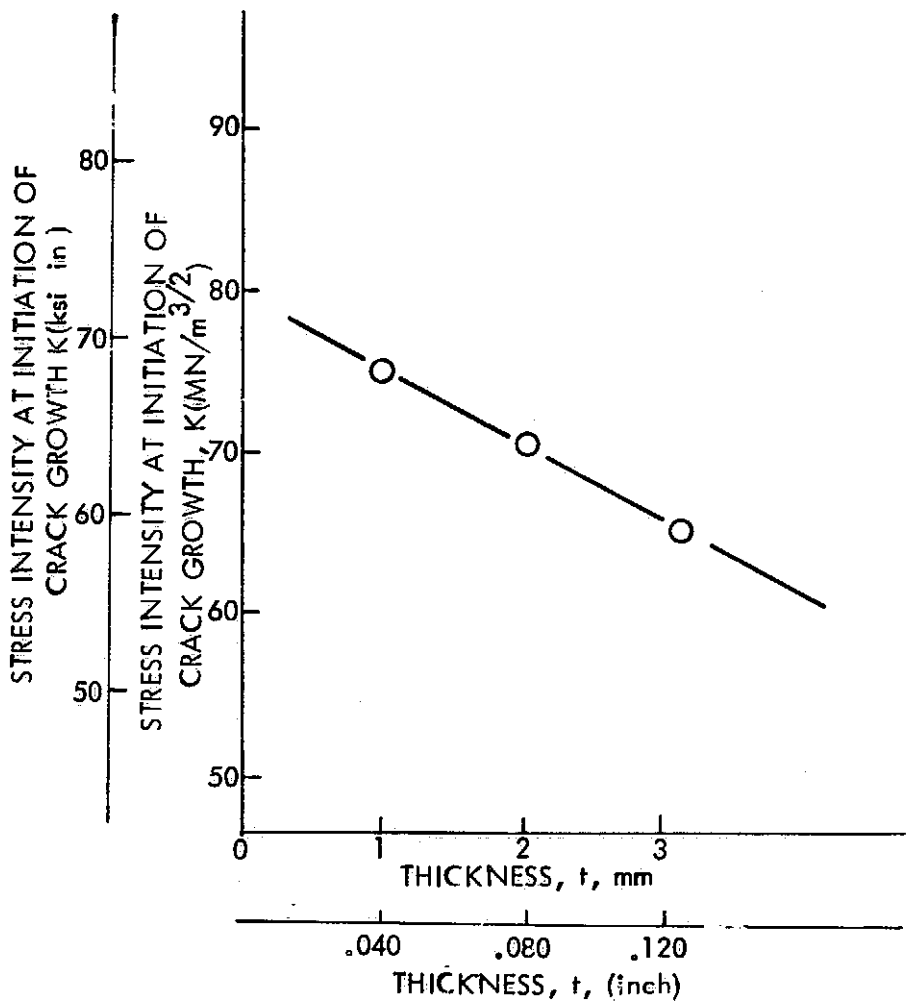

Figure 34: STRESS INTENSITY AT INITIATION OF CRACK GROWTH VERSUS THICKNESS FOR 6Al-4V TITANIUM CENTER CRACK PANELS

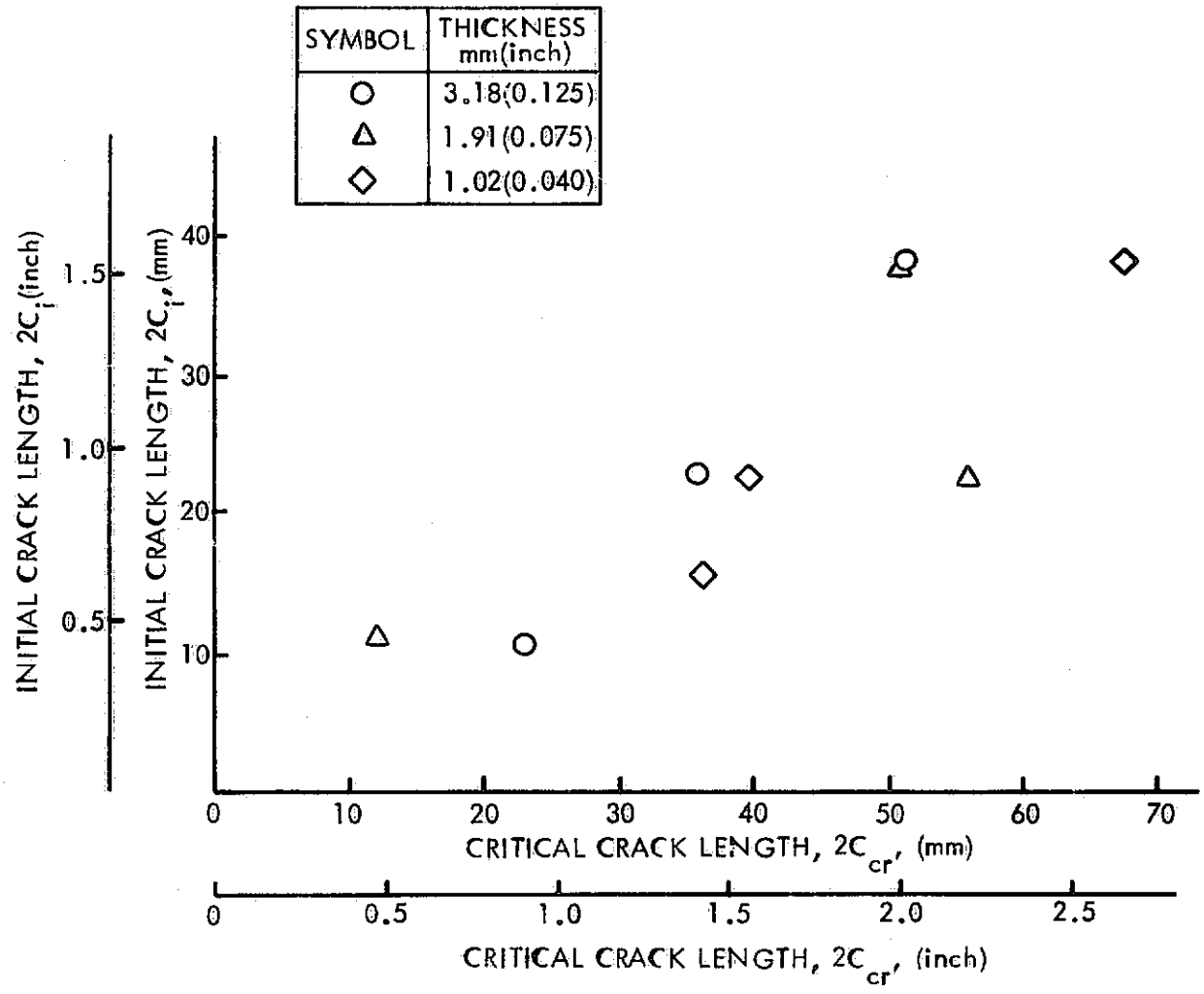

Figure 35 : INITIAL CRACK LENGTH VERSUS CRITICAL CRACK LENGTH FOR 6AI-4V TITANIUM BASE METAL CENTER CRACK PANELS

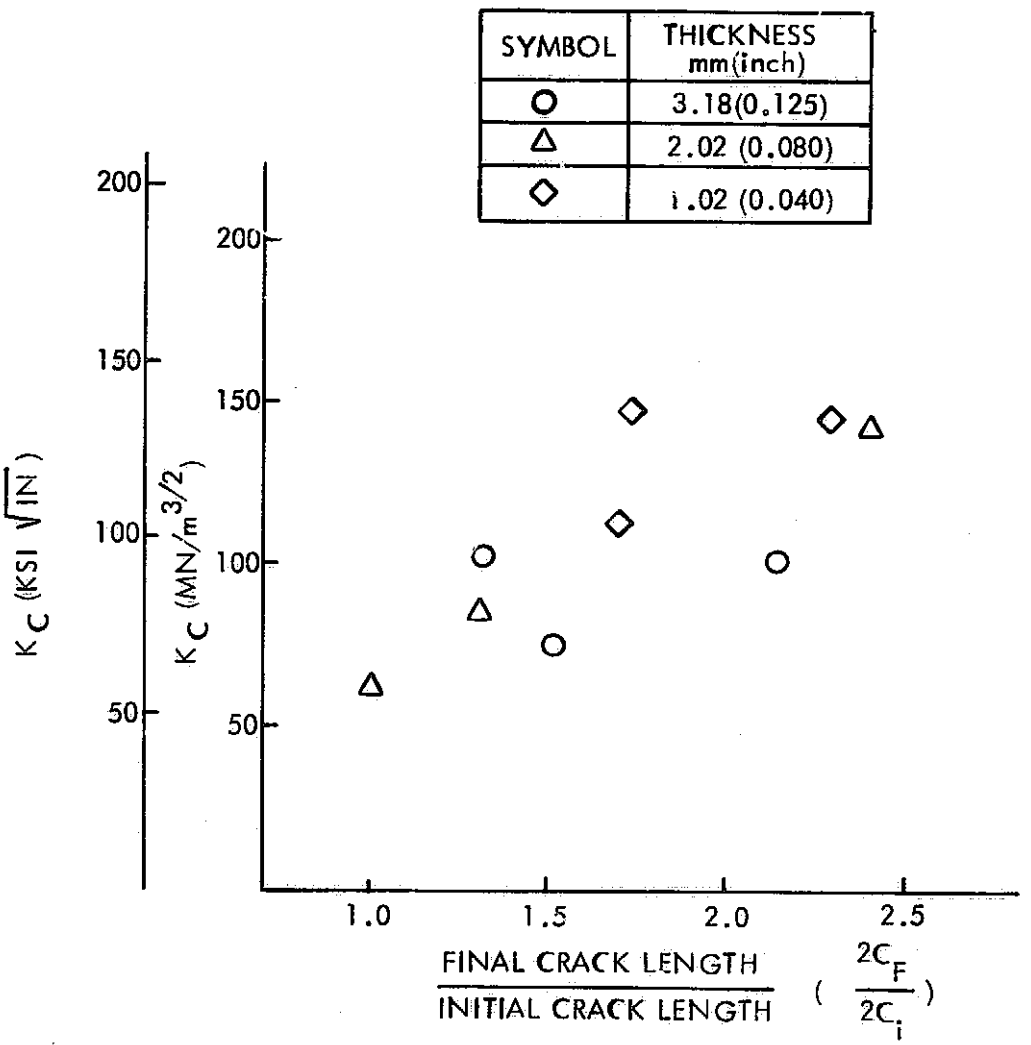

Figure 36 : K_{cr} VERSUS RATIO OF FINAL TO INITIAL CRACK LENGTH FOR 6Al-4V STA TITANIUM CENTER CRACK PANELS

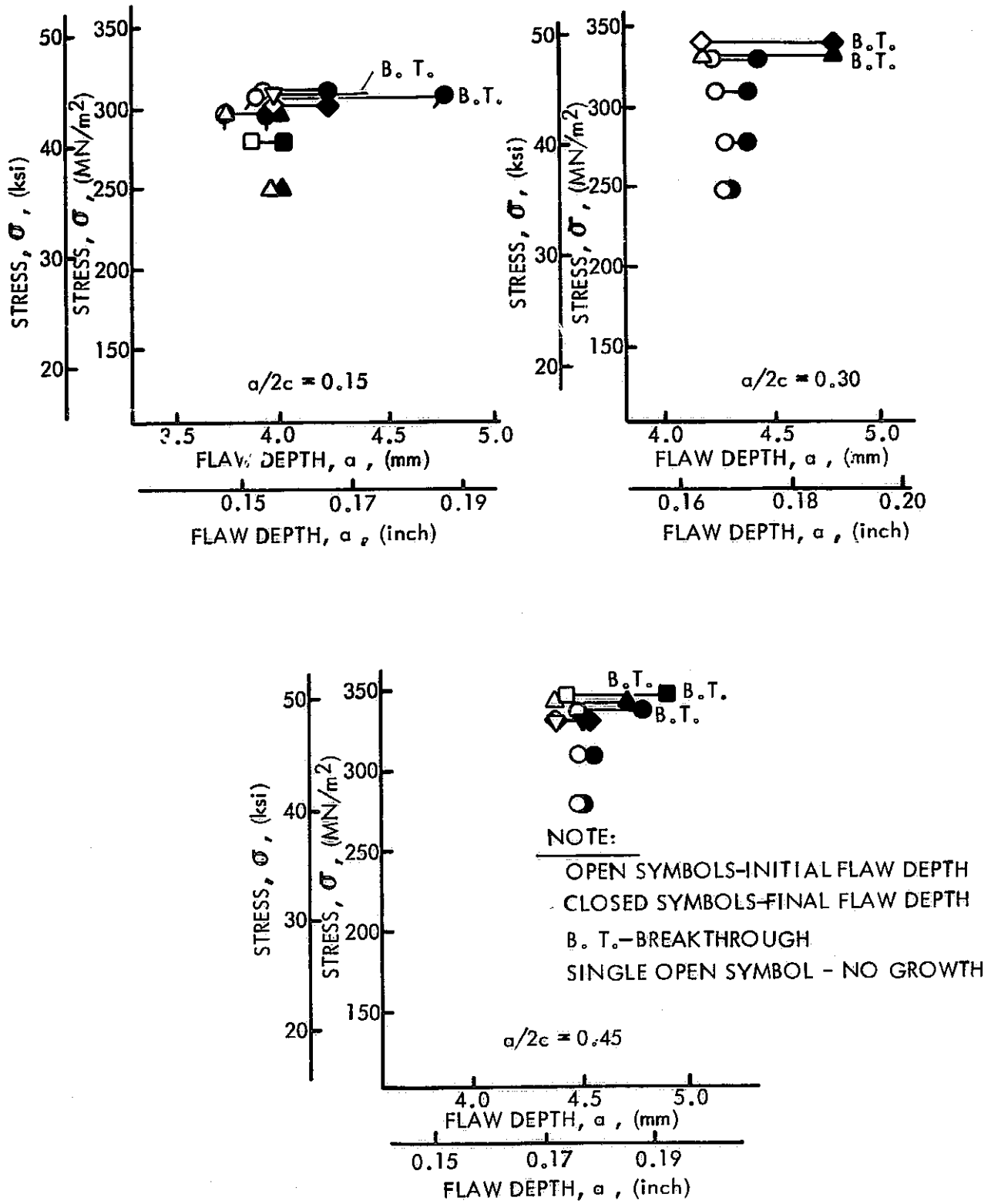

Figure 37 : GROWTH-ON-LOADING TEST RESULTS FOR 4.78mm(0.188 inch) THICK 2219-T87 ALUMINUM BASE METAL AT ROOM TEMPERATURE

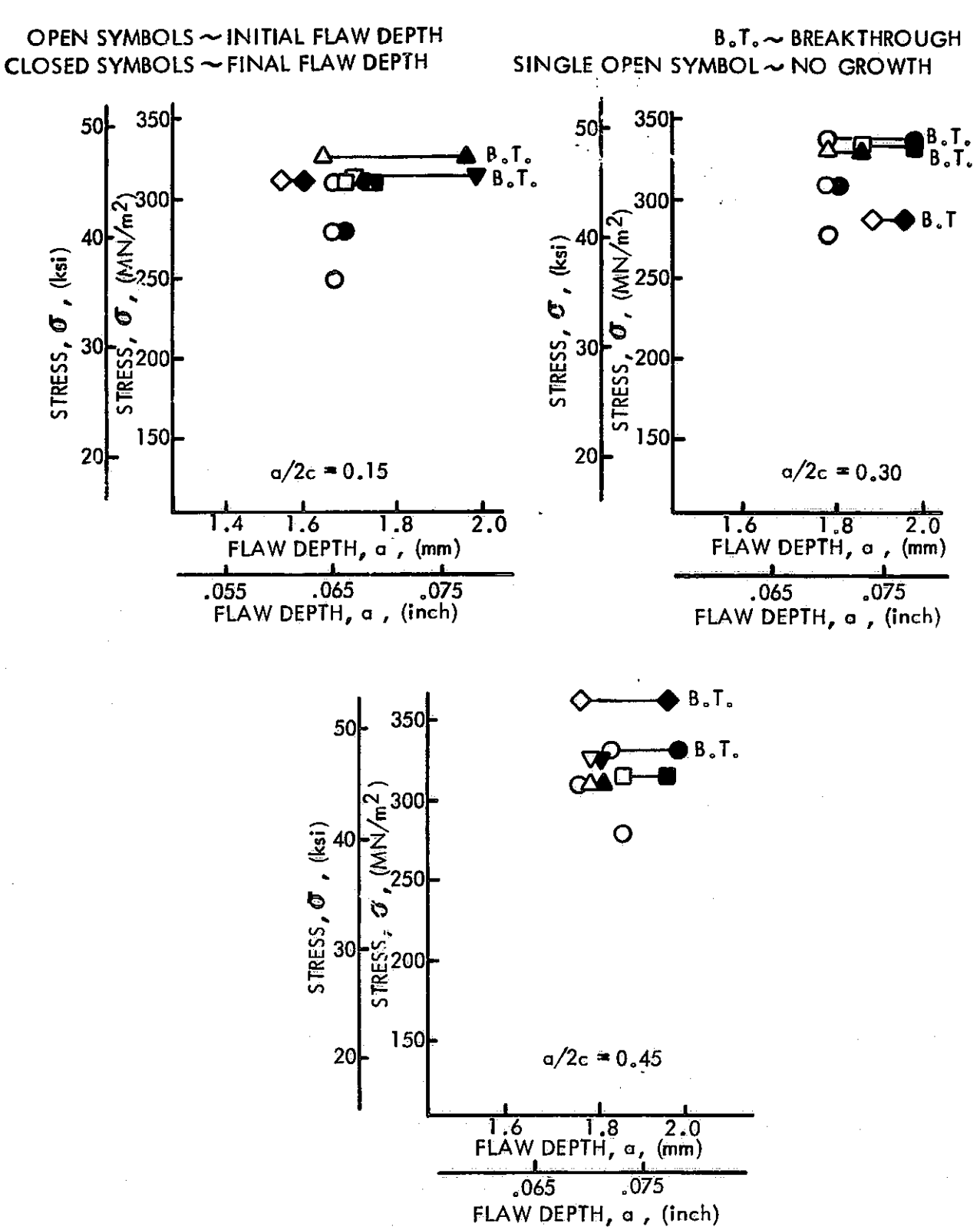

Figure 38 : GROWTH-ON-LOADING TEST RESULTS FOR 1.91mm(0.075 inch) THICK 2219-T87 ALUMINUM BASE METAL AT ROOM TEMPERATURE

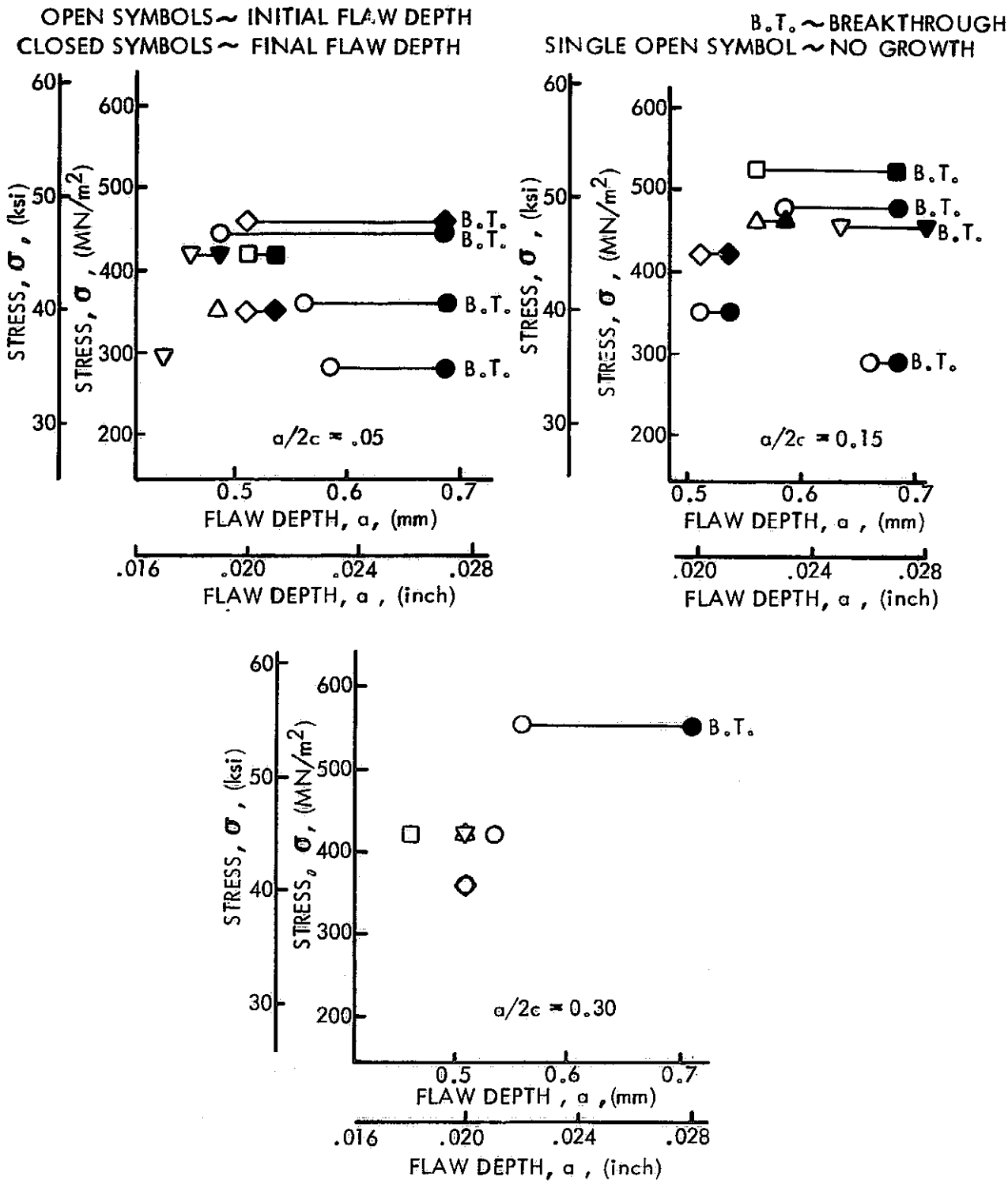

Figure 39 :GROWTH-ON-LOADING TEST RESULTS FOR 0.635mm (0.025 inch) THICK 2219-T87 ALUMINUM BASE METAL AT ROOM TEMPERATURE

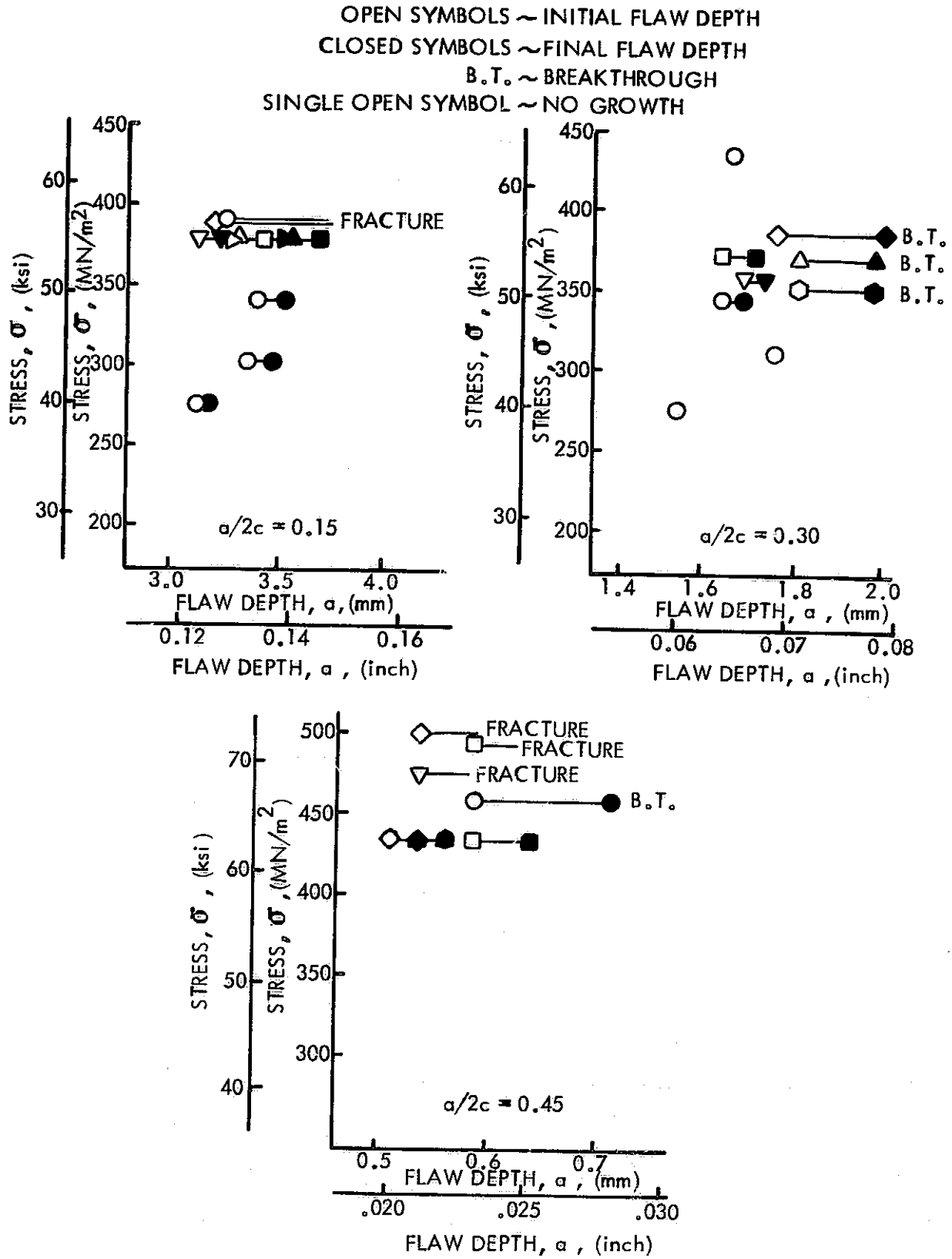

Figure 40 : GROWTH-ON-LOADING TEST RESULTS FOR 2219-T87 ALUMINUM BASE METAL AT LIQUID HYDROGEN TEMPERATURE

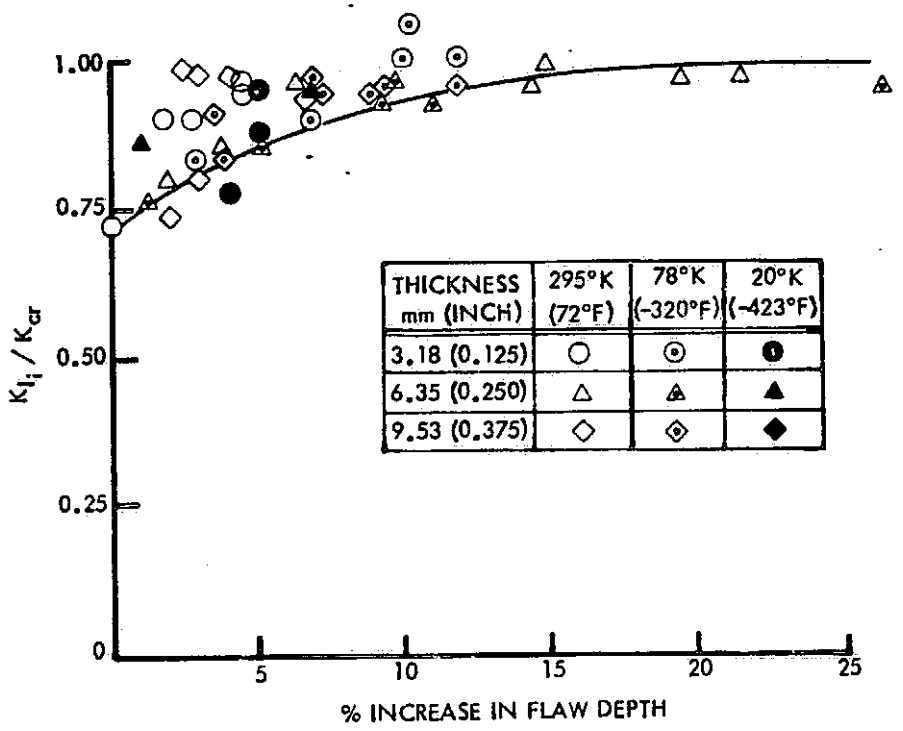

Figure 41 : 2219-T87 ALUMINUM BASE METAL GROWTH-ON-LOADING TEST RESULTS ($a/2c = 0.15$) (REFERENCE 11)

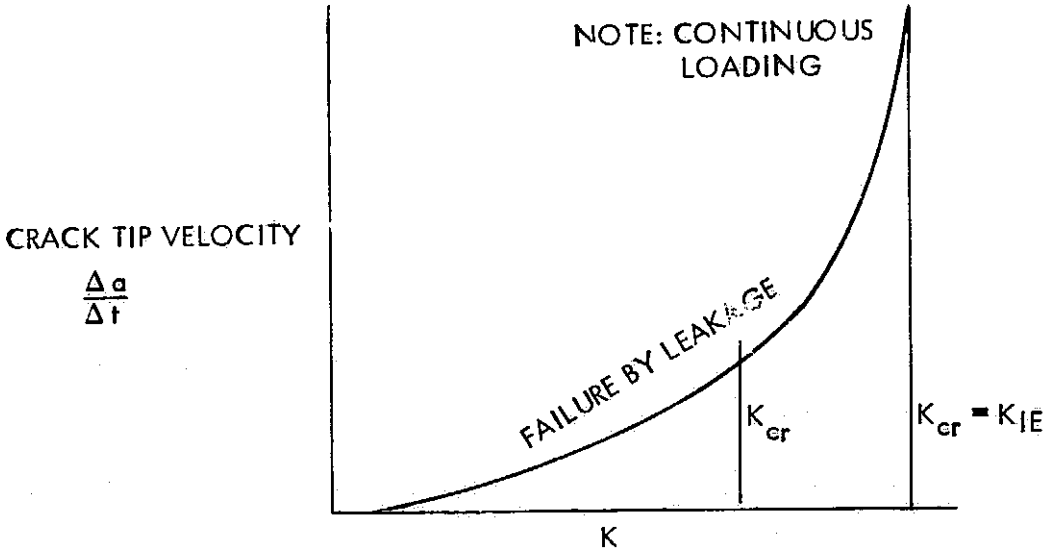

Figure 42: SCHEMATIC REPRESENTATION OF CRACK TIP VELOCITY VERSUS STRESS INTENSITY

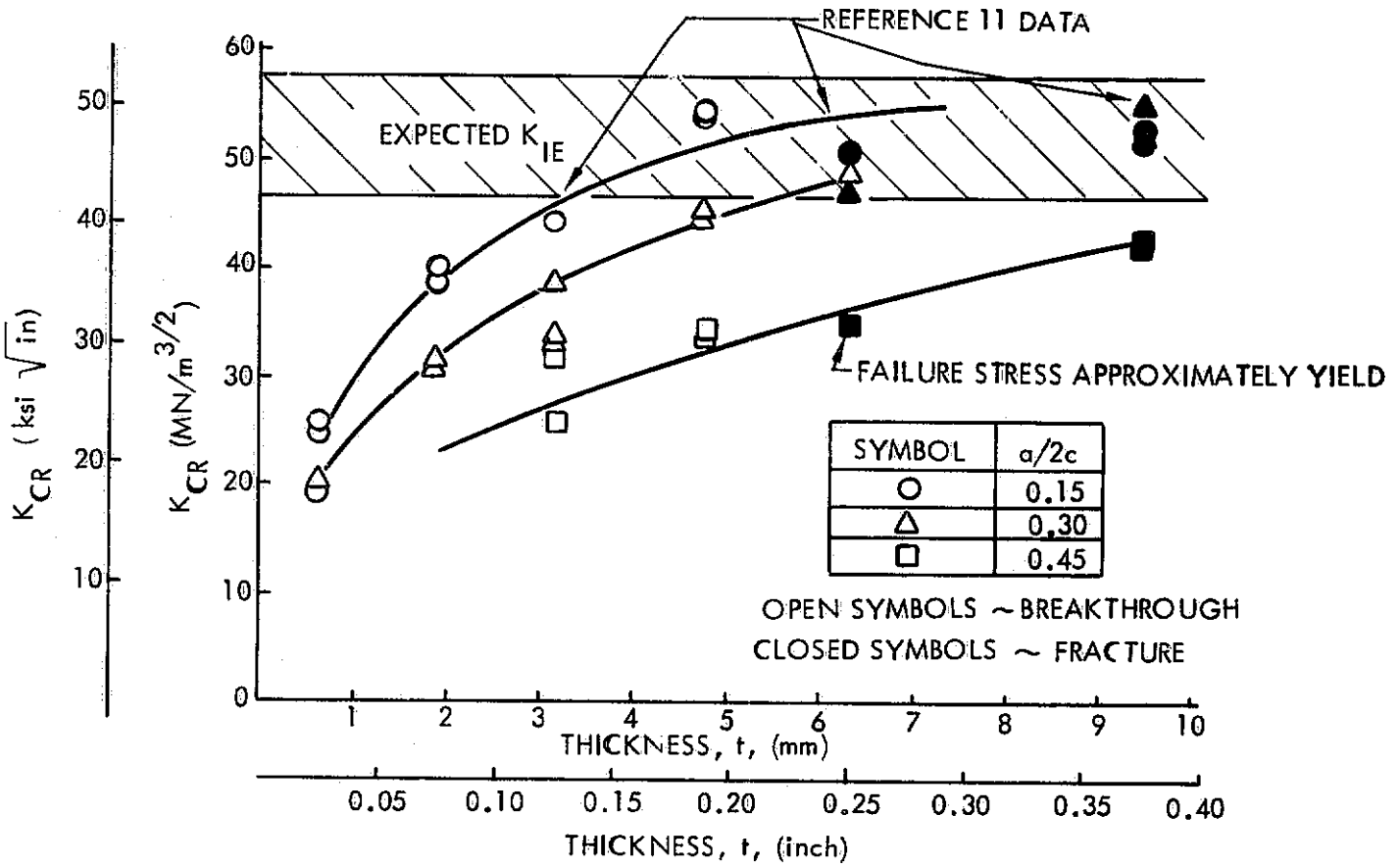

Figure 43 : K_{CR} VERSUS THICKNESS FOR 2219-T87 ALUMINUM BASE METAL AT ROOM TEMPERATURE

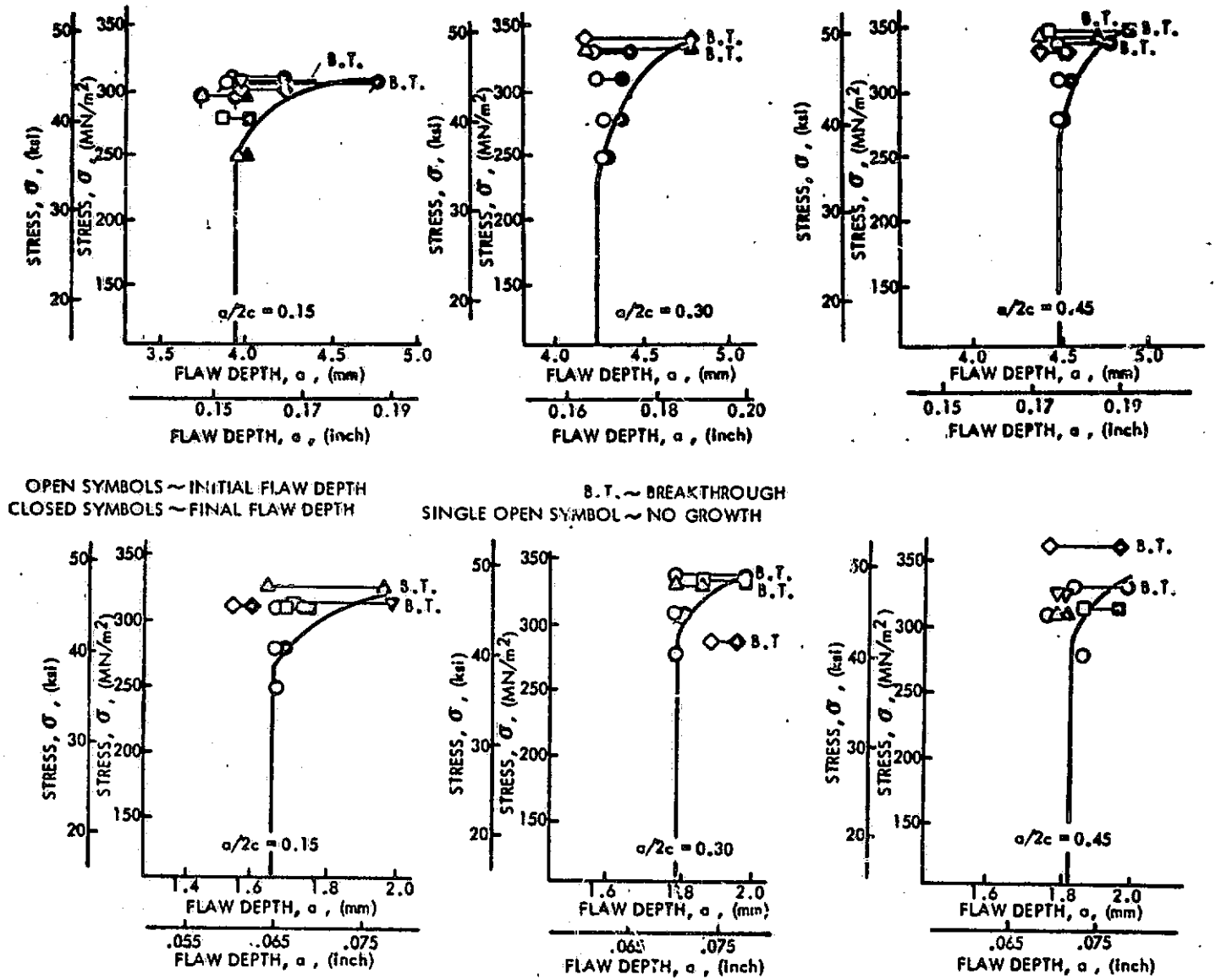

Figure 44 : ASSUMED GROWTH ON LOADING BEHAVIOR FOR 4.78mm AND 1.91mm (0.188 AND 0.075 INCH) THICK 2219-T78 ALUMINUM SPECIMENS

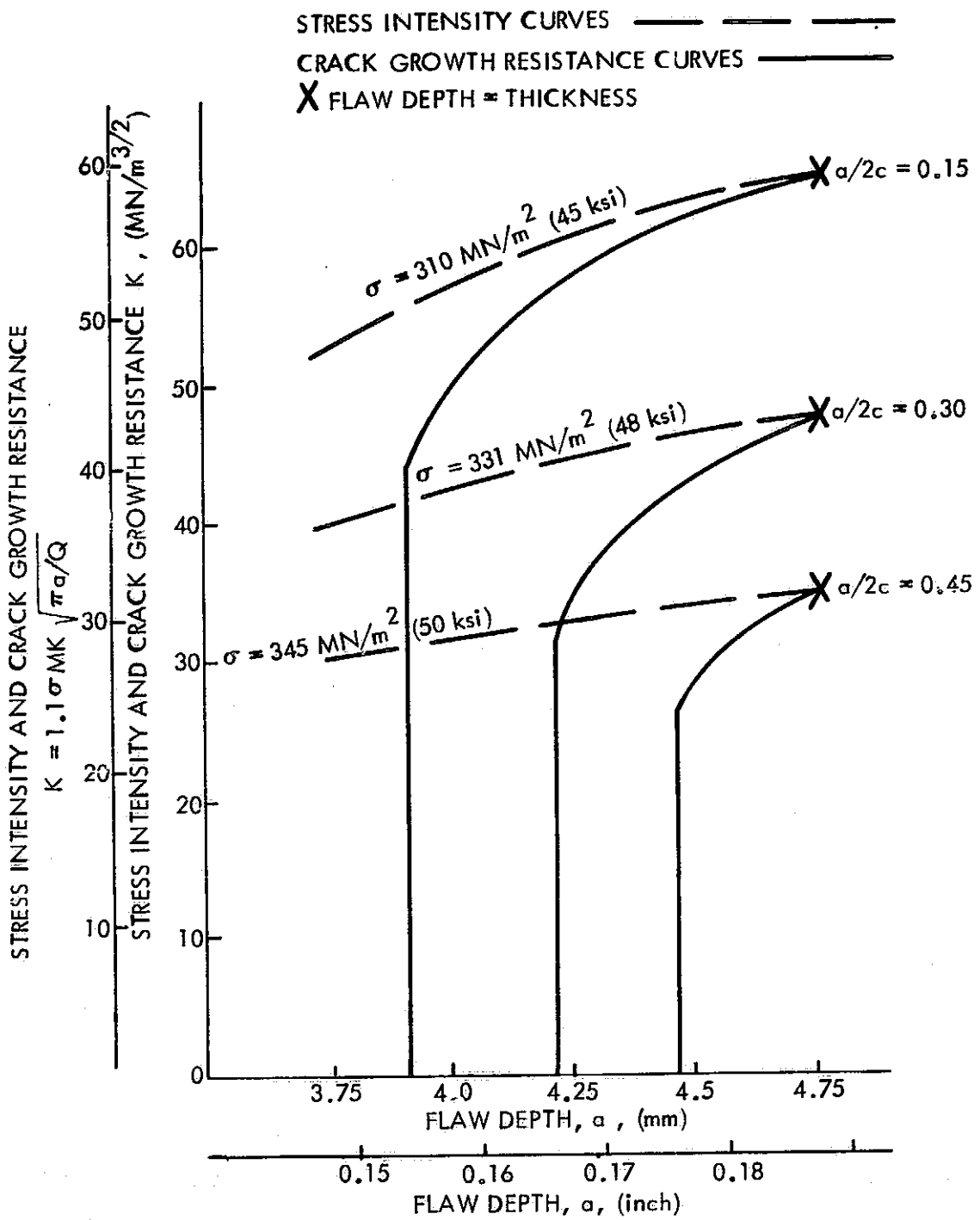

Figure 45 CRACK GROWTH RESISTANCE AND STRESS INTENSITY CURVES (INCLUDING MK) VERSUS CRACK DEPTH FOR ROOM TEMPERATURE 2219-T87 ALUMINUM BASE METAL SPECIMENS (t = 4.77 mm (0.188 inch))

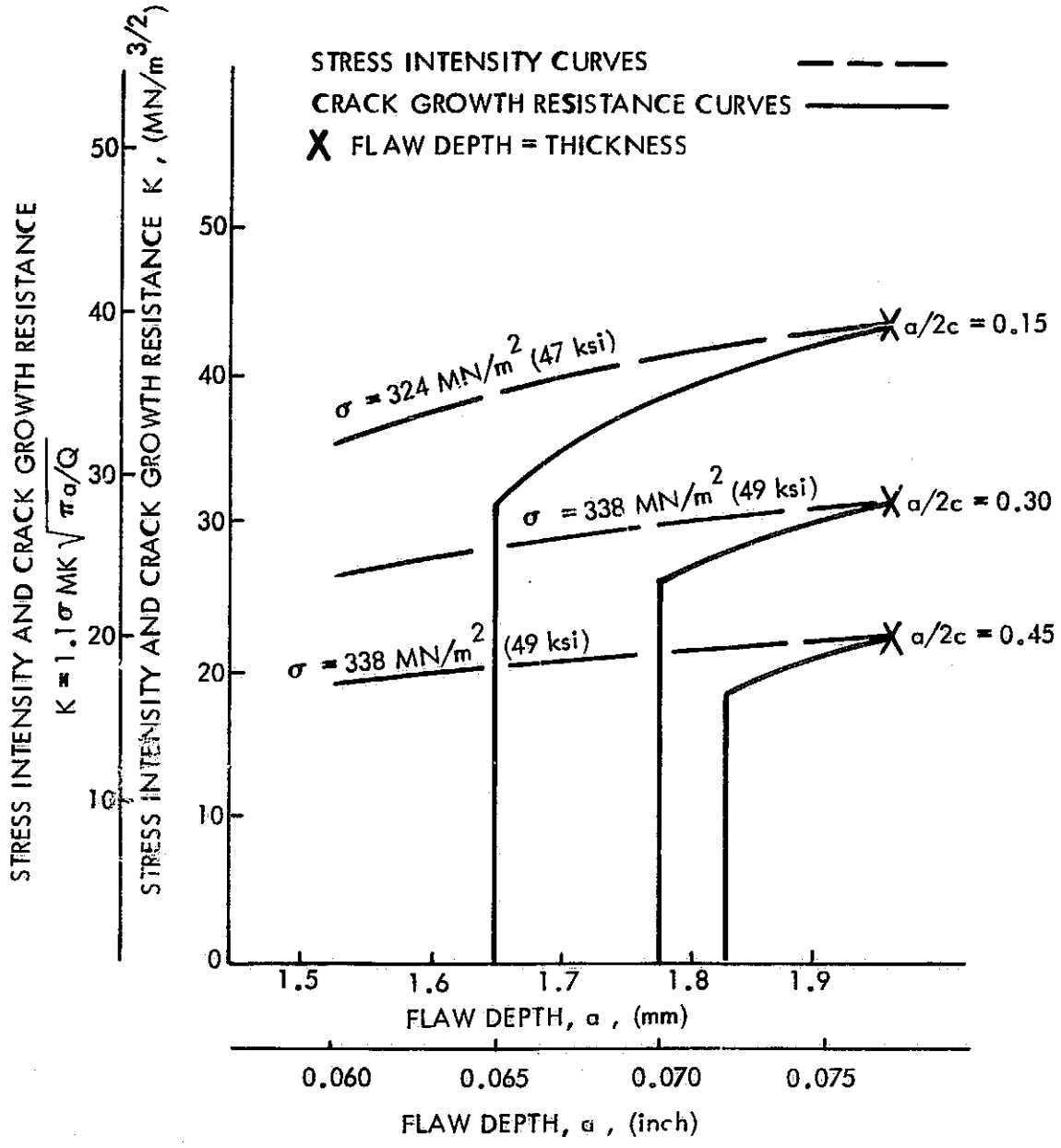

Figure 46 : CRACK GROWTH RESISTANCE AND STRESS INTENSITY (INCLUDING MK) VERSUS FLAW DEPTH FOR ROOM TEMPERATURE 2219-T87 ALUMINUM BASE METAL (t = 1.91 mm (0.075 inch))

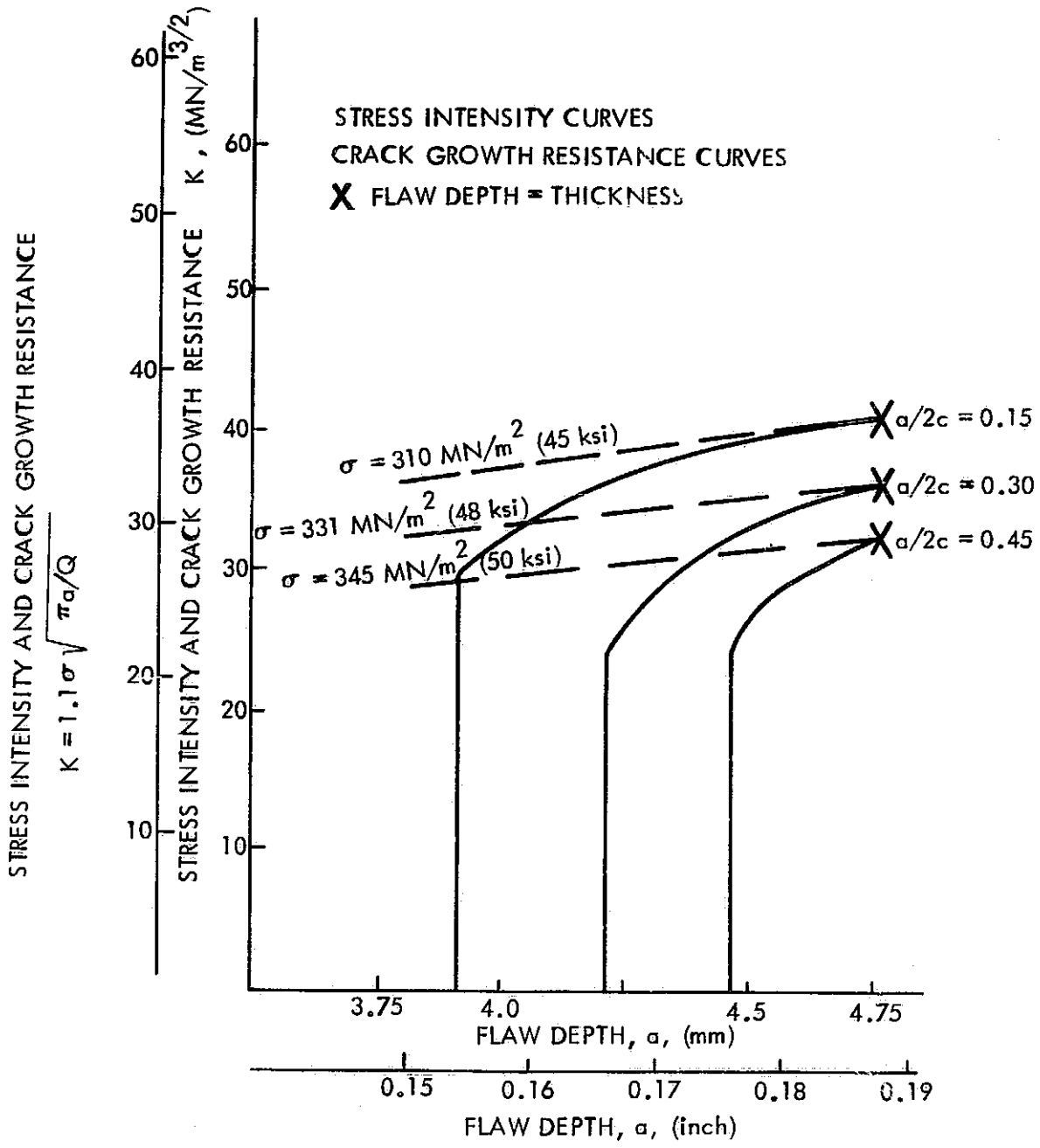

Figure 47 : CRACK GROWTH RESISTANCE AND STRESS INTENSITY CURVES VERSUS FLAW DEPTH FOR ROOM TEMPERATURE 2219-T87 ALUMINUM BASE METAL SPECIMENS (t = 4.77 mm (0.188 inch))

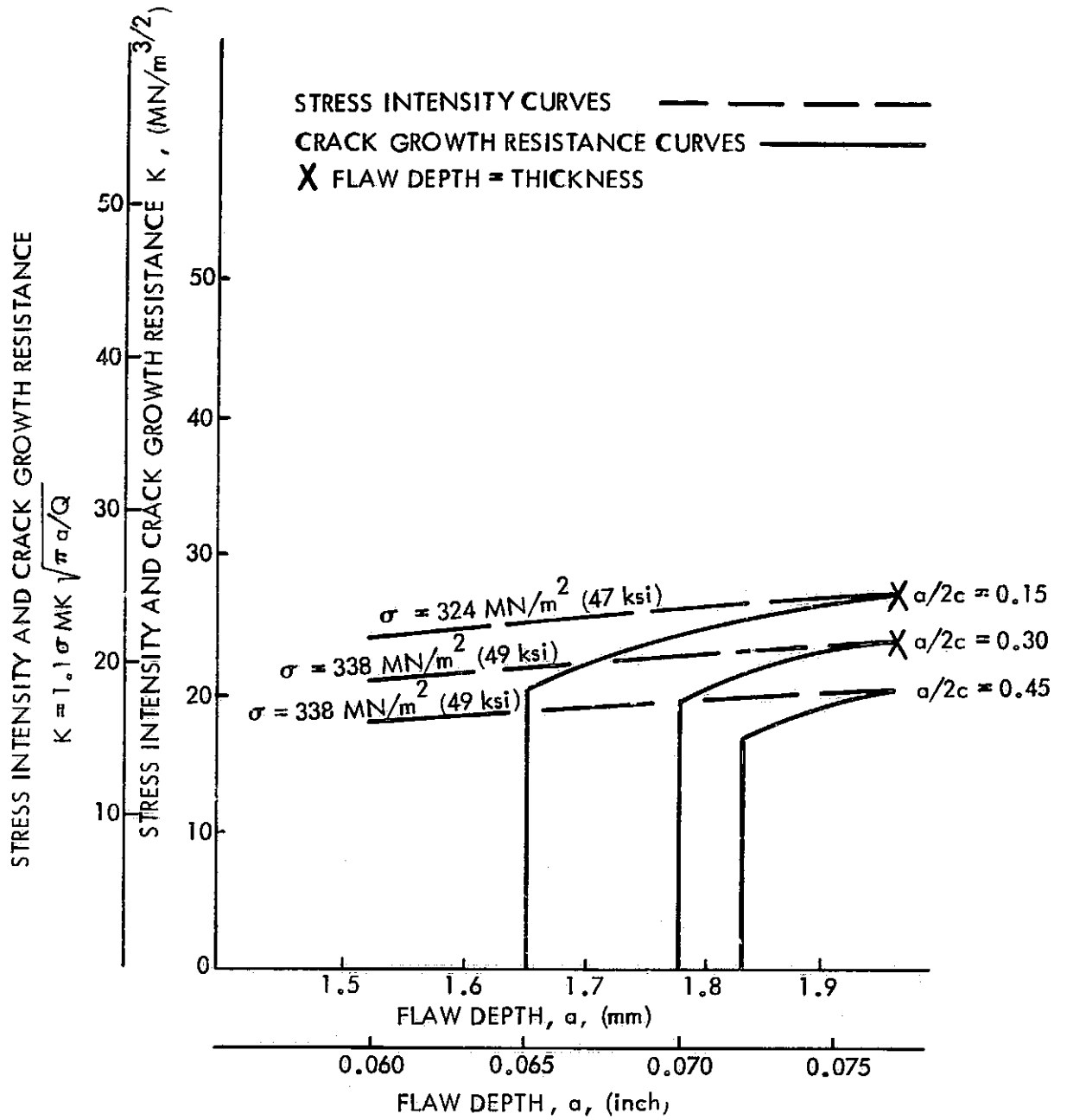

Figure 48 : CRACK GROWTH RESISTANCE AND STRESS INTENSITY VERSUS FLAW DEPTH FOR ROOM TEMPERATURE 2219-T87 ALUMINUM BASE METAL (t = 1.91 mm (0.075 inch))

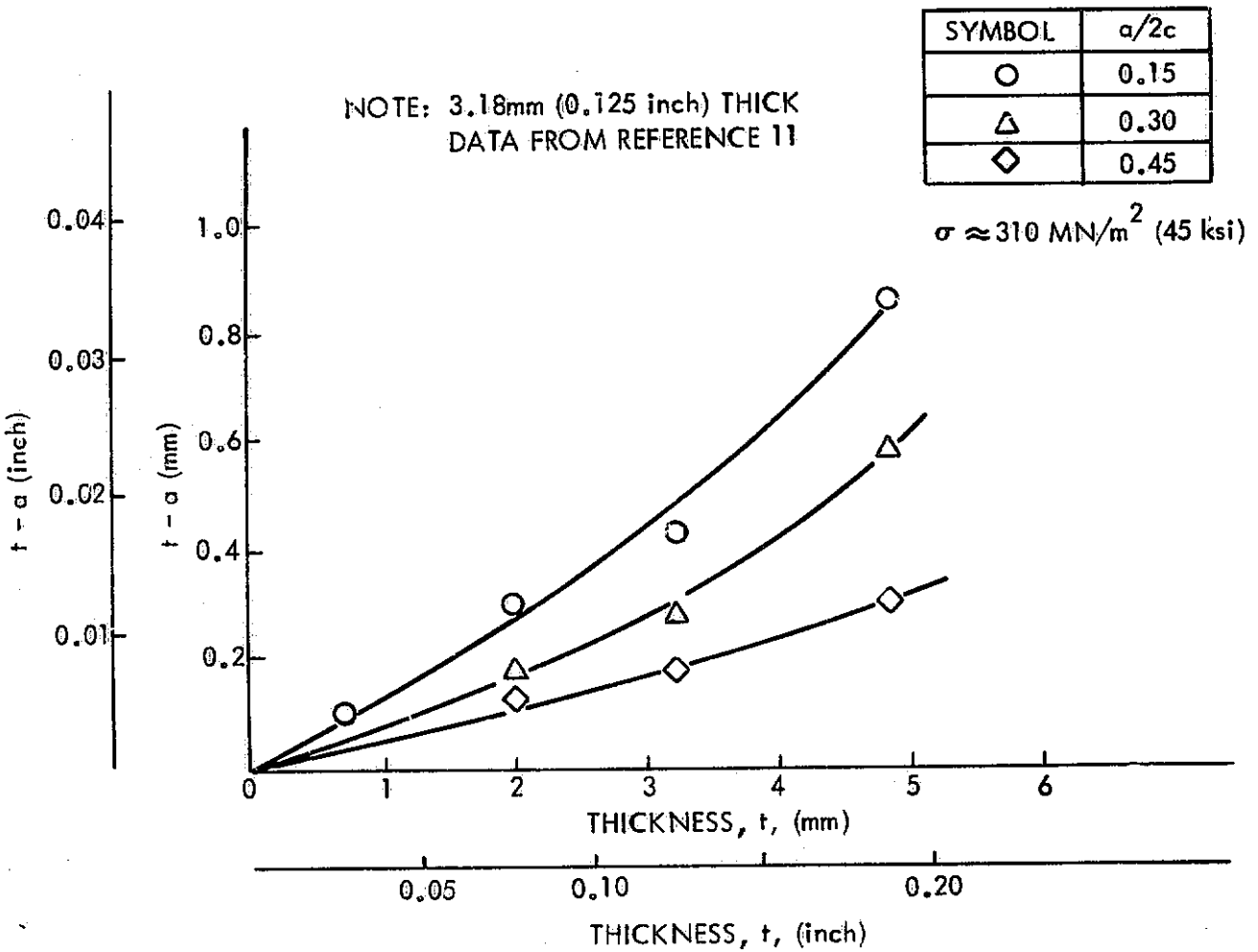

Figure 49: MAXIMUM LIGAMENT FOR BREAKTHROUGH VERSUS THICKNESS FOR ROOM TEMPERATURE 2219-T87 ALUMINUM

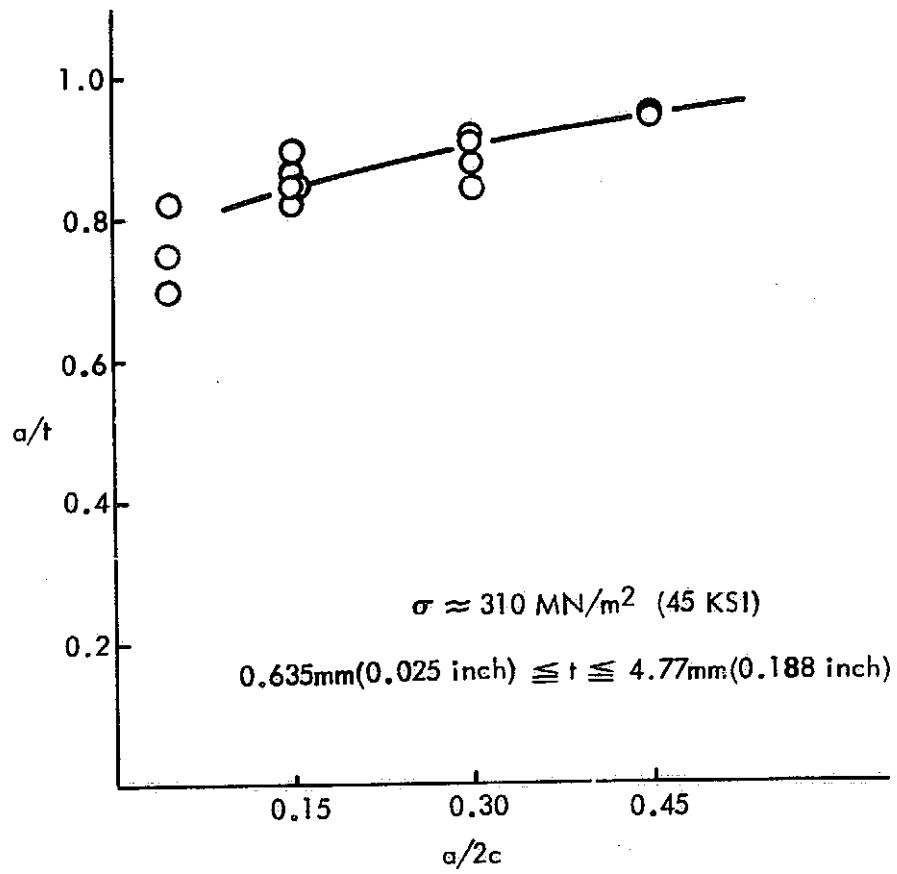

Figure 50 : RELATIONSHIP BETWEEN a/t AND a/2c FOR LEAKAGE RATHER THAN FRACTURE IN THIN GAGE 2219-T87 ALUMINUM AT ROOM TEMPERATURE

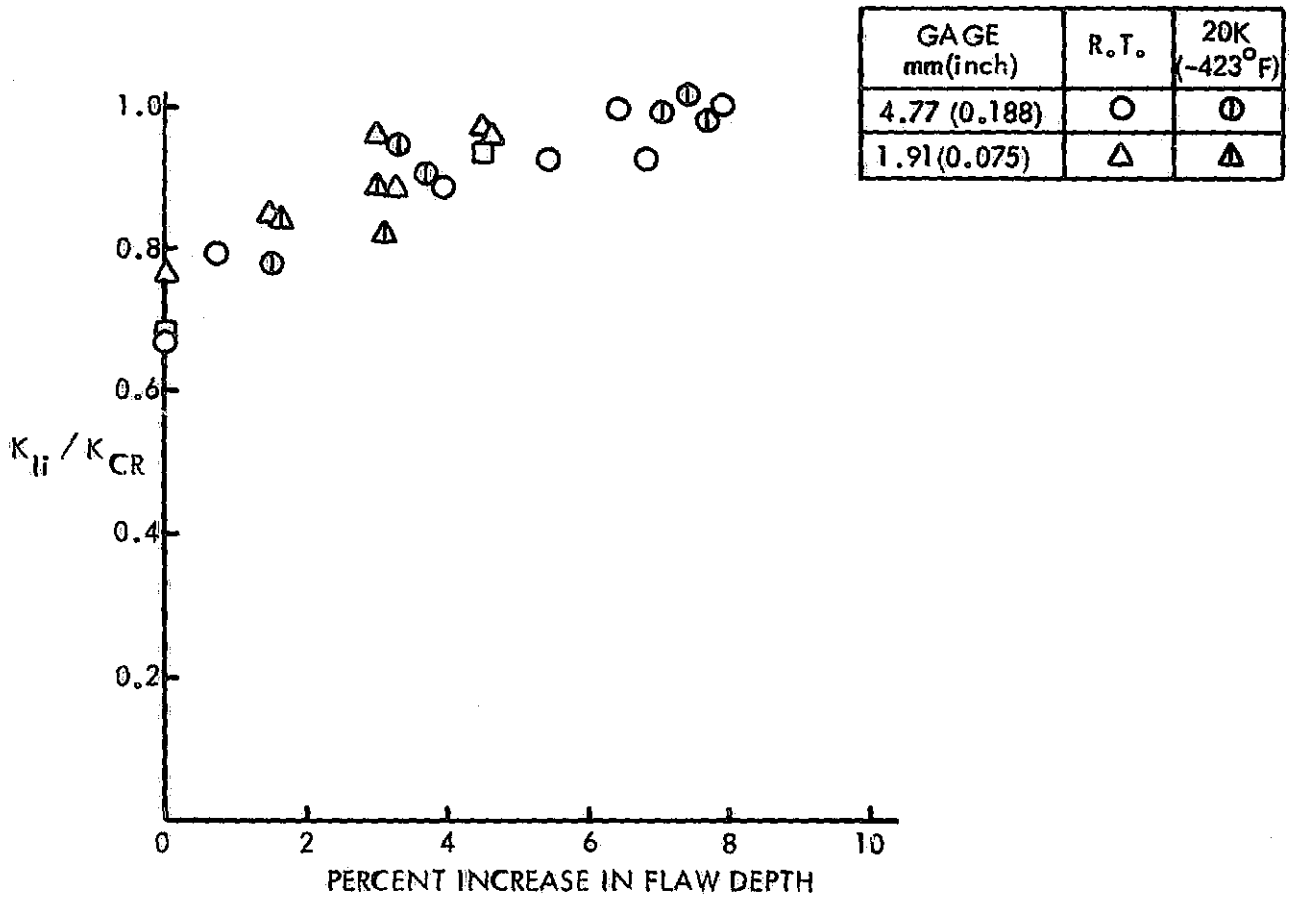

Figure 51 : 2219-T87 ALUMINUM BASE METAL GROWTH ON LOADING TEST RESULTS FOR 4.77mm(0.188 inch) AND 1.91mm(0.075 inch) THICK SURFACE FLAW SPECIMENS (a/2c = 0.15)

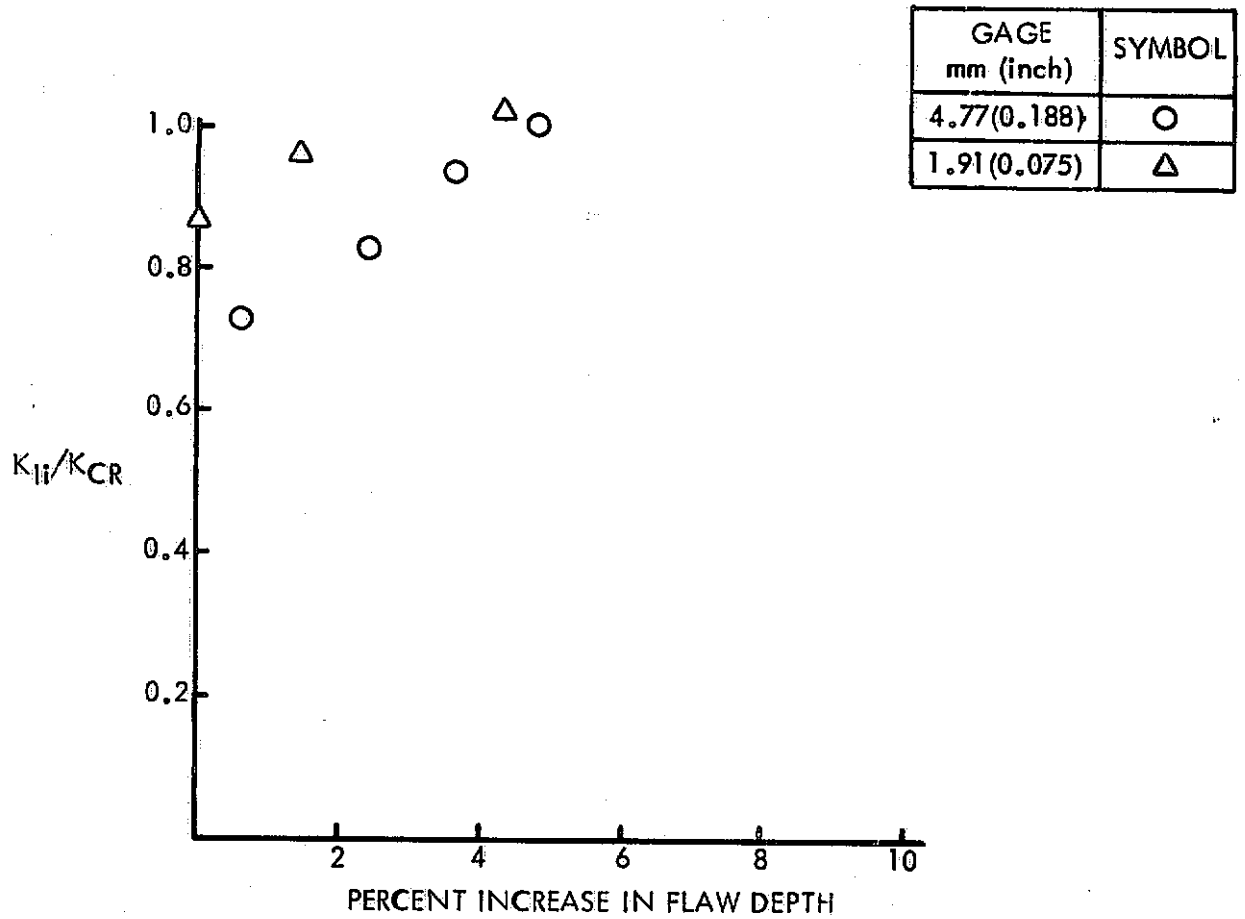

Figure 52 : 2219-T87 ALUMINUM BASE METAL GROWTH-ON-LOADING TEST RESULTS FOR 4.77mm(0.188 inch) AND 1.91mm(0.075 inch) THICK SURFACE FLAWED SPECIMENS (a/2c = 0.30)

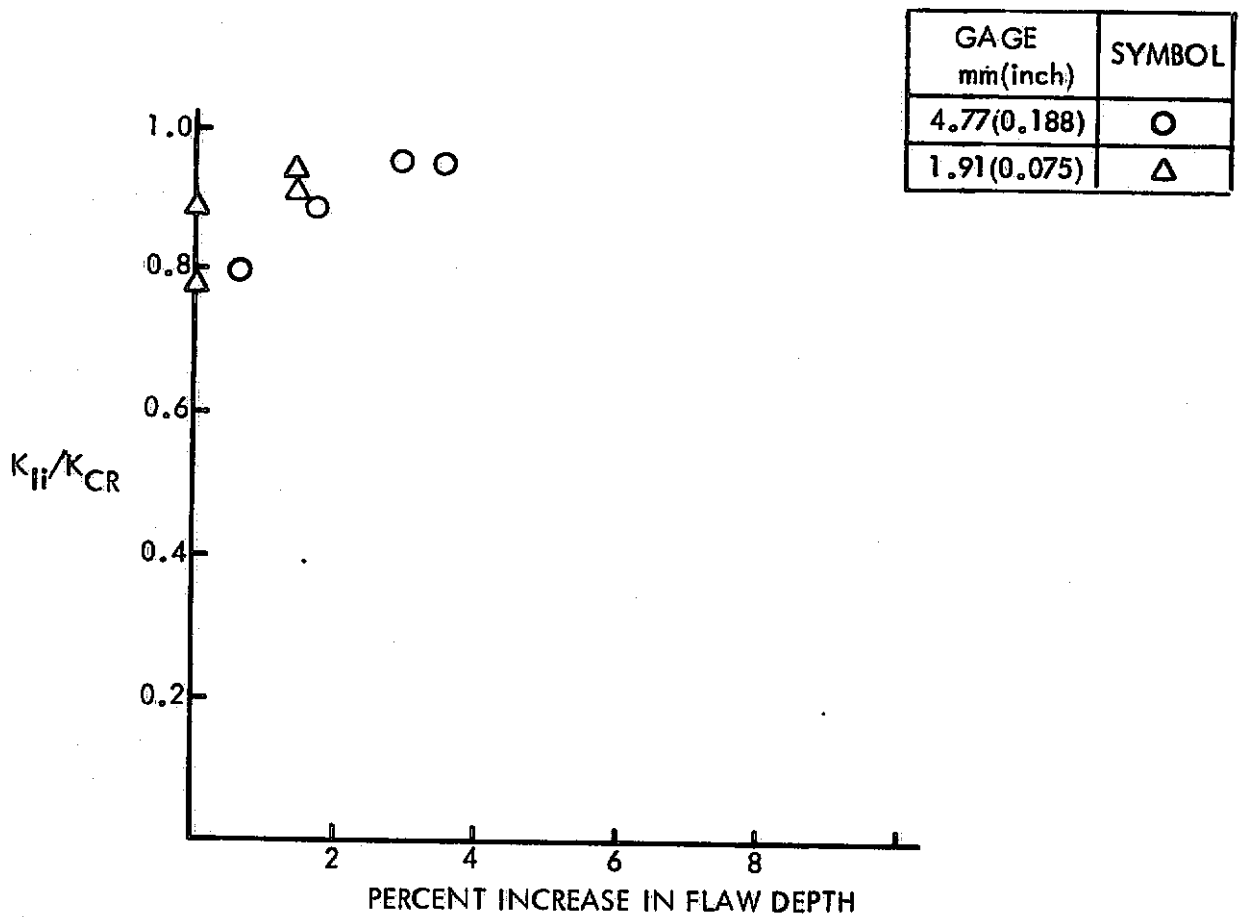

Figure 53 : 2219-T87 ALUMINUM BASE METAL GROWTH-ON-LOADING TEST RESULTS FOR 4.77mm(0.188 inch) AND 1.91mm(0.075 inch) THICK SURFACE FLAWED SPECIMENS (a/2c = 0.40)

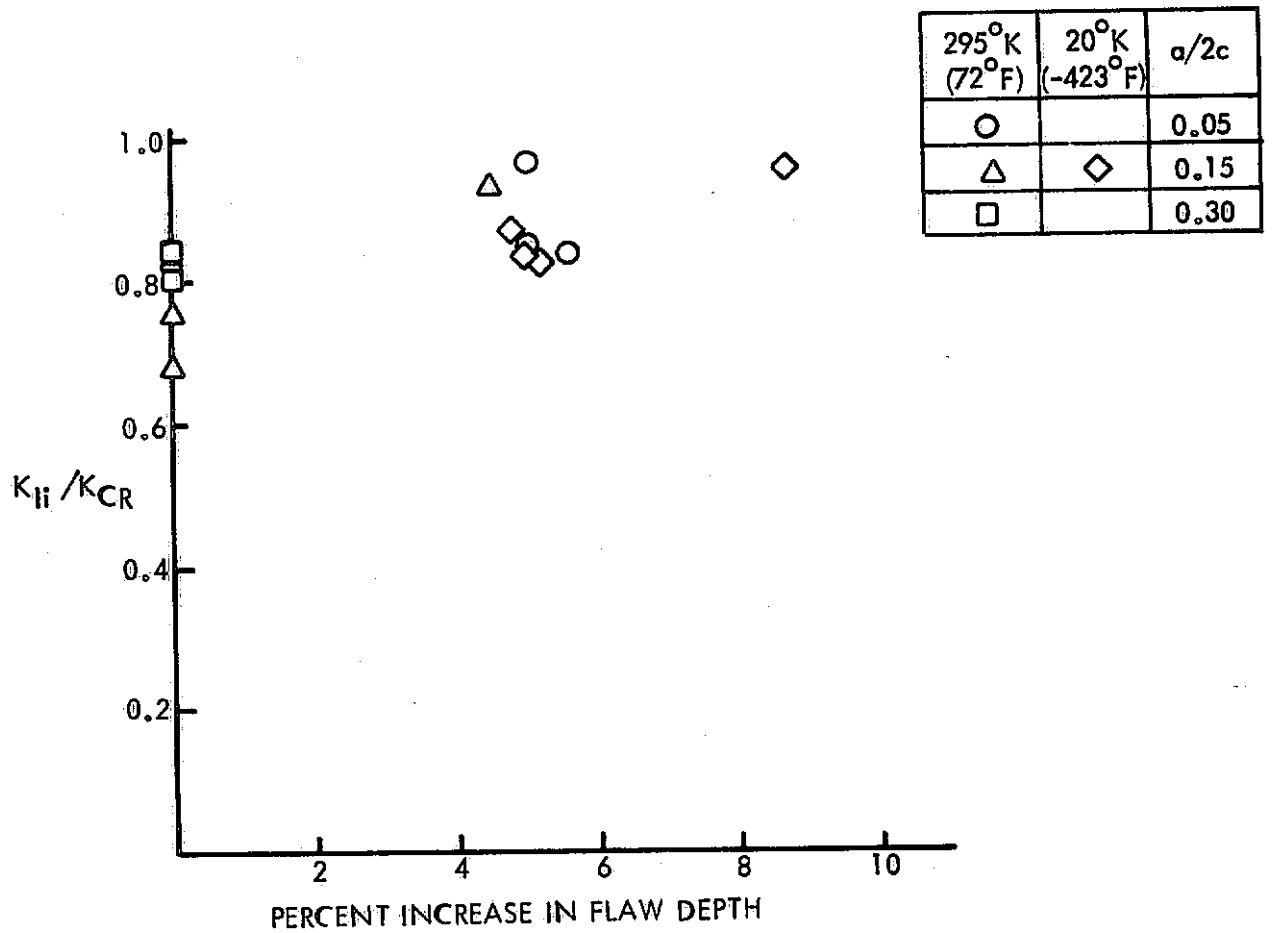

Figure 54 : 2219-T87 ALUMINUM BASE METAL GROWTH-ON-LOADING TEST RESULTS FOR 0.635mm(0.025 inch) THICK SURFACE FLAWED SPECIMENS

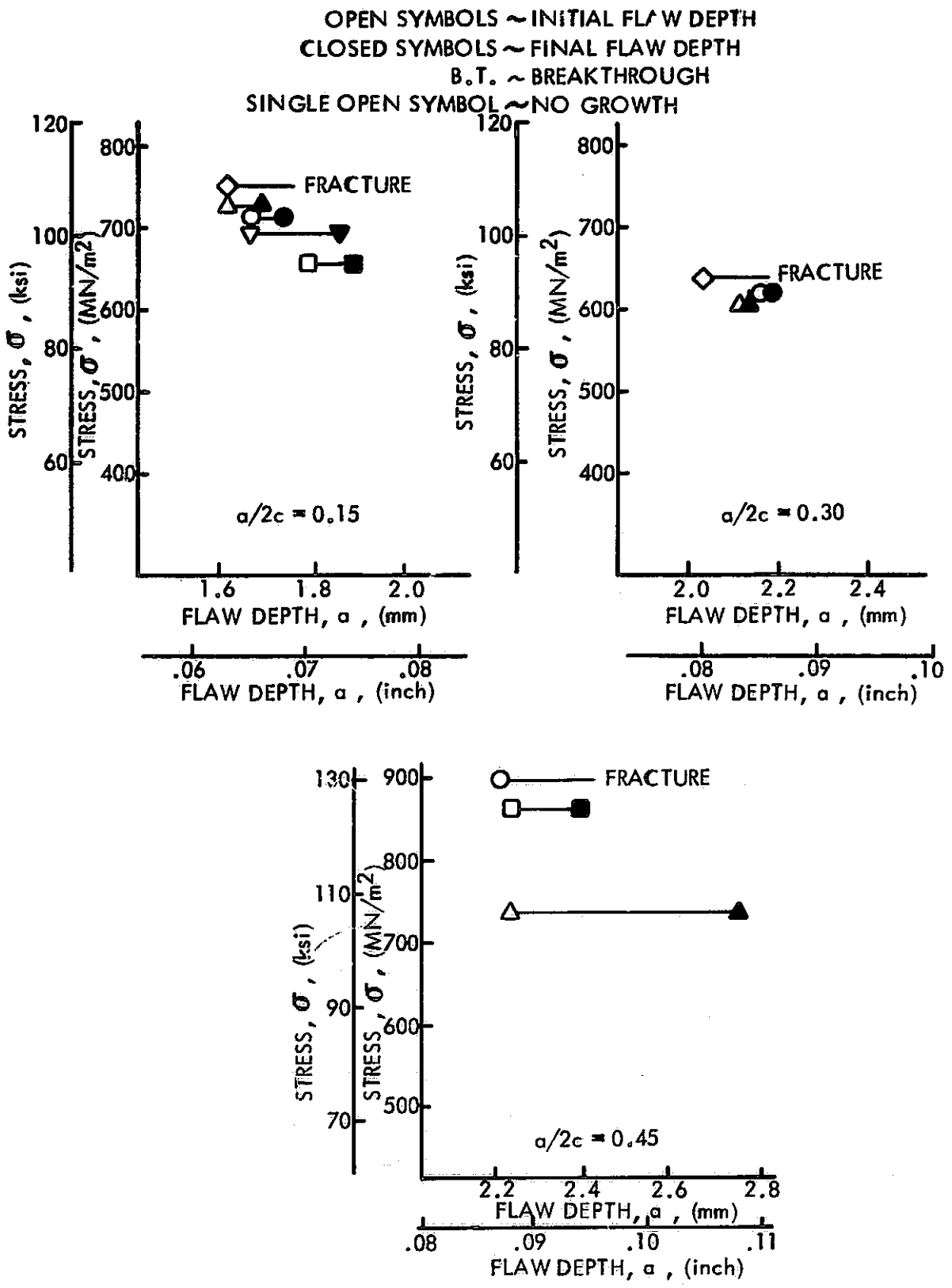

Figure 55 : GROWTH-ON-LOADING TEST RESULTS FOR 3.18mm(0.125 inch) THICK 6Al-4V STA TITANIUM AT ROOM TEMPERATURE

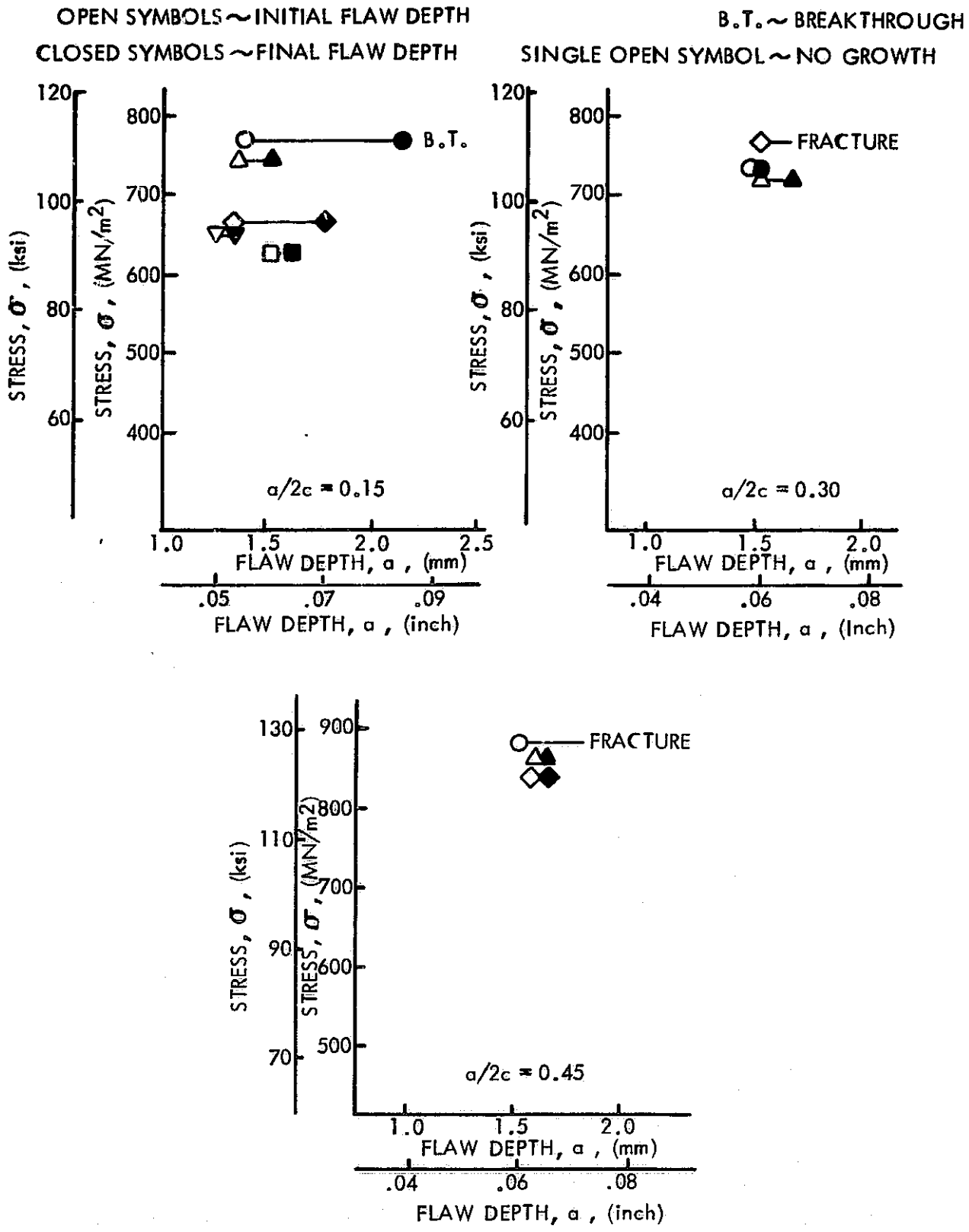

Figure 56 : GROWTH-ON-LOADING TEST RESULTS FOR 2.03mm (0.080 inch) THICK 6Al-4V STA TITANIUM AT ROOM TEMPERATURE

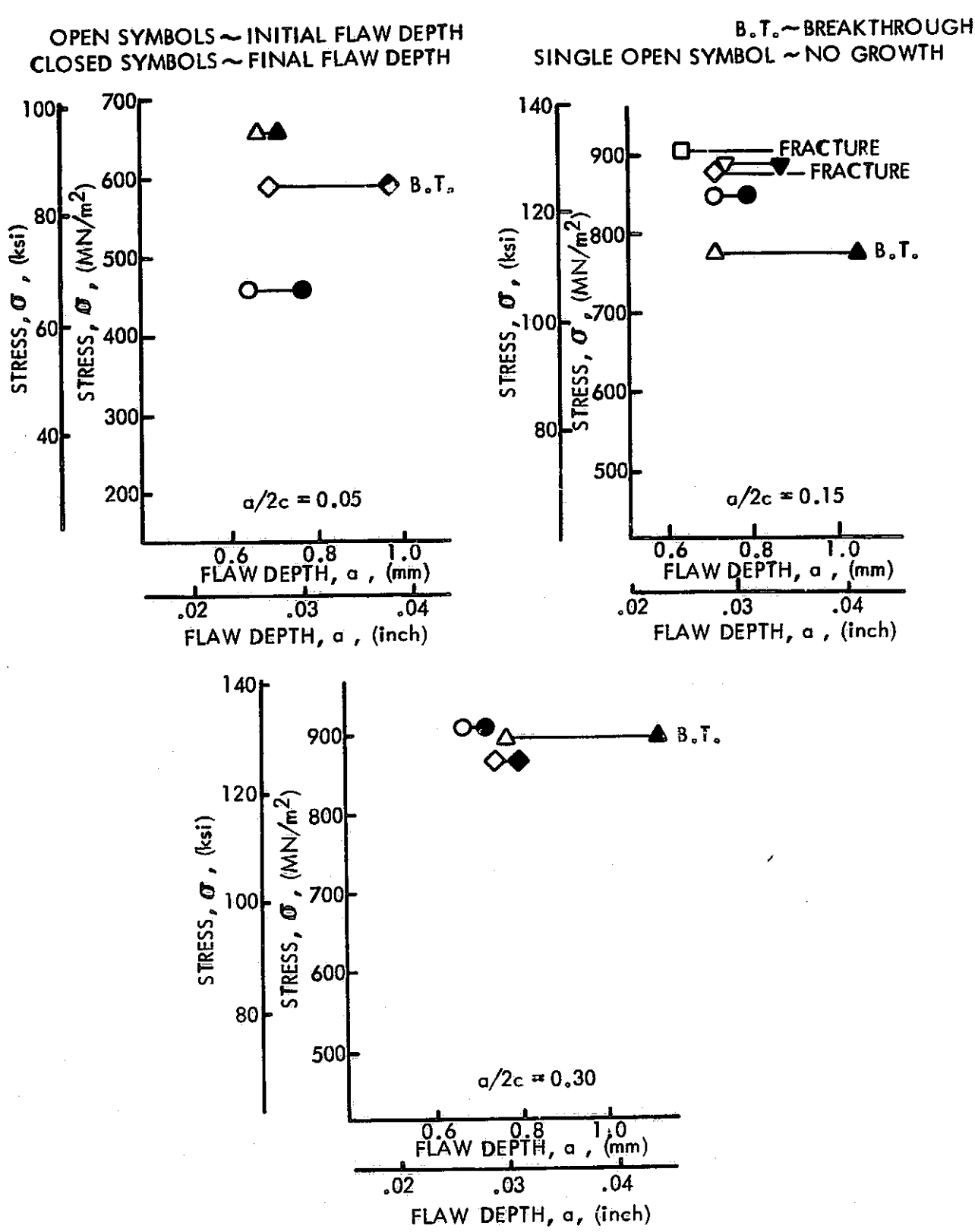

Figure 57 : GROWTH-ON-LOADING TEST RESULTS FOR 1.02mm (0.040 inch) THICK 6Al-4V STA TITANIUM AT ROOM TEMPERATURE

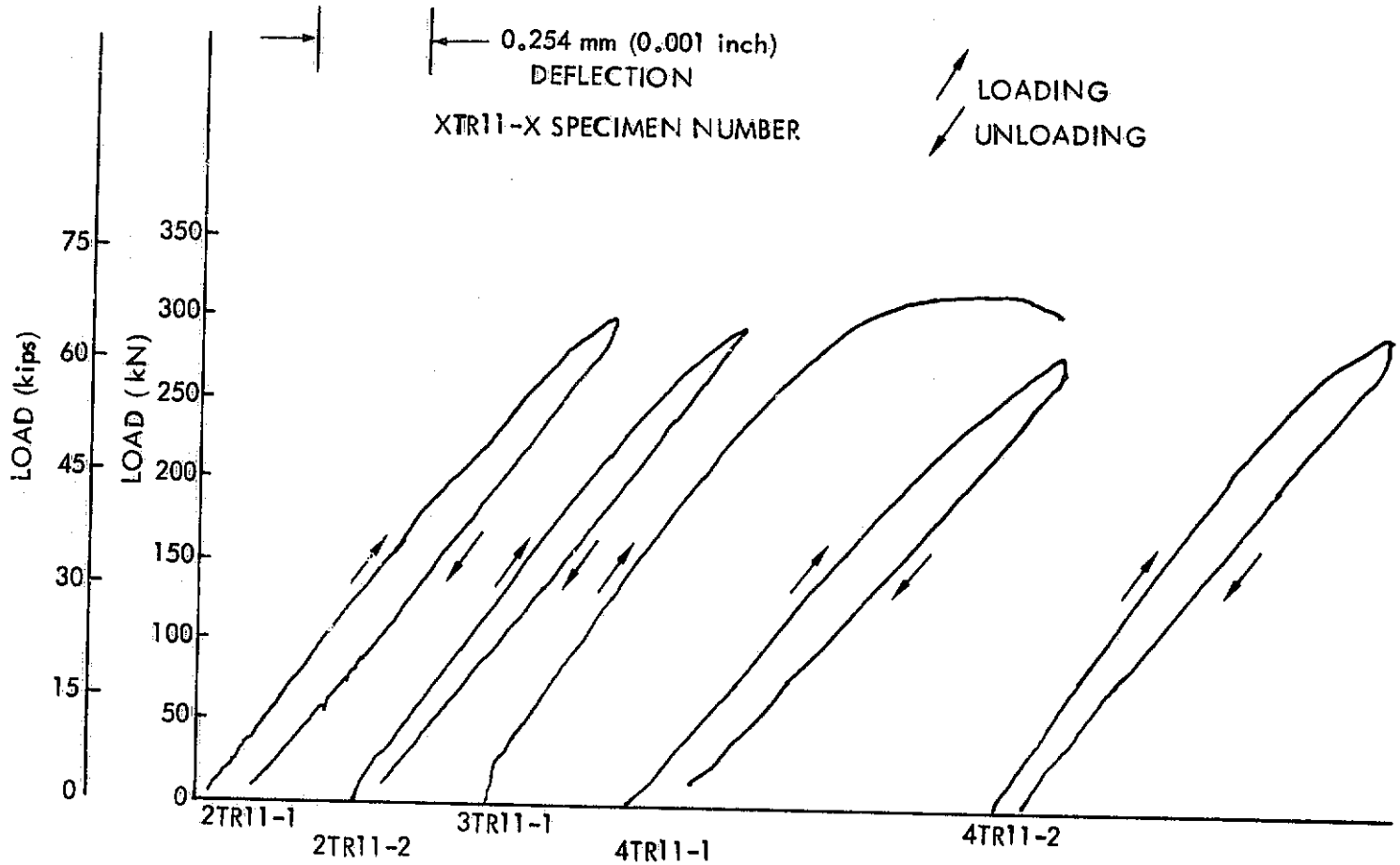

Figure 58 : CRACK OPENING DISPLACEMENT RECORDS FOR 3.18mm (0.125 inch) THICK TITANIUM SURFACE FLAWED SPECIMENS (a/2c = 0.15)

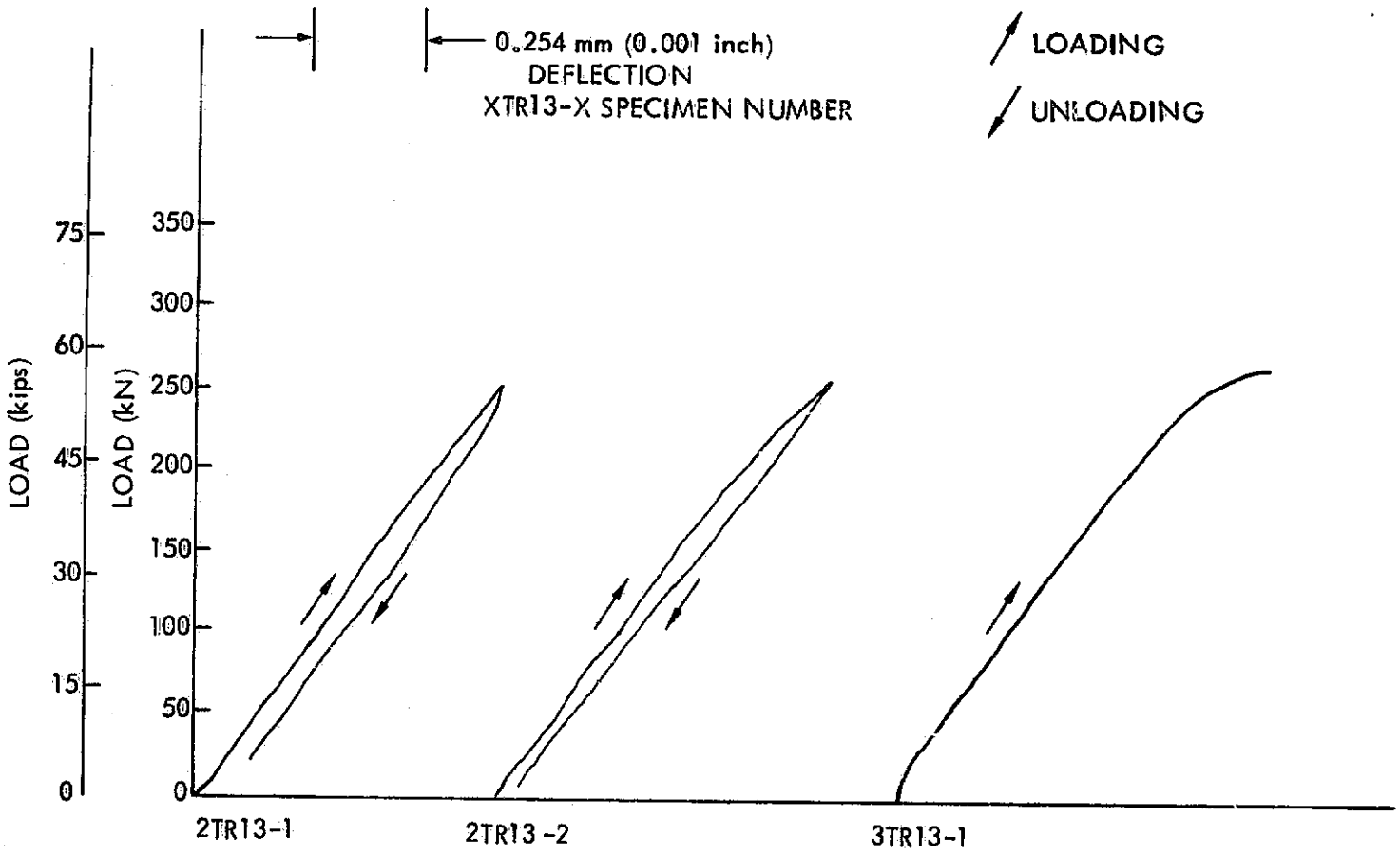

Figure 59: CRACK OPENING DISPLACEMENT RECORDS FOR 3.18mm (0.125 inch) THICK TITANIUM SURFACE FLAWED SPECIMENS (a/2c = 0.30)

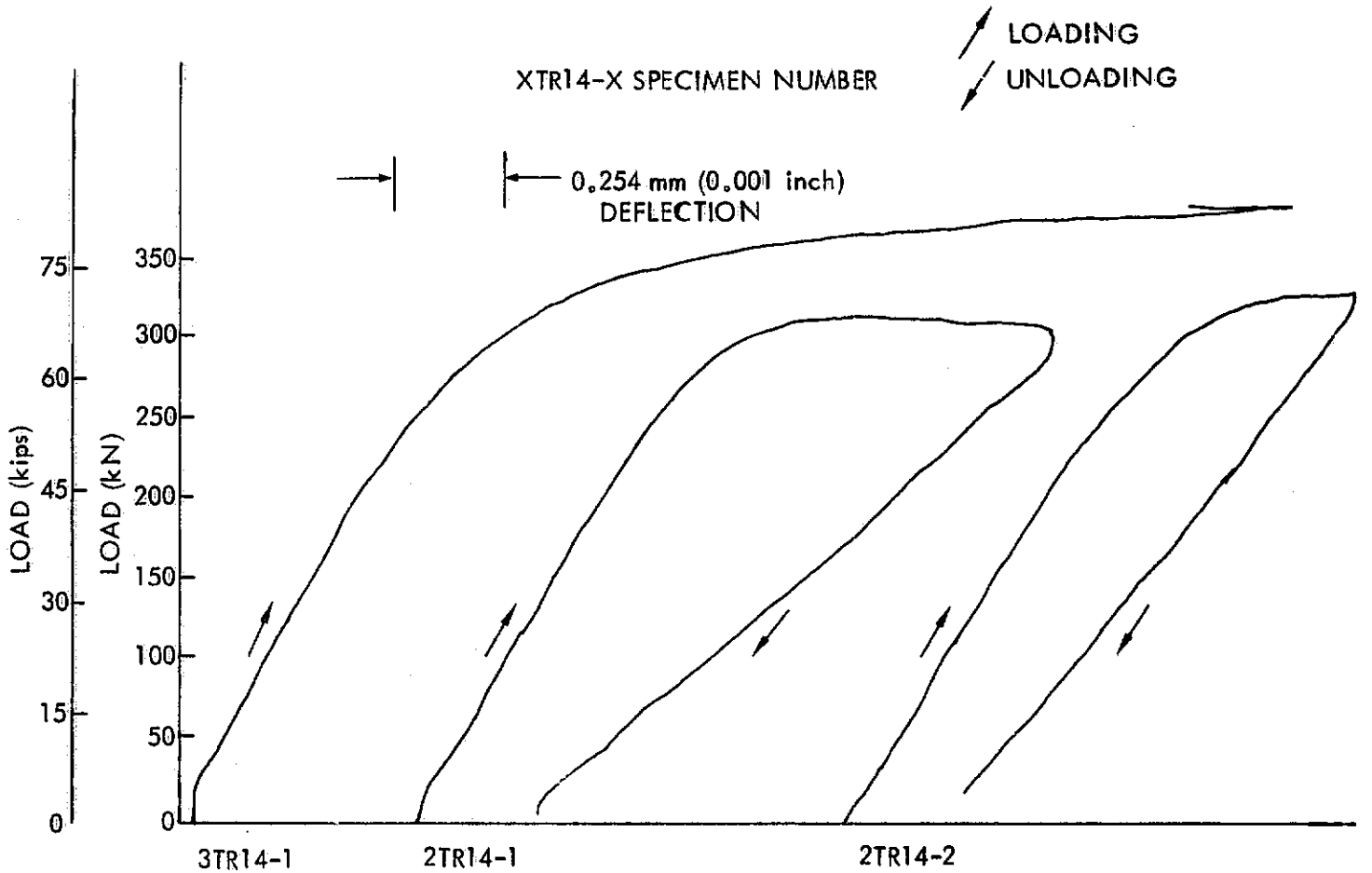

Figure 60: CRACK OPENING DISPLACEMENT RECORDS FOR 3.18mm (0.125 inch) THICK TITANIUM SURFACE FLAWED SPECIMENS ($a/2c = 0.45$)

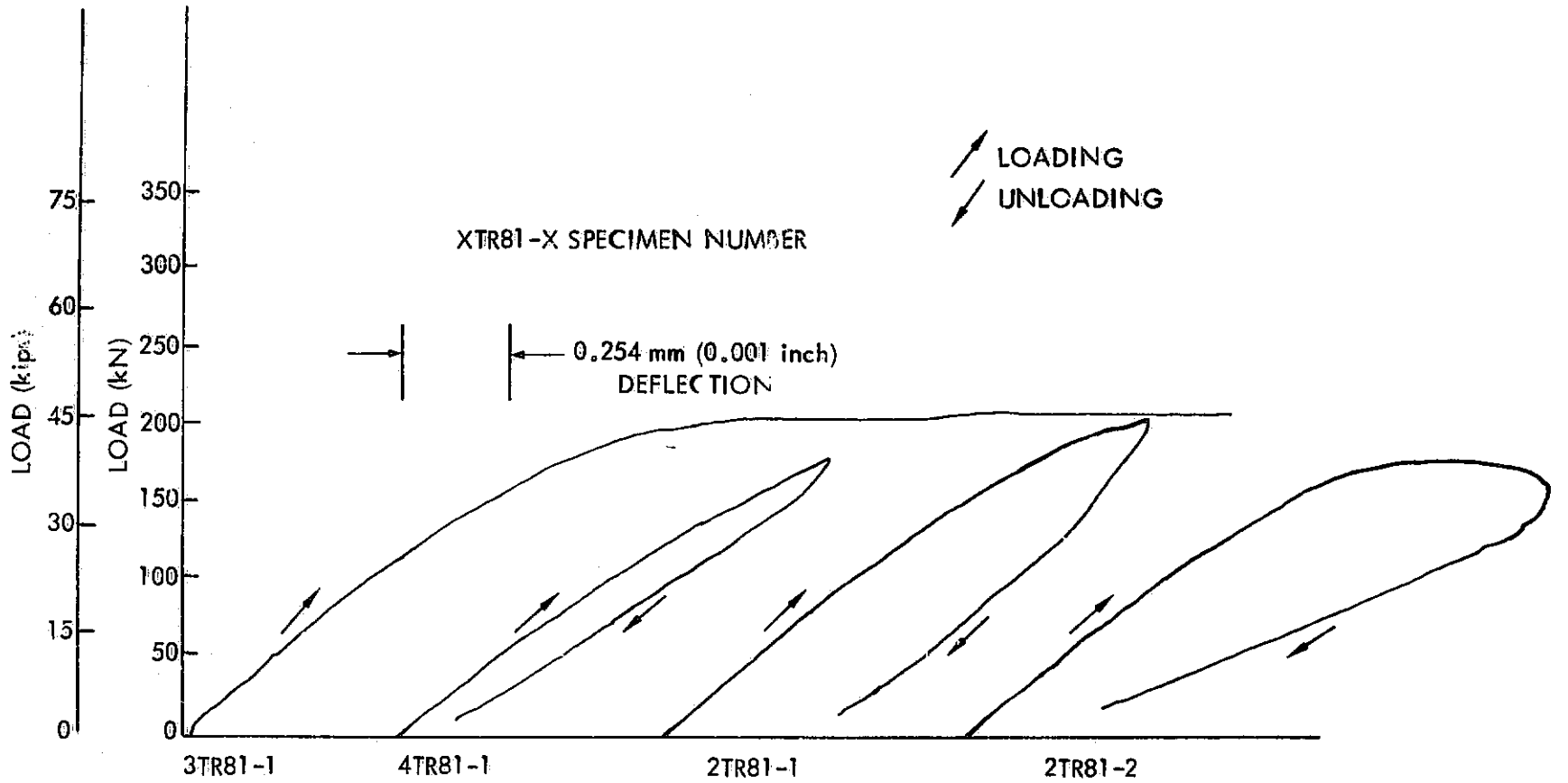

Figure 61: CRACK OPENING DISPLACEMENT RECORDS FOR 2.03mm (0.080 inch) THICK TITANIUM SURFACE FLAWED SPECIMENS (a/2c = 0.15)

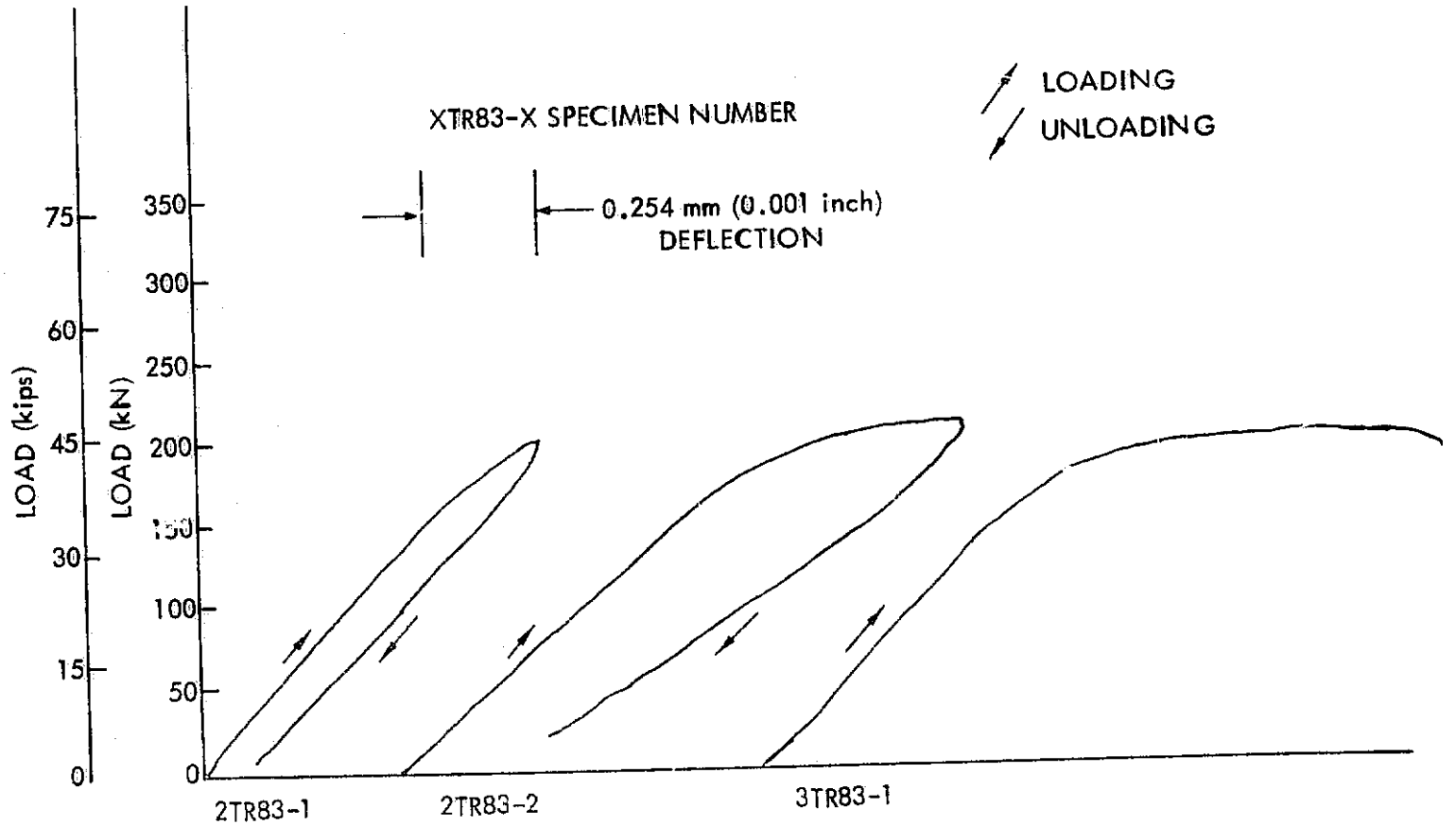

Figure 62: CRACK OPENING DISPLACEMENT RECORDS FOR 2.03mm (0.080 inch) THICK TITANIUM SURFACE FLAWED SPECIMENS ($a/2c = 0.30$)

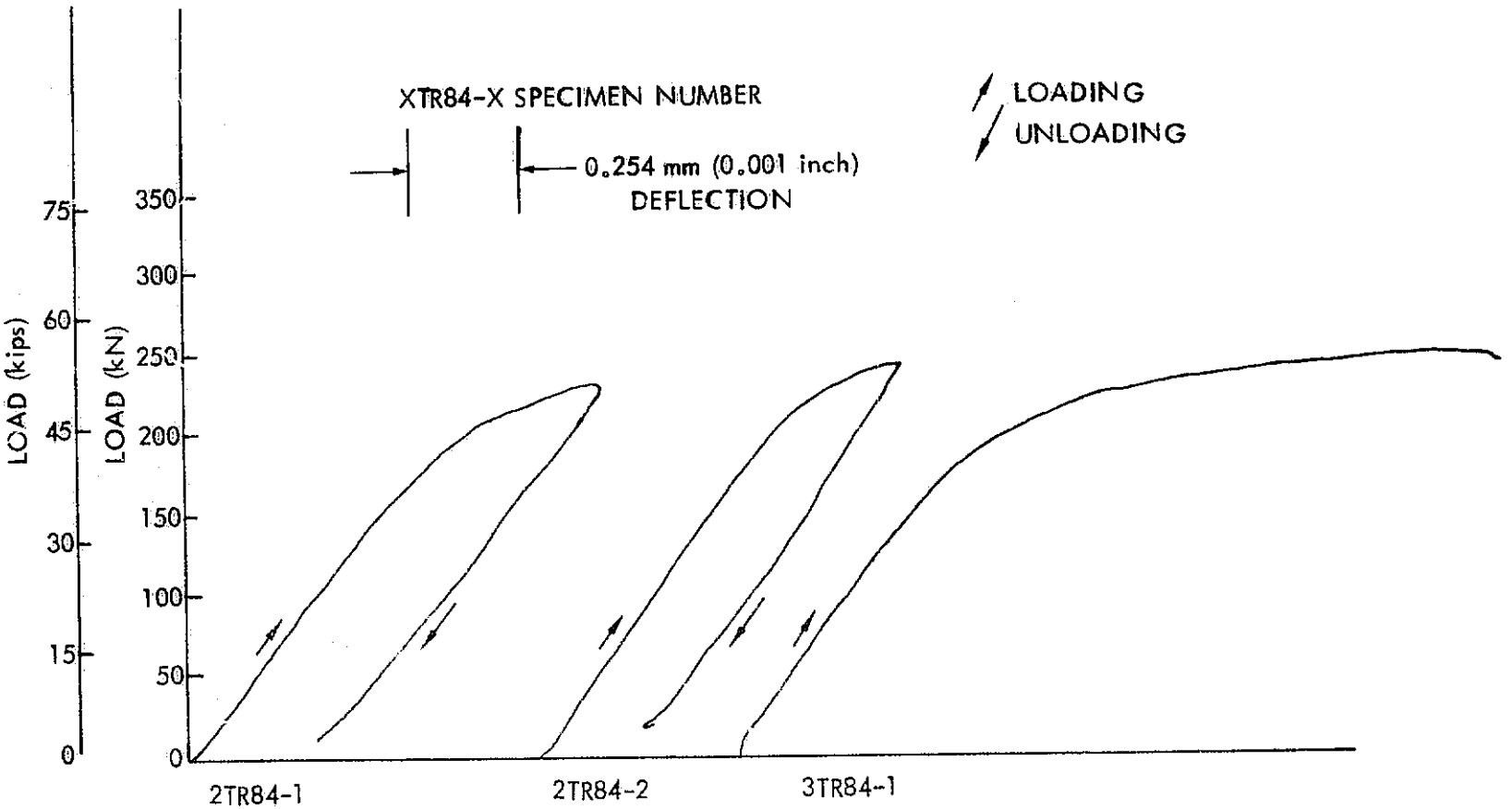

Figure 63: CRACK OPENING DISPLACEMENT RECORDS FOR 2.03mm (0.080 inch) THICK TITANIUM SURFACE FLAWED SPECIMENS ($a/2c \approx 0.45$)

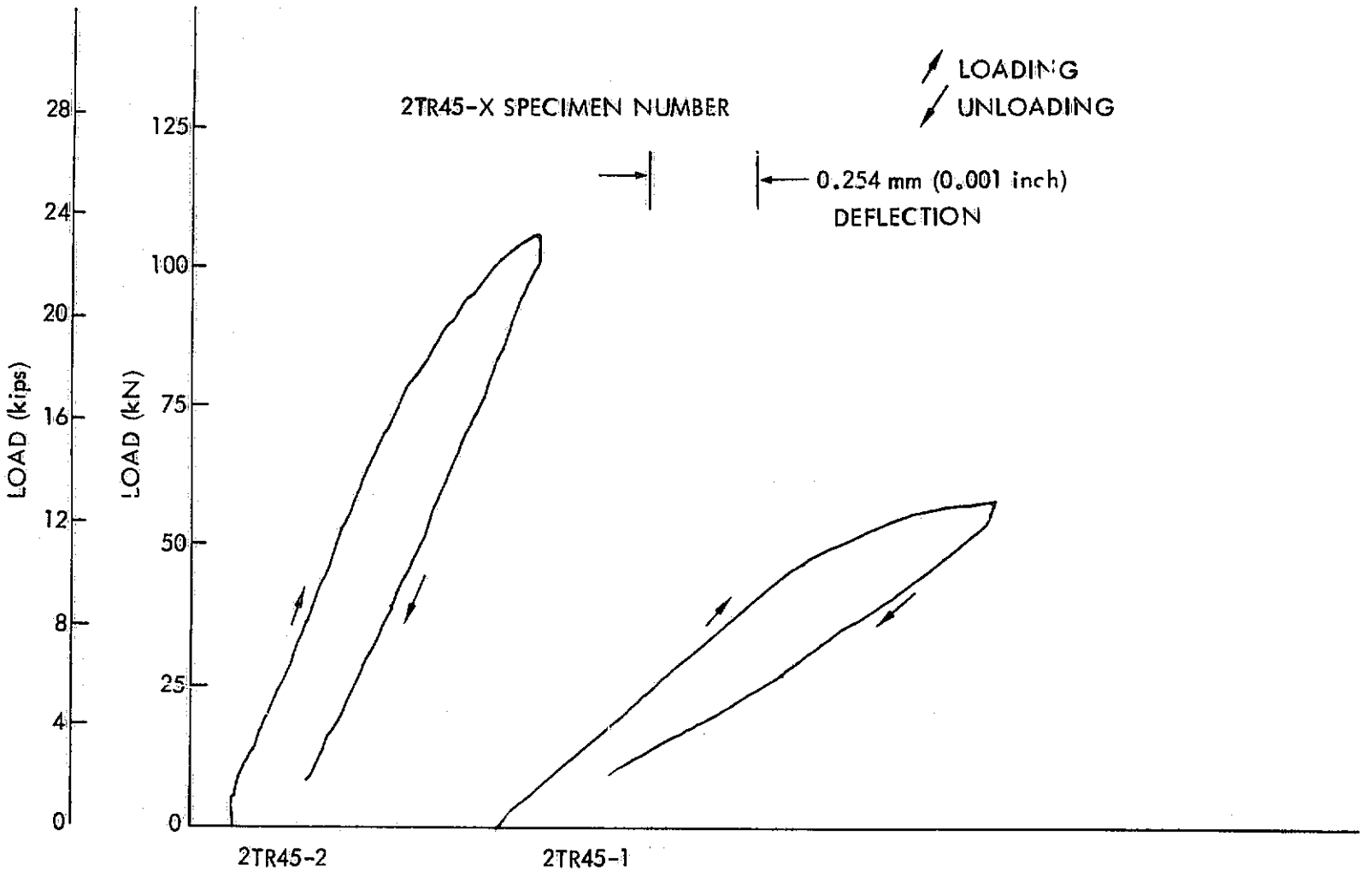

Figure 64: CRACK OPENING DISPLACEMENT RECORDS FOR 1.02mm (0.040 inch) THICK TITANIUM SURFACE FLAWED SPECIMENS (a/2c ≈ 0.05)

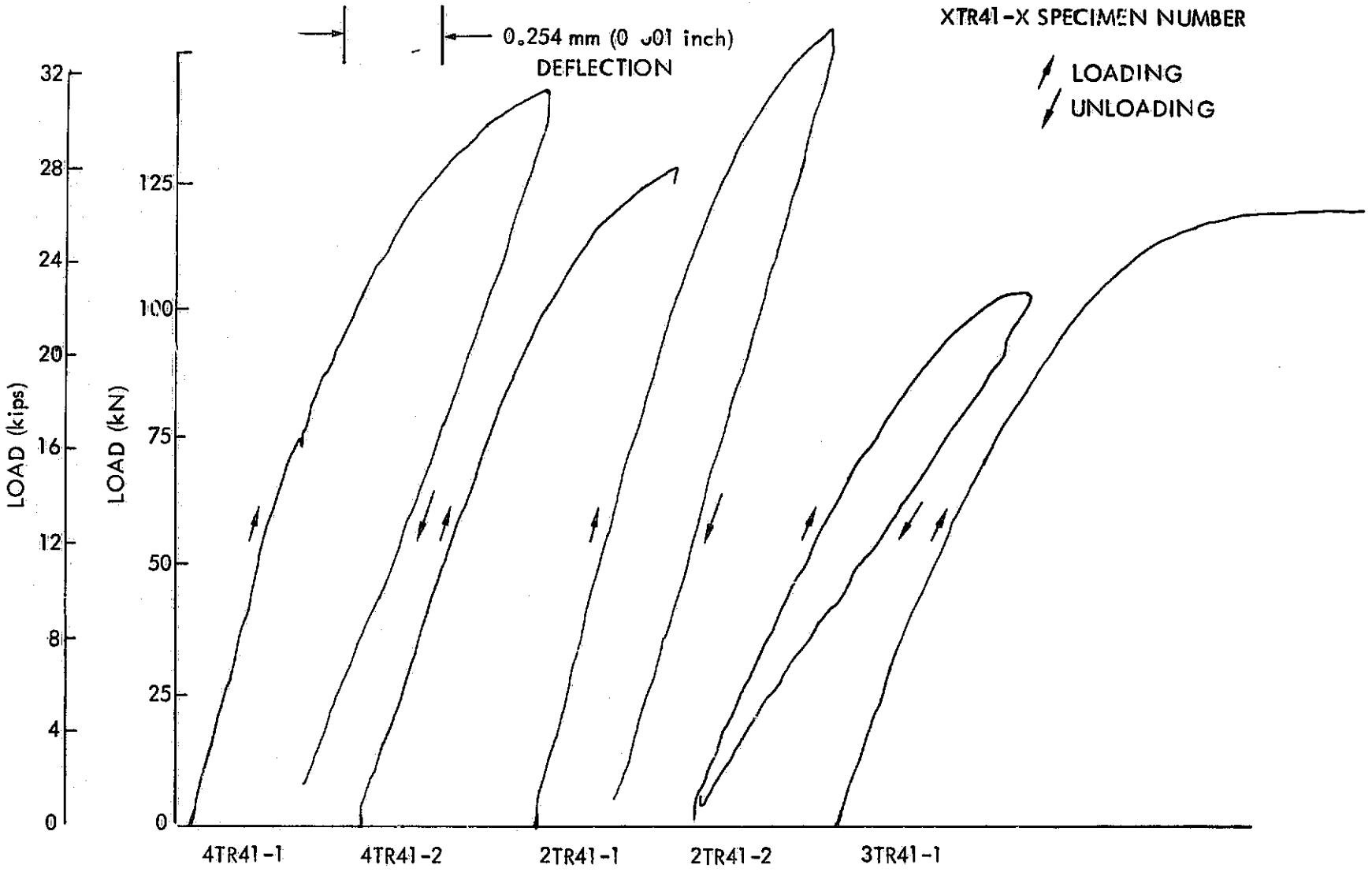

Figure 65: CRACK OPENING DISPLACEMENT RECORDS FOR 1.02mm (0.040 inch) THICK TITANIUM SURFACE FLAWED SPECIMENS (a/2c = 0.15)

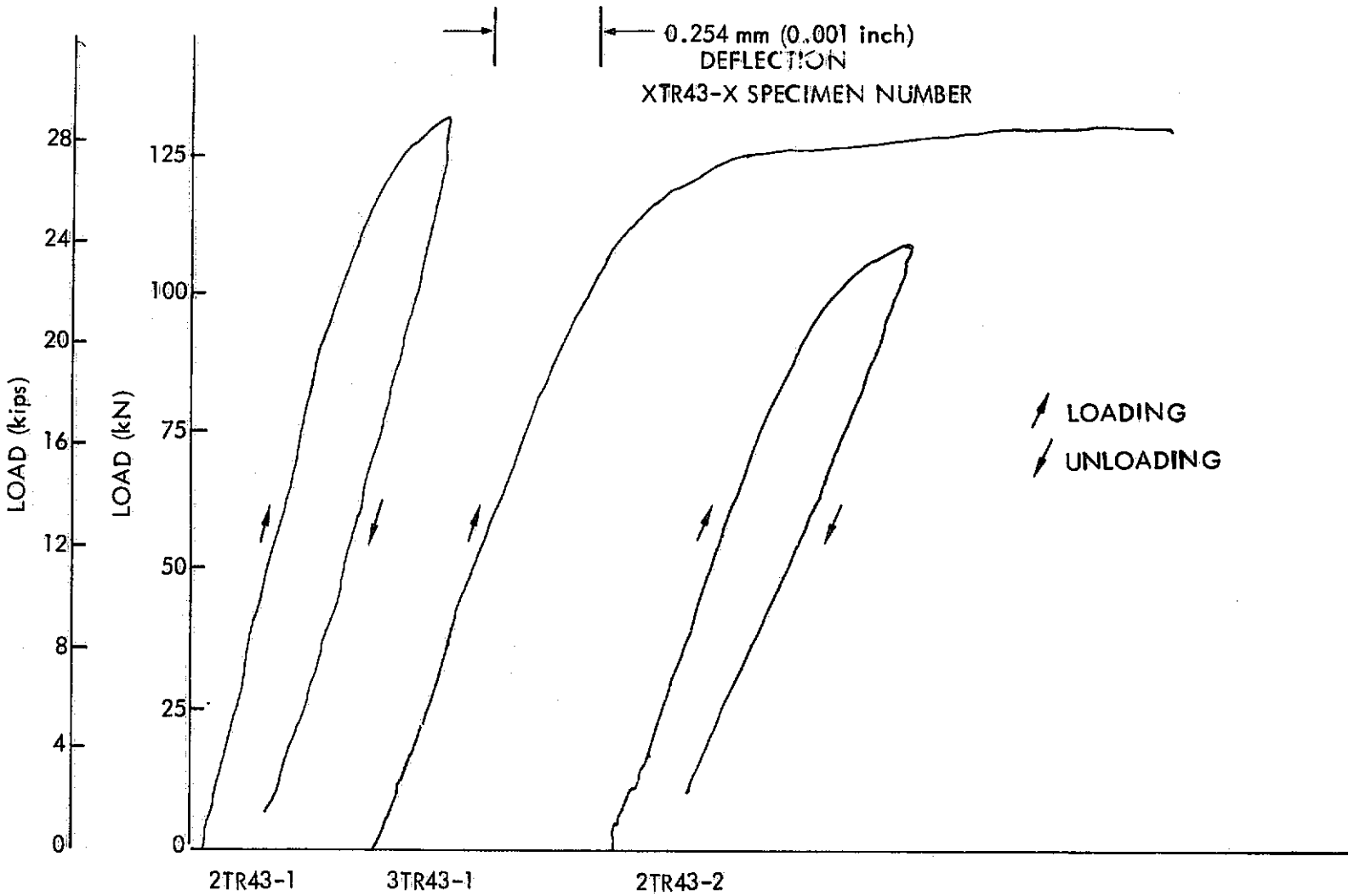

Figure 66: CRACK OPENING DISPLACEMENT RECORDS FOR 1.02mm (0.040 inch) THICK TITANIUM SURFACE FLAWED SPECIMENS (a/2c = 0.30)

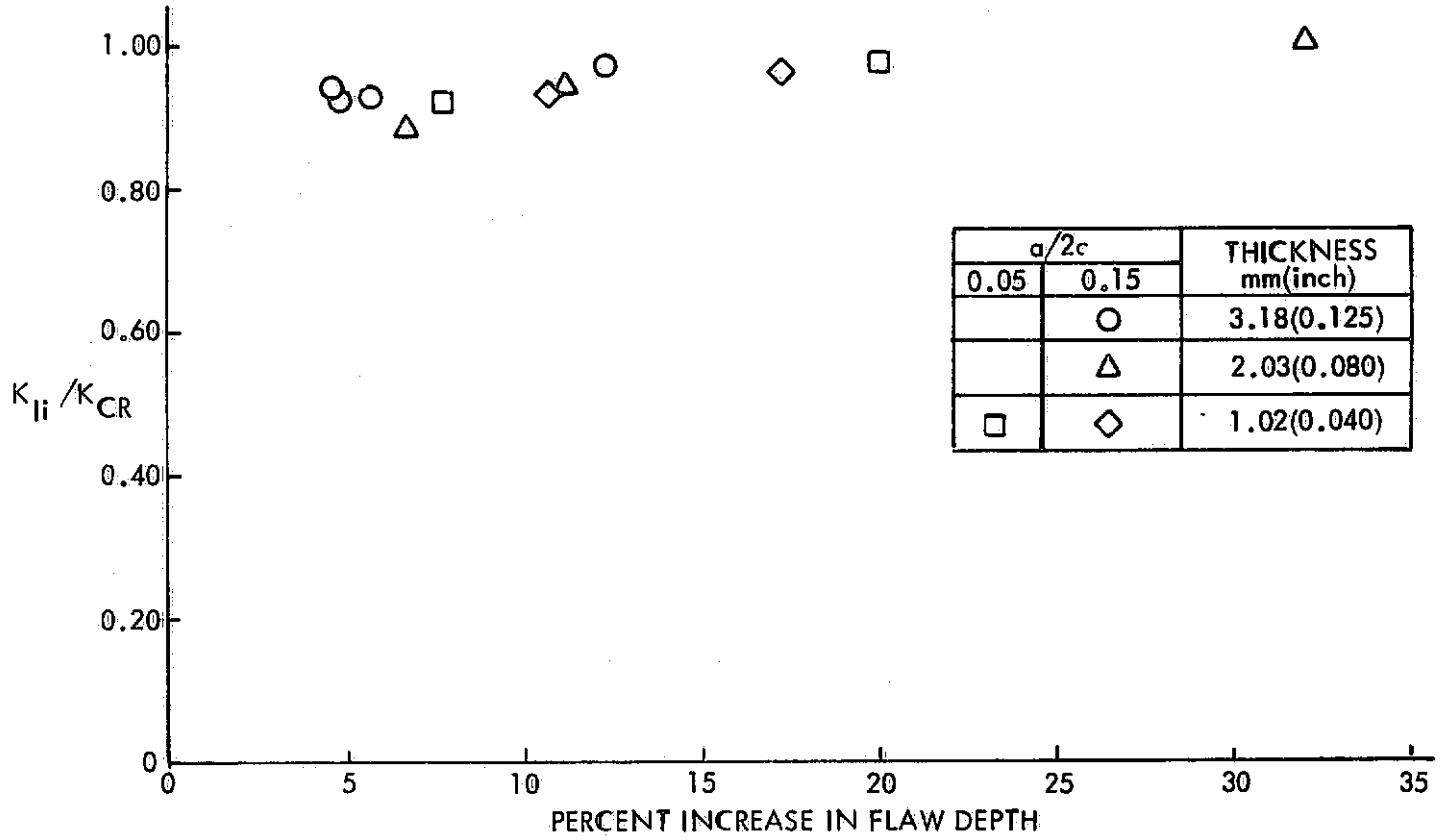

Figure 67 : K_{Ii} / K_{CR} VERSUS PERCENT INCREASE IN FLAW DEPTH FOR ROOM TEMPERATURE 6AI-4V STA TITANIUM (a/2c = 0.15 & 0.05)

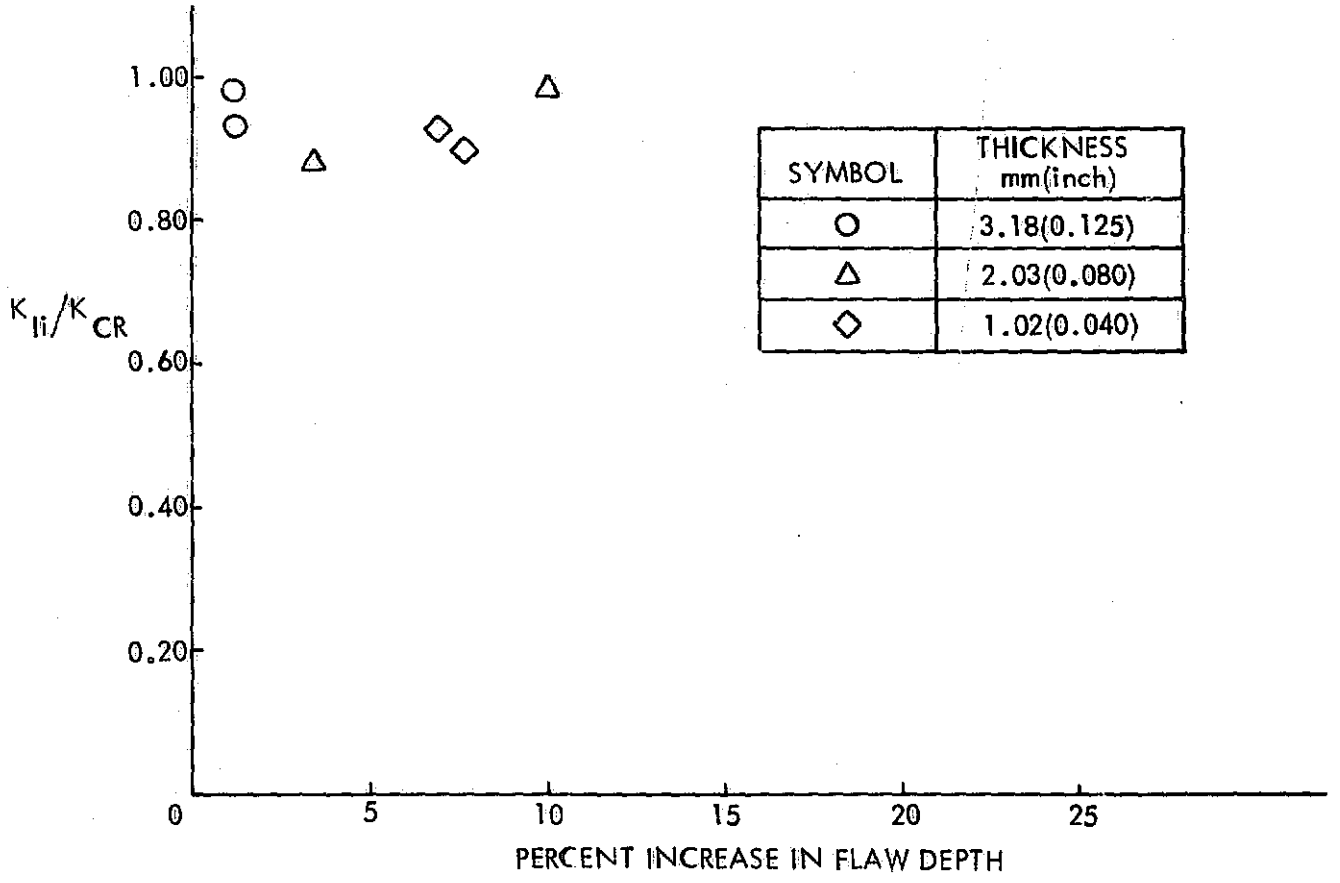

Figure 68 : K_{Ii} / K_{CR} VERSUS PERCENT INCREASE IN FLAW DEPTH FOR ROOM TEMPERATURE 6Al-4V STA TITANIUM (a/2c = 0.30)

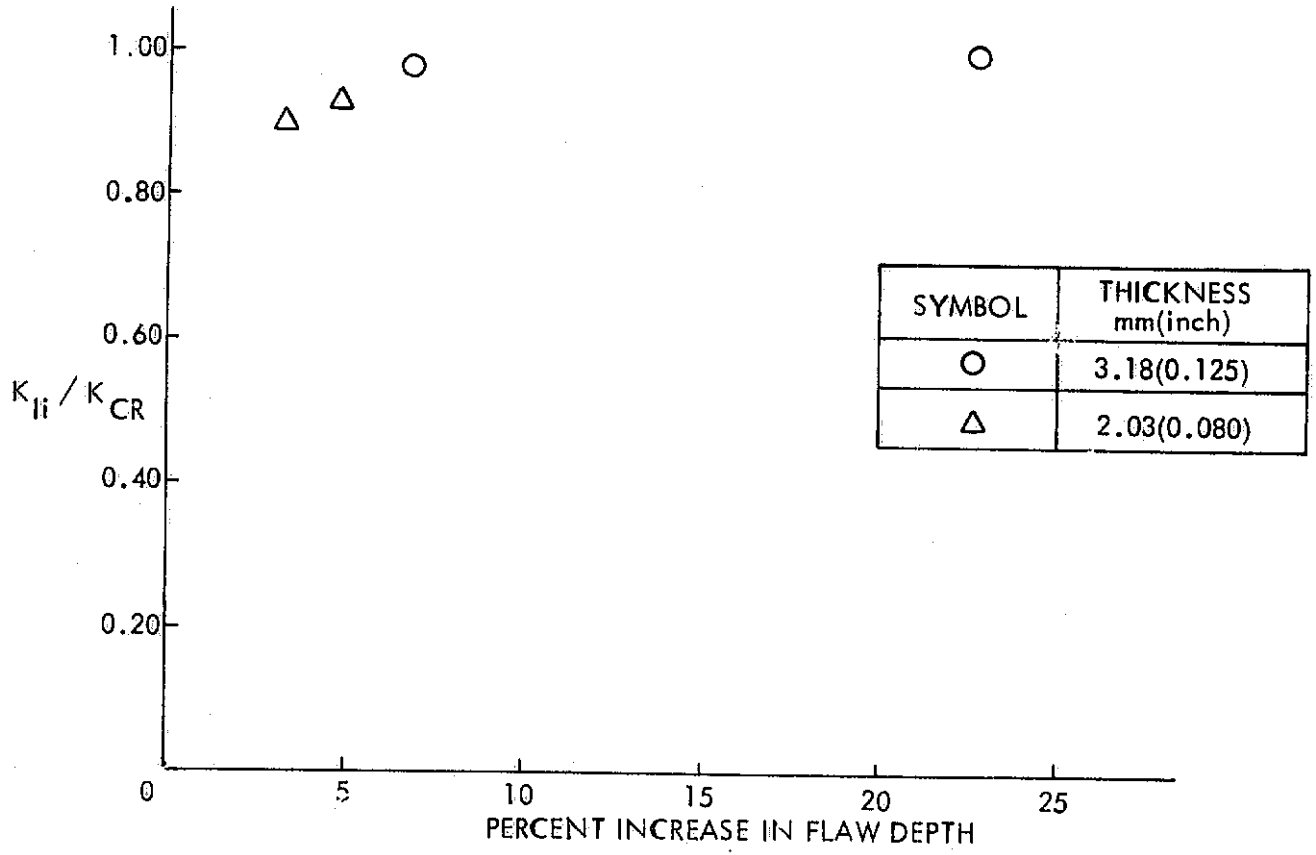

Figure 69 : K_{Ii}/K_{CR} VERSUS PERCENT INCREASE IN FLAW DEPTH FOR ROOM TEMPERATURE 6AI-4V STA TITANIUM ($a/2c = 0.45$)

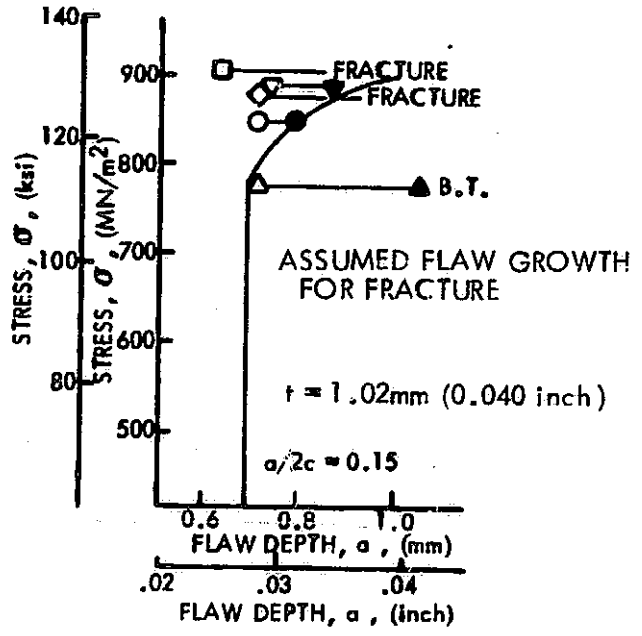

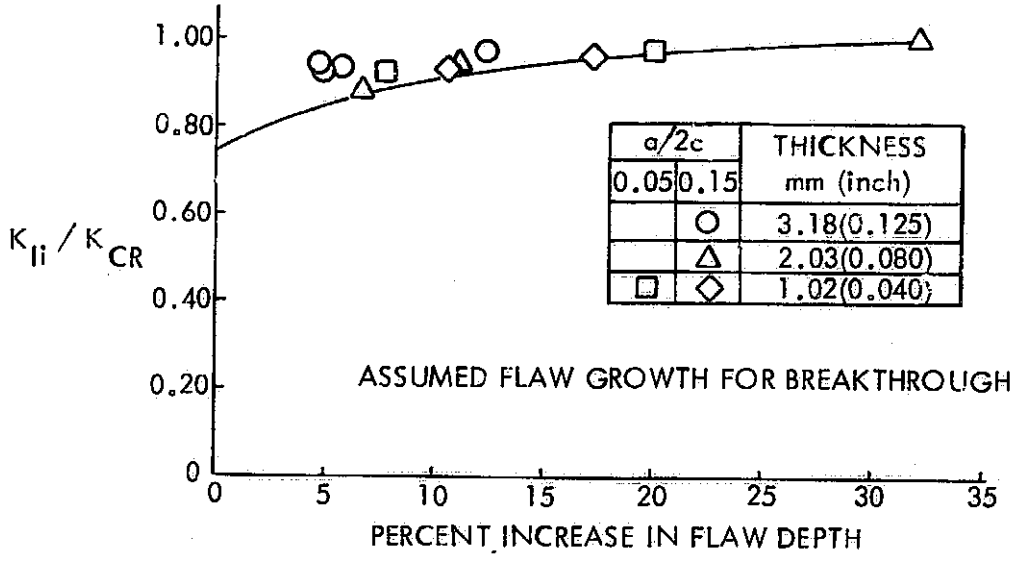

Figure 70: ASSUMED RELATIONSHIPS 6AI-4V STA TITANIUM USED IN CRACK GROWTH RESISTANCE CURVE CALCULATIONS

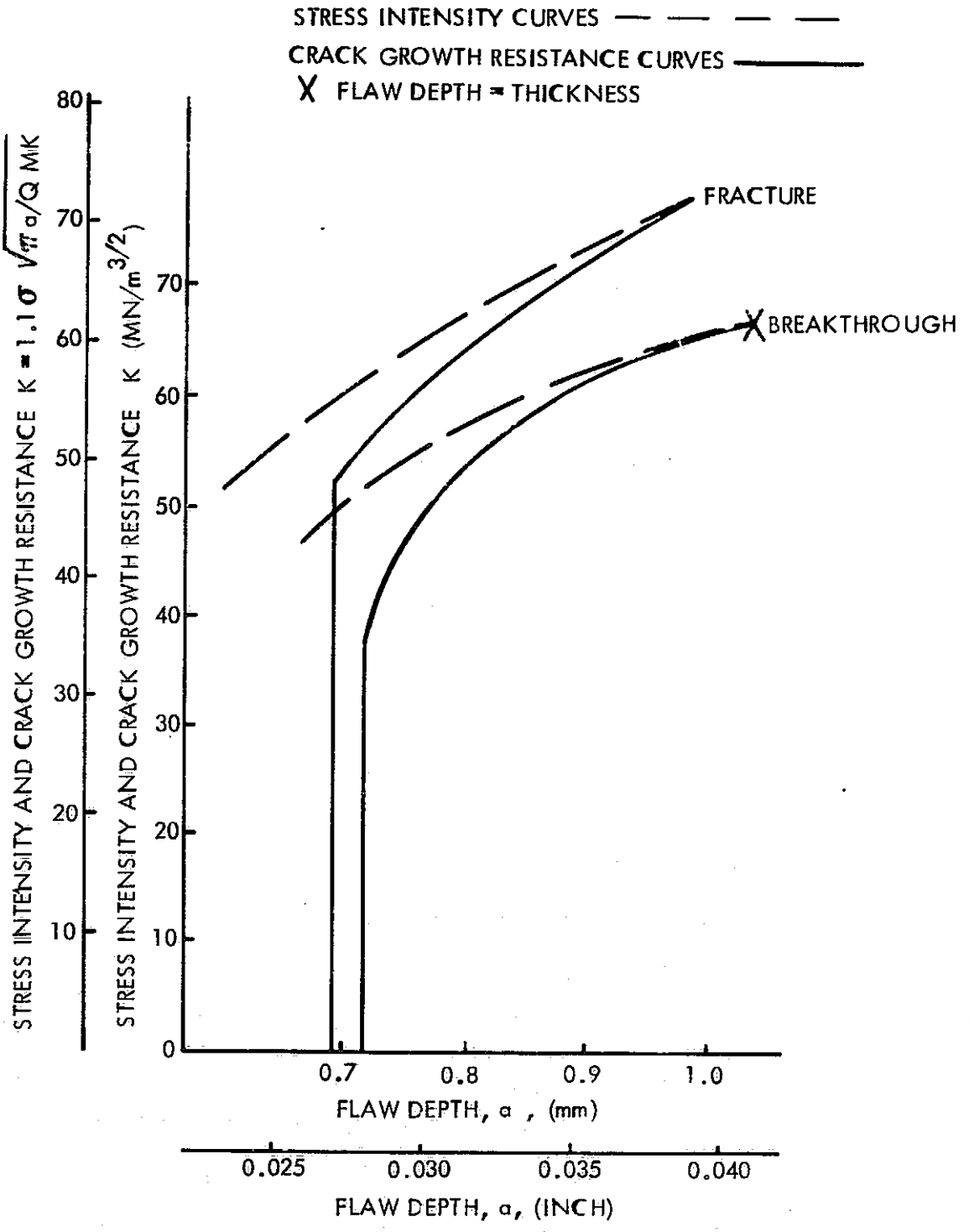

Figure 71 : CRACK GROWTH RESISTANCE AND STRESS INTENSITY CURVES VERSUS CRACK DEPTH FOR ROOM TEMPERATURE 6AI-4V STA TITANIUM BASE METAL (INCLUDES MK CORRECTION)

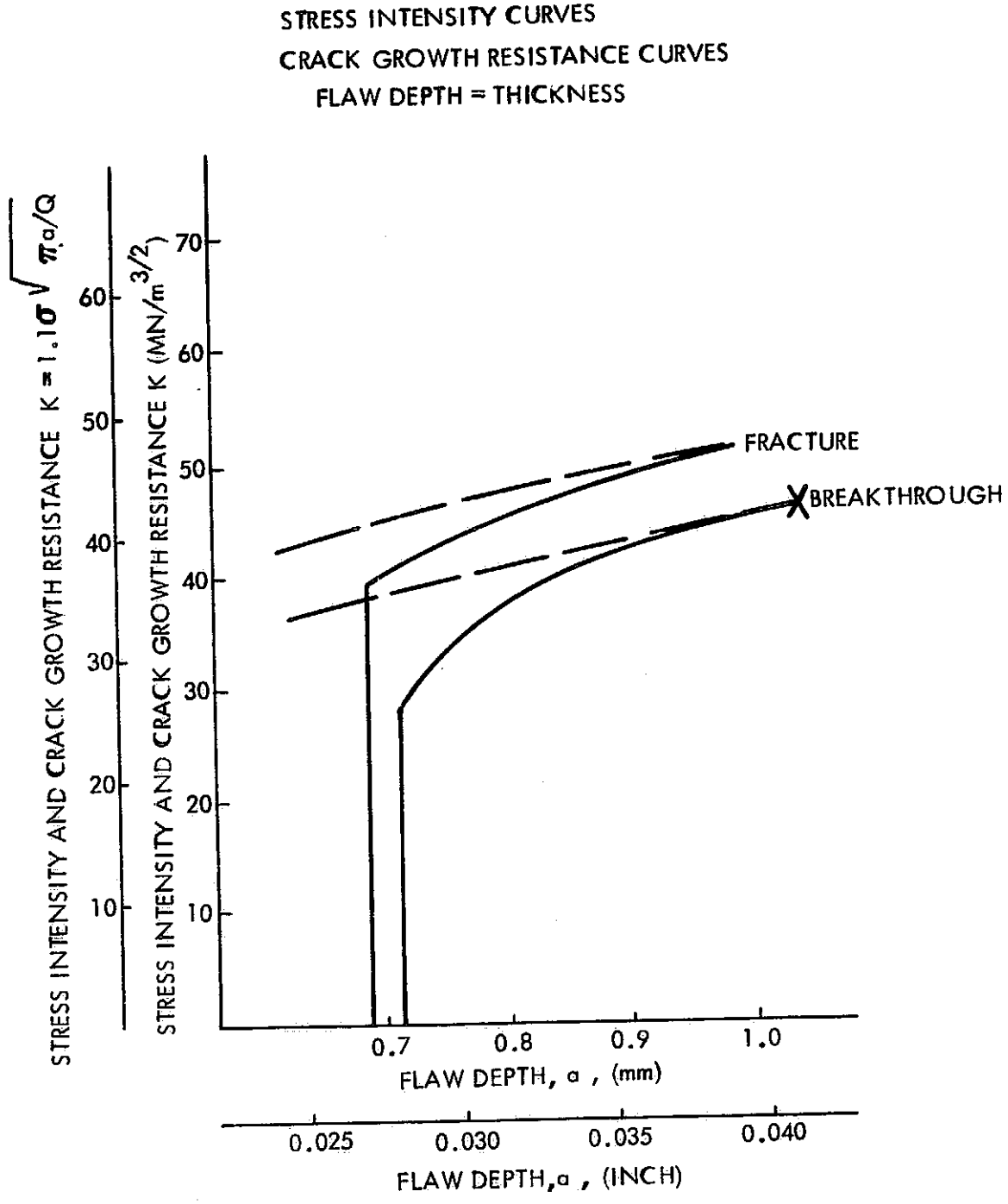

Figure 72 : CRACK GROWTH RESISTANCE AND STRESS INTENSITY CURVES VERSUS CRACK DEPTH FOR ROOM TEMPERATURE 6Al-4V STA TITANIUM BASE METAL

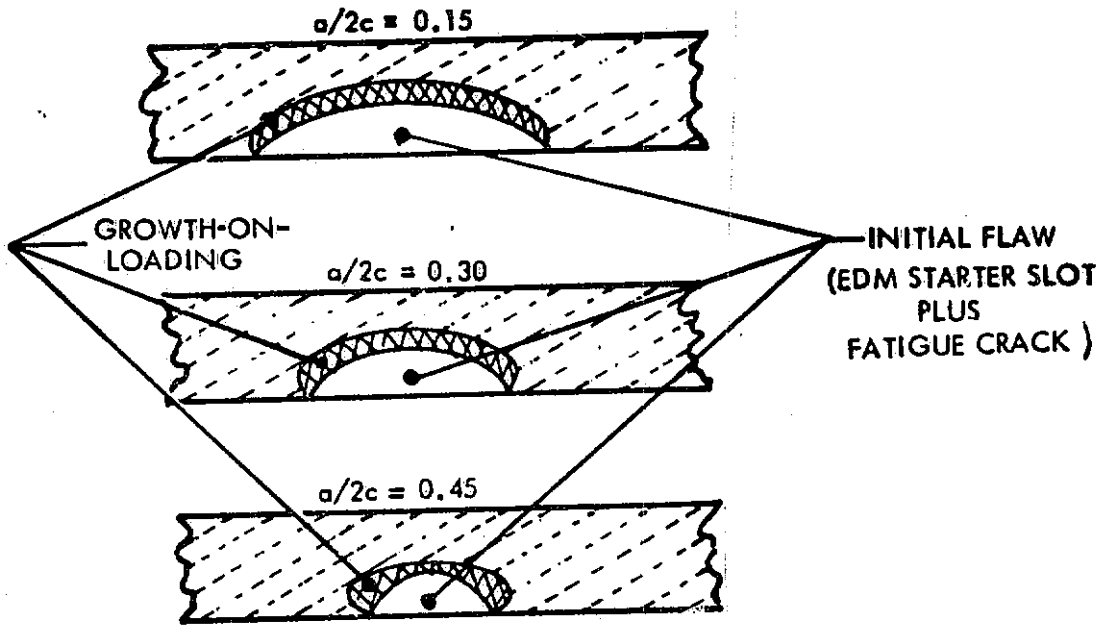

Figure 73: ILLUSTRATION OF GROWTH-ON-LOADING FOR VARIOUS FLAW SHAPES

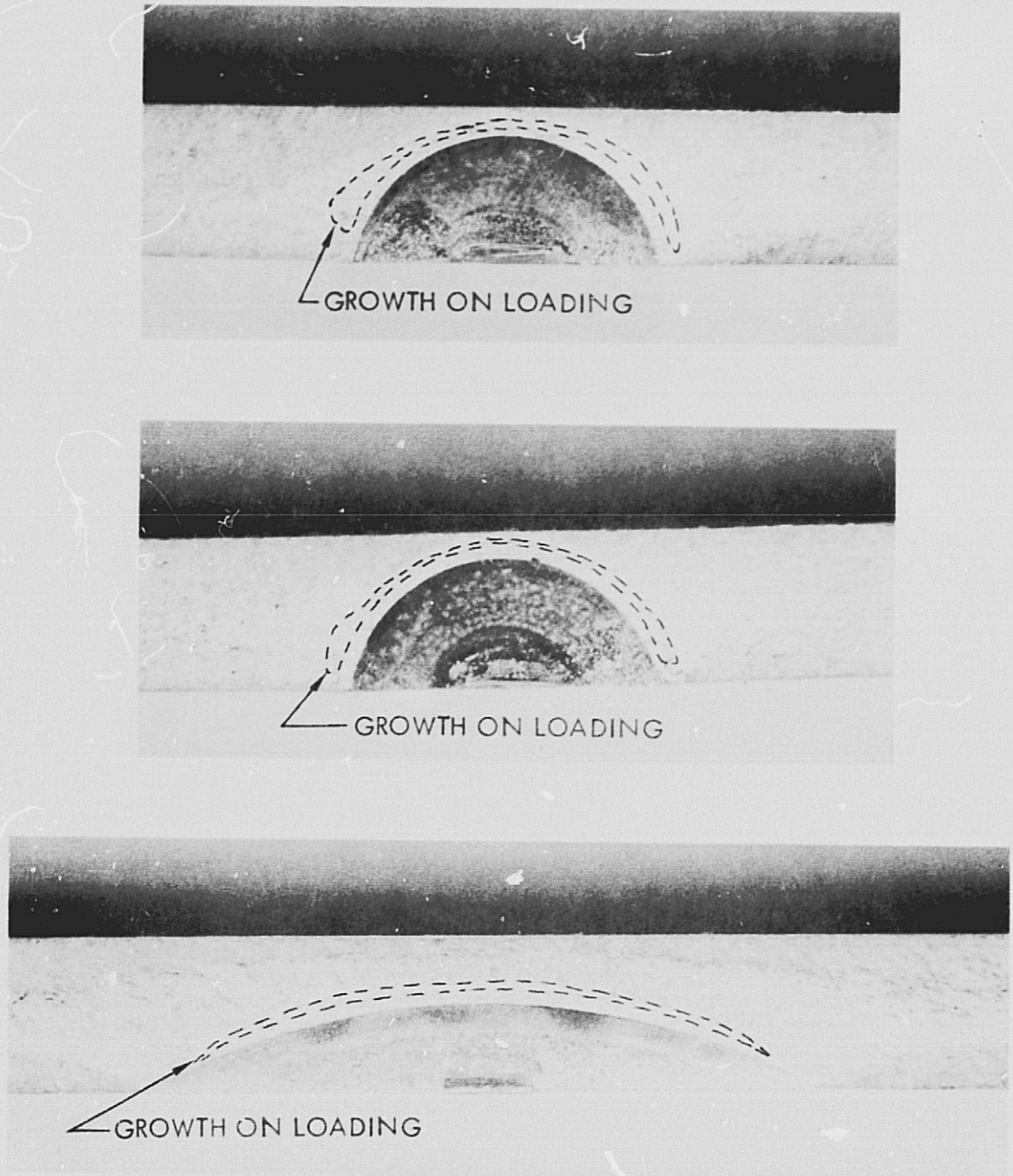

Figure 74: TYPICAL ALUMINUM GROWTH-ON-LOADING SPECIMEN FRACTURE FACES

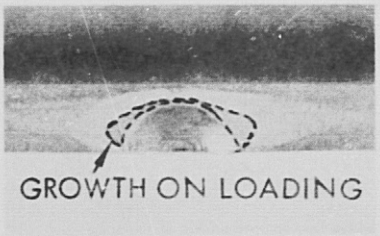

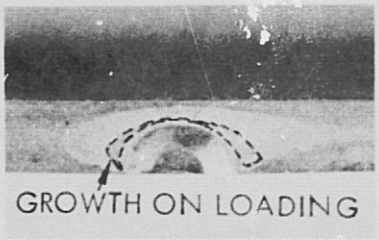

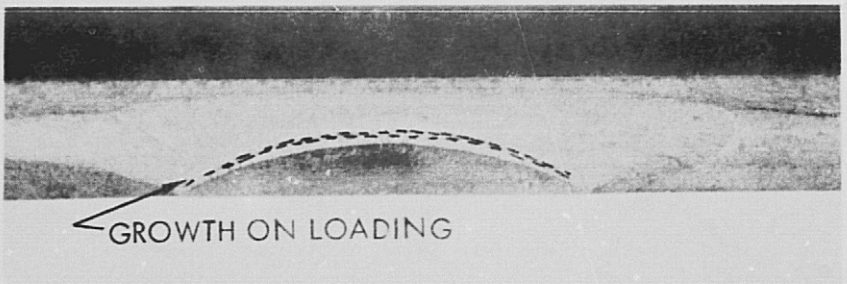

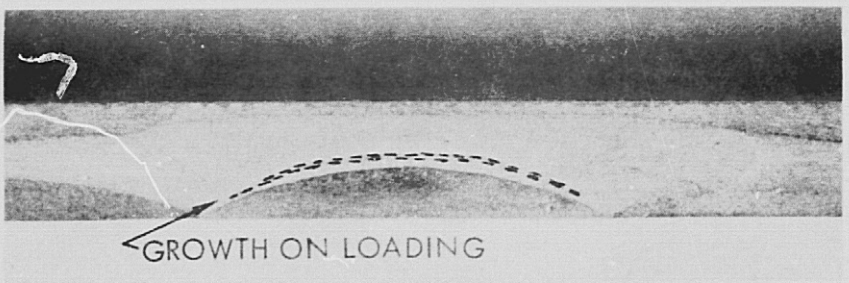

Figure 75: TYPICAL TITANIUM GROWTH-ON-LOADING SPECIMEN FRACTURE FACES

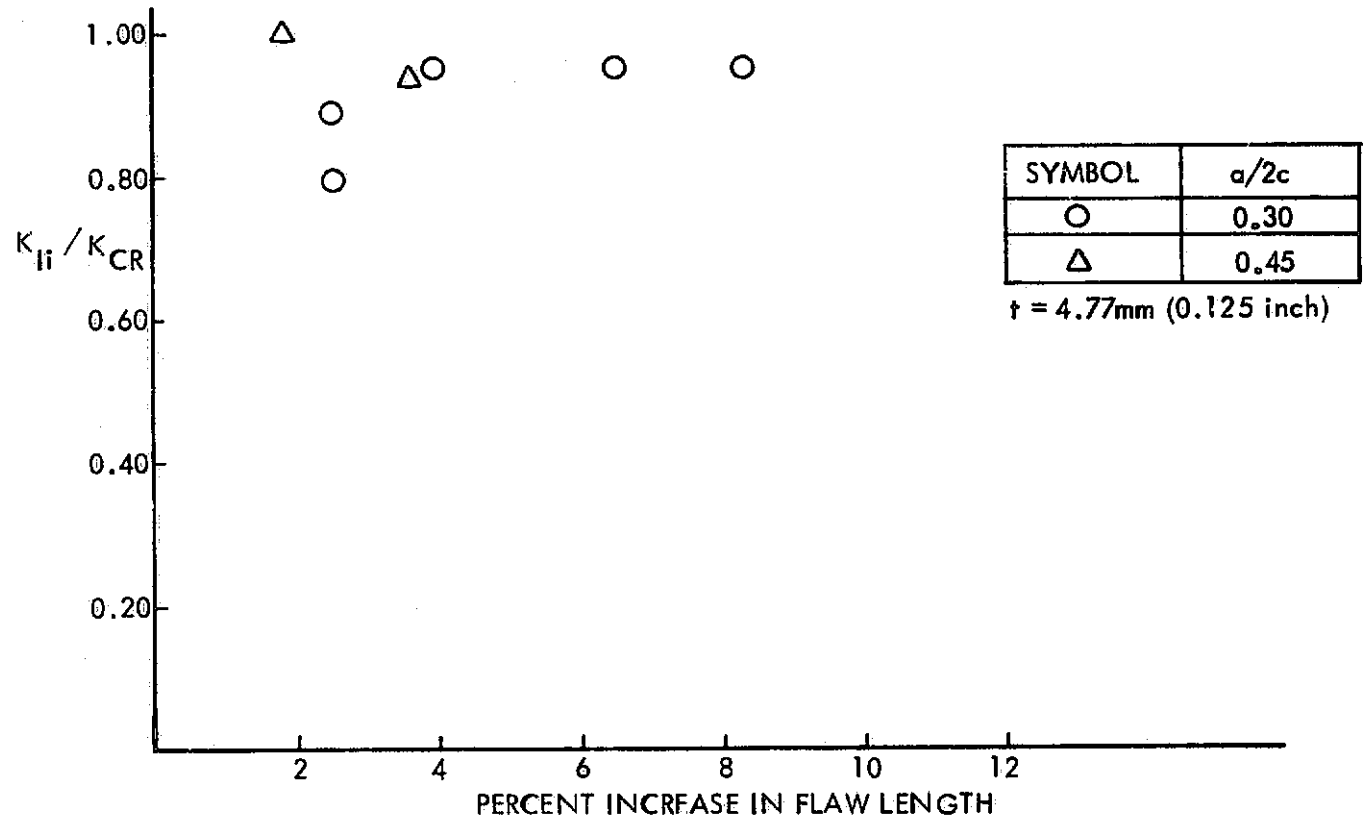

Figure 76 : K_{Ii} / K_{CR} VERSUS PERCENT INCREASE IN FLAW LENGTH FOR ROOM TEMPERATURE 2219-T87 ALUMINUM

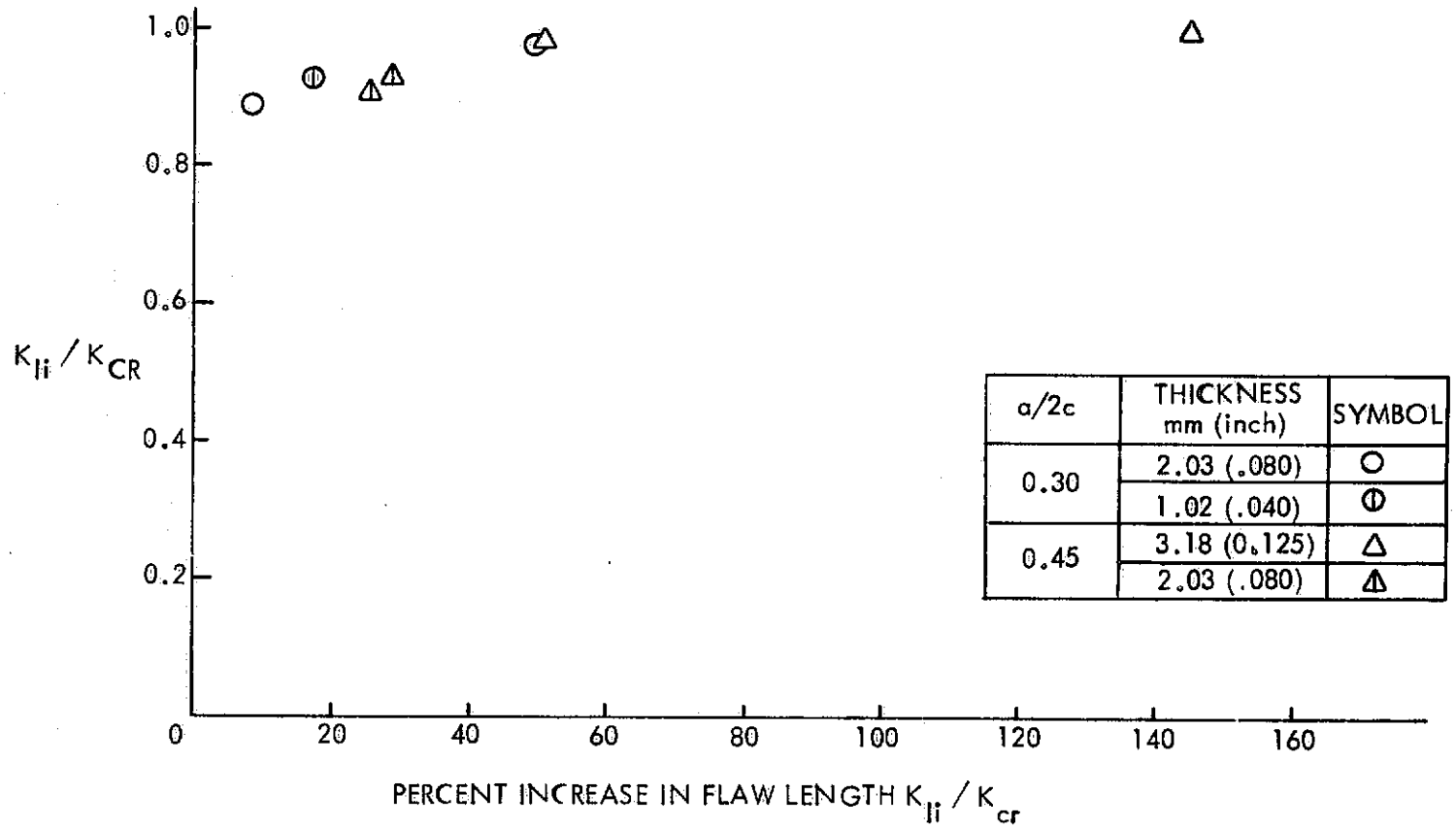

Figure 77: K_{Ii} / K_{CR} VERSUS PERCENT INCREASE IN FLAW LENGTH FOR ROOM TEMPERATURE 6Al-4V STA TITANIUM

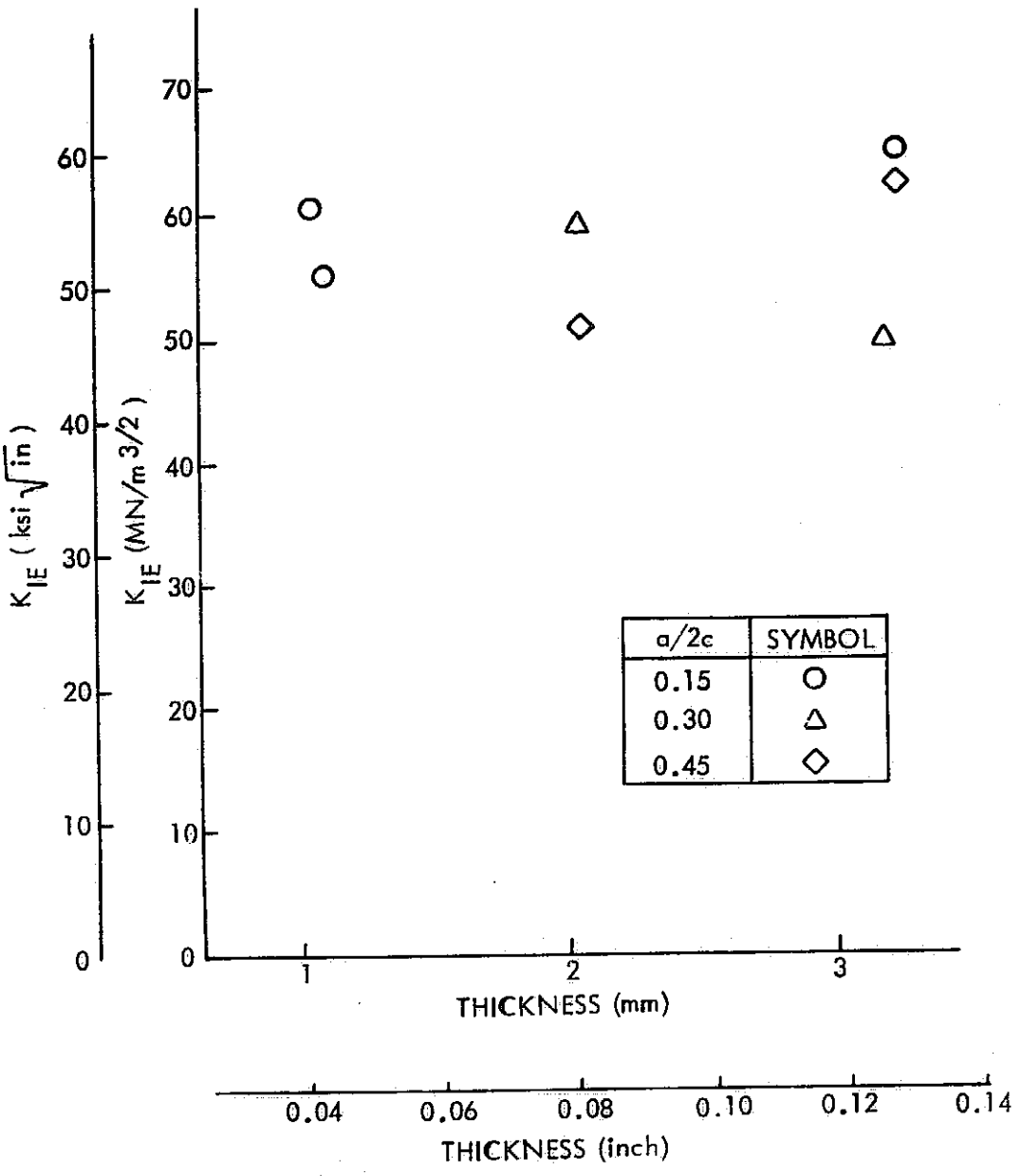

Figure 78 : EFFECT OF THICKNESS ON K_{IE} MEASURED FROM ROOM TEMPERATURE TESTS OF 6Al-4V STA TITANIUM SURFACE FLAW SPECIMENS

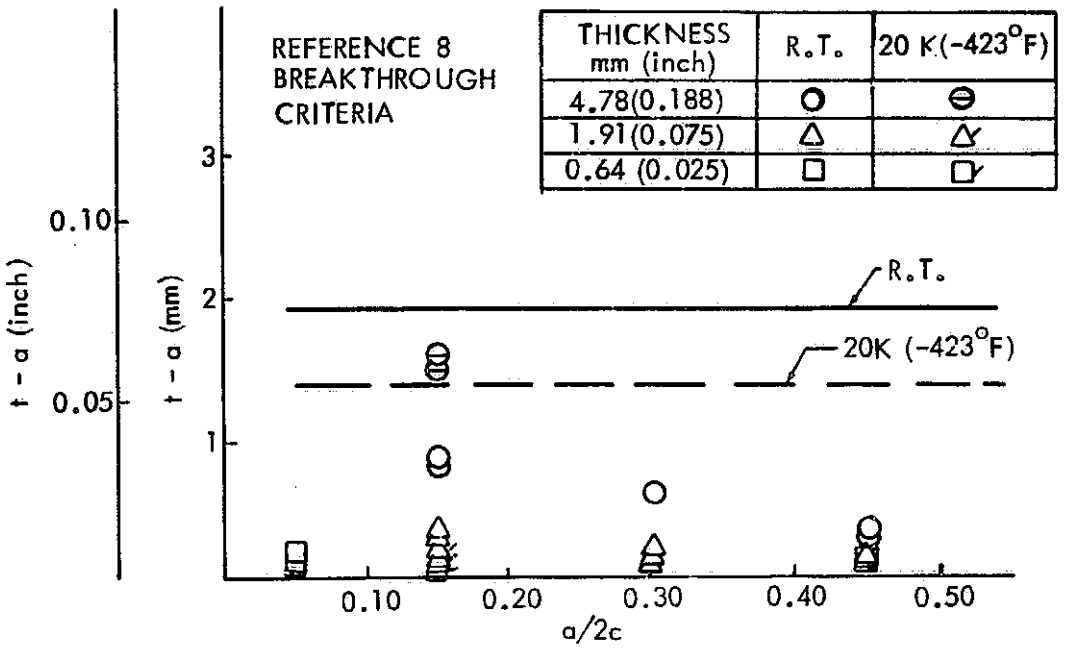

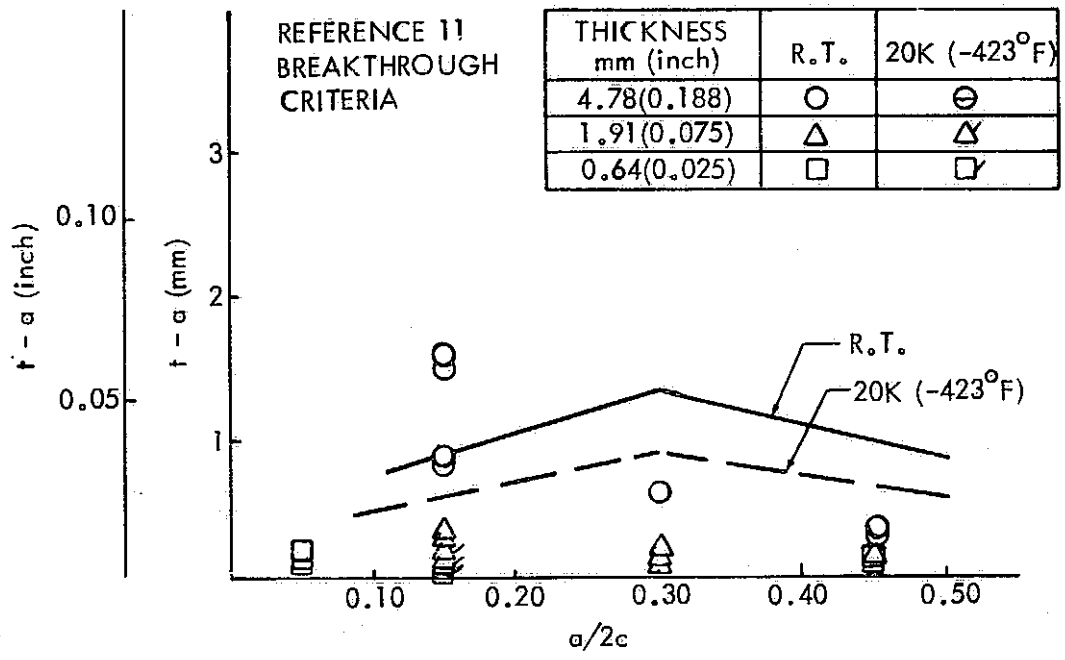

Figure 79: COMPARISON OF ACTUAL AND PREDICTED FAILURE MODES FOR 2219-T87 ALUMINUM SURFACE FLAW SPECIMEN TESTS

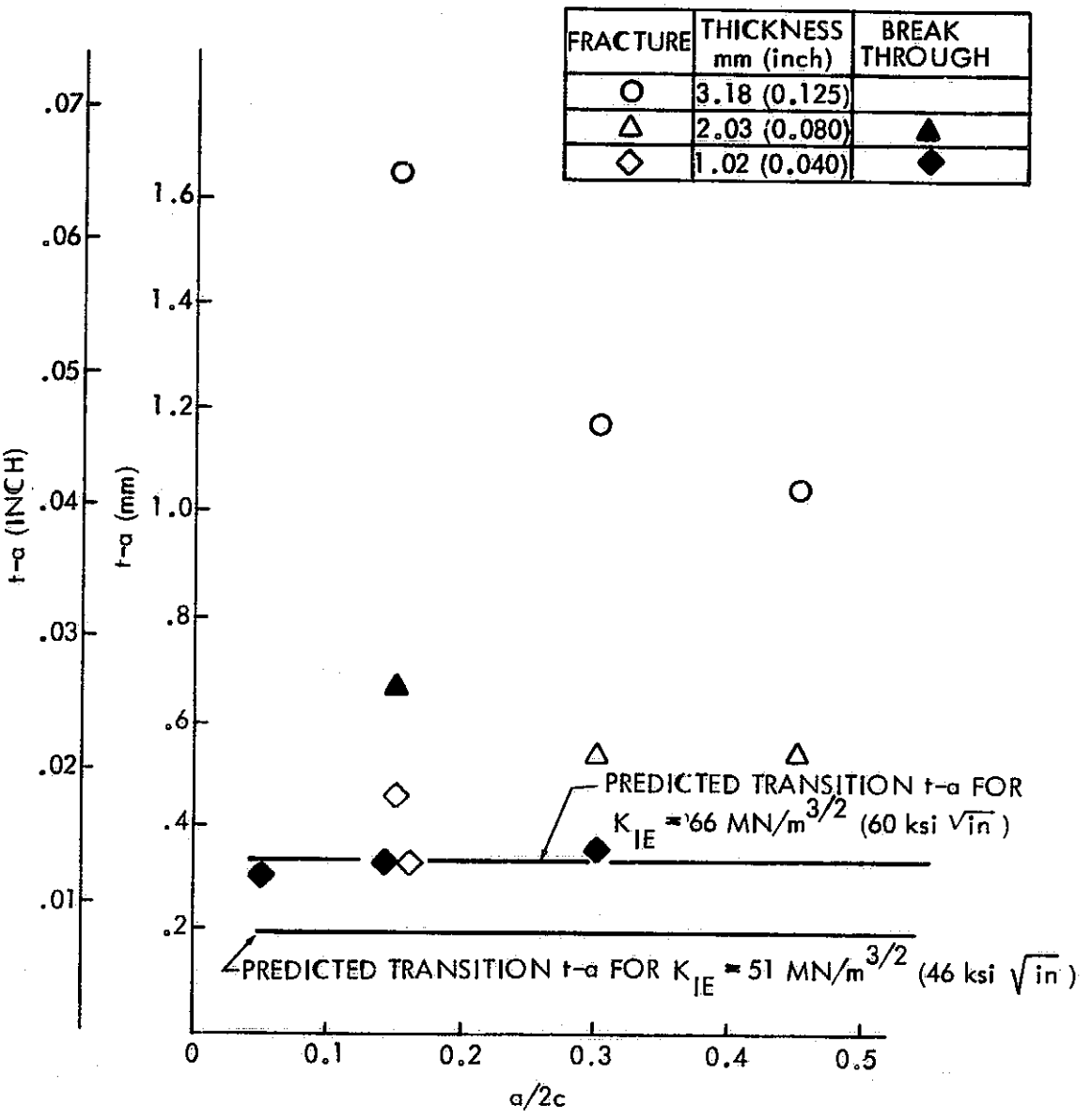

Figure 80 : COMPARISON OF ACTUAL AND PREDICTED (REFERENCE 8)
FAILURE MODE FOR ROOM TEMPERATURE 6Al-4V STA TITANIUM

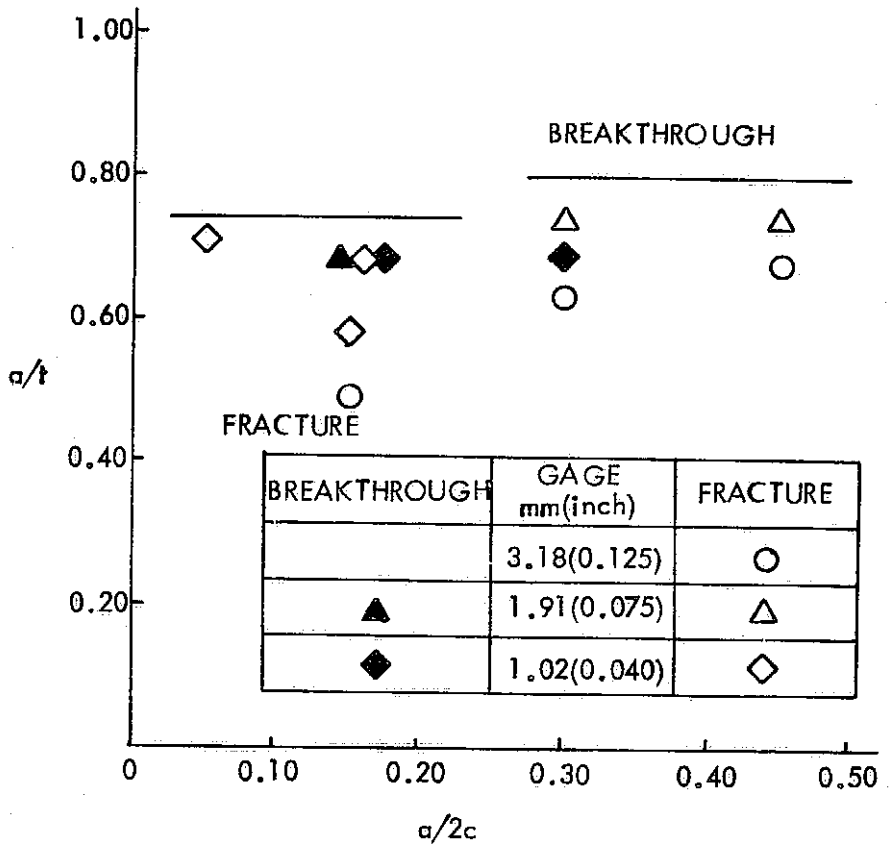

Figure 81: COMPARISON OF ACTUAL AND PREDICTED (REF. 11) FAILURE MODE FOR 6Al-4V STA TITANIUM

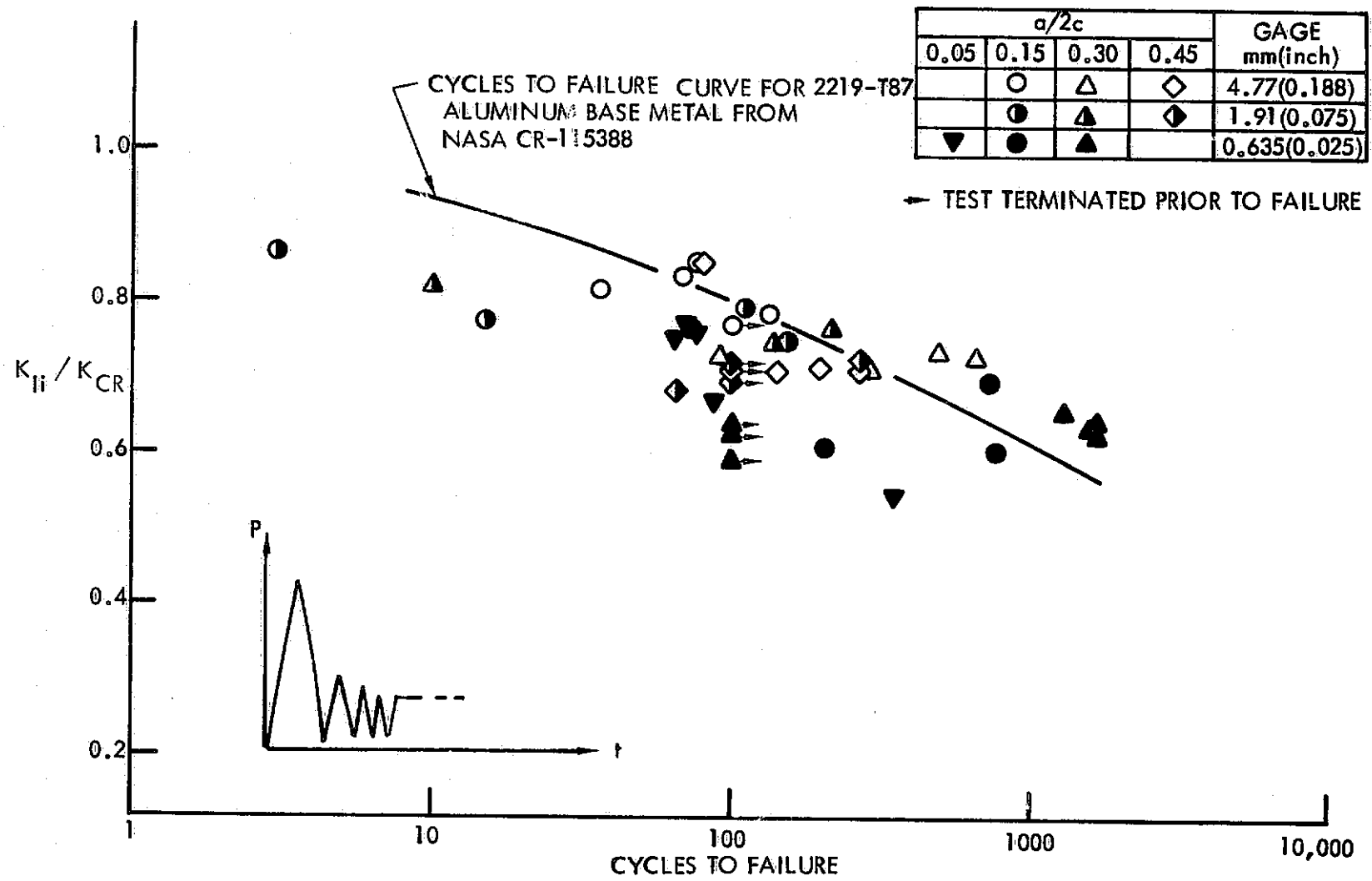

Figure 82 : K_{Ii} / K_{CR} VERSUS CYCLES TO FAILURE FOR 2219-T87 ALUMINUM BASE METAL AT ROOM TEMPERATURE

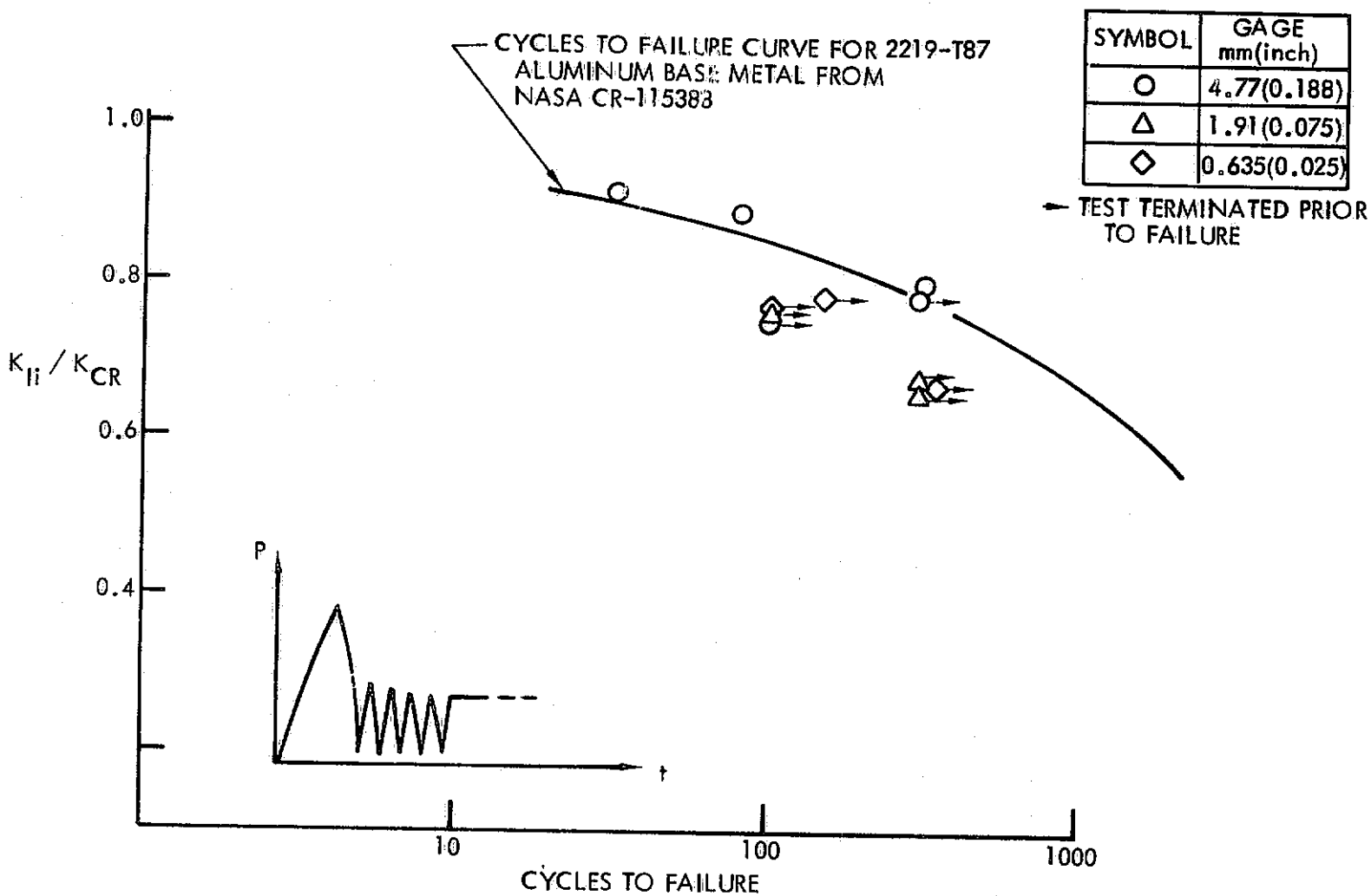

Figure 83 : K_{Ii} / K_{CR} VERSUS CYCLES TO FAILURE FOR 2219-T87 ALUMINUM BASE METAL AT 20K(-423°F)

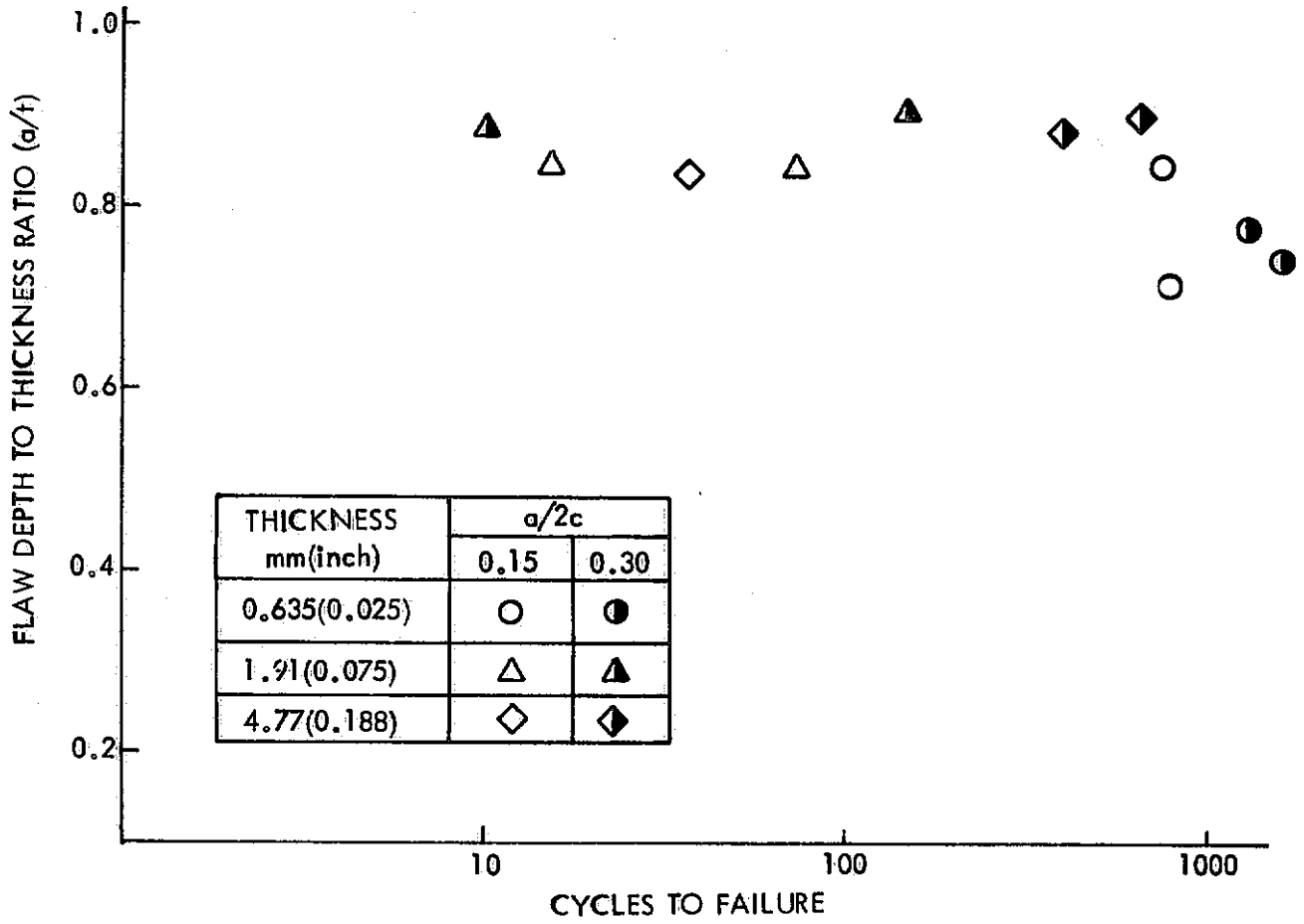

Figure 84: FLAW DEPTH TO THICKNESS RATIO VERSUS CYCLES TO FAILURE FOR ROOM TEMPERATURE 2219-T87 ALUMINUM

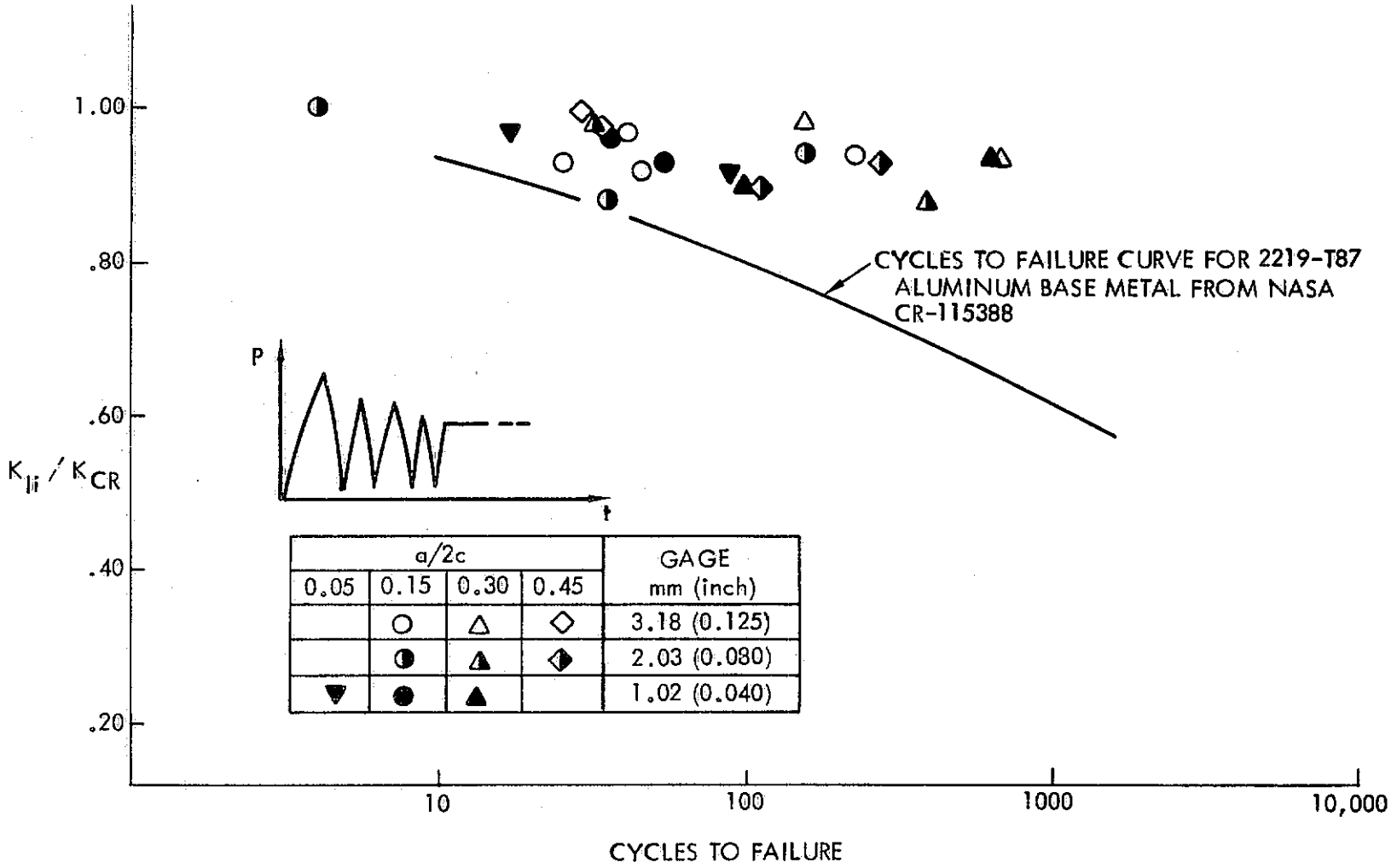

Figure 85 : K_{Ii} / K_{CR} VERSUS CYCLES TO FAILURE FOR 6Al-4V STA TITANIUM AT ROOM TEMPERATURE

Table 1 : CHEMICAL COMPOSITION OF 2219-T87 ALUMINUM AND 6AI-4V TITANIUM SHEET

ELEMENT %	2219-T87 ALUMINUM			6AI-4V TITANIUM		
	SPECIFICATION		MEASURED	SPECIFICATION		MEASURED
	MAXIMUM	MINIMUM		MAXIMUM	MINIMUM	
CARBON				0.08	—	0.02
NITROGEN				0.05	—	0.012
IRON	0.30	—	0.190	0.25	—	0.190
ALUMINUM	BALANCE		BALANCE	6.75	5.50	6.20
VANADIUM	0.15	0.05	0.06	4.50	3.50	4.00
OXYGEN				0.15	—	0.17
TITANIUM	0.10	0.02	0.04	BALANCE		BALANCE
COPPER	6.80	5.80	6.33			
MANGANESE	0.40	0.20	0.30			
MAGNESIUM	0.20	—	0.018			
ZIRCONIUM	0.25	0.10	0.16			
SILICON	0.20	—	0.12			
ZINC	0.10	—	0.03			

Table 2 : ROOM TEMPERATURE 2219-T87 ALUMINUM BASE METAL MECHANICAL PROPERTY TEST RESULTS

MATERIAL CONDITION	SPECIMEN NUMBER	NOMINAL GAGE THICKNESS mm (INCH)	TEST ATMOSPHERE	GRAIN DIRECTION L=LONGITUDINAL T = TRANSVERSE	ULTIMATE STRENGTH MN/m² (KSI)	YIELD STRENGTH MN/m² (KSI)	ELONGATION % IN 50.8 mm (% IN 2.0 INCH)	MODULUS OF ELASTICITY E x 10³ MN/m² (E x 10³ KSI)	POISSON'S RATIO
BASE METAL	AT1-1	4.78 (0.188)	RT AIR	T	473.0 (68.6)	377.2 (54.7)	10		
	AT1-2				472.3 (68.5)	379.2 (55.0)	9		
	1AL-1			L	468.9 (68.0)	382.0 (55.4)	11	76.5 (11.1)	0.299
	1AL-2				467.5 (67.8)	381.3 (55.3)	11	72.4 (10.5)	0.314
	A1/-1	1.91 (0.075)		T	474.4 (68.8)	380.0 (55.1)	9		
	A17-2				476.4 (69.1)	382.0 (55.4)	10		
	7AL-1			L	463.3 (67.2)	378.5 (54.9)	9	73.8 (10.7)	0.312
	7AL-2				462.7 (67.1)	378.5 (54.9)	9	73.1 (10.6)	0.317
	AT3-1	0.635 (0.025)		I	468.9 (68.0)	375.8 (54.5)	8		
	AT3-2				470.9 (68.3)	376.5 (54.6)	9		
	2AL-1			L	467.5 (67.8)	376.5 (54.6)	7	71.7 (10.4)	0.305
	2AL-2				(67.6)	376.5 (51.6)	7	73.8 (10.7)	0.309

Table 3 : LIQUID HYDROGEN TEMPERATURE 2219-T87 ALUMINUM BASE METAL MECHANICAL PROPERTY TEST RESULTS.

MATERIAL CONDITION	SPECIMEN NUMBER	NOMINAL GAGE THICKNESS mm (INCH)	TEST ATMOSPHERE	GRAIN DIRECTION L= LONGITUDINAL T = TRANSVERSE	ULTIMATE STRENGTH MN/m^2 (KSI)	YIELD STRENGTH MN/m^2 (KSI)	ELONGATION % IN 50.8 mm (% IN 2.0 INCH)	REDUCTION IN AREA %	MODULUS OF ELASTICITY $E \times 10^3$ MN/m^2 ($E \times 10^3$ KSI)	POISSON'S RATIO
BASE METAL	AT1-3	3.18 (0.125)	LH_2 20^oK (-423^oF)	T	674.3 (97.8)	462.7 (67.1)	14	17	74.5 (10.8)	
	AT1-4				672.3 (97.5)	466.1 (67.6)	12	16	76.5 (11.1)	
	1AL-3			L	651.6 (94.5)	467.5 (67.8)	14	24	76.5 (11.1)	0.315
	1AL-4				658.5 (95.5)	471.6 (68.4)	13	21	72.4 (10.5)	0.324
	AT2-3	6.35 (0.250)		T	676.4 (98.1)	468.9 (68.0)	12	15	75.2 (10.9)	
	AT2-4				681.9 (98.9)	473.0 (68.6)	13	14	77.2 (11.2)	
	7AL-3			L	662.6 (96.1)	465.4 (67.5)	15	14	77.9 (11.3)	0.320
	7AL-4				664.0 (96.3)	470.2 (68.2)	14	16	75.8 (11.0)	0.344
	AT3-3	9.53 (0.375)		T	655.0 (95.0)	453.0 (65.7)	10	8	74.5 (10.8)	
	AT3-4				675.0 (97.9)	464.0 (67.3)	11	10	73.8 (10.7)	
	2AL-3			L	666.1 (96.6)	463.3 (67.2)	11	12	78.6 (11.4)	0.325
	2AL-4				626.1 (90.8)	446.1 (64.7)	11	14	73.8 (10.7)	0.344

Table 4 : ROOM TEMPERATURE 6Al-4V STA TITANIUM BASE METAL
MECHANICAL PROPERTY TEST RESULTS

MATERIAL, CONDITION	SPECIMEN NUMBER	NOMINAL GAGE THICKNESS mm (INCH)	TEST ATMOSPHERE	GRAIN DIRECTION L= LONGITUDINAL T = TRANSVERSE	ULTIMATE STRENGTH MN/m^2 (KSI)	YIELD STRENGTH MN/m^2 (KSI)	ELONGATION % IN 50.8 mm (% IN 2.0 INCH)	MODULUS OF ELASTICITY $E \times 10^3$ MN/m^2 ($E \times 10^3$ KSI)	POISSON'S RATIO
BASE METAL	T-3	3.18 (0.125)	R.T. Air	T	1247.3 (180.9)	1154.2 (167.4)	10		
	TT-6				1248.7 (181.1)	1142.5 (165.7)	7		
	TL-5			L	1264.5 (183.4)	1132.8 (164.3)	6	122.0 (17.7)	0.281
	TL-6				1252.1 (181.6)	1130.1 (163.9)	7	119.3 (17.3)	0.290
	T-2	2.03 (0.080)		T	1234.9 (179.1)	1126.6 (163.4)	11		
	TT-5				1234.2 (179.0)	1127.3 (163.5)	6		
	TL-3			L	1219.0 (176.8)	1076.3 (156.1)	8	122.7 (17.8)	0.286
	TL-4				1239.7 (179.8)	1082.5 (157.0)	6	116.5 (16.9)	0.288
	T-1	1.02 (0.040)		T	1236.3 (179.3)	1115.6 (161.8)	7		
	TT-4				1230.8 (178.5)	1118.4 (162.2)	6		
	TL-1			L	1267.3 (183.8)	1117.7 (162.1)	6	122.0 (17.7)	0.278
	TL-2				1244.5 (180.5)	1067.3 (154.8)	4	119.3 (17.3)	0.284

Table 5 : ROOM TEMPERATURE 2219-T87 ALUMINUM BASE METAL CENTER CRACK PANEL DATA (t = 4.78 mm (0.188 inch))

SPECIMEN NUMBER	GAGE THICKNESS, t mm (INCH)	GAGE WIDTH, W mm (INCH)	TEST TEMPERATURE	INITIAL FLAW LENGTH, 2c mm (INCH)	STRESS AT START OF CRACK GROWTH, σ_s MN/m^2 (KSI)	MAXIMUM GROSS SECTION STRESS, σ_G MN/m^2 (KSI)	MAXIMUM NET SECTION STRESS, σ_N MN/m^2 (KSI)	CRITICAL CRACK LENGTH, 2c mm (INCH)	K_{cn} $MN/m^{3/2}$ (KSI $\sqrt{IN}$)
1AR-1	4.72 (0.186)	304.8 (12.0)	RT	91.44 (3.60)	131.0 (19.0)	193.1 (28.0)	329.6 (47.8)	128.02 (5.04)	77.1 (70.2)
1AR-2	4.75 (0.187)	304.8 (12.0)	RT	76.71 (3.02)	143.4 (20.8)	208.2 (30.2)	328.9 (47.7)	113.28 (4.46)	75.1 (68.3)
1AR-3	4.78 (0.188)	304.8 (12.0)	RT	26.67 (1.05)			297.9 (43.2)		61.5 (56.0)
1AR-4	4.80 (0.189)	304.8 (12.0)	RT	61.47 (2.42)	150.3 (21.8)	228.9 (33.2)	344.1 (49.9)	102.11 (4.02)	73.1 (66.5)
1AR-5	4.70 (0.185)	304.8 (12.0)	RT	10.67 (0.42)	284.8 (41.3)	351.0 (50.9)	396.5 (57.5)	35.05 (1.38)	45.4 (41.3)
1AR-6	4.62 (0.182)	304.8 (12.0)	RT	15.75 (0.62)	290.3 (42.1)	309.6 (44.9)	351.0 (50.9)	36.07 (1.42)	48.9 (44.5)

Table 6 : ROOM TEMPERATURE 2219-T87 ALUMINUM BASE METAL CENTER CRACK PANEL DATA (t = 1.91mm(0.075 inch))

SPECIMEN NUMBER	GAGE THICKNESS, t mm (INCH)	GAGE WIDTH, W mm (INCH)	TEST TEMPERATURE	INITIAL FLAW LENGTH, 2c mm (INCH)	STRESS AT START OF CRACK GROWTH, σ_s MN/m^2 (KSI)	MAXIMUM GROSS SECTION STRESS, σ_G MN/m^2 (KSI)	MAXIMUM NET SECTION STRESS, σ_N MN/m^2 (KSI)	CRITICAL CRACK LENGTH, 2c mm (INCH)	$K_{c,cn}$ MN/m$^{3/2}$ (KSI$\sqrt{IN}$)
7AR-1	1.93 (0.076)	304.8 (12.0)	RT	91.44 (3.60)	135.8 (19.7)	177.9 (25.8)	297.2 (43.1)	123.95 (4.88)	71.1 (64.7)
7AR-2	2.01 (0.079)	304.8 (12.0)	RT	75.95 (2.99)	139.3 (20.2)	208.2 (30.2)	308.2 (44.7)	100.33 (3.95)	74.6 (67.9)
7AR-3	1.98 (0.078)	304.8 (12.0)	RT	60.96 (2.40)	166.9 (24.2)	225.5 (32.7)	323.4 (46.9)	93.47 (3.68)	71.7 (65.2)
7AR-4	1.93 (0.076)	304.8 (12.0)	RT	15.24 (0.60)	277.2 (40.2)	315.8 (45.8)	357.2 (51.8)	35.56 (1.40)	49.1 (44.7)
7AR-5	1.96 (0.077)	304.8 (12.0)	RT	25.15 (0.99)	270.3 (39.2)	298.6 (43.3)	356.5 (51.7)	49.53 (1.95)	59.9 (54.5)
7AR-6	1.91 (0.075)	304.8 (12.0)	RT	10.16 (0.40)	322.0 (46.7)	346.8 (50.3)	390.9 (56.7)	34.54 (1.36)	43.7 (39.8)

Table 7 : ROOM TEMPERATURE 2219-T87 ALUMINUM BASE METAL CENTER CRACK PANEL DATA (t = 0.64 mm(0.025 inch))

SPECIMEN NUMBER	GAGE THICKNESS, t mm (INCH)	GAGE WIDTH, W mm (INCH)	TEST TEMPERATURE	INITIAL FLAW LENGTH, 2c mm (INCH)	STRESS AT START OF CRACK GROWTH, σ_s MN/m^2 (KSI)	MAXIMUM GROSS SECTION STRESS, σ_G MN/m^2 (KSI)	MAXIMUM NET SECTION STRESS, σ_N MN/m^2 (KSI)	CRITICAL CRACK LENGTH, 2c mm(INCH)	K_{cn} $MN/m^{3/2}$ ($KSI\sqrt{IN}$)
2AR-1	0.787 (0.031)	304.8 (12.0)	RT	91.44 (3.60)	97.2 (14.1)	144.1 (20.9)	251.7 (36.5)	132.08 (5.20)	57.6 (52.4)
2AR-2	0.686 (0.027)	304.8 (12.0)	RT	75.95 (2.99)	120.7 (17.5)	184.1 (26.7)	287.5 (41.7)	111.00 (4.37)	66.0 (60.1)
2AR-3	0.838 (0.033)	304.8 (12.0	RT	60.71 (2.39)	137.2 (19.9)	217.2 (31.5)	317.2 (46.0)	97.28 (3.83)	69.0 (62.8)
2AR-4	0.762 (0.030)	304.8 (12.0)	RT	15.24 (0.60)	274.4 (39.8)	297.2 (43.1)	335.8 (48.7)	35.56 (1.40)	46.2 (42.0)
2AR-5	0.686 (0.027)	304.8 (12.0)	RT	24.64 (0.97)	262.0 (38.0)	289.6 (42.0)	350.3 (50.8)	53.09 (2.09)	57.6 (52.4)
2AR-6	0.813 (0.032)	304.8 (12.0)	RT	12.70 (0.50)		288.2 (41.8)			40.9 (37.2)

Table 8 : LIQUID HYDROGEN TEMPERATURE 2219-T87 ALUMINUM BASE METAL CENTER CRACK PANEL DATA

SPECIMEN NUMBER	GAGE THICKNESS, t mm (INCH)	GAGE WIDTH, W mm (INCH)	TEST TEMPERATURE K (°F)	INITIAL FLAW LENGTH, 2c mm (INCH)	STRESS AT START OF CRACK GROWTH, σ_s MN/m^2 (KSI)	MAXIMUM GROSS SECTION STRESS, σ_G MN/m^2 (KSI)	MAXIMUM NET SECTION STRESS, σ_N MN/m^2 (KSI)	CRITICAL CRACK LENGTH, 2c mm (INCH)	K_{cn} MN/m$^{3/2}$ (KSI$\sqrt{IN}$)
1AH-1	4.72 (0.186)	304.8 (12.0)	20 (-423)	91.95 (3.62)	152.4 (22.1)	193.1 (28.0)	322.7 (46.8)	120.4 (4.74)	77.4 (70.4)
1AH-2	4.78 (0.188)	304.8 (12.0)	20 (-423)	20.83 (0.82)	294.4 (42.7)	347.5 (50.4)	405.4 (58.8)	41.15 (1.62)	63.1 (57.4)
7AH-1	1.93 (0.076)	304.8 (12.0)	20 (-423)	10.41 (0.41)	387.5 (56.2)	422.7 (61.3)	468.9 (68.0)	26.67 (1.05)	54.3 (49.4)
7AH-2	1.96 (0.077)	304.8 (12.0)	20 (-423)	91.95 (3.62)	160.0 (23.2)	220.0 (31.9)	360.6 (52.3)	116.33 (4.58)	88.2 (80.3)
2AH-1	0.787 (0.031)	304.8 (12.0)	20 (-423)	20.57 (0.81)	288.9 (41.9)	358.5 (52.0)	412.3 (59.8)	36.83 (1.45)	64.7 (58.9)
2AH-2	0.711 (0.028)	304.8 (12.0)	20 (-423)	91.44 (3.60)	135.8 (19.7)	231.7 (33.6)	395.1 (57.3)	123.95 (4.88)	92.6 (84.3)

Table 9 : ROOM TEMPERATURE 6Al-4V STA TITANIUM BASE METAL CENTER CRACK PANEL DATA

SPECIMEN NUMBER	GAGE THICKNESS, t mm (INCH)	GAGE WIDTH, W mm (INCH)	TEST TEMPERATURE	INITIAL FLAW LENGTH, 2c mm (INCH)	STRESS AT START OF CRACK GROWTH, σ_s MN/m^2 (KSI)	MAXIMUM GROSS SECTION STRESS, σ_G MN/m^2 (KSI)	MAXIMUM NET SECTION STRESS, σ_N MN/m^2 (KSI)	CRITICAL CRACK LENGTH, 2c mm (INCH)	K_{cn} $MN/m^{3/2}$ ($KSI\sqrt{IN}$)
1TR-1	3.20 (0.126)	127.0 (5.00)	RT	38.86 (1.53)	284.8 (41.3)	329.6 (47.8)	550.9 (79.9)	51.05 (2.01)	85.9 (78.2)
1TR-2	3.28 (0.129)	127.0 (5.00)	RT	23.37 (0.92)	291.0 (42.2)	308.9 (44.8)	428.9 (62.2)	35.56 (1.40)	60.8 (55.3)
1TR-3	3.23 (0.127)	127.0 (5.00)	RT	10.67 (0.42)	488.9 (70.9)	533.0 (77.3)	650.2 (94.3)	22.86 (0.90)	69.8 (63.4)
8TR-1	2.03 (0.080)	127.0 (5.00)	RT	38.61 (1.52)	271.0 (39.3)	275.1 (39.9)	458.5 (66.5)	50.80 (2.00)	71.4 (65.0)
8TR-2	1.88 (0.074)	127.0 (5.00)	RT	23.11 (0.91)	359.9 (52.2)	430.2 (62.4)	765.3 (111.0)	55.63 (2.19)	84.2 (76.6)
8TR-3	2.13 (0.084)	127.0 (5.00)	RT	11.94 (0.47)	454.4 (65.9)	454.4 (65.9)	501.3 (72.7)	11.94 (0.47)	85.5 (77.8)
4TR-1	1.14 (0.045)	127.0 (5.00)	RT	38.86 (1.53)	295.8 (42.9)	373.7 (54.2)	795.0 (115.3)	67.31 (2.65)	97.4 (88.6)
4TR-2	1.07 (0.042)	127.0 (5.00)	RT	15.75 (0.62)	489.5 (71.0)	590.9 (85.7)	825.3 (119.7)	36.07 (1.42)	94.4 (85.9)
4TR-3	1.02 (0.040)	127.0 (5.00)	RT	23.11 (0.91)	349.6 (50.7)	433.0 (62.8)	627.4 (91.0)	39.37 (1.55)	84.7 (77.1)

Table 10 :ROOM TEMPERATURE 2219-T87 ALUMINUM BASE METAL
TEST RESULTS (t = 4.77mm(0.188 inch)) a/2c = .15)

SPECIMEN NUMBER	GAGE THICKNESS, t mm (INCH)	GAGE WIDTH, W mm (INCH)	TEST TEMPERATURE	TEST TYPE	STRESS, σ MN/m^2 (KSI)	INITIAL FLAW DEPTH, a_i mm (INCH)	INITIAL FLAW LENGTH, $2c_i$ mm (INCH)	INITIAL STRESS INTENSITY, K_{i_i} $MN/m^{3/2}$ (KSI$\sqrt{IN}$)	$(a/2c)_i$	$(a/t)_i$	FINAL FLAW DEPTH, a_f mm (INCH)	FINAL FLAW LENGTH, $2c_f$ mm (INCH)	FINAL STRESS INTENSITY, K_{f_f} $MN/m^{3/2}$ (KSI$\sqrt{IN}$)	$(a/2C)_f$	$(a/t)_f$	REMARKS
2AR11-1	4.75 (0.187)	190.5 (7.50)	RT	LUL	302.0 (43.8)	3.96 (0.156)	25.40 (1.00)	54.2 (49.3)	0.156	0.834	(0.166)	25.40 (1.00)	56.3 (51.2)	0.166	0.888	
				CYCLIC	248.2 (36.0)	4.22 (0.166)	25.40 (1.00)	45.4 (41.3)	0.166	0.888	a = t	25.40 (1.00)	46.2 (42.0)	0.187	1.00	10 CPM, 36 CYCLES TO BREAKTHROUGH
				FRACTURE	308.9 (44.8)	a = t	25.40 (1.00)	58.7 (53.4)	0.187	1.00						
2AR11-2	4.80 (0.189)	190.5 (7.50)	RT	LUL	279.2 (40.5)	3.86 (0.152)	25.15 (0.990)	48.1 (43.8)	0.154	0.804	(0.158)	25.15 (0.990)	(45.2)	0.160	0.836	
				CYCLIC	248.5 (36.0)	4.01 (0.158)	25.15 (0.990)	43.6 (39.7)	0.160	0.836	a = t	25.15 (0.990)	(41.8)	0.191	1.00	10 CPM, 133 CYCLES TO BREAKTHROUGH
				FRACTURE	303.4 (44.0)	a = t	25.15 (0.990)	57.3 (52.1)	0.191	1.00						
2AR11-3	4.78 (0.188)	190.5 (7.50)	RT	LUL	248.2 (36.0)	3.96 (0.156)	24.89 (0.980)	43.2 (39.3)	0.159	0.830	(0.157)	24.89 (0.980)	49.7 (39.5)	0.160	0.835	
				LUL	284.8 (41.3)	4.27 (0.168)	24.89 (0.980)	52.5 (47.8)	0.171	0.894	a = t	25.91 (1.02)	54.1 (49.2)	0.184	1.00	
				FRACTURE	291.7 (42.3)	a = t	28.70 (1.13)	57.8 (52.6)	0.166	1.00						
2AR11-4	4.80 (0.189)	190.5 (7.50)	RT	LUL	310.3 (45.0)	3.91 (0.154)	24.89 (0.980)	54.5 (49.6)	0.157	0.815	(0.166)	24.89 (0.980)	57.4 (52.2)	0.169	0.878	
				CYCLIC	264.1 (38.3)	4.22 (0.166)	24.89 (0.980)	47.9 (43.6)	0.169	0.878	a = t	24.89 (0.980)	48.9 (44.5)	0.193	1.00	10 CPM, 78 CYCLES TO BREAKTHROUGH
				FRACTURE	306.8 (44.5)	a = t	24.89 (0.980)	57.7 (52.5)	0.193	1.0						
3AR11-1	4.78 (0.188)	190.5 (7.50)	RT	FRACTURE	308.9 (44.8)	3.96 (0.156)	24.89 (0.980)	55.1 (50.1)	0.159	0.830						BREAKTHROUGH AT 306.8 MN/m^2 (44.5 ksi)
3AR11-2	4.75 (0.187)	190.5 (7.50)	RT	LUL	308.2 (44.7)	3.89 (0.153)	24.89 (0.980)	54.2 (49.3)	0.156	0.818	a = t	28.96 (1.14)	61.7 (56.1)	0.164	1.00	
				FRACTURE	249.6 (36.2)	a = t	46.74 (1.84)	55.8 (50.8)	0.102	1.00						
4AR11-1	4.75 (0.187)	190.5 (7.30)	RT	LUL	296.5 (43.0)	3.73 (0.147)	24.89 (0.980)	50.2 (45.7)	0.150	0.786	3.99 (0.157)	24.89 (0.980)	53.0 (48.2)	0.160	0.840	
				CYCLIC	248.2 (36.0)	3.99 (0.157)	24.89 (0.980)	43.6 (39.7)	0.160	0.840	4.37 (0.172)	24.89 (0.980)	45.4 (41.3)	0.176	0.920	1 CPM, 100 cycles total
				FRACTURE	306.8 (44.5)	4.37 (0.177)	24.89 (0.980	57.4 (52.2)	0.176	0.920						Breakthrough at 2960 MN/m^2 (42.9 ksi)

Table 10 : LIQUID HYDROGEN TEMPERATURE 2219-T87 ALUMINUM BASE METAL TEST RESULTS (t = 4.77mm(0.188 inch)) .

SPECIMEN NUMBER	GAGE THICKNESS, t mm (INCH)	GAGE WIDTH, W mm (INCH)	TEST TEMPERATURE	TEST TYPE	STRESS, σ MN/m^2 (KSI)	INITIAL FLAW DEPTH, a_i mm (INCH)	INITIAL FLAW LENGTH, $2c_i$ mm (INCH)	INITIAL STRESS INTENSITY, K_{I_i} $MN/m^{3/2}$ (KSI$\sqrt{IN}$)	$(a/2c)_i$	$(a/t)_i$	FINAL FLAW DEPTH, a_f mm (INCH)	FINAL FLAW LENGTH, $2c_f$ mm (INCH)	FINAL STRESS INTENSITY, K_{I_f} $MN/m^{3/2}$ (KSI$\sqrt{IN}$)	$(a/2C)_f$	$(a/t)_f$	REMARKS
4AR11-2	4.78 (0.188)	190.5 (7.50)	RT	LUL	296.5 (43.0)	3.73 (0.147)	25.14 (0.990)	50.2 (45.7)	0.148	0.782	3.94 (0.155)	25.14 (0.990)	52.4 (47.7)	0.157	0.824	
				CYCLIC	268.9 (39.0)	3.94 (0.155)	25.14 (0.990)	47.0 (42.8)	0.157	0.824	ast	25.14 (0.990)	50.1 (45.6)	0.190	1.00	1 CPM, 69 cycles to BT
				FRACTURE	305.4 (44.3)	ast	25.14 (0.990)	57.7 (52.5)	0.190	1.00						

Table 11 : ROOM TEMPERATURE 2219-T87 ALUMINUM BASE METAL
TEST RESULTS ($t = 4.77$mm(0.188 inch) $a/2c = .30$)

SPECIMEN NUMBER	GAGE THICKNESS, t mm (INCH)	GAGE WIDTH, W mm (INCH)	TEST TEMPERATURE	TEST TYPE	STRESS, σ MN/m^2 (KSI)	INITIAL FLAW DEPTH, a_i mm (INCH)	INITIAL FLAW LENGTH, $2c_i$ mm (INCH)	INITIAL STRESS INTENSITY, K_{I_i} $MN/m^{3/2}$ (KSI$\sqrt{IN}$)	$(a/2c)_i$	$(a/t)_i$	FINAL FLAW DEPTH, a_f mm (INCH)	FINAL FLAW LENGTH, $2c_f$ mm (INCH)	FINAL STRESS INTENSITY, K_{I_f} $MN/m^{3/2}$ (KSI$\sqrt{IN}$)	$(a/2C)_f$	$(a/t)_f$	REMARKS
2AR13-1	4.75 (0.187)	190.5 (7.50)	R.T.	LUL	310.3 (45.0)	4.22 (0.166)	13.97 (0.550)	41.9 (38.2)	0.302	0.888	4.37 (0.172)	14.48 (0.570)	42.9 (39.0)	0.302	0.920	
				CYCLIC	248.2 (36.0)	4.37 (0.172)	14.48 (0.570)	33.6 (30.6)	0.302	0.920	a=t	15.24 (0.600)	34.4 (31.3)	0.312	1.00	10 CPM, 393 Cycles to Breakthrough
				FRACTURE	338.5 (49.1)	a=t	15.24 (0.600)	48.1 (43.8)	0.312	1.00						
2AR13-2	4.70 (0.185)	190.5 (7.50)	R.T.	LUL	279.2 (40.5)	4.27 (0.168)	13.72 (0.540)	37.0 (33.7)	0.311	0.980	4.37 (0.172)	13.72 (0.540)	36.9 (33.6)	0.319	0.930	
				CYCLIC	248.2 (36.0)	4.37 (0.172)	13.72 (0.540)	32.5 (29.6)	0.319	0.930	a=t	14.99 (0.590)	34.1 (31.0)	0.314	1.00	10 CPM, 278 Cycles to Breakthrough
				FRACTURE	342.7 (49.7)	a=t	14.99 (0.590)	48.4 (44.0)	0.314	1.00						
2AR13-3	4.78 (0.188)	190.5 (7.50)	R.T.	LUL	248.2 (36.0)	4.27 (0.168)	13.72 (0.540)	32.6 (29.7)	0.311	0.894	4.29 (0.169)	13.72 (0.540)	32.6 (29.7)	0.313	0.899	
				LUL	310.3 (45.0)	4.39 (0.173)	13.97 (0.550)	41.8 (38.0)	0.315	0.920	4.50 (0.177)	14.22 (0.560)	42.2 (38.4)	0.316	0.941	
				CYCLIC	248.2 (36.0)	4.50 (0.177)	14.22 (0.560)	33.2 (30.2)	0.316	0.941	a=t	14.73 (0.580)	33.6 (30.6)	0.324	1.00	10 CPM, 91 Cycles to Breakthrough
				FRACTURE	338.5 (49.1)	a=t	14.73 (0.580)	47.0 (42.8)	0.324	1.00						
2AR13-4	4.70 (0.185)	190.5 (7.50)	R.T.	LUL	331.0 (48.0)	4.22 (0.166)	13.97 (0.550)	45.2 (41.1)	0.302	0.897	4.42 (0.174)	14.22 (0.560)	45.4 (41.3)	0.311	0.941	
				CYCLIC	248.2 (36.0)	4.42 (0.174)	14.22 (0.560)	33.3 (30.3)	0.311	0.941	a=t	15.75 (0.620)	35.2 (32.0)	0.298	1.00	10 CPM, 646 Cycles to Breakthrough
				FRACTURE	342.7 (49.7)	a=t	15.75 (0.620)	49.9 (45.4)	0.298	1.00						
3AR13-1	4.78 (0.188)	190.5 (7.50)	R.T.	FRACTURE	339.9 (49.3)	4.17 (0.164)	13.72 (0.540)	45.7 (41.6)	0.304	0.872						Breakthrough at σ=332.3 MN/m^2 (48.2 ksi)
3AR13-2	4.78 (0.188)	190.5 (7.50)	R.T.	LUL	339.9 (49.3)	4.17 (0.164)	13.46 (0.530)	45.2 (41.1)	0.309	0.872	a=t	16.26 (0.640)	50.4 (45.9)	0.294	1.00	
				FRACTURE	330.3 (47.9)	a=t	18.29 (0.720)	53.1 (48.3)	0.261	1.00						

Table 12 : ROOM TEMPERATURE 2219-T87 ALUMINUM BASE METAL
TEST RESULTS (t = 4.77mm(0.188 inch) a/2c = .45)

SPECIMEN NUMBER	GAGE THICKNESS, t mm (INCH)	GAGE WIDTH, W mm (INCH)	TEST TEMPERATURE	TEST TYPE	STRESS, σ MN/m^2 (KSI)	INITIAL FLAW DEPTH, a_i mm (INCH)	INITIAL FLAW LENGTH, $2c_i$ mm (INCH)	INITIAL STRESS INTENSITY, K_{I_i} MN/m$^{3/2}$ (KSI$\sqrt{IN}$)	$(a/2c)_i$	$(a/t)_i$	FINAL FLAW DEPTH, a_f mm (INCH)	FINAL FLAW LENGTH, $2c_f$ mm (INCH)	FINAL STRESS INTENSITY, K_{I_f} MN/m$^{3/2}$ (KSI$\sqrt{IN}$)	$(a/2C)_f$	$(a/t)_f$	REMARKS
2AR14-1	4.70 (0.185)	190.5 (7.50)	R.T.	LUL	310.3 (45.0)	4.47 (0.176)	9.91 (0.390)	31.5 (28.7)	0.451	0.951	4.55 (0.179)	10.16 (0.400)	32.1 (29.2)	0.447	0.968	
				CYCLIC	248.2 (36.0)	4.55 (0.179)	10.16 (0.400)	25.4 (23.1)	0.447	0.968	a=t	10.80 (0.425)	26.5 (24.1)	0.435	1.00	10 CPM, 269 Cycles to B.T. 274 Total
				FRACTURE	353.7 (51.3)	a=t	10.80 (0.425)	38.0 (34.6)	0.435	1.00						
2AR14-2	4.75 (0.187)	190.5 (7.50)	R.T.	LUL	279.2 (40.5)	4.47 (0.176)	9.91 (0.390)	28.2 (25.7)	0.451	0.941	4.50 (0.177)	10.16 (0.400)	28.8 (26.2)	0.442	0.947	
				CYCLIC	248.2 (36.0)	4.50 (0.177)	10.16 (0.400)	25.5 (23.2)	0.442	0.947	a=t	10.67 (0.420)	26.0 (23.7	0.445	1.00	10 CPM, 141 Cycles to B.T. 143 Total
				FRACTURE	348.9 (50.6)	a=t	10.67 (0.420)	37.4 (34.0)	0.445	1.00						
2AR14-3	4.78 (0.188)	190.5 (7.50)	R.T.	LUL	337.9 (49.0)	4.47 (0.176)	10.16 (0.400)	35.4 (32.2)	0.440	0.936	a=t	10.67 (0.420)	36.0 (32.8)	0.448	1.00	
				FRACTURE	353.7 (51.3)	a=t	10.67 (0.420)	37.8 (34.4)	0.448	1.00						
2AR14-4	4.78 (0.188)	190.5 (7.50)	R.T.	LUL	331.0 (48.0)	4.37 (0.172)	9.78 (0.385)	33.7 (30.7)	0.447	0.915	4.52 (0.178)	10.16 (0.400)	34.5 (31.4)	0.445	0.947	
				CYCLIC	248.2 (36.0)	4.52 (0.178)	10.15 (0.400)	25.4 (23.1)	0.445	0.947	a=t	10.67 (0.420)	25.9 (23.6)	0.448	1.00	10 CPM, 197 Cycles to B.T.
				FRACTURE	353.0 (51.2)	a=t	10.67 (0.420)	37.8 (34.4)	0.448	1.00						
3AR14-1	4.88 (0.192)	190.5 (7.50)	R.T.	FRACTURE	355.8 (51.6)	4.42 (0.174)	10.03 (0.395)	37.3 (33.9)	0.441	0.906						Breakthrough at 346.1 MN/m^2 (50.2 ksi)
3AR14-2	4.70 (0.185)	190.5 (7.50)	R.T.	LUL	343.4 (49.8)	4.37 (0.172)	9.65 (0.380)	34.7 (31.6)	0.453	0.930	a=t	10.67 (0.420)	36.9 (33.6)	0.440	1.00	
				FRACTURE	357.2 (51.8)	a=t	10.92 (0.430)	39.5 (35.9)	0.430	1.00						
4AR14-1	4.67 (0.184)	190.5 (7.50)	R.T.	LUL	331.0 (48.0)	4.37 (0.172)	9.78 (0.385)	33.7 (30.7)	.447	0.935	4.50 (0.177)	10.67 (0.420)	36.2 (32.9)	0.421	0.962	
				CYCLIC	248.2 (36.0)	4.50 (0.177)	10.67 (0.420)	26.6 (24.2)	.421	0.962	4.62 (0.182)	10.92 (0.430)	26.9 (24.5)	0.423	0.989	1 CPM, 100 cycles Total
				FRACTURE	359.2 (52.1)	4.62 (0.182)	10.92 (0.430)	39.9 (36.3)	.423	0.989						Breakthrough at 334.4 MN/m^2 (48.5 ksi)

Table 12 : ROOM TEMPERATURE 2219-T87 ALUMINUM BASE METAL
TEST RESULTS (t = 4.77mm(0.188 inch) a/2c = .45)

SPECIMEN NUMBER	GAGE THICKNESS, t mm (INCH)	GAGE WIDTH, W mm (INCH)	TEST TEMPERATURE	TEST TYPE	STRESS, σ MN/m^2 (KSI)	INITIAL FLAW DEPTH, a_i mm (INCH)	INITIAL FLAW LENGTH, $2c_i$ mm (INCH)	INITIAL STRESS INTENSITY, K_{I_i} $MN/m^{3/2}$ (KSI$\sqrt{IN}$)	$(a/2c)_i$	$(a/t)_i$	FINAL FLAW DEPTH, a_f mm (INCH)	FINAL FLAW LENGTH, $2c_f$ mm (INCH)	FINAL STRESS INTENSITY, K_{I_f} $MN/m^{3/2}$ (KSI$\sqrt{IN}$)	$(a/2C)_f$	$(a/t)_f$	REMARKS
4AR14-2	4.75 (0.187)	190.5 (7.50)	R.T.	LUL	331.0 (48.0)	4.37 (0.172)	9.78 (0.385)	33.7 (30.7)	0.447	0.920	4.50 (0.177)	10.41 (0.410)	35.4 (32.2)	0.432	0.947	
				CYCLIC	297.9 (43.2)	4.50 (0.177)	10.41 (0.410)	31.5 (28.7)	0.432	0.947	a=t	10.54 (0.415)	31.2 (28.4)	0.451	1.00	1 CPM, 79 cycles to B.T.
				FRACTURE	358.5 (52.0)	a=t	10.54 (0.415)	38.0 (34.6)	0.451	1.00						

Table 13 : ROOM TEMPERATURE 2219-T87 ALUMINUM BASE METAL
TEST RESULTS ($t = 1.91$mm(0.075 inch) $a/2c = .15$)

SPECIMEN NUMBER	GAGE THICKNESS, t mm (INCH)	GAGE WIDTH, W mm (INCH)	TEST TEMPERATURE	TEST TYPE	STRESS, σ MN/m^2 (KSI)	INITIAL FLAW DEPTH, a_i mm (INCH)	INITIAL FLAW LENGTH, $2c_i$ mm (INCH)	INITIAL STRESS INTENSITY, K_{I_i} $MN/m^{3/2}$ (KSI$\sqrt{IN}$)	$(a/2c)_i$	$(a/t)_i$	FINAL FLAW DEPTH, a_f mm (INCH)	FINAL FLAW LENGTH, $2c_f$ mm (INCH)	FINAL STRESS INTENSITY, K_{I_f} $MN/m^{3/2}$ (KSI$\sqrt{IN}$)	$(a/2C)_f$	$(a/t)_f$	REMARKS
2AR71-1	1.96 (0.077)	127.0 (5.00)	RT	LUL	310.3 (45.0)	1.65 (0.065)	11.43 (0.450)	37.3 (33.9)	0.144	0.844	1.73 (0.068)	11.43 (0.450)	38.4 (34.9)	0.151	0.833	
				CYCLIC	248.2 (36.0)	1.73 (0.068)	11.43 (0.450)	30.0 (27.3)	0.151	0.883	a=t	11.43 (0.450)	30.7 (27.9)	0.171	1.00	10 cpm, 72 cycles to breakthrough
				FRACTURE	344.1 (49.9)	a=t	11.43 (0.450)	44.2 (40.2)	0.171	1.00						
2AR71-2	1.98 (0.078)	127.0 (5.00)		LUL	279.2 (40.5)	1.65 (0.065)	11.43 (0.450)	32.9 (29.9)	0.144	0.833	1.68 (0.066)	11.43 (0.450)	33.3 (30.3)	0.147	0.846	
				CYCLIC	248.2 (36.0)	1.68 (0.066)	11.43 (0.450)	29.2 (26.6)	0.147	0.846	a=t	11.43 (0.450)	30.8 (28.0)	0.173	1.00	10 cpm, 156 cycles to breakthrough
				FRACTURE	340.6 (49.4)	a=t	11.43 (0.450)	43.7 (39.8)	0.173	1.00						
2AR71-3	1.98 (0.078)	127.0 (5.00)		LUL	310.3 (45.0)	1.52 (0.060)	11.30 (0.445)	34.4 (31.3)	0.135	0.769	1.57 (0.062)	11.30 (0.445)	35.4 (32.2)	0.139	0.795	
				CYCLIC	279.2 (40.5)	1.57 (0.062)	11.30 (0.445)	31.4 (28.6)	0.139	0.795	a=t	11.30 (0.445)	34.8 (31.7)	0.175	1.00	10 cpm, 110 cycles to BT
				FRACTURE	338.5 (49.1)	a=t	11.30 (0.445)	43.2 (39.3)	0.175	1.00						
2AR71-4	1.98 (0.078)	127.0 (5.00)		LUL	248.2 (36.0)	1.65 (0.065)	11.94 (0.470)	29.2 (26.6)	0.138	0.833	1.65 (0.065)	11.94 (0.470)	29.2 (26.6)	0.138	0.83	
				LUL	286.8 (41.6)	1.73 (0.068)	11.94 (0.470)	35.4 (32.2)	0.145	0.872	a=t	11.94 (0.470)	36.6 (33.3)	0.166	1.00	
				FRACTURE	336.5 (48.8)	a=t	11.94 (0.470)	43.9 (39.9)	0.166	1.00						
3AR71-1	1.96 (0.077)	127.0 (5.00)		FRACTURE	345.4 (50.1)	1.63 (0.064)	11.81 (0.465)	42.1 (38.3)	0.138	0.831						Breakthrough at σ=126.1 MN/m^2 (47.3 ksi)
3AR71-2	1.98 (0.078)	127.0 (5.00)		LUL	313.7 (45.5)	1.70 (0.067)	11.43 (0.450)	38.2 (34.8)	0.149	0.859	a=t	11.43 (0.450)	39.8 (36.2)	0.173	1.00	
				FRACTURE	326.1 (47.3)	a=t	13.46 (0.530)	44.2 (40.2)	0.147	1.00						
4AR71-1	1.98 (0.078)	127.0 (5.00	R.T.	LUL	310.3 (45.0)	1.68 (0.066)	11.43 (0.450)	37.7 (34.3)	0.144	0.846	1.75 (0.069)	11.43 (0.450)	38.5 (35.0)	0.153	0.895	
				CYCLIC	248.2 (36.0)	1.75 (0.069)	11.43 (0.450)	30.0 (27.3)	0.153	0.885	a=t	11.43 (0.450)	30.8 (28.0)	0.173	1.00	1 CPM, 15 cycles to BT
				FRACTURE	345.4 (50.1)	a=t	11.43 (0.450)	44.4 (40.4)	0.173	1.00						

Table 13 : ROOM TEMPERATURE 2219-T87 ALUMINUM BASE METAL
TEST RESULTS (t = 1.91mm(0,075 inch) a/2c = .15)

SPECIMEN NUMBER	GAGE THICKNESS, t mm (INCH)	GAGE WIDTH, W mm (INCH)	TEST TEMPERATURE	TEST TYPE	STRESS, σ MN/m^2 (KSI)	INITIAL FLAW DEPTH, a_i mm (INCH)	INITIAL FLAW LENGTH, $2c_i$ mm (INCH)	INITIAL STRESS INTENSITY, K_{I_i} $MN/m^{3/2}$ (KSI$\sqrt{IN}$)	$(a/2c)_i$	$(a/t)_i$	FINAL FLAW DEPTH, a_f mm (INCH)	FINAL FLAW LENGTH, $2c_f$ mm (INCH)	FINAL STRESS INTENSITY, K_{I_f} $MN/m^{3/2}$ (KSI$\sqrt{IN}$)	$(a/2C)_f$	$(a/t)_f$	REMARKS
4AR71-2	1.98 (0.078)	127.0 (5.00)	RT	LUL	310.3 (45.0)	1.68 (0.066)	11.30 (0.445)	37.4 (34.0)	0.148	0.846	1.73 (0.068)	11.30 (0.445)	38.0 (34.6)	0.153	0.872	
				CYCLIC	279.2 (40.5)	1.73 (0.068)	11.30 (0.445)	33.7 (30.7)	0.153	0.872	a=t	11.30 (0.445)	34.8 (31.7)	0.175	1.00	1 CPM, 3 cycles to BT
				FRACTURE	339.9 (49.3)	a=t	11.30 (0.445)	43.4 (39.5)	0.175	1.00						

Table 14 : ROOM TEMPERATURE 2219-T87 ALUMINUM BASE METAL
TEST RESULTS ($t = 1.91$mm(0.075 inch)$a/2c = .30$)

SPECIMEN NUMBER	GAGE THICKNESS, t mm (INCH)	GAGE WIDTH, W mm (INCH)	TEST TEMPERATURE	TEST TYPE	STRESS, σ MN/m^2 (KSI)	INITIAL FLAW DEPTH, a_i mm (INCH)	INITIAL FLAW LENGTH, $2c_i$ mm (INCH)	INITIAL STRESS INTENSITY, K_{i_i} $MN/m^{3/2}$ (KSI$\sqrt{IN}$)	$(a/2c)_i$	$(a/t)_i$	FINAL FLAW DEPTH, a_f mm (INCH)	FINAL FLAW LENGTH, $2c_f$ mm (INCH)	FINAL STRESS INTENSITY, K_{i_f} $MN/m^{3/2}$ (KSI$\sqrt{IN}$)	$(a/2C)_f$	$(a/t)_f$	REMARKS
2AR73-1	1.98 (0.078)	127.0 (5.00)	RT	LUL	339.2 (49.2)	78 (0.070)	6.25 (0.246)	31.4 (28.6)	0.285	0.897	a=t	6.86 (0.270)	32.9 (29.9)	0.289	1.00	
				FRACTURE	365.4 (53.0)	a=t	6.86 (0.270)	35.7 (32.5)	0.270	1.00						
2AR73-2	1.98 (0.078)	127.0 (5.00)	RT	LUL	279.2 (40.5)	1.78 (0.070)	6.35 (0.250)	25.7 (23.4)	0.280	0.897	1.78 (0.070)	6.35 (0.250)	25.7 (23.4)	0.280	0.897	
				CYCLIC	248.2 (36.0)	1.78 (0.070)	6.35 (0.250)	22.6 (20.6)	0.280	0.897	a=t	6.48 (0.255)	22.5 (20.5)	0.306	1.00	10 CPM, 216 cycles to BT
				FRACTURE	362.0 (52.5)	a=t	6.48 (0.255)	34.0 (30.9)	0.306	1.00						
2AR73-3	1.96 (0.077)	127.0 (5.00)		LUL	310.3 (45.0)	1.78 (0.070)	6.25 (0.246)	28.5 (25.9)	0.285	0.909	1.80 (0.071)	6.25 (0.246)	28.4 (25.8)	0.289	0.922	
				CYCLIC	248.2 (36.0)	1.80 (0.071)	6.25 (0.246)	22.3 (20.3)	0.289	0.922	a=t	6.40 (0.252)	22.3 (20.3)	0.306	1.00	10 CPM, 143 cycles to BT
				FRACTURE	360.6 (52.3)	a=t	6.40 (0.252)	33.6 (30.6)	0.306	1.00						
2AR73-4	2.00 (0.079)	127.0 (5.00		LUL	331.0 (48.0)	1.78 (0.070)	6.25 (0.246)	30.4 (27.7)	0.285	0.886	1.85 (0.073)	6.25 (0.246)	30.4 (27.7)	0.297	0.92	
				CYCLIC	275.8 (40.0)	1.85 (0.073)	6.25 (0.246)	24.8 (22.6)	0.297	0.924	a=t	6.35 (0.250)	24.8 (22.6)	0.316	1.00	10 CPM, 10 cycles to BT
				FRACTURE	359.9 (52.2)	a=t	6.35 (0.250)	33.2 (30.2)	0.316	1.00						
3AR73-1	1.96 (0.077)	127.0 (5.00)		FRACTURE	367.5 (53.3)	1.88 (0.074)	6.25 (0.246)	34.0 (30.9)	0.301	0.961						Breakthrough at 288.9 MN/m^2 (41.9 ksi)
3AR73-2	1.98 (0.078)	127.0 (5.00)		LUL	337.3 (48.2)	1.85 (0.073)	6.32 (0.249)	30.8 (28.0)	0.293	0.936	a=t	6.32 (0.249)	30.3 (27.6)	0.313	1.00	
				FRACTURE	345.4 (50.1)	a=t	8.76 (0.345)	39.1 (35.6)	0.226	1.00						

Table 15 : ROOM TEMPERATURE 2219-T87 ALUMINUM BASE METAL
TEST RESULTS(t = 1.91mm(0.075 inch) a/2c = .45)

SPECIMEN NUMBER	GAGE THICKNESS, t mm (INCH)	GAGE WIDTH, W mm (INCH)	TEST TEMPERATURE	TEST TYPE	STRESS, σ MN/m^2 (KSI)	INITIAL FLAW DEPTH, a_i mm (INCH)	INITIAL FLAW LENGTH, $2c_i$ mm (INCH)	INITIAL STRESS INTENSITY, K_{i_i} $MN/m^{3/2}$ (KSI$\sqrt{IN}$)	$(a/2c)_i$	$(a/t)_i$	FINAL FLAW DEPTH, a_f mm (INCH)	FINAL FLAW LENGTH, $2c_f$ mm (INCH)	FINAL STRESS INTENSITY, K_{f_f} $MN/m^{3/2}$ (KSI$\sqrt{IN}$)	$(a/2C)_f$	$(a/t)_f$	REMARKS
2AR74-1	1.96 (0.077)	127.0 (5.00)	RT	LUL	310.3 (45.0)	1.78 (0.070)	4.32 (0.170)	21.7 (19.7)	0.412	0.909	(0.071)	1.80 (0.170)	4.32 (19.8)	21.8 0.418	0.922	
				CYCLIC	248.2 (36.0)	1.80 (0.071)	4.32 (0.170)	17.0 (15.5)	0.418	0.922	a=t	(0.180)	4.57 (15.8)	17.4 0.428	1.00	10 cpm, 269 cycles to BT
				FRACTURE	368.2 (53.4)	a=t	4.57 (0.180)	26.5 (24.1)	0.428	1.00						
2AR74-2	1.96 (0.077)	127.0 (5.00)	RT	LUL	279.2 (40.5)	1.85 (0.073)	4.17 (0.164)	18.5 (16.8)	0.445	0.948	1.85 (0.073)	4.17 (0.164)	18.5 (16.8)	0.445	0.948	
				CYCLIC	248.2 (36.0)	1.85 (0.073)	4.17 (0.164)	16.3 (14.8)	0.445	0.948	a=t	4.42 (0.174)	16.8 (15.3)	0.443	1.00	10 cpm, 65 cycles to BT
				FRACTURE	368.9 (53.5)	a=t	4.42 (0.174)	25.6 (23.3)	0.443	1.00						
2AR74-3	1.98 (0.078)	127.0 (5.00)	RT	LUL	333.0 (48.3)	1.83 (0.072)	4.42 (0.174)	23.6 (21.5)	0.414	0.923	a=t	4.83 (0.190)	24.7 (22.5)	0.411	1.00	
				FRACTURE	368.9 (53.5)	a=t	4.83 (0.190)	27.7 (25.2)	0.411	1.00						
2AR74-4	1.98 (0.078)	127.0 (5.00)	RT	LUL	327.5 (47.5)	a=t	4.22 (0.166)	21.4 (19.5)	0.470	1.00	a=t	4.22 (0.166)	21.4 (19.5)	0.470	1.00	
				CYCLIC	248.2 (36.0)	a=t	4.22 (0.166)	15.9 (14.5)	0.470	1.00	a=t	4.24 (0.168)	16.2 (14.7)	0.464	1.00	
				FRACTURE	373.0 (54.1)	a=t	4.27 (0.168)	24.9 (22.7)	0.464	1.00						
3AR74-1	1.96 (0.077)	127.0 (5.00)	RT	FRACTURE	377.2 (54.7)	1.75 (0.069)	4.27 (0.168)	26.6 (24.2)	0.411	0.896						Breakthrough at σ=362.0 MN/m^2(52.5 ksi)
3AR74-2	1.96 (0.077)	127.0 (5.00)	RT	LUL	315.1 (45.7)	1.85 (0.073)	4.47 (0.176)	22.3 (20.3)	0.415	0.948	a=t	4.47 (0.176)	21.9 (19.9)	0.437	1.00	
				FRACTURE	355.1 (51.5)	a=t	7.01 (0.276)	35.3 (32.1)	0.279	1.00						
4AR74-1	1.96 (0.077)	127.0 (5.00)	RT	LUL	310.3 (45.0)	1.75 (0.069)	4.17 (0.164)	21.1 (19.2)	0.421	0.896	1.75 (0.069)	4.17 (0.164)	21.1 (19.2)	0.421	0.896	
				CYCLIC	248.2 (36.0)	1.75 (0.069)	4.17 (0.164)	16.6 (15.1)	0.421	0.896	1.83 (0.072)	4.37 (0.172)	17.1 (15.6)	0.419	0.935	11 cpm, 100 cycles total
				FRACTURE	371.6 (53.9)	1.83 (0.072)	4.37 (0.172)	26.4 (24.0)	0.419	0.935						Breakthrough at σ=354.5 MN/m^2(51.4 ksi)

Table 15 : ROOM TEMPERATURE 2219-T87 ALUMINUM BASE METAL
TEST RESULTS (t = 1.91mm(0.075 inch) a/2c = .45)

SPECIMEN NUMBER	GAGE THICKNESS, t mm (INCH)	GAGE WIDTH, W mm (INCH)	TEST TEMPERATURE	TEST TYPE	STRESS, σ MN/m^2 (KSI)	INITIAL FLAW DEPTH, a_i mm (INCH)	INITIAL FLAW LENGTH, $2c_i$ mm (INCH)	INITIAL STRESS INTENSITY, K_i $MN/m^{3/2}$ (KSI$\sqrt{IN}$)	$(a/2c)_i$	$(a/t)_i$	FINAL FLAW DEPTH, a_f mm (INCH)	FINAL FLAW LENGTH, $2c_f$ mm (INCH)	FINAL STRESS INTENSITY, K_f $MN/m^{3/2}$ (KSI$\sqrt{IN}$)	$(a/2C)_f$	$(a/t)_f$	REMARKS
4AR74-2	1.98 (0.078)	127.0 (5.00)	RT	LUL	327.5 (47.5)	1.78 (0.070)	4.22 (0.166)	22.4 (20.4)	0.422	0.897	1.80 (0.071)	4.22 (0.166)	22.3 (20.3)	0.428	0.910	
				CYCLIC	248.2 (36.0)	1.80 (0.071)	4.22 (0.166)	16.7 (15.2)	0.428	0.910	a=t	4.47 (0.176)	16.9 (15.4)	0.443	1.00	1 CPM, 100 cycles total
				FRACTURE	366.8 (53.2)	a=t	4.47 (0.176)	25.6 (23.3)	0.443	1.00						

Table 16 : ROOM TEMPERATURE 2219-T87 ALUMINUM BASE METAL
TEST RESULTS (t = 0.635mm(0.025 inch) a/2c = .05)

SPECIMEN NUMBER	GAGE THICKNESS, t mm (INCH)	GAGE WIDTH, W mm (INCH)	TEST TEMPERATURE	TEST TYPE	STRESS, σ MN/m^2 (KSI)	INITIAL FLAW DEPTH, a_i mm (INCH)	INITIAL FLAW LENGTH, $2c_i$ mm (INCH)	INITIAL STRESS INTENSITY, K_{I_i} MN/m$^{3/2}$ (KSI$\sqrt{IN}$)	$(a/2c)_i$	$(a/t)_i$	FINAL FLAW DEPTH, a_f mm (INCH)	FINAL FLAW LENGTH, $2c_f$ mm (INCH)	FINAL STRESS INTENSITY, K_{I_f} MN/m$^{3/2}$ (KSI$\sqrt{IN}$)	$(a/2C)_f$	$(a/t)_f$	REMARKS
2AR25-1	0.686 (0.027)	127.0 (5.00)	R.T.	FRACTURE	336.5 (48.8)	0.584 (0.023)	11.94 (0.470)	29.5 (26.8)	0.049	0.852						BREAKTHROUGH AT 241.3 MN/m^2 (35.0 ksi)
2AR25-2	0.686 (0.027)	127.0 (5.00)	R.T.	FRACTURE	335.8 (48.7)	0.483 (0.019)	10.16 (0.400)	23.2 (21.1)	0.047	0.704						BREAKTHROUGH AT 322.7 MN/m^2 (46.8 ksi)
2AR25-1A	0.686 (0.027)	127.0 (5.00)	R.T.	FRACTURE	347.5 (50.4)	0.559 (0.022)	10.92 (0.430)	28.9 (26.3)	0.051	0.815						BREAKTHROUGH AT 280.6 MN/m^2 (40.7 ksi)
2AR25-4	0.686 (0.027)	127.0 (5.00)	R.T.	LUL	275.8 (40.0)	0.508 (0.020)	10.67 (0.420)	19.7 (17.9)	0.048	0.741	0.533 (0.021)	10.67 (0.420)	20.9 (19.0)	0.050	0.778	
				CYCLIC	248.2 (36.0)	0.533 (0.021)	10.67 (0.420)	18.6 (16.9)	0.050	0.778	a = t	10.67 (0.420)	22.5 (20.5)	0.064	1.00	10 CPM, 76 CYCLES TO B.T.
				LUL	337.9 (49.0)	a = t	10.67 (0.420)	32.0 (29.1)	0.064	1.00						
3AR25-1	0.686 (0.027)	127.0 (5.00)	R.T.	FRACTURE	342.7 (49.7)	0.508 (0.020)	10.16 (0.400)	25.2 (22.9)	0.050	0.741						BREAKTHROUGH AT 328.9 MN/m^2 (47.7 ksi)
3AR25-2	0.737 (0.029)	127.0 (5.00)	R.T.	LUL	275.8 (40.0)	0.483 (0.019)	10.41 (0.410)	17.6 (16.0)	0.046	0.655	0.483 (0.019)	10.41 (0.410)	17.6 (16.0)	0.046	0.655	
				CYCLIC	248.2 (36.0)	0.483 (0.019)	10.41 (0.410)	15.6 (14.2)	0.046	0.655	a = t	10.41 (0.410)	23.1 (21.0)	0.071	1.00	1 CPM, 87 CYCLES TO B.T.
				FRACTURE	319.9 (46.4)	a = t	10.41 (0.410)	30.7 (27.9)	0.071	1.00						
2AR25-5	0.711 (0.028)	127.0 (5.00)	R.T.	LUL	248.2 (36.0)	0.432 (0.017)	10.16 (0.400)	14.2 (12.9)	0.042	0.607	0.432 (0.017)	10.16 (0.400)	14.2 (12.9)	0.042	0.607	
				CYCLIC	223.4 (32.4)	0.432 (0.017)	10.16 (0.400)	12.6 (11.5)	0.042	0.607	a = t	10.16 (0.400)	20.2 (18.4)	0.070	1.00	10 CPM, 349 CYCLES TO B.T.
				FRACTURE	335.8 (48.7)	a = t	10.16 (0.400)	32.0 (29.1)	0.070	1.00						
4AR25-1	0.686 (0.027)	127.0 (5.00)	R.T.	LUL	310.3 (45.0)	0.508 (0.020)	10.16 (0.400)	22.4 (20.4)	0.050	0.741	0.533 (0.021)	10.16 (0.400)	23.7 (21.6)	0.062	0.778	
				CYCLIC	248.2 (36.0)	0.533 (0.021)	10.16 (0.400)	18.5 (16.8)	0.052	0.778	a = t	10.16 (0.400)	22.4 (20.4)	0.067	1.00	1 CPM, 71 CYCLES TO B.T.
				FRACTURE	337.2 (48.9)	a = t	10.16 (0.400)	31.7 (28.8)	0.067	1.00						

Table 16 : ROOM TEMPERATURE 2219-T87 ALUMINUM BASE METAL
TEST RESULTS (t = 0.635mm(0.025 inch) a/2c = .05)

SPECIMEN NUMBER	GAGE THICKNESS, t mm (INCH)	GAGE WIDTH, W mm (INCH)	TEST TEMPERATURE	TEST TYPE	STRESS, σ MN/m^2 (KSI)	INITIAL FLAW DEPTH, a_i mm (INCH)	INITIAL FLAW LENGTH, $2c_i$ mm (INCH)	INITIAL STRESS INTENSITY, K_{I_i} $MN/m^{3/2}$ (KSI$\sqrt{IN}$)	$(a/2c)_i$	$(a/t)_i$	FINAL FLAW DEPTH, a_f mm (INCH)	FINAL FLAW LENGTH, $2c_f$ mm (INCH)	FINAL STRESS INTENSITY, K_{I_f} $MN/m^{3/2}$ (KSI$\sqrt{IN}$)	$(a/2C)_f$	$(a/t)_f$	REMARKS
4AR25-2	0.711 (0.028)	27.0 (5.00)	R. T.	LUL	310.3 (45.0)	0.457 (0.018)	11.18 (0.440)	19.5 (17.7)	0.041	0.643	0.483 (0.019)	11.18 (0.440)	20.7 (18.8)	0.043	0.679	
				CYCLIC	297.2 (40.5)	0.483 (0.019)	11.18 (0.440)	18.4 (16.7)	0.043	0.679	a = t	11.18 (0.440)	26.2 (23.8)	0.064	1.00	1 CPM, 64 CYCLES TO R.T.
				FRACTURE	337.2 (48.9)	a = t	11.18 (0.440)	32.4 (29.5)	0.064	1.00						

Table 17 : ROOM TEMPERATURE 2219-T87 ALUMINIUM BASE METAL
TEST RESULTS (t = 0.635mm(0.025 inch) a/2c = .15)

SPECIMEN NUMBER	GAGE THICKNESS, t mm (INCH)	GAGE WIDTH, W mm (INCH)	TEST TEMPERATURE	TEST TYPE	STRESS, σ MN/m² (KSI)	INITIAL FLAW DEPTH, a_i mm (INCH)	INITIAL FLAW LENGTH, $2c_i$ mm (INCH)	INITIAL STRESS INTENSITY, K_{I_i} MN/m$^{3/2}$ (KSI$\sqrt{IN}$)	$(a/2c)_i$	$(a/t)_i$	FINAL FLAW DEPTH, a_f mm (INCH)	FINAL FLAW LENGTH, $2c_f$ mm (INCH)	FINAL STRESS INTENSITY, K_{I_f} MN/m$^{3/2}$ (KSI$\sqrt{IN}$)	$(a/2C)_f$	$(a/t)_f$	REMARKS
2AR21-1	0.686 (0.027)	127.0 (5.00)	R.T.	FRACTURE	365.4 (53.0)	0.660 (0.026)	4.17 (0.164)	28.4 (25.8)	0.159	0.963						BREAKTHROUGH AT 245.5 MN/m² (35.6 ksi)
2AR21-2	0.686 (0.027)	127.0 (5.00)	R.T.	FRACTURE	364.1 (52.8)	0.584 (0.023)	3.91 (0.154)	27.6 (25.1)	0.169	0.852						BREAKTHROUGH AT 339.2 MN/m² (49.2 ksi)
2AR21-3	0.711 (0.028)	127.0 (5.00)	R.T.	LUL	310.3 (45.0)	0.508 (0.020)	3.96 (0.156)	19.1 (17.4)	0.128	0.714	0.508 (0.020)	3.96 (0.156)	19.1 (17.4)	0.128	0.714	
				CYCLIC	248.2 (36.0)	0.508 (0.020)	3.96 (0.156)	15.3 (13.9)	0.128	0.714	a = t	3.96 (0.156)	18.1 (16.5)	0.179	1.00	10CPM, 761 CYCLES TO B.T.
				FRACTURE	353.7 (51.3)	a = t	3.96 (0.156)	26.9 (24.5)	0.179	1.00						
2AR21-4	0.660 (0.026)	127.0 (5.00)	R.T.	LUL	331.0 (48.0)	0.559 (0.022)	3.96 (0.156)	23.6 (21.5)	0.141	0.846	0.584 (0.023)	3.96 (0.156)	24.2 (22.0)	0.147	0.885	
				CYCLIC	248.2 (36.0)	0.584 (0.023)	3.96 (0.156)	17.6 (16.0)	0.147	0.885	a = t	3.96 (0.156)	18.0 (16.4)	0.167	1.00	10 CPM, 728 CYCLES TO B.T.
				FRACTURE	366.1 (53.1)	a = t	3.96 (0.156)	27.9 (25.4)	0.167	1.00						
2AR21-1A	0.686 (0.027)	127.0 (5.00)	R.T.	LUL	275.8 (40.0)	0.508 (0.020)	4.06 (0.160)	17.3 (15.7)	0.125	0.741	0.508 (0.020)	4.06 (0.160)	17.3 (15.7)	0.125	0.741	
				CYCLIC	248.2 (36.0)	(0.508) (0.020)	4.06 (0.160)	15.5 (14.1)	0.125	0.741	a = t	4.06 (0.160)	18.2 (16.6)	0.169	1.00	10 CPM, 201 CYCLES TO B.T.
				FRACTURE	362.0 (52.5)	a = t	4.06 (0.160)	27.9 (25.4)	0.169	1.00						
3AR21-1	0.686 (0.027)	127.0 (5.00)	R.T.	FRACTURE	374.4 (54.3)	0.559 (0.022)	4.01 (0.158)	26.7 (24.3)								BREAKTHROUGH AT 362.0 MN/m² (52.5 ksi)
3AR21-2	0.711 (0.028)	127.0 (5.00)	R.T.	LUL	328.2 (47.6)	0.635 (0.025)	4.11 (0.162)	24.7 (22.5)	0.154	0.893	a = t	4.11 (0.162)	25.2 (22.9)	0.173	1.00	
				FRACTURE	368.9 (53.5)	a = t	4.11 (0.162)	28.6 (26.0)	0.173	1.00						

Table 18 : ROOM TEMPERATURE 2219-T87 ALUMINUM BASE METAL
TEST RESULTS (t = 0.635mm(0.025 inch) a/2c = .30)

SPECIMEN NUMBER	GAGE THICKNESS, t mm (INCH)	GAGE WIDTH, W mm (INCH)	TEST TEMPERATURE	TEST TYPE	STRESS, σ MN/m^2 (KSI)	INITIAL FLAW DEPTH, a_i mm (INCH)	INITIAL FLAW LENGTH, $2c_i$ mm (INCH)	INITIAL STRESS INTENSITY, K_{I_i} $MN/m^{3/2}$ (KSI$\sqrt{IN}$)	$(a/2c)_i$	$(a/t)_i$	FINAL FLAW DEPTH, a_f mm (INCH)	FINAL FLAW LENGTH, $2c_f$ mm (INCH)	FINAL STRESS INTENSITY, K_{I_f} $MN/m^{3/2}$ (KSI$\sqrt{IN}$)	$(a/2C)_f$	$(a/t)_f$	REMARKS
2AR23-2	0.686 (0.027)	127.0 (5.00)	R.T.	LUL	310.3 (45.0)	0.533 (0.021)	2.41 (0.095)	17.0 (15.5)	0.221	0.778	0.533 (0.021)	2.41 (0.095)	17.0 (15.5)	0.221	0.778	
				CYCLIC	248.2 (36.0)	0.533 (0.021)	2.41 (0.095)	13.3 (12.1)	0.221	0.778	a = t	2.90 (0.114)	15.6 (14.2)	0.237	1.00	10CPM, 1288 CYCLES TO B.T.
				FRACTURE	368.2 (53.4)	a = t	2.90 (0.114)	24.2 (22.0)	0.237	1.00						
2AR23-2	0.686 (0.027)	127.0 (5.00)	R.T.	LUL	310.3 (45.0)	0.508 (0.020)	2.31 (0.091)	16.3 (14.8)	0.220	0.741	0.508 (0.020)	2.31 (0.091)	16.3 (14.8)	0.220	0.741	
				CYCLIC	248.2 (36.0)	0.508 (0.020)	2.51 (0.099)	12.7 (11.6)	0.220	0.741	a = t	2.51 (0.099)	14.3 (13.0)	0.273	1.00	10CPM, 1554 CYCLES TO B.T.
2AR23-3	0.686 (0.027)	127.0 (5.00)	R.T.	LUL	279.2 (40.5)	0.508 (0.020)	2.44 (0.096)	14.8 (13.5)	0.208	0.741	0.508 (0.020)	2.44 (0.096)	14.8 (13.5)	0.208	0.741	
				CYCLIC	248.2 (36.0)	0.508 (0.020)	2.44 (0.096)	13.1 (11.9)	0.208	0.741	a = t	2.67 (0.105)	14.8 (13.5)	0.257	1.00	10 CPM, 1605 CYCLES TO B.T.
				FRACTURE	377.2 (54.7)	a = t	2.67 (0.105)	23.6 (21.5)	0.257	1.00						
2AR23-3	0.686 (0.027)	127.0 (5.00)	R.T.	LUL	279.2 (40.5)	0.508 (0.020)	2.29 (0.090)	14.4 (13.1)	0.222	0.741	0.508 (0.020)	2.29 (0.090)	14.4 (13.1)	0.222	0.741	
				CYCLIC	248.2 (36.0)	0.508 (0.020)	2.29 (0.090)	12.6 (11.5)	0.222	0.741	a = t	2.54 (0.100)	14.4 (13.1)	0.270	1.00	10CPM, 1622 CYCLES TO B.T.
3AR23-2	0.686 (0.027)	127.0 (5.00)	R.T.	FRACTURE	371.6 (53.9)	a = t	2.74 (0.108)	23.6 (21.5)	0.250	1.00						
2AR23-4	0.711 (0.028)	127.0 (5.00)	R.T.	FRACTURE	383.4 (55.6)	0.559 (0.022)	2.37 (0.092)	20.7 (18.8)	0.239	0.785						BREAKTHROUGH AT 376.5 MN/m^2 (54.6 ksi)
4AR23-1A	0.686 (0.027)	127.0 (5.00)	R.T.	LUL	310.3 (45.0)	0.457 (0.018)	2.34 (0.092)	15.4 (14.0)	0.196	0.667	0.457 (0.018)	2.34 (0.092)	15.4 (14.0)	0.196	0.667	
				CYCLIC	248.2 (36.0)	0.457 (0.018)	2.34 (0.092)	12.0 (10.9)	0.196	0.667	0.457 (0.018)	2.34 (0.092)	12.0 (10.9)	0.196	0.667	1 CPM, 100 CYCLES TOTAL
				FRACTURE	377.2 (54.7)	0.457 (0.018)	2.34 (0.092)	19.2 (17.5)	0.196	0.667						
4AR23-1A	0.686 (0.027)	127.0 (5.00)	R.T.	LUL	310.3 (45.0)	0.508 (0.020)	2.39 (0.094)	16.5 (15.0)	0.213	0.741	0.508 (0.020)	2.39 (0.094)	16.5 (15.0)	0.213	0.741	
				CYCLIC	248.2 (36.0)	0.508 (0.020)	2.39 (0.094)	13.0 (11.8)	0.213	0.741	0.533 (0.021)	2.39 (0.094)	13.3 (12.1)	0.223	0.778	1 CPM, 100 CYCLES TOTAL

Table 18 : ROOM TEMPERATURE 2219-T87 ALUMINUM BASE METAL
TEST RESULTS (t = 0.635mm(0.025 inch) a/2c = .30)

SPECIMEN NUMBER	GAGE THICKNESS, t mm (INCH)	GAGE WIDTH, W mm (INCH)	TEST TEMPERATURE	TEST TYPE	STRESS, σ MN/m^2 (KSI)	INITIAL FLAW DEPTH, a_i mm (INCH)	INITIAL FLAW LENGTH, $2c_i$ mm (INCH)	INITIAL STRESS INTENSITY, K_{I_i} $MN/m^{3/2}$ (KSI$\sqrt{IN}$)	$(a/2c)_i$	$(a/t)_i$	FINAL FLAW DEPTH, a_f mm (INCH)	FINAL FLAW LENGTH, $2c_f$ mm (INCH)	FINAL STRESS INTENSITY, K_{I_f} $MN/m^{3/2}$ (KSI$\sqrt{IN}$)	$(a/2C)_f$	$(a/t)_f$	REMARKS
4AR23-1	0.686 (0.027)	127.0 (5.00)	R.T.	LUL	279.2 (40.5)	0.508 (0.020)	2.34 (0.092)	14.5 (13.2)	0.217	0.741	0.508 (0.020)	2.34 (0.092)	14.5 (13.2)	0.217	0.741	
				CYCLIC	248.2 (36.0)	0.508 (0.020)	2.34 (0.092)	12.7 (11.6)	0.217	0.741	0.533 (0.021)	2.34 (0.092)	13.2 (12.0)	0.228	0.778	1 CPM, 100 CYCLES TOTAL
				FRACTURE	362.7 (52.6)	0.533 (0.021)	2.34 (0.092)	20.0 (18.2)	0.228	0.778						
4AR23-1	0.686 (0.027)	127.0 (5.00)	R.T.	LUL	279.2 (40.5)	0.508 (0.020)	2.39 (0.094)	14.7 (13.4)	0.213	0.741	0.508 (0.020)	2.39 (0.094)	14.7 (13.4)	0.213	0.741	
				CYCLIC	248.2 (36.0)	0.508 (0.020)	2.39 (0.094)	13.0 (11.8)	0.213	0.741	0.533 (0.021)	2.39 (0.094)	13.4 (12.2)	0.223	0.778	1 CPM, 100 CYCLES TOTAL

Table 19: LIQUID HYDROGEN 2219-T87 ALUMINUM BASE METAL
TEST RESULTS ($t = 4.77mm(0.188)$ $a/2c = .15$)

SPECIMEN NUMBER	GAGE THICKNESS, t mm (INCH)	GAGE WIDTH, W mm (INCH)	TEST TEMPERATURE K (°F)	TEST TYPE	STRESS, σ MN/m^2 (KSI)	INITIAL FLAW DEPTH, a_i mm (INCH)	INITIAL FLAW LENGTH, $2c_i$ mm (INCH)	INITIAL STRESS INTENSITY, K_{I_i} $MN/m^{3/2}$ (KSI$\sqrt{IN}$)	$(a/2c)_i$	$(a/t)_i$	FINAL FLAW DEPTH, a_f mm (INCH)	FINAL FLAW LENGTH, $2c_f$ mm (INCH)	FINAL STRESS INTENSITY, K_{I_f} $MN/m^{3/2}$ (KSI$\sqrt{IN}$)	$(a/2C)_f$	$(a/t)_f$	REMARKS
2AH11-1	4.80 (0.189)	190.5 (7.50)	20 (-423)	LUL	379.2 (55.0)	3.30 (0.130)	20.32 (0.800)	54.5 (49.6)	0.162	0.688	3.56 (0.140)	20.32 (0.800)	57.6 (52.4)	0.175	0.741	
				CYCLIC	303.4 (44.0)	3.56 (0.140)	20.32 (0.800)	45.1 (41.0)	0.175	0.741	4.24 (0.167)	20.32 (0.800)	50.2 (45.7)	0.209	0.884	3 CPM. 300 CYCLES TOTAL
				FRACTURE	390.3 (56.6)	4.24 (0.167)	20.32 (0.800)	66.2 (60.2)	0.209	0.884						BREAKTHROUGH AT (55.2 ksi)
2AH11-2	4.72 (0.186)	190.5 (7.50)	20 (-423)	LUL	341.3 (49.5)	3.40 (0.134)	20.57 (0.810)	50.2 (45.7)	0.165	0.720	3.53 (0.139)	20.57 (0.810)	51.7 (47.0)	0.172	0.747	
				CYCLIC	303.4 (440)	3.53 (0.139)	20.57 (0.810)	45.5 (41.4)	0.172	0.747	a = t	21.08 (0.830)	51.5 (46.9)	0.224	1.00	3 CPM, 310 CYCLES TO B.T.
				FRACTURE	371.6 (53.9)	a = t	21.08 (0.830)	64.2 (58.4)	0.224	1.00						
2AH11-3	4.83 (0.190)	190.5 (7.50)	20 (-423)	LUL	303.4 (44.0)	3.35 (0.132)	20.57 (0.810)	43.4 (39.5)	0.163	0.695	3.40 (0.134)	20.57 (0.810)	44.0 (40.0)	0.165	0.705	
			RT	CYCLIC	248.2 (36.0)	3.40 (10.134)	20.57 (0.810)	35.9 (32.7)	0.165	0.705	a=t	22.10 (0.870)	43.3 (39.4)	0.218	1.00	10 CPM, 449 cycles to BT
			RT	FRACTURE	308.9 (44.8)	a=t	22.10 (0.870)	54.8 (49.9)	0.218	1.00						
3AH11-2	4.78 (0.188)	190.5 (7.50)	20 (-423)	FRACTURE	389.6 (56.5)	3.20 (0.126)		(0.815)	55.3 (50.3)	0.155	0.688					
3AH11-3	4.83 (0.190)	190.5 (7.50)	20 (-423)	LUL	275.8 (40.0)	3.12 (0.123)	20.57 (0.810)	37.1 (33.8)	0.152	0.670						
			RT	CYCLIC	248.2 (36.0)	3.12 (0.123)	20.57 (0.810)	33.7 (30.7)	0.152	0.647	3.12 (0.123)	20.57 (0.810)	37.1 (33.8)	0.152	0.647	
4AH11-1	4.83 (0.190)	190.5 (7.50)	RT	FRACTURE	313.7 (45.4)	a=t	22.35 (0.880)	56.0 (51.0)	0.216	0.647	a=t	22.35 (0.880)	43.5 (39.6)	0.216	1.00	10 CPM, 530 cycles to BT
				CYCLIC	303.4 (44.0)	3.23 (0.127)	20.83 (0.820)	42.1 (38.3)	0.155	0.668	3.43 (0.135)	20.83 (0.820)	44.1 (40.1)	0.165	0.711	1CPM, 100 CYCLES TOTAL
				FRACTURE	405.4 (58.8)	3.43 (0.135)	20.83 (0.820)	60.7 (55.2)	0.165	0.711						
4AH11-2	4.75 (0.187)	190.5 (7.50)	20 (-423)	LUL	379.2 (55.0)	3.43 (0.135)	20.83 (0.820)	56.8 (51.7)	0.165	0.722	3.68 (0.145)	20.83 (0.820)	59.9 (54.5)	0.177	0.775	
				CYCLIC	341.3 (49.5)	3.68 (0.145)	20.83 (0.820)	53.3 (48.5)	0.177	0.775						SPECIMEN FAILED ON 32nd CYCLE
3AH11-1	4.72 (0.186)	190.5 (7.50)	20 (-423)	FRACTURE	390.9 (56.7)	3.25 (0.128)	20.57 (0.810)	56.4 (51.3)	0.158	0.688						

Table 19 : LIQUID HYDROGEN TEMPERATURE 2219-T87 ALUMINUM
BASE METAL TEST RESULTS (t = 4.77mm(0.188 inch))

SPECIMEN NUMBER	GAGE THICKNESS, t mm (INCH)	GAGE WIDTH, W mm (INCH)	TEST TEMPERATURE K (°F)	TEST TYPE	STRESS, σ MN/m^2 (KSI)	INITIAL FLAW DEPTH, a_i mm (INCH)	INITIAL FLAW LENGTH, $2c_i$ mm (INCH)	INITIAL STRESS INTENSITY, K_{I_i} $MN/m^{3/2}$ (KSI$\sqrt{IN}$)	$(a/2c)_i$	$(a/t)_i$	FINAL FLAW DEPTH, a_f mm (INCH)	FINAL FLAW LENGTH, $2c_f$ mm (INCH)	FINAL STRESS INTENSITY, K_{I_f} $MN/m^{3/2}$ (KSI$\sqrt{IN}$)	$(a/2C)_f$	$(a/t)_f$	REMARKS
2AH11-4	4.78 (0.188)	190.5 (7.50)	20 (-423)	LUL	379.2 (55.0)	3.28 (0.129)	20.83 (0.320)	55.2 (50.2)	0.157	0.686	3.51 (0.138)	20.83 (0.820)	58.1 (52.9)	0.168	0.734	
				CYCLIC	341.3 (49.5)	3.51 (0.138)	20.83 (0.820)	51.5 (46.9)	0.168	0.734						3 CPM, Specimen Failed on 80th cycle

Table 20 : LIQUID HYDROGEN TEMPERATURE 2219-T87 ALUMINUM BASE METAL TEST RESULTS ($t = 1.91$ mm (0.075 inch))

SPECIMEN NUMBER	GAGE THICKNESS, t mm (INCH)	GAGE WIDTH, W mm (INCH)	TEST TEMPERATURE K (°F)	TEST TYPE	STRESS, σ MN/m^2 (KSI)	INITIAL FLAW DEPTH, a_i mm (INCH)	INITIAL FLAW LENGTH, $2c_i$ mm (INCH)	INITIAL STRESS INTENSITY, K_{I_i} $MN/m^{3/2}$ (KSI$\sqrt{IN}$)	$(a/2c)_i$	$(a/t)_i$	FINAL FLAW DEPTH, a_f mm (INCH)	FINAL FLAW LENGTH, $2c_f$ mm (INCH)	FINAL STRESS INTENSITY, K_{I_f} $MN/m^{3/2}$ (KSI$\sqrt{IN}$)	$(a/2C)_f$	$(a/t)_f$	REMARKS
2AH71-1	1.96 (0.077)	127.0 (5.00)	20 (-423)	LUL	344.8 (50.0)	1.63 (0.064)	10.92 (0.430)	39.8 (36.2)	0.149	0.831	1.68 (0.066)	10.92 (0.430)	40.7 (37.0)	0.153	0.857	
			20 (-423)	CYCLIC	275.8 (40.0)	1.68 (0.066)	10.92 (0.430)	32.0 (29.1)	0.153	0.857	1.83 (0.072)	10.92 (0.430)	33.0 (30.0)	0.167	0.935	2 CPM 300 Cycles Total
			20 (-423)	FRACTURE	442.7 (64.2)	1.83 (0.072)	10.92 (0.430)	55.7 (50.7)	0.167	0.935						Breakthrough at 408.9 MN/m^2 (59.3 ksi)
2AH71-2	1.98 (0.078)	127.0 (5.00)	20 (-423)	LUL	311.7 (45.2)	1.73 (0.068)	10.92 (0.430)	36.8 (33.5)	0.158	0.872	1.75 (0.069)	10.92 (0.430)	37.1 (33.8)	0.160	0.885	
			20 (-423)	CYCLIC	275.8 (40.0)	1.75 (0.069)	10.92 (0.430)	32.6 (29.7)	0.160	0.885	1.88 (0.074)	10.92 (0.430)	33.1 (30.1)	0.172	0.949	2 CPM 300 Cycles Total
			20 (-423)	FRACTURE	442.0 (64.1)	1.88 (0.074)	10.92 (0.430)	55.8 (50.8)	0.172	0.949						Breakthrough at 346.8 MN/m^2 (50.3 ksi)
2AH71-3	1.98 (0.078)	127.0 (5.00)	20 (-423)	LUL	275.8 (40.0)	1.52 (0.060)	11.18 (0.440)	29.6 (26.9)	0.136	0.769	1.52 (0.060)	11.18 (0.440)	29.6 (26.9)	0.136	0.769	
			R.T.	FRACTURE	337.8 (49.0)	a=t	11.43 (0.450)	43.3 (39.4)	0.173	1.00						
2AH71-4	1.98 (0.078)	127.0 (5.00)	20 (-423)	LUL	370.3 (53.7)	1.80 (0.071)	11.56 (0.455)	46.3 (42.1)	0.156	0.910	a=t	11.56 (0.455)	46.8 (42.6)	0.171	1.00	Breakthrough at 342.0 MN/m^2 (49.6 ksi)
			20 (-423)	FRACTURE	444.0 (64.4)	a=t	11.56 (0.455)	57.7 (52.6)	0.171	1.00						
3AH71-1	1.98 (0.078)	127.0 (5.00)	20 (-423)	FRACTURE	439.9 (63.8)	1.80 (0.071)	11.43 (0.450)	56.2 (51.1)	0.158	0.910						Breakthrough at 352.3 MN/m^2 (51.1 ksi)
3AH71-2	2.00 (0.079)	127.0 (5.00)	20 (-423)	FRACTURE	435.1 (63.1)	1.75 (0.069)	11.30 (0.445)	54.4 (49.5)	0.155	0.873						Breakthrough at 386.8 MN/m^2 (56.1 ksi)
3AH71-3	1.98 (0.078)	127.0 (5.00)	20 (-423)	LUL	436.5 (63.3)	1.65 (0.065)	10.67 (0.420)	52.3 (47.6)	0.155	0.833	a=t	10.67 (0.420)	55.2 (50.2)	0.186	1.00	
			R.T.	FRACTURE	310.3 (45.0)	a=t	10.67 (0.420)	38.1 (34.7)	0.186	1.00						
4AH71-1	1.93 (0.076)	127.0 (5.00)	20 (-423)	LUL	358.5 (52.0)	1.68 (0.066)	11.05 (0.435)	42.9 (39.0)	0.156	0.868	1.73 (0.068)	11.05 (0.435)	43.6 (39.7)	0.156	0.895	
			20 (-423)	CYCLIC	310.3 (45.0)	1.73 (0.068)	11.05 (0.435)	37.3 (33.9)	0.156	0.895	1.83 (0.072)	11.05 (0.435)	37.6 (34.2)	0.166	0.947	1 CPM 101 Cycles Total
			20 (-423)	FRACTURE	438.5 (63.6)	1.83 (0.072)	11.05 (0.435)	55.4 (50.4)	0.166	0.947						Breakthrough at 377.2 MN/m^2 (54.7 ksi)

Table 20: LIQUID HYDROGEN TEMPERATURE 2219-T87 ALUMINUM BASE METAL TEST RESULTS ($t = 1.91$ mm (0.075 inch))

SPECIMEN NUMBER	GAGE THICKNESS, t mm (INCH)	GAGE WIDTH, W mm (INCH)	TEST TEMPERATURE K (°F)	TEST TYPE	STRESS, σ MN/m² (KSI)	INITIAL FLAW DEPTH, a_i mm (INCH)	INITIAL FLAW LENGTH, $2c_i$ mm (INCH)	INITIAL STRESS INTENSITY, K_{I_i} MN/m$^{3/2}$ (KSI $\sqrt{IN}$)	$(a/2c)_i$	$(a/t)_i$	FINAL FLAW DEPTH, a_f mm (INCH)	FINAL FLAW LENGTH, $2c_f$ mm (INCH)	FINAL STRESS INTENSITY, K_{I_f} MN/m$^{3/2}$ (KSI $\sqrt{IN}$)	$(a/2C)_f$	$(a/t)_f$	REMARKS
4AH71-2	1.96 (0.077)	127.0 (5.00)	20 (-423)	LUL	372.3 (54.0)	1.63 (0.064)	11.18 (0.440)	40.7 (37.0)	0.145	0.831	1.65 (0.065)	11.18 (0.440)	41.4 (37.6)	0.148	0.844	
				CYCLIC	310.3 (45.0)	1.65 (0.065)	11.18 (0.440)	34.4 (31.3)	0.148	0.844	1.78 (0.070)	11.18 (0.440)	37.6 (34.2)	0.159	0.909	1 CPM, 100 Cycles Total
				FRACTURE	446.1 (64.7)	1.78 (0.070)	11.18 (0.440)	56.6 (51.5)	0.159	0.909						Breakthrough at 398.5 MN/m² (57.8 ksi)

Table 21 : LIQUID HYDROGEN TEMPERATURE 2219-T87 ALUMINUM
BASE METAL TEST RESULTS (t = 0.635mm(0.025 inch))

SPECIMEN NUMBER	GAGE THICKNESS, t mm (INCH)	GAGE WIDTH, w mm (INCH)	TEST TEMPERATURE K (°F)	TEST TYPE	STRESS, σ MN/m² (KSI)	INITIAL FLAW DEPTH, a_i mm (INCH)	INITIAL FLAW LENGTH, $2c_i$ mm (INCH)	INITIAL STRESS INTENSITY, K_{Ii} MN/m$^{3/2}$ (KSI$\sqrt{IN}$)	$(a/2c)_i$	$(a/t)_i$	FINAL FLAW DEPTH, a_f mm (INCH)	FINAL FLAW LENGTH, $2c_f$ mm (INCH)	FINAL STRESS INTENSITY, K_{If} MN/m$^{3/2}$ (KSI$\sqrt{IN}$)	$(a/2c)_f$	$(a/t)_f$	REMARKS
2AH21-1	0.686 (0.027)	127.0 (5.00)	20 (-423)	LUL	434.4 (63.0)	0.508 (0.020)	3.71 (0.146)	27.5 (25.0)	0.137	0.741	0.533 (0.021)	3.71 (0.146)	28.7 (26.1)	0.144	0.778	
				CYCLIC	347.5 (50.4)	0.559 (0.022)	3.71 (0.146)	22.3 (20.3)	0.144	0.778	0.635 (0.025)	3.71 (0.146)	24.7 (22.5)	0.171	0.926	2 CPM, 350 cycles total
				FRACTURE	383.3 (55.1)	0.635 (0.025)	3.71 (0.146)	35.9 (32.7)	0.171	0.926						Breakthrough at 452.3 MN/m² (65.6 ksi)
2AH21-2	0.711 (0.028)	127.0 (5.00)	20 (-423)	LUL	433.7 (62.9)	0.533 (0.021)	3.81 (0.150)	28.6 (26.0)	0.140	0.750	0.559 (0.022)	3.81 (0.150)	29.2 (26.6)	0.147	0.786	
				CYCLIC	389.6 (56.5)	0.559 (0.022)	3.81 (0.150)	25.8 (23.5)	0.147	0.786	0.635 (0.025)	3.81 (0.150)	28.4 (25.8)	0.167	0.893	2 CPM, 150 cycles total
				FRACTURE	480.6 (69.7)	0.635 (0.025)	3.81 (0.150)	36.0 (32.8)	0.167	0.893						Breakthrough at 450.9 MN/m² (65.4 ksi)
3AH21-3	0.686 (0.027)	127.0 (5.00)	20 (-423)	LUL	439.2 (63.7)	0.483 (0.019)	3.81 (0.150)	27.0 (24.6)	0.127	0.704	0.508 (0.020)	3.81 (0.150)	28.4 (25.8)	0.133	0.741	
			R.T.	FRACTURE	328.9 (47.7)	a=t	13.46 (0.53)	31.1 (28.3	0.051	1.00						
2AH21-4	0.711 (0.028)	127.0 (5.00)	20 (-423)	FRACTURE	477.1 (69.2)	0.584 (0.023)	3.86 (0.152)	34.2 (31.1)	0.151	0.821						Breakthrough at 458.5 MN/m² (66.5 ksi)
3AH21-1	0.711 (0.028)	127.0 (5.00)	20 (-423)	FRACTURE	493.7 (71.6)	0.584 (0.023)	3.81 (0.150)	35.2 (32.0)	0.153	0.821						BT Instrumentation Inoperative
3AH21-2	(0.025)	127.0 (5.00)	20 (-423)	FRACTURE	475.1 (68.9)	0.533 (0.021)	3.76 (0.148)	33.6 (30.6)	0.142	0.840						No BT Instrumentation
3AH21-3	0.686 (0.027)	127.0 (5.00)	20 (-423)	FRACTURE	499.9 (72.5)	0.533 (0.021)	3.81 (0.150)	33.8 (30.8)	140	0.778						BT Instrumentation Inoperative
4AH21-1	0.686 (0.027)	127.0 (5.00)	20 (-423)	LUL	434.4 (63.0)	0.483 (0.020)	3.73 (0.147)	27.5 (25.0)	0.136	0.741	0.533 (0.021)	3.73 (0.147)	28.7 (26.1)	0.143	0.770	
				CYCLIC	347.5 (50.4)	0.533 (0.021)	3.73 (0.147)	22.3 (20.3)	0.143	0.778	0.584 (0.023)	3.73 (0.147)	24.1 (21.9)	0.156	0.852	1 CPM, 100 cycles total
				FRACTURE	471.6 (68.4)	0.584 (0.023)	3.73 (0.147)	34.2 (31.1)	0.156	0.852						Breakthrough at 449.6 MN/m² (65.2 ksi)
4AH21-2	0.686 (0.027)	127.0 (5.00)	20 (-423)	LUL	433.0 (62.8)	0.584 (0.023)	3.96 (0.156)	31.4 (28.6)	0.147	0.852	0.635 (0.025)	3.96 (0.156)	32.5 (29.6)	0.160	0.926	
				CYCLIC	392.3 (56.9)	0.635 (0.025)	3.96 (0.156)	29.0 (26.4)	0.160	0.926	a=t	3.96 (0.156)	29.8 (27.1)	0.163	1.00	1 CPM, 15 cycles to BT
				FRACTURE	463.3 (67.2)	a=t	3.96 (0.156)	36.1 (32.8)	0.163	1.00						

Table 22 : ROOM TEMPERATURE 6Al-4V STA TITANIUM BASE METAL
TEST RESULTS ($t = 3.18mm(0.125\ inch)\ a/2c = .15$)

SPECIMEN NUMBER	GAGE THICKNESS, t mm (INCH)	GAGE WIDTH, W mm (INCH)	TEST TEMPERATURE	TEST TYPE	STRESS, σ MN/m^2 (KSI)	INITIAL FLAW DEPTH, a_i mm (INCH)	INITIAL FLAW LENGTH, $2c_i$ mm (INCH)	INITIAL STRESS INTENSITY, K_{I_i} $MN/m^{3/2}$ ($KSI\sqrt{IN}$)	$(a/2c)_i$	$(a/t)_i$	FINAL FLAW DEPTH, a_f mm (INCH)	FINAL FLAW LENGTH, $2c_f$ mm (INCH)	FINAL STRESS INTENSITY, K_{I_f} $MN/m^{3/2}$ ($KSI\sqrt{IN}$)	$(a/2C)_f$	$(a/t)_f$	REMARKS
2TR11-1	3.25 (0.128)	127.0 (5.00)	RT	LUL	711.6 (103.2)	1.65 (0.065)	11.43 (0.450)	63.0 (57.3)	0.144	0.508	1.73 (0.068)	11.43 (0.450)	65.1 (59.2)	0.151	0.531	
				CYCLIC	569.5 (82.6)	1.73 (0.068)	11.43 (0.450)	51.3 (46.7)	0.151	0.531	2.90 (0.114)	18.54 (0.730)	86.8 (79.0)	0.156	0.891	10 CPM, 222 CYCLES TO FRACTURE
2TR11-2	3.18 (0.125)	127.0 (5.00)	RT	LUL	724.0 (105.0)	1.60 (0.063)	11.18 (0.440)	63.1 (57.4)	0.143	0.504	1.68 (0.066)	11.18 (0.440)	65.2 (59.3)	0.150	0.528	
				CYCLIC	651.6 (94.5)	1.68 (0.066)	11.18 (0.440)	58.2 (53.0)	0.150	0.528	2.79 (0.110)	13.72 (0.540)	87.9 (80.0)	0.204	0.880	10 CPM, 45 CYCLES TO FRACTURE
3TR11-1	3.25 (0.128)	127.0 (5.00)	RT	FRACTURE	748.8 (108.6)	1.60 (0.063)	11.93 (0.470)	65.7 (59.8)	0.134	0.492						
4TR11-1	3.27 (0.129)	127.0 (5.00)	R.T.	LUL	654.3 (94.9)	1.78 (0.070)	11.43 (0.450)	60.3 (54.9)	0.155	0.543	1.88 (0.074)	11.43 (0.450)	62.6 (57.0)	0.164	0.574	
				CYCLIC	588.8 (85.4)	1.88 (0.074)	11.43 (0.450)	56.3 (51.2)	0.164	0.574	2.24 (0.088)	11.43 (0.450)	62.9 (57.2)	0.196	0.682	1 CPM, 25 cycles to FRACTURE
4TR11-2	3.27 (0.129)	127.0 (5.00)	R.T.	LUL	690.9 (100.2)	1.65 (0.065)	11.68 (0.460)	61.0 (55.5)	0.141	0.504	1.85 (0.073)	11.68 (0.460)	65.8 (59.9)	0.159	0.566	
				CYCLIC	587.5 (85.2)	1.85 (0.073)	11.68 (0.460)	55.6 (50.6)	0.154	0.556	2.24 (0.088)	11.68 (0.460)	63.3 (57.6)	0.191	0.682	1 CPM, 41 CYCLES TO FRACTURE

Table 23 : ROOM TEMPERATURE 6AI-4V STA TITANIUM BASE METAL
TEST RESULTS (t = 3.18mm (0.125 inch) a/2c = .30)

SPECIMEN NUMBER	GAGE THICKNESS, t mm (INCH)	GAGE WIDTH, W mm (INCH)	TEST TEMPERATURE	TEST TYPE	STRESS, σ MN/m^2 (KSI)	INITIAL FLAW DEPTH, a_i mm (INCH)	INITIAL FLAW LENGTH, $2c_i$ mm (INCH)	INITIAL STRESS INTENSITY, K_{I_i} $MN/m^{3/2}$ (KSI$\sqrt{IN}$)	$(a/2c)_i$	$(a/t)_i$	FINAL FLAW DEPTH, a_f mm (INCH)	FINAL FLAW LENGTH, $2c_f$ mm (INCH)	FINAL STRESS INTENSITY, K_{I_f} $MN/m^{3/2}$ (KSI$\sqrt{IN}$)	$(a/2C)_f$	$(a/t)_f$	REMARKS
2TR13-1	1.38 (0.126)	127.0 (5.00)	RT	LUL	604.7 (87.7)	2.11 (0.083)	6.60 (0.260)	48.6 (44.2)	0.319	0.659	2.13 (0.084)	6.60 (0.260)	48.7 (44.3)	0.323	0.667	
				CYCLIC	484.0 (70.2)	2.13 (0.084)	6.60 (0.260)	38.8 (35.3)	0.323	0.667	a = t	10.41 (0.410)	(49.7)	.307	1.00	10 CPM, 685 CYCLES TO B.T.
				FRACTURE	599.9 (87.0)	a = t	10.41 (0.410)	68.1 (62.0)	0.307	1.00						
2TR13-2	1.38 (0.126)	127.0 (5.00)	RT	LUL	620.6 (90.0)	2.16 (0.085)	6.60 (0.260)	50.1 (45.6)	0.327	0.675	2.18 (0.086)	6.60 (0.260)	50.2 (45.7)	0.331	0.683	
				CYCLIC	558.5 (81.0)	2.18 (0.086)	6.60 (0.260)	45.1 (41.0)	0.331	0.683	a = t	10.41 (0.410)	63.3 (57.6)	0.307	1.00	10 CPM, 152 CYCLES TO B.T.
				FRACTURE	498.5 (72.3)	a = t	10.41 (0.410)	56.3 (51.2)	0.307	1.00						
3TR13-1	1.38 (0.126)	127.0 (5.00)	RT	FRACTURE	636.4 (92.3)	2.03 (0.080)	6.60 (0.260)									

Table 24 : ROOM TEMPERATURE 6Al-4V STA TITANIUM BASE METAL
TEST RESULTS (t = 3.18mm (0.125 inch) a/2c = .45)

SPECIMEN NUMBER	GAGE THICKNESS, t mm (INCH)	GAGE WIDTH, W mm (INCH)	TEST TEMPERATURE	TEST TYPE	STRESS, σ MN/m^2 (KSI)	INITIAL FLAW DEPTH, a_i mm (INCH)	INITIAL FLAW LENGTH, $2c_i$ mm (INCH)	INITIAL STRESS INTENSITY, K_{I_i} MN/m$^{3/2}$ (KSI$\sqrt{IN}$)	$(a/2c)_i$	$(a/t)_i$	FINAL FLAW DEPTH, a_f mm (INCH)	FINAL FLAW LENGTH, $2c_f$ mm (INCH)	FINAL STRESS INTENSITY, K_{I_f} MN/m$^{3/2}$ (KSI$\sqrt{IN}$)	$(a/2c)_f$	$(a/t)_f$	REMARKS
2TR14-1	3.23 (0.127)	127.0 (5.00)	R.T.	LUL	735.7 (106.7)	2.24 (0.088)	5.08 (0.200)	49.5 (45.0)	0.440	0.695	2.74 (0.108)	12.45 (0.490)	94.4 (85.9)	0.220	0.450	
				CYCLIC	588.1 (85.3)	2.74 (0.108)	12.45 (0.490)	74.6 (67.9)	0.220	0.850	3.05 (0.120)	12.70 (0.500)	76.5 (69.6)	0.240	0.945	10 CPM, 29 Cycles To Fracture
2TR14-2	3.23 (0.127)	127.0 (5.00)	R.T.	LUL	861.9 (125.0)	2.24 (0.088)	5.08 (0.200)	58.4 53.1	0.440	0.693	2.39 (0.094)	7.62 (0.300)	79.3 (72.2)	0.313	0.740	
				CYCLIC	775.7 (112.5)	2.39 (0.094)	7.62 (0.300)		0.313	0.740	2.79 (0.110)	8.13 (0.320)	76.5 (69.6)	0.344	0.866	10 CPM, 33 Cycles To Fracture
3TR14-1	3.25 (0.128)	127.0 (5.00)	R.T.	FRACTURE	900.5 (130.6)	2.21 (0.087)	5.33 (0.210)	63.2 (57.5)	0.414	0.680						

Table 25 : ROOM TEMPERATURE 6Al-4V STA TITANIUM BASE METAL
TEST RESULTS (t = 2.03mm(0.080 inch) a/2c = .15)

SPECIMEN NUMBER	GAGE THICKNESS, t mm (INCH)	GAGE WIDTH, W mm (INCH)	TEST TEMPERATURE	TEST TYPE	STRESS, σ MN/m^2 (KSI)	INITIAL FLAW DEPTH, a_i mm (INCH)	INITIAL FLAW LENGTH, $2c_i$ mm (INCH)	INITIAL STRESS INTENSITY, K_i $MN/m^{3/2}$ (KSI$\sqrt{IN}$)	$(a/2c)_i$	$(a/t)_i$	FINAL FLAW DEPTH, a_f mm (INCH)	FINAL FLAW LENGTH, $2c_f$ mm (INCH)	FINAL STRESS INTENSITY, K_f $MN/m^{3/2}$ (KSI$\sqrt{IN}$)	$(a/2C)_f$	$(a/t)_f$	REMARKS
2TR81-1	2.13 (0.084)	127.0 (5.00)	R.T.	LUL	744.7 (108.0)	1.37 (0.054)	10.16 (0.400)	68.5 (62.3)	0.135	0.643	1.52 (0.060)	10.16 (0.400)	74.5 (67.8)	0.150	0.714	
				CYCLIC	595.7 (86.4)	1.52 (0.060)	10.16 (0.400)	58.8 (53.5)	0.150	0.714	a=t	10.16 (0.400)	69.5 (63.2)	0.210	1.00	10 CPM, 155 Cycles to B.T.
				FRACTURE	664.0 (96.3)	a=t	10.16 (0.400)	77.9 (70.9)	0.210	1.00						
2TR81-2	2.03 (0.080)	127.0 (5.00)	R.T.	LUL	665.4 (96.5)	1.35 (0.053)	9.65 (0.380)	60.6 (55.1)	0.139	0.663	1.78 (0.070)	12.19 (0.480)	[illegible] (74.1)	0.146	0.875	
				CYCLIC	599.2 (86.9)	1.78 (0.070)	12.19 (0.480)	72.9 (66.3)	0.146	0.875	1.88 (0.074)	12.45 (0.490)	75.0 (68.2)	0.151	0.925	10 CPM, 4 Cycles to Fracture
3TR81-1	2.06 (0.081)	127.0 (5.00)	R.T.	FRACTURE	784.0 (113.7)	1.40 (0.055)	9.14 (0.360)	73.0 (66.4)	0.153	0.679						Breakthrough at 770.9 MN/m^2 (111.8 ksi)
4TR81-1	2.13 (0.084)	127.0 (5.00)	R.T.	LUL	627.4 (91.0)	1.52 (0.060)	9.91 (0.390)	61.7 (56.1)	0.154	0.714	1.63 (0.064)	9.91 (0.390)	65.0 (59.1)	0.164	0.762	
				CYCLIC	555.4 (82.0)	1.63 (0.064)	9.91 (0.390)	58.1 (52.9)	0.164	0.762	a=t	9.91 (0.390)	65.0 (59.1)	0.215	1.00	1 CPM, 35 cycles to BT
				FRACTURE	573.0 (83.1)	a=t	9.91 (0.390)	65.9 (60.0)	0.215	1.00						
4TR81-2	2.11 (0.083)	127.0 (5.00)	R.T.	LUL	654.3 (94.9)	1.27 (0.050)	9.91 (0.390)	55.6 (50.6)	0.128	0.602	1.35 (0.053)	9.91 (0.390)	56.6 (51.5)	0.136	0.639	
				CYCLIC	588.8 (85.4)	1.35 (0.053)	9.91 (0.390)	52.6 (47.9)	0.136	0.639	a=t	10.67 (0.420)	74.1 (67.4)	0.198	1.00	1 CPM, 75 cycles to BT
				FRACTURE	605.6 (87.8)	a=t	10.67 (0.420)	76.5 (69.6)	0.198	1.00						

Table 26 : ROOM TEMPERATURE 6AI-4V STA TITANIUM BASE METAL
TEST RESULTS (t = 2.03mm (0.080 inch) a/2c = .30)

SPECIMEN NUMBER	GAGE THICKNESS, t mm (INCH)	GAGE WIDTH, W mm (INCH)	TEST TEMPERATURE	TEST TYPE	STRESS, σ MN/m^2 (KSI)	INITIAL FLAW DEPTH, a_i mm (INCH)	INITIAL FLAW LENGTH, $2c_i$ mm (INCH)	INITIAL STRESS INTENSITY, K_{I_i} $MN/m^{3/2}$ (KSI$\sqrt{IN}$)	$(a/2c)_i$	$(a/t)_i$	FINAL FLAW DEPTH, a_f mm (INCH)	FINAL FLAW LENGTH, $2c_f$ mm (INCH)	FINAL STRESS INTENSITY, K_{I_f} $MN/m^{3/2}$ (KSI$\sqrt{IN}$)	$(a/2C)_f$	$(a/t)_f$	REMARKS
2TR83-1	2.08 (0.082)	127.0 (5.00)	R.T.	LUL	732.9 (106.3)	1.47 (0.058)	5.18 (0.204)	54.7 (49.8)	0.284	0.707	1.52 (0.060)	5.49 (0.216)	57.3 (52.1)	0.278	0.732	
				CYCLIC	586.1 (85.0)	1.52 (0.060)	5.49 (0.216)	45.3 (41.2)	0.278	0.732	a=t	7.62 (0.300)	58.1 (52.9)	0.273	1.00	10 CPM, 387 Cycles to B.T.
				FRACTURE	732.2 (106.2)	a=t	7.62 (0.300)	73.4 (66.8)	0.273	1.00						
2TR83-2	2.16 (0.085)	127.0 (5.00)	R.T.	LUL	720.5 (104.5)	1.52 (0.060)	5.33 (0.210)	54.5 (49.6)	0.210	0.706	1.68 (0.066)	7.95 (0.313)	70.0 (63.7)	0.313	0.776	
				CYCLIC	648.8 (94.1)	1.68 (0.066)	7.95 (0.313)	62.6 (57.0)	0.313	0.776	a=t	8.13 (0.320)	67.0 (61.0)	0.320	1.00	10 CPM, 33 Cycles to B.T.
				FRACTURE	649.6 (94.2)	a=t	8.13 (0.320)	67.1 (61.1)	0.320	1.00						
3TR83-1	2.06 (0.081)	127.0 (5.00)	R.T.	FRACTURE	771.6 (111.9)	1.52 (0.060)	5.33 (0.210)	59.8 (54.4)	0.286	0.741						

Table 27 : ROOM TEMPERATURE 6Al-4V STA TITANIUM BASE METAL
TEST RESULTS (t = 2.03mm (0.080 inch) a/2c = .45)

SPECIMEN NUMBER	GAGE THICKNESS, t mm (INCH)	GAGE WIDTH, W mm (INCH)	TEST TEMPERATURE	TEST TYPE	STRESS, σ MN/m^2 (KSI)	INITIAL FLAW DEPTH, a_i mm (INCH)	INITIAL FLAW LENGTH, $2c_i$ mm (INCH)	INITIAL STRESS INTENSITY, K_{I_i} $MN/m^{3/2}$ (KSI$\sqrt{IN}$)	$(a/2c)_i$	$(a/t)_i$	FINAL FLAW DEPTH, a_f mm (INCH)	FINAL FLAW LENGTH, $2a_f$ mm (INCH)	FINAL STRESS INTENSITY, K_{I_f} $MN/m^{3/2}$ (KSI$\sqrt{IN}$)	$(a/2C)_f$	$(a/t)_f$	REMARKS
2TR84-1	2.08 (0.082)	127.0 (5.00)	R.T.	LUL	837.7 (121.5)	1.57 (0.062)	3.56 (0.140)	48.2 (43.9)	0.443	0.756	1.65 (0.065)	4.57 (0.180)	59.2 (53.9)	0.361	0.793	
				CYCLIC	670.2 (97.2)	1.65 (0.065)	4.57 (0.180)	46.8 (42.6)	0.361	0.793	a=t	6.60 (0.260)	60.8 (55.3)	0.260	1.00	10 CPM, 277 cycles to BT
				FRACTURE	784.7 (113.8)	a=t	6.60 (0.260)	71.8 (65.3)	0.260	1.00						
2TR84-2	2.11 (0.083)	127.0 (5.00)	R.T.	LUL	861.9 (125.0)	1.60 (0.063)	3.40 (0.134)	47.8 (43.5)	0.470	0.759	1.65 (0.065)	4.27 (0.168)	57.4 (52.2)	0.387	0.783	
				CYCLIC	775.7 (112.5)	1.65 (0.065)	4.27 (0.168)	51.3 (46.7)	0.387	0.783	a=t	6.48 (0.255)	69.8 (63.5)	0.325	1.00	10 CPM, 113 cycles to BT
				FRACTURE	817.1 (118.5)	a=t	6.48 (0.255)	46.6 (42.4)	0.325	1.00						
3TR84-1	2.06 (0.081)	127.0 (5.00	R.T.	FRACTURE	881.9 (127.9)	1.52 (0.060)	3.56 (0.140)	51.2 (46.6)	0.429	0.741						

Table 28 : ROOM TEMPERATURE 6Al-4V STA TITANIUM BASE METAL
TEST RESULTS (t = 1.02mm (0.040 inch) a/2c = .05)

SPECIMEN NUMBER	GAGE THICKNESS, t mm (INCH)	GAGE WIDTH, W mm (INCH)	TEST TEMPERATURE	TEST TYPE	STRESS, σ MN/m^2 (KSI)	INITIAL FLAW DEPTH, a_i mm (INCH)	INITIAL FLAW LENGTH, $2c_i$ mm (INCH)	INITIAL STRESS INTENSITY, K_{I_i} $MN/m^{3/2}$ (KSI$\sqrt{IN}$)	$(a/2c)_i$	$(a/t)_i$	FINAL FLAW DEPTH, a_f mm (INCH)	FINAL FLAW LENGTH, $2c_f$ mm (INCH)	FINAL STRESS INTENSITY, K_{I_f} $MN/m^{3/2}$ (KSI$\sqrt{IN}$)	$(a/2C)_f$	$(a/t)_f$	REMARKS
2TR45-1	0.99 (0.039)	127.0 (5.00)	R.T.	LUL	455.8 (66.1)	0.635 (0.025)	14.99 (0.590)	31.7 (28.8)	0.042	0.641	0.762 (0.030)	14.99 (0.590)	39.1 (35.6)	0.051	0.769	
				CYCLIC	410.3 (59.5)	0.762 (0.030)	14.99 (0.590)	35.2 (32.0)	0.051	0.769	a=t	14.99 (0.590)	41.2 (39.3)	0.066	1.00	10 CPM, 17 CYCLES TO BT
				FRACTURE	548.2 (79.5)	a=t	14.99 (0.590)	58.2 (53.0)	0.066	1.00						
2TR45-2	1.24 (0.049)	127.0 (5.00)	R.T.	LUL	659.2 (95.6)	0.660 (0.026)	14.48 (0.570)	42.5 (38.7)	0.046	0.531	0.711 (0.028)	14.48 (0.570)	45.7 (41.6)	0.049	0.571	
				CYCLIC	564.7 (81.9)	0.711 (0.028)	14.48 (0.570)	38.8 (35.3)	0.049	0.571	a=t	14.48 (0.570)	65.3 (59.4)	0.086	1.00	10 CPM, 88 CYCLES TO BT
				FRACTURE	605.4 (87.8)	a=t	14.48 (0.570)	70.2 (63.9)	0.086	1.00						
3TR45-1	0.97 (0.038)	127.0 (5.00)	R.T.	FRACTURE	646.8 (93.8)	0.686 (0.027)	14.48 (0.570)	50.8 (46.2)	0.047	0.711						~~BREAKTHROUGH AT~~ (85.1 ksi)

Table 29 : ROOM TEMPERATURE 6Al-4V STA TITANIUM BASE METAL
TEST RESULTS (t = 1.02mm (0.040 inch) a/2c = .15)

SPECIMEN NUMBER	GAGE THICKNESS, t mm (INCH)	CAGE WIDTH, W mm (INCH)	TEST TEMPERATURE	TEST TYPE	STRESS, σ MN/m^2 (KSI)	INITIAL FLAW DEPTH, a_i mm (INCH)	INITIAL FLAW LENGTH, $2c_i$ mm (INCH)	INITIAL STRESS INTENSITY, K_{I_i} $MN/m^{3/2}$ (KSI$\sqrt{IN}$)	$(a/2c)_i$	$(a/t)_i$	FINAL FLAW DEPTH, a_f mm (INCH)	FINAL FLAW LENGTH, $2c_f$ mm (INCH)	FINAL STRESS INTENSITY, K_{I_f} $MN/m^{3/2}$ (KSI$\sqrt{IN}$)	$(a/2C)_f$	$(a/t)_f$	REMARKS
2TR41-1	1.42 (0.056)	127.0 (5.00)	R.T.	LUL	849.5 (123.2)	0.711 (0.028)	5.33 (0.210)	50.7 (46.1)	0.133	0.500	0.787 (0.031)	5.33 (0.210)	54.5 (49.6)	0.148	0.554	
				CYCLIC	765.3 (111.0)	0.787 (0.031)	5.33 (0.210)	48.6 (44.2)	0.148	0.554	a=t	6.10 (0.240)	70.1 (63.8)	0.233	1.00	1 CPM, 54 CYCLES TO BT
				FRACTURE	799.1 (115.9)	a=t	6.10 (0.240)	73.4 (66.8)	0.233	1.00						
2TR41-2	1.04 (0.041)	127.0 (5.00)	R.T.	LUL	776.4 (112.6)	0.711 (0.028)	5.33 (0.210)	53.5 (48.7)	0.133	0.683	a=t	5.59 (0.220)	67.9 (61.8)	0.186	1.00	
				FRACTURE	818.4 (118.7)	a=t	5.59 (0.220)	72.0 (65.5)	0.180	1.00						
3TR41-1	1.04 (0.041)	127.0 (5.00)	R.T.	FRACTURE	881.2 (127.8)	0.711 (0.028)	5.33 (0.210)	61.5 (56.0)	0.133	0.683						
4TR41-1	1.22 (0.048)	127.0 (5.00)	R.T.	LUL	890.1 (129.1)	(0.029)	5.59 (0.220)	59.3 (54.0)	0.132	0.604	0.864 (0.034)	5.59 (0.220)	67.4 (61.3)	0.155	0.708	
				CYCLIC	802.2 (116.2)	0.864 (0.034)	5.59 (0.220)	59.9 (54.5)	0.155	0.708	a=t	5.59 (0.220)	70.7 (64.3)	0.218	1.00	1 CPM, 36 CYCLES TO BT
				FRACTURE	893.5 (129.6)	a=t	5.59 (0.220)	79.6 (72.4)	0.218	1.00						
4TR41-2	1.09 (0.043)	127.0 (5.00)	R.T.	FRACTURE	906.0 (131.4)	0.635 (0.025)	5.18 (0.204)	55.9 (50.9)	0.123	0.581						

Table 30 : ROOM TEMPERATURE 6Al-4V STA TITANIUM BASE METAL
TEST RESULTS (t = 1.02mm (0.040 inch) a/2c = .30)

SPECIMEN NUMBER	GAGE THICKNESS, t mm (INCH)	GAGE WIDTH, W mm (INCH)	TEST TEMPERATURE	TEST TYPE	STRESS, σ MN/m^2 (KSI)	INITIAL FLAW DEPTH, a_i mm (INCH)	INITIAL FLAW LENGTH, $2c_i$ mm (INCH)	INITIAL STRESS INTENSITY, K_{I_i} $MN/m^{3/2}$ (KSI$\sqrt{IN}$)	$(a/2c)_i$	$(a/t)_i$	FINAL FLAW DEPTH, a_f mm (INCH)	FINAL FLAW LENGTH, $2c_f$ mm (INCH)	FINAL STRESS INTENSITY, K_{I_f} $MN/m^{3/2}$ (KSI$\sqrt{IN}$)	$(a/2C)_f$	$(a/t)_f$	REMARKS
2TR43-1	1.12 (0.044)	127.0 (5.00	R.T.	LUL	908.8 (131.8)	0.660 (0.026)	3.05 (0.120)	49.1 (44.7)	0.217	0.591	0.711 (0.028)	3.05 (0.120)	51.0 (46.4)	0.233	0.636	
				CYCLIC	817.7 (118.6)	0.711 (0.028)	3.05 (0.120)	45.4 (41.3)	0.233	0.636	a=t	3.43 (0.135)	53.7 (48.9)	0.326	1.00	10 CPM, 100 CYCLES TO BT
				FRACTURE	838.4 (121.6)	a=t	3.43 (0.135)	55.2 (50.2)	0.326	1.00						
2TR43-2	0.97 (0.038)	127.0 (5.00)	R.T.	LUL	863.3 (125.2)	0.737 0.029	3.05 (0.120)	52.3 (47.6)	0.242	0.763	0.787 (0.031)	3.56 (0.140)	59.3 (54.0)	0.215	0.816	
				CYCLIC	733.6 (106.4)	0.787 (0.031)	3.56 (0.140)	49.8 (45.3)	0.215	0.816	a=t	4.22 (0.166)	55.7 (50.7)	0.229	1.00	10 CPM 631 CYCLES TO BT
				FRACTURE	766.7 (111.2)	a=t	4.22 (0.166)	58.5 (53.2)	0.229	1.00						
3TR43-1	1.12 (0.044)	127.0 (5.00)	R.T.	FRACTURE	930.1 (134.9)	0.762 (0.030)	3.06 (0.120)	53.9 (49.0)	(0.250)	0.687						BREAKTHROUGH AT 895.7 MN/m^2 (129.9 ksi)

Table 31: ROOM TEMPERATURE 6Al-4V STA TITANIUM BASE METAL STATIC FRACTURE TEST RESULTS

SPECIMEN NUMBER	GAGE THICKNESS mm (inch)	FLAW SHAPE a/2c	FRACTURE TOUGHNESS K_{IE} $MN/m^{3/2}$ (ksi $\sqrt{in}$)
3TR11-1	3.18 (0.125)	0.15	65.7 (59.8)
3TR13-1		0.30	50.1 (45.6)
3TR14-1		0.45	63.2 (57.2)
3TR83-1	2.03 (0.080)	0.30	59.8 (54.4)
3TR84-1		0.45	51.2 (46.6)
3TR41-1	1.02 (0.040)	0.15	61.5 (56.0)
4TR41-2		0.15	55.9 (50.9)